University of Strathclyde

Doctoral Thesis

Recycling of Polyethylene Terephthalate (PET) through Ionic Liquid-Catalysed Glycolysis: Mechanistic Insights and Sustainable Strategies

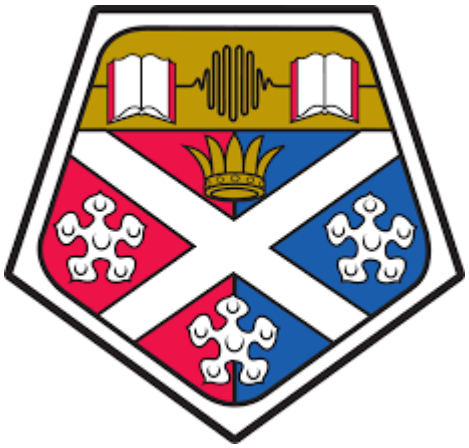

Stuart Conroy

Supervisor: Dr. Xiaolei Zhang

A thesis submitted in the fulfilment of the requirements for the degree of Doctor of Philosophy in the Department of Chemical and Process Engineering

Declaration of Authorship

This thesis is the result of the author's original research. It has been composed by the author and has not been previously submitted for examination which has led to the award of a degree.

Signed:

Stuart Conroy

11/07/2025

Abstract

Since their discovery in the early 20th century and subsequent industrial scale production beginning in the 1950s, plastics have become near-ubiquitous across modern society. Their extensive application in packaging and manufacturing has seen incredible growth, largely attributed to their durability, which ironically has also led to widespread environmental damage. Polyethylene terephthalate (PET), is a thermoplastic used for primarily food packaging and textiles. While its recycling rate is actually greater than alternative plastics, the volume in which it is produced means much more work is needed to be done to improve the end-of-life management.

Catalysed PET glycolysis has been identified as a promising process for the chemical recycling of PET waste, to its monomer bis(2-hydroxyethyl) terephthalate (BHET). In recent years, ionic liquids (ILs) have garnered interest as catalysts for PET glycolysis, due to their non-flammability and tuneability. However, while some metal-based ILs have shown exceptional activity and reusability, their high toxicity and cost of synthesis are a major hurdle to their scalability. Alternatively, choline-based ILs have been proposed as non-metal, non-toxic and cheaply-produced alternatives to their metal-containing counterparts. Despite the sustainability of these catalysts, issues such as low activity and unclear recyclability still remain. This thesis aims to bridge the gap in performance between choline- and metal-based ILs, while retaining the green credentials and low-cost of the former.

Density functional theory (DFT) calculations were employed to screen two non-metal choline-based ILs, [Ch][For] and [Ch][OAc], and two imidazolium-based ILs, [bmim]Cl and $[bmim]_2[CoCl_4]$. Subsequently, the ILs identified as being the most promising, $[bmim]_2[CoCl_4]$ and [Ch][OAc], were further evaluated using experimental

techniques. Experimentally-derived BHET yields and DFT-calculated energy barriers revealed the metal IL's superior catalytic performance, however BHET yields were low compared to literature standards. It was proposed that this was a result of moisture contamination hindering the degradation process, as well as potential re-depolymerisation of the monomer. The role of moisture was later explored via DFT and experiment, highlighting its hindering effects when in contact with the hygroscopic ILs within the reaction.

Further DFT analyses elucidated the catalytic mechanism of both, indicating that the metal IL's enhanced activity was influenced by the unique coordination ability of the anion's cobalt centre, while the organic IL was limited to non-covalent interactions. Results revealed that the mechanistic role of the cation, in both cases, was limited, challenging the conventional reaction mechanism commonly described in literature. The results indicate the insufficiency of "off-the-shelf" catalytic mechanisms, emphasising the need for bespoke analysis of individual catalytic systems.

A number of approaches to enhance the effectiveness and sustainability of the process were explored. Microwave (MW) heating was found to rapidly heat cobalt-containing reaction samples, while organic IL-containing systems responded poorly. The results indicated that [Ch][OAc] is unsuitable for future studies of MW-assisted PET glycolysis, unless combined with some form of MW-absorbing "cladding" materials.

Finally, a waste biomass-derived, KOH-activated biochar (BC) catalyst support was introduced as a potential method of enhancing the IL performance, especially in the organic case. The [Ch][OAc]-catalysed process observed a

remarkable 24% increase in BHET yield, which was attributed to the catalyst's efficient dispersion across the BC surface, as well as a potential synergistic catalytic role played by the support. Raman spectroscopy of separated BC indicated the potential reusability of the [Ch][OAc]-BC catalyst. These findings demonstrate the potential for use of a green, cheaply synthesised BC-supported [Ch][OAc] IL catalyst for PET glycolysis.

Acknowledgements

I would like to thank my supervisor Dr Xiaolei Zhang for her continued support and guidance, without which this thesis would not be possible. She has provided me with amazing opportunities and it has been a pleasure to work under her guidance.

Thanks to the other academics and staff that have aided in my experiments: Jun Li as my second supervisor, Elliot Ross who produced and provided biochar samples, Stuart Robertson who provided guidance on Schlenk line chemistry, those at the microwave facility at the University of York and the Strathclyde CPE lab technicians.

I have met some amazing people in my time here and am sure I have made some friends for life. To Robbie and Nisha, our lunches were always the highlight of my day. Thanks also to the other PhDs who helped make the department a great place to work: Tam, Elliot, Jordan, Tom, to name a few. A special mention must go to Fraser who recommended the position to me in the first place and for joining me in the library during the COVID days.

Of my civilian friends, I owe the most thanks to Matthew and Michael for putting up with living with me. To them and the others, Kane, Matt, Adam, Martin, Lewis, Marra – the weekends were always a welcome distraction.

To Dot, the final 6 months of this PhD was one of the most challenging periods of my life, but your constant support helped me see the light at the end of the tunnel.

To my family, especially my brother and grandparents, thank you for all your support and I can't wait to celebrate together. Lastly, my deepest gratitude is to my parents, to whom I owe everything. This thesis is dedicated to them, thank you.

Publications

Papers included in thesis:

Chapter 2:

S. Conroy, X. Zhang*, Theoretical insights into chemical recycling of polyethylene terephthalate (PET), *Polym Degrad Stab.*, 223 (2024). 110729-110741, https://doi.org/10.1016/j.polymdegradstab.2024.110729

Chapters 4-6:

S. Conroy, F. Norris, E. Ross, S. D. Robertson, Y. Xu, A. J. Fletcher, X. Zhang*, Advancing sustainable polyethylene terephthalate (PET) glycolysis with ionic liquid-based catalysts (In preparation)

Papers not included in this thesis:

- M. Thangamuthu, K. Vankayala, L. Xiong, **S. Conroy**, X. Zhang* and J. Tang*, "Tungsten Oxide-Based Z-Scheme for Visible Light-Driven Hydrogen Production from Water Splitting", *ACS Catal.*, 13, (**2023**), 9113-9124, https://doi.org/10.1021/acscatal.3c01312

- R. Guo, Y. Zeng, L. Lin, D. Hu, C. Lu, **S. Conroy**, S. Zhang, C. Zeng, H. Luo, Z. Jiang, X. Zhang, X. Tu* and K. Yan*, "CO_2-Assisted Controllable Synthesis of PdNi Nanoalloys for Highly Selective Hydrogenation of Biomass-Derived 5- Hydroxymethylfurfural", *Angew. Chem. Int. Ed.*,64, (**2025**), 1-9, https://doi.org/10.1002/anie.202418234

- C. McCready, K. Sladekova, **S. Conroy**, J. R. B. Gomes, A. J. Fletcher and M. Jorge*, "Quantifying the Uncertainty of Force Field Selection on Adsorption Predictions in MOFs", *J. Chem. Theory Comput.* 20, (**2024**), 4869-4884, https://doi.org/10.1021/acs.jctc.4c00287

- Y. Ma, **S. Conroy**, A. Shaw, I. M. Alliati, B. F. Sels*, X. Zhang* and X. Tu*, "Plasma-Enabled Selective Synthesis of Biobased Phenolics from Lignin-Derived Feedstock", *JACS Au*, 3, (**2023**), 3101-3110, https://doi.org/10.1021/jacsau.3c00468

Contents

List of Figures

List of Tables

List of abbreviations

Abbreviation	Definition	Abbreviation	Definition
PET	Polyethylene terephthalate	**QTAIM**	Quantum theory of atoms in molecules
IL	Ionic liquid	**RDG**	Reduced density gradient
SDG	Sustainable development goal	**TS**	Transition state
BHET	Bis(2-hydroxyethyl) terephthalate	**IRC**	Intrinsic reaction coordinate
DMT	Dimethyl terephthalate	**ADCH**	Atomic dipole moment corrected Hirshfeld
EG	Ethylene glycol	**SMD**	Solvation model based on density
TPA	Terephthalic acid	**ESP**	Electrostatic potential
sCCO$_2$	Supercritical CO_2	**GGA**	General gradient approximation
BHETA	Bis(2-hydroxy ethylene) terephthalamide	**FT-IR**	Fourier transform infrared spectroscopy
DES	Deep eutectic solvent	**NMR**	Nuclear magnetic resonance
MW	Microwave	**SCGs**	Spent coffee grounds
BC	Biochar	**KF**	Karl-Fischer
DFT	Density functional theory	**LDA**	Local (spin) density approximation
Zn(OAc)$_2$	Zinc acetate	**PCM**	Polarisable continuum model
Bmim	1-butyl-3-methylimidazolium	**SCF**	Self-consistent field
Ch	Choline	**PES**	Potential energy surface
For	Formate	**BCP**	Bond critical point
SILP	Supported ionic liquid phase	**vdW**	van der Waals
SILLP	Supported ionic liquid-like phase	**ATR**	Attenuated total reflectance
MHET	Mono(2-hydroxyethyl) terephthalic acid	**ECP**	Effective core potential
MWCNT	Multi-walled carbon nanotubes	**DMSO-d6**	Deuterated dimethyl sulfoxide
GO	Graphene oxide	**E(2)**	Second-order perturbation stabilisation energy

HOMO	Highest occupied molecular orbital	**eρ**	Electron density
LUMO	Lowest unoccupied molecular orbital	**∇^2eρ**	Laplacian of the density
LP	Lone pair	**AC**	Activated carbon
MD	Molecular dynamics	**H-bond**	Hydrogen bond
NBO	Natural bond orbital		

Chapter 1
Introduction

Plastic waste represents one of the most significant environmental challenges of the 21st century, with the commonly used thermoplastic polyethylene terephthalate (PET) being one of the major contributors. In recent years, the limitations of current recycling methods have become increasingly apparent, resulting in significant research into novel chemical recycling processes. Of these, PET glycolysis has been identified as a promising technique, which, when combined with efficient, green catalysts such as ionic liquids (ILs), may be capable of supporting the plastic circular economy. This introductory chapter examines the role of PET recycling within the circular economy, outlines the various plastic recycling strategies currently available and introduces recent technological advancements. The chapter concludes with the aims and objectives of this research and the thesis outline.

1.1 Plastic waste problem and circular economy

The use of plastic materials derived from fossil fuel-based feedstocks offers great advantages to industry, medicine and daily life. Due to their strength, flexibility and low production cost, plastics have become ubiquitous within society and are completely unparalleled to any other material used in packaging and construction, the two major sectors of their use [1]. The United Nations estimates that more than 400 million tonnes of plastic is produced globally each year, as of 2025 [2], with such a rate of production inevitably leading to significant amounts of waste generation. Although recycling methods are available, a mix of collection costs, insufficient infrastructure, and lack of demand from companies for recycled virgin material mean that the recycling rate of plastic is still low. It is estimated that only 9.5% of all plastic produced in history has ever been recycled [3]. When plastics are not recycled, they are often sent to landfill where they accumulate and cause environmental harm. Due to the mismanagement and overcapacity of coastal landfills, plastic waste often finds its way into the sea, where it can damage marine life and cause litter accumulation across oceans and beaches. Indeed, it was estimated in 2025 that 19-23 million tonnes of plastic leaks into aquatic ecosystems in including oceans, rivers and lakes, every year [4].

Throughout the second half of the 20th century, grassroots environmental movements across the United States and Europe began to see their warnings about the dangers of overproduction translated into domestic sustainability policy [5]. The mantra of “reduce, reuse, recycle” has since been adopted by many governments and organisations globally. This concept presents a hierarchy of goals; first to prevent waste through reducing plastic use across all societal sectors and second, if plastic

must be used, to avoid single-use products where possible. However, despite this outlook becoming more prevalent in recent years with the development of circular economy frameworks, the ubiquity of plastic products across the planet means that its existence as a waste product remains unavoidable. Therefore, much contemporary research has gone into optimising plastic recycling methods, to both reduce the use of petroleum resources and prevent plastic build-up in landfills and oceans.

The principles of the circular economy align closely with multiple United Nations Sustainable Development Goals (SDGs) [6]. The SDGs relevant to this research are displayed in **Figure 1.1**. SDG 12 (Responsible Consumption and Production) advocates for sustainable resource management and waste reduction, promoting efficient recycling systems and innovative recovery methods. SDG 9 (Industry, Innovation, and Infrastructure) highlights the importance of technological advancements in sustainable industrial processes, while SDG 13 (Climate Action) emphasises the need to reduce carbon emissions associated with raw material extraction and waste disposal. Furthermore, SDG 14 (Life Below Water) is directly linked to plastic pollution, by the well-observed suffering of marine environments from the accumulation of discarded plastics within them. By implementing circular solutions, such as improved plastic recycling and waste management, it is possible to reduce marine pollution across the planet's oceans and protect aquatic ecosystems.

Figure 1.1 *United Nations Sustainable Development Goals (SDGs) relevant to this work.*

By integrating circular economy principles into polymer recycling and material recovery, a more sustainable and resilient system can be established, mitigating environmental harm while reducing reliance on virgin resources. This transition is essential in addressing the global challenges of waste, pollution and resource depletion.

1.2 Polyethylene Terephthalate (PET)

One of the most commonly produced synthetic plastics, and the most common thermoplastic resin of the polyester family, PET is a thermoplastic found in food and drinks packaging and in synthetic fibres for clothing [7]. It has a number of properties which make it an excellent material for these utilisations, such as resistance to water, excellent mechanical strength and thermal stability [8]. The current industrially-established production methods are shown in **Figure 1.2**, where bis(2-hydroxyethyl) terephthalate (BHET) serves as an intermediate during the production process. PET is manufactured *via* either: A) the esterification process of terephthalic acid (TPA) with ethylene glycol (EG), or B) the transesterification polycondensation of dimethyl terephthalate (DMT) with EG. It should be noted that whilst traditionally both methods make use of chemicals derived from petroleum resources, recent research has begun

to explore the derivation of TPA and EG from bio-based feedstock such as cellulose and hemicellulose [9].

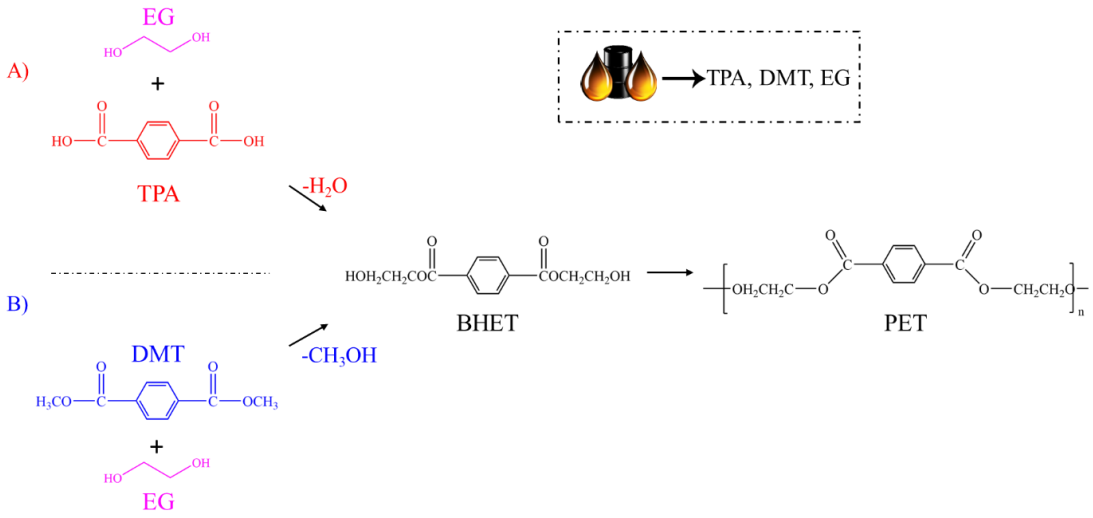

Figure 1.2. *The two main production routes of PET, via A) Direct esterification of TPA to BHET and B) Transesterification of DMT to BHET.*

PET was first discovered in 1941 by Whinfield and Dickson, chemists who worked for The Calico Printer's Association, a textile company in Manchester, England [10]. Five years later, in 1946, the American chemical corporation DuPont bought all legal rights for the material [11]. Initially, PET was used largely for advancements in X-ray technology, until the early 1970s, when DuPont produced the first PET plastic soft drinks bottle [12]. Since the 1980s, PET use, especially in food and drinks packaging, has been significantly expanded, with production expected to rise even further in the coming years.

PET is considered to be a non-biodegradable polymer, that is, when it is disposed to landfill it accumulates there for many years, causing harm to the environment. Due to its popularity, PET makes up a large percentage of global waste, accounting for 8% by weight and 12% by volume of the world's solid waste [13].

While it is difficult to determine the global rate, it is understood that PET is generally recycled more favourably than other plastics, due to existing infrastructure and the prevalence of deposit-return-schemes [14]. This compares favourably to the overall plastic recycling rate of 10% in 2024 [15], however, because of the sheer volume of PET being produced, the amount that is recycled needs to be increased significantly if EU targets of a 50% recycling rate on all plastic materials are to be met. Current waste management systems are incapable of effectively disposing of PET waste, resulting in much of it going to landfill. In addition to the negative environmental impact of this, the landfilled plastic represents a significant potential for energy footprint recovery. As a consequence of this, there is currently great interest in finding new, efficient ways to improve the PET waste situation and support the circular economy.

1.3 PET recycling methods

Thermoplastics such as PET can be repeatedly softened and hardened by heating and cooling, and have attractive properties such as chemical stability and hardness. However, these properties, created by the long carbon chains located along the polymers' backbone, are also the cause of the PET's inability to be broken down naturally. Much research in recent years has gone into finding solutions for the plastic crisis, with recycling solutions for the universally prevalent PET particularly sought after. Numerous recycling methods have been explored, including primary, secondary, tertiary and quaternary, as shown in **Figure 1.3**.

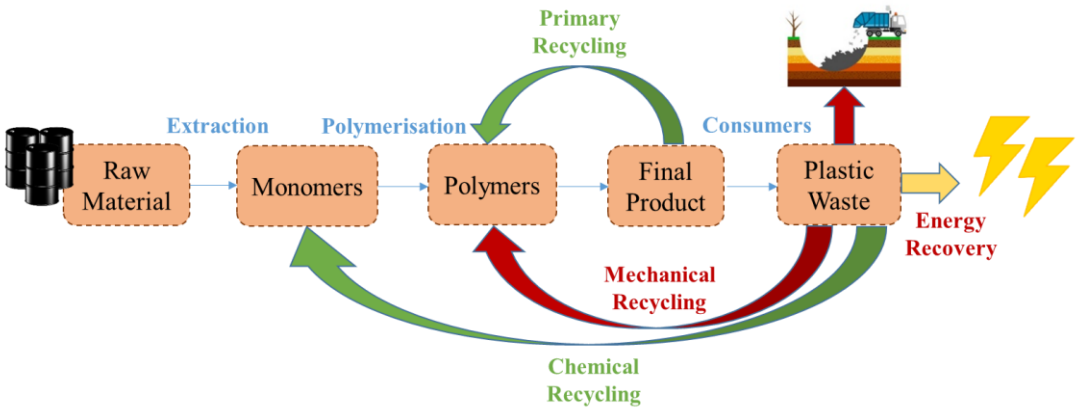

Figure 1.3. *Summary of primary, secondary, tertiary and quaternary plastic recycling methods.*

1.3.1 Primary Recycling

Primary recycling is the simplest and most economical method of plastic recycling. It is defined as the recycling of pre-consumer material, employing the use of defected plastic that has been discarded from the production line. Due to its status as a pre-consumer plastic, there is no contamination or mixing of plastic combinations, thus making pre-processing and separation methods unnecessary. However, primary recycling requires high purity of the feedstock, which makes it unsuitable for any post-consumer plastic without significant pre-processing [16].

1.3.2 Secondary Recycling

Secondary recycling (as outlined in **Figure 1.4**) is the most common method of plastic recycling and involves the separation and processing of waste plastic using mechanical methods. PET waste material is collected and transported to sorting facilities, where it is either manually separated from other plastic waste or separated automatically through the use of near infrared or X-ray-based technologies [17]. In addition to separation from other plastic types, the PET waste is also separated by colour, as mechanical recycling can only be used for transparent or light-blue PET,

due to the incompatibility with the presence of dyes [18]. Extensive cleaning will also be carried out, especially with PET waste derived from food packaging, before the waste is reduced in size and melt extrusion is carried out.

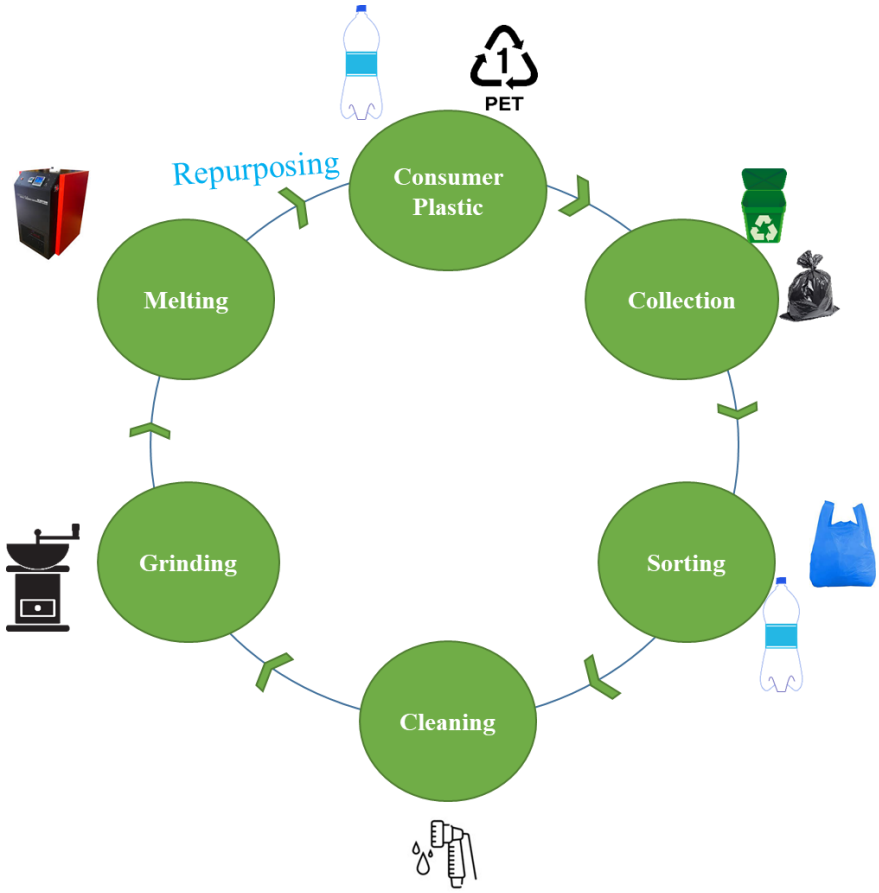

Figure 1.4. *Steps of secondary (mechanical) recycling of PET wastes.*

Secondary recycling has several advantages which mean it remains the most commonly used recycling technique for PET waste. The processes often make use of existing PET production infrastructure, meaning less initial investment is required and the detrimental environmental effect is limited [19]. However, difficulties arise with this method when used with PET due to the deterioration of polymer properties that results from a reduction in molecular weight during processing [20]. For example, the strain-at-break decreases from 47% for virgin PET to 0.7% for recycled PET after 5 cycles of secondary recycling techniques [21]. Additionally, the presence of

unavoidable contaminants such as PVC and paper in the waste stream can result in the hydrolysis of PET's ester linkages during thermal processing [22]. The "yellowing" of mechanically recycled PET, caused by side-reactions initiated by contaminants such as water or acidic groups, makes the recycled PET unusable for reuse in plastic bottle production [23]. For mechanically recycled PET to be made suitable for reuse as plastic bottles, it is usually mixed with virgin PET.

1.3.3 Quaternary Recycling

Another option for recycling of plastic material is quaternary recycling or energy recovery. This is the name for the process of burning plastic waste to produce energy in the form of heat or electricity. Such a process is only considered when other recycling methods offer no economic potential [24]. According to the Big Plastic Count, 2024 , around 58% of plastic waste is incinerated globally. While this is likely an overestimation based on the extrapolation of a small sample size, it is widely acknowledged that the incineration rate is far greater than the recycling rate, due to difficulties in recycling including sorting and cleaning [25]. Incinerating plastic waste is unfavourable as it releases large amounts of CO_2, as well as releasing potentially harmful toxins such as dioxins and polychlorinated biphenyls [26].

1.3.4 Tertiary Recycling

A promising method for recycling of plastics, specifically PET, is tertiary recycling, also known as chemical recycling. Tertiary recycling has a higher level of complexity than other recycling techniques and results in the breaking down of polymer backbones to form monomers, oligomers and other valuable intermediates. Such processes can be carried out using chemical, thermal or biological degradation methods. The main advantage of tertiary recycling is that it allows for the plastic

recycling loop to be fully closed and the recycled plastic loses none of its attractive properties [27]. Various tertiary recycling and upcycling techniques have been studied including thermo-chemical processes and solvolysis.

Thermo-chemical upcycling techniques such as gasification and pyrolysis have been studied extensively in the past as approaches to produce valuable chemicals which can be further processed for use as fuels and other high-value compounds. However, when used with PET plastic, a high concentration of benzoic acid is formed, making the liquid product unusable as a fuel, while manufacturing difficulties may present due to the high corrosivity [28,29]. Conversely, when polyethylene is pyrolysed, liquid oil comparable to gasoline, kerosene and diesel is produced [30]. During the gasification of PET, there is well-documented difficulty in the management of tar generated from the aromatic hydrocarbons present [31].

Tertiary recycling of PET is more commonly carried out using solvolysis rather than pyrolysis. Depending on the solvent to be used, there are various types of solvolysis including: hydrolysis, alcoholysis, glycolysis, aminolysis and ammonolysis, as shown in **Figure 1.5**. Aminolysis and ammonolysis techniques are not used on an industrial scale due to the technologies still being in their infancies [7]. Hydrolysis, alcoholysis and glycolysis are the prevalent solvolysis processes in tertiary recycling of PET. In addition to the production of monomers, the oligomers produced from the degradation process can be used to manufacture secondary valuable products such as epoxy resins and polyurethanes [13]

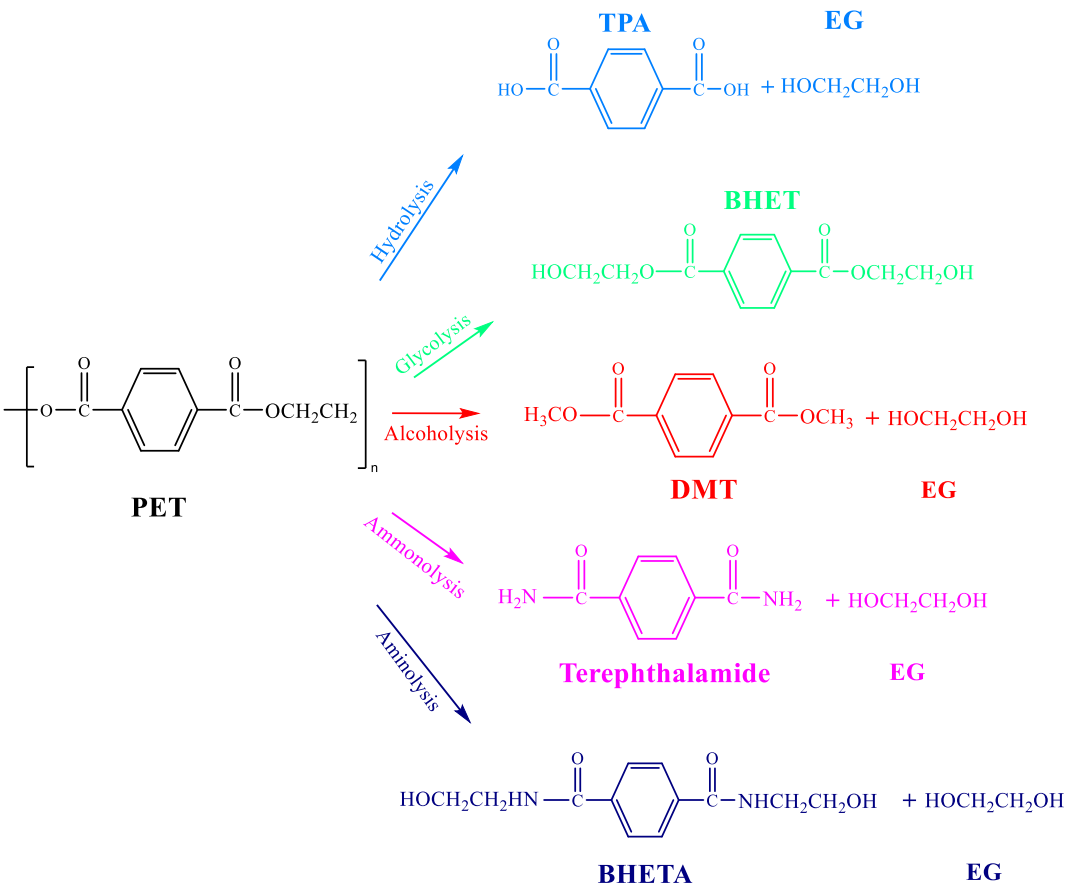

Figure 1.5. *Popular PET tertiary recycling methods via solvolysis [32].*

1.3.4.1 Alcoholysis

Alcoholysis involves the degradation of PET to its monomer DMT and EG *via* the reaction with an alcohol. The most commonly used alcohol is methanol, leading to the process often being named methanolysis, though other alcohols such as ethanol have also been employed previously [33,34]. Methanolysis of PET is currently being used by Loop Industries [35], with Eastman also having developed their own process [36]. The methanolysis process can be carried out alongside transesterification catalysts or with the aid of supercritical conditions [37–39]. Generally, the reaction is carried out at lower temperatures than other solvolysis techniques, however higher pressures are required. The introduction of co-solvents has been seen to significantly

improve the kinetics of the reaction, allowing for considerably lower temperatures and shorter reaction times [40].

The methanolysis process has the advantage of producing a monomer for which processing infrastructure already exists, meaning it can be directly re-introduced into the PET production process, or even installed within the production line [7]. However, the process also suffers from some limitations. The main disadvantage arises from the trend for TPA to be used primarily as the raw material for PET production, reducing the demand for DMT [7]. From an environmental and process safety perspective, the use of methanol, as a highly toxic and flammable solvent, is also undesirable [41]. Moreover, the product mixture is significantly more complex than other solvolysis methods, with a combination of DMT, glycols, phthalate derivatives and alcohols being produced [41]. Separation and refinement of this complex mixture can be time-consuming and expensive. Finally, the high pressures required in the process contribute to substantial capital and operating costs, further limiting its industrial appeal.

1.3.4.2 Hydrolysis

Hydrolysis involves the degradation of PET to its monomer TPA using water molecules in an acidic, alkaline or neutral medium. There is growing interest in PET hydrolysis due to the popularity of the TPA-based PET production route, which removes methanol from both the production and recycling process [42]. Hydrolysis of PET materials of varying quality has been validated on a pilot plant scale by INEOS Aromatics, as of July 2023 [43]. Despite this, hydrolysis is generally carried out at higher temperatures and pressures when compared to other solvolysis processes, due to water being a weaker nucleophile than alcohols or glycols [44].

Acidic hydrolysis is most commonly carried out using concentrated sulphuric acid, however other mineral acids such as nitric acid and phosphoric acid have also been used. The reduced pH induced by the acidic medium allows for the increased selective production of TPA [45]. In order to improve the reaction kinetics, supercritical CO_2 ($sCCO_2$) has been employed [46,47]. The introduction of $sCCO_2$ allows for the reaction to take place at both the interfacial surface of the PET particles and within its bulk. Additionally, phase transfer catalysts (PTCs) have been used to allow for milder reaction conditions [48,49]. The role of these catalysts is to transfer hydroxide ions more efficiently from the aqueous phase to the surface of the PET particles [49,50]. Despite this, acid hydrolysis suffers from the high corrosiveness of the process, which causes difficulties on an industrial scale and the generation of large amounts of inorganic salts which need to be removed during post-process neutralisation [51].

Alkaline hydrolysis is carried out in an aqueous alkaline solution, most commonly sodium hydroxide or potassium hydroxide in a concentration of 4-20% alkaline [44]. The strongly basic medium acts as a catalyst, allowing for the production of EG and a corresponding terephthalic salt, which can then be acidified with a strong acid to produce the final product TPA [52]. Similar to the acidic process, alkaline hydrolysis has been carried out successfully alongside additional catalysts such as trioctylmethylammonium bromide [53], benzalkonium chloride [54] and tributylhexadecylphosphonium bromide [50]. Additional techniques such as co-solvation and ultrasound have also been used [55,56]. Despite the initial alkaline conditions, the introduction of large amounts of acid to neutralise the terephthalic salt causes corrosion issues similar to the acidic process.

Neutral hydrolysis is performed using a stream of water or steam, most commonly in the presence of catalysts such as alkali metal salts. The neutral process has attracted much attention due to reduced costs, as the large amounts of acid and/or alkali can be avoided by carrying the process out at longer reaction times of 24 hours [57]. The process mechanism shows great promise from an environmental perspective, as it avoids the use of toxic solvents and catalysts, whilst abandoning the use of corrosive acids further simplifies the process [57]. Nevertheless, more work needs to be done to reduce the energy demands caused by the long reaction times of the neutral process hydrolysis process before it can be considered a viable industrial method of PET tertiary recycling.

1.3.4.3 Ammonolysis

During the ammonolysis process, ammonia is used to break down the PET chain into the monomer terephthalamide. Although not inherently valuable in itself, terephthalamide can be further converted into value-added products such as p-xylylenediamine and 1,4-bis (amino- ethyl) cyclohexane [58]. Owing to the presence of the nitrogen atom, the $-NH_3$ functional group has a more basic nature than the -OH nucleophile used to cleave the PET chain in the other solvolysis methods. This creates the potential for more ambient reaction conditions and improved kinetics.

1.3.4.4 Aminolysis

Aminolysis of PET involves the use of a functional group which contains a nitrogen atom with a lone-pair of electrons. The most commonly used amine is ethanolamine due to its promotion of the monomer bis(2-hydroxy ethylene) terephthalamide (BHETA). Additionally, larger amines such as diethanolamide are avoided due to their propensity to cause significant steric hindrance, which can deter

the degradation process [59]. BHETA is a valuable chemical which can be used to produce valuable poly(ester amides), which represent an emerging category within various industries, due to their combination of attractive polyester and polyamide characteristics [60]. Within the ethanolamine molecule, there are two nucleophilic centres capable of attacking the carbonyl group of PET: the amine group ($-NH_2$) and the hydroxyl group (-OH). The amine group is more likely to attack the PET chain due to its increased basicity compared to the hydroxyl. Both ammonolysis and aminolysis are still in their relative infancies compared to hydrolysis and alcoholysis, however there are some concerns over the toxicity and expense of using ammonia or its derivatives as nucleophiles [61].

1.4 PET Glycolysis

The most common PET solvolysis method in use in the chemical industry today is PET glycolysis. Glycolysis involves the use of glycols to degrade PET to BHET *via* the breaking of ester linkages which are replaced by hydroxyl terminals. The most commonly used glycol is EG, however diethylene glycol, propylene glycol and polyethylene glycol have also been used, amongst others. Glycolysis of PET was first patented in the US in 1961, using an alkali earth metal catalyst [62]. In the time since, the process has been greatly streamlined and is used commercially by companies such as Goodyear, Shell, DuPont and others [63].

PET glycolysis is generally considered favourable to other solvolysis methods due to its shorter reaction time and milder reaction conditions, as well as the associated reduced separation and purification costs. Additionally, as BHET is produced as an intermediate for both TPA- and DMT-based PET production, it can be entered directly into either production stream [64]. Modelled studies comparing the technoeconomic

and environmental metrics of different recycling methods have commonly concluded that glycolysis offers the best performance [65,66]. As uncatalysed glycolysis is a sluggish process, certain changes need to be made to the process to make it more economically viable. In order to improve the kinetics of a glycolysis process, there are a number of methods available, with the introduction of a transesterification catalyst being the most common. Recent research progress has predominantly focused on developing more efficient and reusable catalysts, making the process more efficient and environmentally friendly. Advances include the design of novel metal-based, metal-free and hybrid catalytic systems that operate under milder conditions and deliver higher yields of valuable monomers. These technologies can be supplemented by the assistance of microwave heating or organic solvents. Supercritical conditions also allow for improved reaction kinetics and have the main advantage of not requiring a catalyst. These additional measures are however not without their disadvantages. Supercritical methods have to operate at high operating conditions (the critical temperature and pressure of EG are 446.7 °C and 7.7 MPa, respectively [67]) whilst the use of organic solvents has become an unattractive notion in recent years due to their negative environmental impact [68].

1.5 Catalysed PET glycolysis

The conventional catalysed PET glycolysis process often makes use of heavy metal salts, the use of which is being phased out by industry due to difficult separation and toxicity issues [69]. Resultingly, recent studies of PET glycolysis have focused on the development of efficient and environmentally friendly catalysts. Novel technologies include ILs [70], metal oxides [71], deep eutectic solvents (DESs) [72] and high surface area catalyst supports [73], among others. With increasing research

efforts, monomer yields have risen significantly, with many catalysts being capable of producing > 90% BHET yield. However, scalability-hindering problems remain.

Of the most effective catalysts, the majority are metal-containing, adding expense and toxicity as well as potential leaching issues. In contrast, environmentally friendly non-metal catalysts often suffer from separation issues and lower activity. ILs in particular present a possible solution to many of the aforementioned issues. Known for their highly tuneable and non-volatile nature, ILs offer a cheaper and more environmentally benign alternative to the metal-containing catalysts being studied elsewhere. However, to enhance their suitability for industrial use, the observed BHET yields need to be competitive with metal-based catalysts. Additionally, the separation of ILs from product mixtures needs to be improved to increase their economic compatibility. It is these elements, BHET yield enhancement and ease of separation of ILs from product mixtures, which represent a potential gap in the research. By solving these issues, the green credentials of ILs could be exploited on an industrial scale.

1.6 Aim and objectives of this thesis

ILs have emerged as promising PET glycolysis catalysts due to their tunability and non-volatility. Organic ILs, in particular, represent a cheap and green alternative to the conventional metal catalysts commonly used in industry. However, the current technology suffers from separation issues and lower BHET yields, which limits the scalability. The work enclosed in this thesis was developed to understand and enhance the IL-catalysed PET glycolysis process, with a focused view of making it more cost-effective, efficient and sustainable. The main research objectives consist of the following:

1) To computationally screen a range of metal-based and organic ILs using density functional theory (DFT) calculations to evaluate their catalytic activity in the PET glycolysis reaction.
2) To experimentally assess the catalytic performance of the most promising ILs identified through DFT screening.
3) To elucidate the detailed reaction mechanism of IL-catalysed PET glycolysis using quantum chemical methods, with a comparative focus on metal and non-metal ILs.
4) To investigate the influence of microwave (MW) heating on IL-catalysed glycolysis and compare its effects with those of conventional thermal methods.
5) To examine the role of moisture in the glycolysis process, relating it to real-world plastic waste systems.
6) To evaluate the potential of waste biomass-derived activated biochar (BC) as a catalyst support and determine its impact on the efficiency and sustainability of the process.

1.7 Thesis outline

This thesis presents a combined experimental and computational investigation of IL-catalysed PET glycolysis. The current chapter, **Chapter 1**, introduced the main aim and objectives of the research: to tackle the PET waste problem through sustainable IL-catalysed glycolysis. **Chapter 2** provides a comprehensive review of the literature related to catalysed glycolysis and the corresponding reaction mechanisms, as well as the integration of biochar with chemical processes. The chapter concludes with an identification of the research gap and novelty of this work. **Chapter**

3 provides an overview of the full methodology whilst detailing the theoretical background related to the computational work and experimental characterisation. The first results chapter, **Chapter 4**, combines computational screening of ILs for PET glycolysis, with experimental testing of the catalysts found to be the most promising. **Chapter 5** theoretically evaluates the intrinsic reaction mechanisms of IL-catalysed glycolysis, defining the key differences between metal and organic ILs and relating the mechanisms to those previously established in the literature. **Chapter 6** investigates methods to enhance the sustainability, economics and efficiency of the process through three approaches: 1) Using microwave heating to reduce reaction times and energy demands, 2) Investigating the hindering effects of moisture, relating the results more closely to real-world plastic waste, and 3) Evaluating the use of biochar derived from waste biomass as a catalyst support for IL-catalysed PET glycolysis. Finally, **Chapter 7** summarises the work enclosed in the thesis and proposes future work on the basis of the obtained results.

References

[1] L. Lebreton, A. Andrady, Future scenarios of global plastic waste generation and disposal, Palgrave Commun 5 (2019) 1–11. https://doi.org/10.1057/s41599-018-0212-7.

[2] United Nations, Beat plastic pollution, United Nations: World Environment Day (2025). https://www.un.org/pl/node/71013#:~:text=Beat%20plastic%20pollution,to%20be%20used%20only%20once. (accessed October 2, 2025).

[3] R. Geyer, J.R. Jambeck, K.L. Law, Production, use, and fate of all plastics ever made, Sci Adv 3 (2017) 25–29. https://doi.org/10.1126/sciadv.1700782.

[4] UNEP, Plastic Pollution, (2025). https://www.unep.org/plastic-pollution (accessed November 17, 2025).

[5] A.T. Williams, N. Rangel-Buitrago, The past, present, and future of plastic pollution, Mar Pollut Bull 176 (2022). https://doi.org/10.1016/j.marpolbul.2022.113429.

[6] UN, Transforming Our World: The 2030 Agenda for Sustainable Development, 2015.

[7] G.P. Karayannidis, D.S. Achilias, Chemical recycling of poly(ethylene terephthalate), Macromol Mater Eng 292 (2007) 128–146. https://doi.org/10.1002/mame.200600341.

[8] J. Xin, Q. Zhang, J. Huang, R. Huang, Q.Z. Jaffery, D. Yan, Q. Zhou, J. Xu, X. Lu, Progress in the catalytic glycolysis of polyethylene terephthalate, J Environ Manage 296 (2021) 113267. https://doi.org/10.1016/j.jenvman.2021.113267.

[9] E.E. Kwon, J. Lee, Polyethylene terephthalate production from a carbon neutral resource, J Clean Prod 469 (2024). https://doi.org/10.1016/j.jclepro.2024.143210.

[10] J. Rex Whinfield, J. Tennant Dickson, Polymeric Linear Terephthalic Esters, 1945.

[11] O. Kahn-Freund, English Contracts and American Anti-Trust Law . The Nylon Patent Case Author (s): O . Kahn-Freund Source : The Modern Law Review , Jan ., 1955 , Vol . 18 , No . 1 (Jan ., 1955), pp . 65-70 Published by : Wiley on behalf of the Modern Law Review Stable, Mod Law Rev 18 (1955) 65–70. https://doi.org/1091162.

[12] K.S. Carmichael, United States Patent (19), 1973.

[13] G.M. Mohamad Sadeghi, M. Sayaf, From PET waste to novel polyurethanes, in: Mater. Recycl. Trends Perspect., 2012: pp. 357–390. https://doi.org/10.5772/31642.

[14] British Plastics Federation, Plastic Recycling, (2022). https://www.bpf.co.uk/Sustainability/Plastics_Recycling.aspx (accessed November 17, 2025).

[15] Q. Liu, S. Martinez-Villarreal, S. Wang, N. Ngoc Thanh Tien, M. Kammoun, Q. De Roover, C. Len, A. Richel, The role of plastic chemical recycling processes in a circular economy context, Chem. Eng. J. 498 (2024). https://doi.org/10.1016/j.cej.2024.155227.

[16] V. Sinha, M.R. Patel, J. V Patel, Pet waste management by chemical recycling: A review, J Polym Environ 18 (2010) 8–25. https://doi.org/10.1007/s10924-008-0106-7.

[17] I. Vollmer, M.J.F. Jenks, M.C.P. Roelands, R.J. White, T. van Harmelen, P. de Wild, G.P. van der Laan, F. Meirer, J.T.F. Keurentjes, B.M. Weckhuysen, Beyond mechanical recycling: Giving new life to plastic waste, Angew. Chem. Int. Ed. 59 (2020) 15402–15423. https://doi.org/10.1002/anie.201915651.

[18] M.D. de Dios Caputto, R. Navarro, J.L. Valentín, Á. Marcos-Fernández, Chemical upcycling of poly(ethylene terephthalate) waste: Moving to a circular model, J. Polym. Sci. 60 (2022) 3269–3283. https://doi.org/10.1002/pol.20220137.

[19] F. Welle, Twenty years of PET bottle to bottle recycling - An overview, Resour Conserv Recycl 55 (2011) 865–875. https://doi.org/10.1016/j.resconrec.2011.04.009.

[20] V. Dulio, R. Po, R. Borrelli, A. Guarini, C. Santini, Characterization of low-molecular-weight oligomers in recycled poly(ethylene terephthalate), Angew.

Makromol. Chem. 225 (1995) 109–122. https://doi.org/10.1002/apmc.1995.052250110.

[21] M.D.M.C. Lopez, A.I.A. Pernas, M.J.A. Lopez, A.L. Latorre, J.M.L. Vilarino, M.V.G. Rodriguez, Assessing changes on poly (ethylene terephthalate) properties after recycling: Mechanical recycling in laboratory versus postconsumer recycled material, Mater Chem Phys 147 (2014) 884–894. https://doi.org/10.1016/j.matchemphys.2014.06.034.

[22] A. Pawlak, M. Pluta, J. Morawiec, A. Galeski, M. Pracella, Characterization of scrap poly(ethylene terephthalate), Eur Polym J 36 (2000) 1875–1884. https://doi.org/10.1016/S0014-3057(99)00261-X.

[23] J.D. Badia, E. Strömberg, S. Karlsson, A. Ribes-Greus, The role of crystalline, mobile amorphous and rigid amorphous fractions in the performance of recycled poly (ethylene terephthalate) (PET), Polym Degrad Stab 97 (2012) 98–107. https://doi.org/10.1016/j.polymdegradstab.2011.10.008.

[24] S.M. Al-Salem, P. Lettieri, J. Baeyens, Recycling and recovery routes of plastic solid waste (PSW): A review, Waste Manag. 29 (2009) 2625–2643. https://doi.org/10.1016/j.wasman.2009.06.004.

[25] OECD, Global Plastics Outlook, 2022. https://doi.org/10.1787/de747aef-en.

[26] R. Verma, K.S. Vinoda, M. Papireddy, A.N.S. Gowda, Toxic pollutants from plastic waste - A review, Procedia Environ Sci 35 (2016) 701–708. https://doi.org/10.1016/j.proenv.2016.07.069.

[27] A. Lee, M.S. Liew, Tertiary recycling of plastics waste: an analysis of feedstock, chemical and biological degradation methods, J Mater Cycles Waste Manag 23 (2020) 32–43. https://doi.org/10.1007/s10163-020-01106-2.

[28] M.-W. Ho, Waste Plastics into Fuel Oil?, Science in Society (2015). https://www.i-sis.org.uk/Waste_Plastics_into_Fuel_Oil.php (accessed May 17, 2021).

[29] S.D.A. Sharuddin, F. Abnisa, W.M.A.W. Daud, M.K. Aroua, A review on pyrolysis of plastic wastes, Energy Convers Manag 115 (2016) 308–326. https://doi.org/10.1016/j.enconman.2016.02.037.

[30] B.K. Sharma, B.R. Moser, Production, characterization and fuel properties of alternative diesel fuel from pyrolysis of waste plastic grocery bags, Fuel Process. Technol. 122 (2014) 79–90. https://doi.org/10.1016/j.fuproc.2014.01.019.

[31] J.K. Kim, Y.S. Jeong, J.W. Kim, J.S. Kim, Two-stage thermochemical conversion of polyethylene terephthalate using steam to produce a clean and H2- and CO-rich syngas, Energy 276 (2023). https://doi.org/10.1016/j.energy.2023.127651.

[32] S. Conroy, X. Zhang, Theoretical insights into chemical recycling of polyethylene terephthalate (PET), Polym Degrad Stab 223 (2024) 110729. https://doi.org/10.1016/j.polymdegradstab.2024.110729.

[33] C.S. Nunes, M.J. Vieira Da Silva, D. Cristina Da Silva, A.D.R. Freitas, F.A. Rosa, A.F. Rubira, E.C. Muniz, PET depolymerisation in supercritical ethanol catalysed by [Bmim][BF 4], RSC Adv 4 (2014) 20308–20316. https://doi.org/10.1039/c4ra00262h.

[34] L. Zhou, X. Lu, Z. Ju, B. Liu, H. Yao, J. Xu, Q. Zhou, Y. Hu, S. Zhang, Alcoholysis of polyethylene terephthalate to produce dioctyl terephthalate using choline chloride-based deep eutectic solvents as efficient catalysts, Green Chem. 21 (2019) 897–906. https://doi.org/10.1039/c8gc03791d.

[35] H. Essaddam, Polyethylene Terephthalate Depolymerization, WO2017007965A1, 2017.

[36] T. Pecorini, E.J. Moskala, D.M. Lange, R.W. Seymour, Process for the Preparation of Polyesters with High Recycle Content, WO2013025186A1, 2013.

[37] S. Mishra, A.S. Goje, Kinetic and thermodynamic study of methanolysis of poly(ethylene terephthalate) waste powder, Polym Int 52 (2003) 337–342. https://doi.org/10.1002/pi.1147.

[38] B.-K. Kim, G.-C. Hwang, S.-Y. Bae, S.-C. Yi, H. Kumazawa, Depolymerization of Polyethyleneterephthalate in Supercritical Methanol, J Appl Polym Sci 81 (2001) 2102–2108. https://doi.org/10.1002/app.1645.

[39] J.T. Du, Q. Sun, X.F. Zeng, D. Wang, J.X. Wang, J.F. Chen, ZnO nanodispersion as pseudohomogeneous catalyst for alcoholysis of polyethylene terephthalate, Chem Eng Sci 220 (2020). https://doi.org/10.1016/j.ces.2020.115642.

[40] D.D. Pham, J. Cho, Low-energy catalytic methanolysis of poly(ethyleneterephthalate), Green Chem. 23 (2021) 511. https://doi.org/10.1039/D0GC03536J.

[41] A.B. Raheem, Z.Z. Noor, A. Hassan, M.K. Abd Hamid, S.A. Samsudin, A.H. Sabeen, Current developments in chemical recycling of post-consumer polyethylene terephthalate wastes for new materials production: A review, J Clean Prod 225 (2019) 1052–1064. https://doi.org/10.1016/j.jclepro.2019.04.019.

[42] G. Giannotta, R. Po', N. Cardi, E. Tampellini, E. Occhiello, F. Garbassi, Processing effects on poly(ethylene terephthalate) from bottle scraps, Polym Eng Sci 34 (1994) 1–23. https://doi.org/10.1002/pen.760341508.

[43] INEOS Aromatics, Circular Economy: Infinia recycling, (2023). https://www.ineos.com/businesses/ineos-aromatics/sustainability/ineos-

infinia/#:~:text=Infinia%20recycling%20technology,be%20recycled%20again%20and%20again. (accessed July 8, 2025).

[44] B. Shojaei, M. Abtahi, M. Najafi, Chemical recycling of PET: A stepping-stone toward sustainability, Polym Adv Technol 31 (2020) 2912–2938. https://doi.org/10.1002/pat.5023.

[45] S.D. Mancini, M. Zanin, Optimization of neutral hydrolysis reaction of post-consumer PET for chemical recycling, Prog. Rubber Plast. Recycl. Technol. 20 (2004) 117–132. https://doi.org/10.1177/147776060402000202.

[46] W.Z. Guo, H. Lu, X.K. Li, G.P. Cao, Tungsten-promoted titania as solid acid for catalytic hydrolysis of waste bottle PET in supercritical CO2, RSC Adv 6 (2016) 43171–43184. https://doi.org/10.1039/c6ra06298a.

[47] X.K. Li, H. Lu, W.Z. Guo, G.P. Cao, H.L. Liu, Y.H. Shi, Reaction kinetics and mechanism of catalyzed hydrolysis of waste PET using solid acid catalyst in supercritical CO2, AIChE J. 61 (2015) 200–214. https://doi.org/10.1002/aic.14632.

[48] S.D. Mancini, M. Zanin, Post consumer pet depolymerization by acid hydrolysis, Polym.–Plast. Technol. Eng. 46 (2007) 135–144. https://doi.org/10.1080/03602550601152945.

[49] L. Zhang, Kinetics of hydrolysis of poly(ethylene terephthalate) wastes catalyzed by dual functional phase transfer catalyst: A mechanism of chain-end scission, Eur J Pharmacol 742 (2014) 1–5. https://doi.org/10.1016/j.eurpolymj.2014.08.007.

[50] R. López-Fonseca, J.R. González-Velasco, J.I. Gutiérrez-Ortiz, A shrinking core model for the alkaline hydrolysis of PET assisted by

tributylhexadecylphosphonium bromide, Chem. Eng. J. 146 (2009) 287–294. https://doi.org/10.1016/j.cej.2008.09.039.

[51] T. Yoshioka, T. Motoki, A. Okuwaki, Kinetics of hydrolysis of poly(ethylene terephthalate) powder in sulfuric acid by a modified shrinking-core model, Ind Eng Chem Res 40 (2001) 75–79. https://doi.org/10.1021/ie000592u.

[52] A. Oku, L.C. Hu, E. Yamada, Alkali decomposition of poly(ethylene terephthalate) with sodium hydroxide in nonaqueous ethylene glycol: A study on recycling of terephthalic acid and ethylene glycol, J Appl Polym Sci 63 (1997) 595–601. https://doi.org/10.1002/(SICI)1097-4628(19970131)63:5<595::AID-APP7>3.0.CO;2-P.

[53] M.B. Polk, L.L. Leboeuf, M. Shah, W. Chee-Youb, X. Hu, W. Ding, Nylon 66, nylon 46, and pet phase-transfer-catalyzed alkaline depolymerization at atmospheric pressure, Polym Plast Technol Eng 38 (1999) 459–470. https://doi.org/10.1080/03602559909351593.

[54] J. Das, A.B. Halgeri, V. Sahu, P.A. Parikh, Alkaline hydrolysis of poly(ethylene terephthalate) in presence of a phase transfer catalyst, Indian J. Chem. Technol. 14 (2007) 173–177.

[55] S. Zhang, W. Xu, R. Du, X. Zhou, X. Liu, S. Xu, Y.Z. Wang, Cosolvent-promoted selective non-aqueous hydrolysis of PET wastes and facile product separation, Green Chem. (2022) 3284–3292. https://doi.org/10.1039/d2gc00328g.

[56] C.S. Bhogle, A.B. Pandit, Ultrasound-Assisted alkaline hydrolysis of waste poly(ethylene terephthalate) in aqueous and non-aqueous media at low temperature, Indian Chem. Eng. 60 (2018) 122–140. https://doi.org/10.1080/00194506.2017.1310634.

[57] C.N. Onwucha, C.O. Ehi-Eromosele, S.O. Ajayi, M. Schaefer, S. Indris, H. Ehrenberg, Uncatalyzed neutral hydrolysis of waste PET bottles into pure terephthalic acid, Ind Eng Chem Res (2022). https://doi.org/10.1021/acs.iecr.2c04117.

[58] P. Gupta, S. Bhandari, Chemical depolymerization of PET bottles via ammonolysis and aminolysis, Elsevier Inc., 2019. https://doi.org/10.1016/b978-0-12-811361-5.00006-7.

[59] V.A. Popoola, Polyester formation: Aminolytic degradation and proposed mechanisms of the reaction, J Appl Polym Sci 36 (1988) 1677–1683. https://doi.org/10.1002/app.1988.070360716.

[60] M. Winnacker, B. Rieger, Poly(ester amide)s: Recent insights into synthesis, stability and biomedical applications, Polym Chem 7 (2016) 7039–7046. https://doi.org/10.1039/c6py01783e.

[61] E. Barnard, J.J. Rubio Arias, W. Thielemans, Chemolytic depolymerisation of PET: A review, Green Chem. 23 (2021) 3765–3789. https://doi.org/10.1039/d1gc00887k.

[62] J.T. Mccdowell, * Seed eilee United States Patent Office, 1965.

[63] J. Xin, Q. Zhang, J. Huang, R. Huang, Q.Z. Jaffery, D. Yan, Q. Zhou, J. Xu, X. Lu, Progress in the catalytic glycolysis of polyethylene terephthalate, J Environ Manage 296 (2021) 113267. https://doi.org/10.1016/j.jenvman.2021.113267.

[64] S.H. Park, S.H. Kim, Poly (ethylene terephthalate) recycling for high value added textiles, Fash. Text. 1 (2014) 1–17. https://doi.org/10.1186/s40691-014-0001-x.

[65] T. Uekert, A. Singh, J.S. DesVeaux, T. Ghosh, A. Bhatt, G. Yadav, S. Afzal, J. Walzberg, K.M. Knauer, S.R. Nicholson, G.T. Beckham, A.C. Carpenter, Technical, economic, and environmental comparison of closed-loop recycling technologies for

common plastics, ACS Sustain Chem Eng 11 (2023) 965–978. https://doi.org/10.1021/acssuschemeng.2c05497.

[66] T. Ghosh, G. Avery, A. Bhatt, T. Uekert, J. Walzberg, A. Carpenter, Towards a circular economy for PET bottle resin using a system dynamics inspired material flow model, J Clean Prod 383 (2023). https://doi.org/10.1016/j.jclepro.2022.135208.

[67] M. Imran, B.K. Kim, M. Han, B.G. Cho, D.H. Kim, Sub-and supercritical glycolysis of polyethylene terephthalate (PET) into the monomer bis(2-hydroxyethyl) terephthalate (BHET), Polym Degrad Stab 95 (2010) 1686–1693. https://doi.org/10.1016/j.polymdegradstab.2010.05.026.

[68] L. Bartolome, M. Imran, B.G. Cho, W.A. Al-Masry, D.H. Kim, Recent developments in the chemical recycling of PET, in: Mater. Recycl. Trends Perspect., 2012: pp. 65–84. https://doi.org/10.5772/33800.

[69] S.R. Shukla, V. Palekar, N. Pingale, Zeolite Catalyzed glycolysis of poly(ethylene terephthalate) bottle waste, J Appl Polym Sci 110 (2008) 501–506. https://doi.org/10.1002/app.28656.

[70] F. Forouzeshfar, M.R. Coleman, J.G. Lawrence, Glycolysis of poly (ethylene terephthalate) using DBU-based ionic liquid catalysts, Catal Today 450 (2025). https://doi.org/10.1016/j.cattod.2025.115187.

[71] Y. Zhao, M. Liu, R. Zhao, F. Liu, X. Ge, S. Yu, Heterogeneous CaO(SrO, BaO)/MCF as highly active and recyclable catalysts for the glycolysis of poly(ethylene terephthalate), Res. Chem. Intermed. 44 (2018) 7711-7729. https://doi.org/10.1007/s11164-018-3582-y(0123456789().,-volV)(0123456789().,-volV).

[72] E. Sert, E. Yılmaz, F.S. Atalay, Chemical recycling of polyethlylene terephthalate by glycolysis using deep eutectic solvents, J Polym Environ 27 (2019) 2956–2962. https://doi.org/10.1007/s10924-019-01578-w.

[73] A.M. Al-Sabagh, F.Z. Yehia, D.R.K. Harding, G. Eshaq, A.E. ElMetwally, Fe3O4-boosted MWCNT as an efficient sustainable catalyst for PET glycolysis, Green Chem. 18 (2016) 3997–4003. https://doi.org/10.1039/c6gc00534a.

Chapter 2
Literature Review

This chapter presents a comprehensive review of the literature related to catalysed polyethylene terephthalate (PET) glycolysis, introducing numerous traditional and novel technologies. While the PET degradation mechanism is generally well-established, some discrepancies in the literature exist. These studies, which are essential to elucidating catalytic influence, are collated here. The use of microwave (MW) heating to intensify chemical processes and reduce energy demands is explored in the context of PET glycolysis, using both organic and metal-based catalysts. Additionally, the application of biochar (BC) as a support material in catalytic systems is discussed. Numerous catalysed PET glycolysis approaches are summarised, highlighting their contribution to three essential pillars: economics, sustainability and effectiveness. The chapter concludes with a summary of the research gap and the positioning of the present study within it, in the context of the three aforementioned pillars.

2.1 Catalysed PET glycolysis

Traditionally, transesterification catalysts have been widely used for the PET glycolysis process. Such catalysts act to reduce the activation energy of the process, improve the yield and selectivity of bis(2-hydroxyethyl) terephthalate (BHET), and encourage full conversion of PET. A variety of catalysts including heavy metal salts, metal oxides, organocatalysts, ionic liquids (ILs) and supported metals have been reported for use in PET glycolysis, with the main focus of recent research being the design and application of highly active, sustainable and cost-effective materials.

2.1.1 Heavy metal salts

The most commonly used PET glycolysis catalysts are heavy metal salts such as zinc acetate ($Zn(OAc)_2$). In 1989, Chujo et al. [1] investigated the use of various metal acetates as catalysts for PET glycolysis, finding that $Zn(OAc)_2$ was the most successful. Aguado et al. [2], achieved a high BHET yield of 84% using $Zn(OAc)_2$ as a catalyst. Despite this high yield, industry has recently sought to avoid using heavy metal salts as catalysts for such processes because of their toxicity and associated harm to the environment [3]. Additionally, they are very difficult to recycle and can often only be used once. This single-use characteristic means that significant quantities of the catalyst are required for use, rendering the process unviable at an industrial scale, and adding to its unfavourability.

In an effort to reduce the environmental effect of the catalyst, milder metal catalysts have been proposed as alternatives to heavy metal salts. Mild alkalis such as sodium carbonate and sodium bicarbonate have been tested and found to have comparable catalytic effects to zinc and lead acetate [4]. Similarly, metal chlorides were investigated as milder alternatives and were found to have a reasonably high

BHET yield of 73.24% [5]. Despite these results, the process still suffered from the problem of catalyst separation. Many alkali metal salts are soluble in EG, making their separation from the product mixture more difficult and therefore impairing the product purity. In a similar fashion to heavy metal use, the inability to recycle these milder metal catalysts also makes their use on an industrial scale unsuitable for the process [6].

2.1.2 Metal oxides

With changing opinions regarding the desired properties of catalysts, many novel chemicals and materials have been investigated, with a focus on facilitating separation from product mixtures. Metal oxides have garnered attention in recent years, with mixed metal oxide spinels [7] and basic oxide clusters both being shown to achieve > 80% BHET yields [8]. Yun et al. [9] developed a magnetic catalyst by integrating ZnO with Fe_3O_4, which was capable of achieving a very high BHET yield of 92.3%, as well as being easily separated using an external magnetic field and reused. These results from these novel catalysts indicate the importance, especially in industry, of producing catalysts which are capable of being easily separated and subsequently reused. Despite these advancements, such catalysts are at present expensive to produce and contain metal elements which may harm the environment.

2.1.3 Organocatalysts

Organocatalysts have emerged as attractive alternatives to traditional metal-based catalysts due to their overall more environmentally friendly profile, thanks to the avoidance of toxic heavy metals. Numerous organocatalysts have been successfully trialled for the glycolysis process, producing competitive BHET yields greater than 80% [10–12]. Compared to metal-based catalysts however, they suffer

from various effects which hinder their scalability, such as high loading rates and low thermal stability [10]. Work by Jehanno et al. [13] aimed to improve the thermal stability of organocatalysts, by designing a protic ionic salt made up of 1,5,7-triazabicyclo[4.4.0]dec-5-ene and methane sulfonic acid (TBD:MSA), capable of withstanding temperatures greater than 400 °C and recycled for use up to 5 times. The work provided a major breakthrough in the state of the art, as BHET yields of > 90% were achieved, while evidencing the reusability and stability. However, issues preventing industrial application still remain, such as the high cost of organic bases (like TBD) and the difficulty in fully separating the homogeneous catalysts from product mixtures [14]. This work, despite highlighting the promise of green homogeneous catalysts in PET glycolysis, also emphasises the myriad of properties essential to future catalyst design, such as stability, separability, activity and cost.

Organic deep eutectic solvents (DESs) represent a promising catalytic technology with attractive properties including low volatility and high tuneability, at significantly lower cost [15]. Composed of readily-available, biodegradable compounds, DESs are generally more environmentally friendly and easier to synthesise than alternative catalysts. To date, there has been limited research carried out on DES-catalysed PET glycolysis, however, some early results suggest promise. Urea-based DESs are among the most studied of the type, with variations producing BHET yields of 78.7% and 82%, respectively [16,17]. Whilst these and other DESs have shown comparable catalytic activity in PET depolymerisation, their thermal stability and recyclability may still lag behind other catalyst systems. Nevertheless, their greener profile and economic viability make them attractive candidates for sustainable plastic recycling in the future. However, their use in PET glycolysis

remains in its relative infancy, with further work needed to optimise performance and understand long-term scalability.

2.1.4 Ionic liquids

Ionic liquids (ILs) have for many years been identified as promising catalysts for PET glycolysis, since Wang et al. [18] used 1-butyl-3-methylimidazolium chloride ([Bmim]Cl) as a solvent to dissolve PET in 2009. ILs are generally described as salts consisting exclusively of ions that are liquids at low temperatures, typically below 100 °C [19]. Although the physical properties of ILs vary significantly with the choice of ions, several characteristics are commonly shared across most types. They include thermal stability, nonflammability, nonvolatility, nontoxicity, and immiscibility with numerous organic solvents [20]. It is these properties in particular which eliminate the numerous safety issues commonly associated with many organic solvents. Due to their tuneable properties, these catalysts have been demonstrated to be effective, environmentally friendly, and financially viable. However, the challenge remains that these three vital attributes rarely coexist simultaneously.

Metal-containing ILs are shown to effectively catalyse the reaction, enhancing BHET yields and PET conversion, whilst reducing reaction time. A major breakthrough in the study of IL catalysis was made by Wang et al. [21], who tested several transition metal-containing ILs including $[bmim]_2[CoCl_4]$ and $[bmim]_2[ZnCl_4]$, and found that the Co-based IL achieved a PET conversion, BHET selectivity and BHET mass fraction of 100%, 81.1% and 95.7%, respectively. This compares favourably to other metal ILs, such as $[bmim][FeCl_4]$ and $[bmim]_2[NiCl_4]$, which achieved PET conversions of 94.7% and 45%, respectively. The product mixture was separated with ease and the catalysts were reused 6 times without any

decrease in catalytic activity. More recent publications have seen the activity associated with metal ILs increase even further. A combined protic IL/metal salt (PIL-$Zn(OAc)_2$) catalyst was synthesised and used to produce a BHET yield of 91.25% [22], while also showing capability of reuse for over 8 cycles, with only a modest decrease in yield. The catalyst was biphasic as it was homogeneous at the reaction temperature and heterogeneous when cooled, allowing for excellent molecular interaction with reactants and ease of separation. Combining the enhanced molecular contact with reactants while retaining facile separability has been identified as a key feature for future catalyst design. Several organometallic ILs such as $[C_6TMG]Cl/2ZnCl_2$ [23], $[HO_3S\text{-}(CH_2)_4\text{-}mim]Cl\text{-}FeCl_3$ [24] and poly ($[BVMIM]Zn_mCl_n$) [25] have achieved exceptional BHET yields of over 90%, exemplifying the effective catalysis associated with metallic ILs. A comprehensive review of IL-catalysed PET glycolysis by Kumar et al. [26], determined that of the 25 best-performing ILs, 72% were heavy metal-containing, showing their prevalence in the current state of the art.

While the activity and reusability of metal-containing ILs catalysts mentioned above show promise for scalability, there remains some major drawbacks. Firstly, large-scale production of metal ILs requires large amounts of raw materials which are not readily obtainable from renewable sources [26]. Additionally, the leaching of transition metals into secondary reaction mixtures is well-documented, requiring costly extraction methods such as ion-exchange and membrane separation [27]. Therefore, while the activity and reusability of the metal ILs is impressive, more work needs to be done to make the process more cost-effective and environmentally friendly.

Although non-metal ILs lack toxic heavy metals, it is misleading to suggest that they are inherently less toxic. Using EC_{50} values, an indicator of toxicity, the $[C_8mim]Cl$ IL was found to be significantly more toxic than methanol, itself considered to be a toxic solvent [26]. Generally, the observation of longer alkyl chains attached to the IL cation leads to an increase in toxicity [28]. These findings emphasise that non-metal does not necessarily correlate to non-toxic and it has been observed that commonly investigated cations such as those based on imidazolium, phosphonium, ammonium, pyridinium and quinolinium have high toxicity compared to other ILs [29]. In order to reduce the toxicity of the ILs, there are a number of solutions. Increasing the polarity of the alkyl chains through introduction of certain functional groups has been seen to improve the EC_{50} by an order of magnitude or more [30]. Additionally, ILs composed of bio-derived ions such as choline cations have been determined to be substantially less toxic than the commonly used bmim cation [31]. Overall, the toxicity of the anion in organic ILs is considered secondary to that of the cation, however it is noted that their broader diversity does not allow for comprehensive analysis [28]. Generally, organic ILs produce lower BHET yields than metal-based ILs due to their reduced catalytic activity. Therefore, IL catalyst design must carefully balance the reduction of toxicity, while maintaining high catalytic effectiveness.

As an alternative to relatively toxic imidazolium-based and expensive metal-based ILs, Liu et al. [32] proposed the use of a biocompatible choline acetate ([Ch][OAc]) IL for use in PET glycolysis, achieving a high yield of 85.2%, as well as testing other carboxylate-based anions such as formate (For). Other studies using the same catalyst observed yields between 64-66% [33,34]. Choline as a cation is

commonly used in deep eutectic solvents (DESs) and has been shown to promote PET depolymerisation, whilst the acetate anion is often used as a counter ion to imidazolium-based cations for the same process. Economically, choline-based ILs (£315/kg) cost roughly one third the cost per kilogram, compared to imidazolium-based ones (£916/kg) and this price is further offset through the improved longevity brought on by the BC support [35]. Although effective, non-toxic and cheap to produce, the reusability of these organic ILs is unclear. This is largely a consequence of the fact that using dissolved homogeneous ILs as glycolysis catalysts often leads to difficult separation processes. Reusability is a key pillar of catalyst design due to its associated cost saving implications, therefore any bio-based ILs being synthesised for potential commercialisation must consider this factor.

The use of a catalyst support to immobilise ILs helps to negate one of their main deficiencies, product mixture separation [36]. Anchoring of ILs on such supports can be achieved through chemical or physical adsorption, known as supported ionic liquid-like phase (SILLP) and supported ionic liquid phase (SILP), respectively [37]. Generally, the adsorption energy for physisorption is less than 80 kJ/mol, indicative of weak forces such as van der Waals (vdW), while for chemisorption it ranges between 80 – 240 kJ/mol due to covalent bonding [38,39]. Only small amounts of IL are needed to coat the surface of the material, so the cost of production is greatly reduced when compared to bulk IL systems. The physisorption method of immobilisation is a simple process, requiring only the mixing of an IL solution with the catalyst support before filtration, washing and drying is carried out [40]. Strong H-bonding between the ILs and the support's surface functional groups (usually -OH groups) are the most significant interactions, however vdW and electrostatic interactions, as well as π-π-

stacking in the case of commonly used aromatic cations, also help to bind the ILs [41]. The main disadvantage of SILP catalysts is the potential for leaching or detachment of the IL, due to insufficient strength of the interactions between the catalyst and its support. The use of SILLP catalysts chemically adsorbed to the catalyst support avoids this problem, as the IL is covalently bonded to the material. Typically, the IL is bonded to the surface *via* the Lewis acid cation, which can be grafted using an existing IL. Alternatively, a precursor can be anchored and subsequently subjected to quaternisation, in order to build the IL structure directly on the catalyst support.

As well as their difficult separation, IL's hygroscopicity creates a tendency to absorb moisture which can cause significant alterations in their catalytic properties and therefore their effectiveness [42]. Wang et al.'s exploration of [bmim]Cl for use in PET glycolysis found that anionic interactions with water molecules could significantly decrease the conversion of PET and selectivity of BHET, by 40% and 10%, respectively, suggesting that chain scission rather than product formation is the process most inhibited by water [43]. In addition to interference, extraneous H_2O present in the reaction mixture is capable of hydrolysing BHET to mono(2-hydroxyethyl) terephthalic acid (MHET), thus reducing the monomer yield [14,44]. The potential sources of moisture in waste PET are numerous and must be mitigated to prevent adverse effects on the process. Firstly, post-consumer PET waste, particularly derived from food and drink packaging, is initially very high in moisture content and requires energy-intensive drying processes for it to be removed to an adequate level [45]. Even laboratory standard PET pellets are capable of absorbing 0.3-0.7 wt% water under ambient conditions [46]. The presence of water may also inhibit the crystallisation of the final product by increasing the solubility [47,48]. In

addition to potentially highly hygroscopic catalysts, the solvent being used, EG, is highly hygroscopic and therefore must be distilled to as pure a concentration as possible. Therefore, lab-scale studies should make use of Schlenk lines and gloveboxes where possible.

The progress in IL technology for PET glycolysis has been substantial, with many organo- and organometallic variations achieving very high BHET yields. However, limitations to their use beyond the research setting remain. As this section has demonstrated, the ease of separation, expense, and toxicity of the catalysts is still, in many cases, incompatible with scalability. Future catalyst design must view these factors as essential properties in order to enhance the suitability of IL catalysts for industrial use.

2.1.5 Metal catalysts supported by highly porous materials

Catalyst supports offer several advantages in catalytic systems, including improved thermal and chemical stability, enhanced dispersion of active species, and facilitated catalyst recovery and reuse. The large pore volume and high surface area of supports such as zeolites allows them to act effectively due to the large number of active sites present on their surface and within their pores [49]. This, combined with the material's own catalytic capabilities, allows for a synergistic effect of both support and catalysis. In addition to zeolites, similarly structured materials such as activated carbon [50], graphite [51] and graphene oxide [52] have also been used.

Various high surface area catalyst supports have been used effectively for PET glycolysis, as summarised by

Table 2.1. In each of the cases featured, it was found that the degradation reaction was significantly enhanced by the large surface area provided by the catalyst

support. This was explicitly shown in a study by Imran et al. [53], where both silica nanoparticles and microparticles were compared as supports for the dispersion of various metal oxides. The results produced a BHET yield of > 90%, with the optimal value being found when Mn_3O_4 was dispersed across the surface of the silica nanoparticles rather than the microparticles. Therefore, the result was attributed to the increased surface area and pore volume of the nanoparticles compared to the microparticles and the numerous active sites present.

Table 2.1. *Supported metal catalyst performance for PET glycolysis.*

	Catalyst	Temp. (°C)	Pressure (MPa)	Time (min)	BHET Yield (%)	No. times recycled	Ref.
1	Fe_3O_4-boosted MWCNT	190	0.101	120	100	8	[54]
2	MnO_2@HGO	200	-	10	100	5	[55]
3	rGO\[TESPMI]$_2CoCl_4$	190	0.101	180	95.2	5	[56]
4	ZnO/SBA-15	197	-	60	95.2	6	[57]
5	γ-Fe_2O_3/N-doped graphene	300	-	60	90	10	[58]

A number of causes are proposed for the remarkably high BHET yields shown in

Table 2.1. When Fe_3O_4-boosted multi-walled carbon nanotubes (MWCNT) are used, there is a synergistic effect exerted by both catalyst and support. Upon dispersion of MWCNT in EG, the solvent molecules undergo a conformational change caused by H-bonding with the CNT walls. These interactions increase the polarity of the EG molecules, allowing them to interact strongly with adjacent EGs, seemingly acting as a catalyst themselves by enhancing the partial negative charge on the hydroxyl group of oxygen. Simultaneously, the metal cations of magnetite play a more

traditional role by protonating the carbonyl oxygen of PET [54]. The use of a Co-based IL grafted on graphene as a heterogeneous catalyst led to a degradation mechanism in three-parts, in addition to the traditionally-described PET-cation, EG-anion interactions: 1) Similar to Fe_3O_4-boosted MWCNT, the support activates EG molecules *via* H-bonding, 2) strong π-π interactions adsorb and stabilise the PET molecule to graphene *via* the aromatic rings, and 3) inadvertent nitrogen doping of graphene during the synthesis process may enhance the catalyst somewhat [59]. The most remarkable result, a 100% BHET yield in just 10 minutes, was achieved using 2D holey MnO_2/graphene oxide (GO) nanosheets [60]. The study attributes the excellent kinetics to the abundant nanopores present, enabling uniform deposition of MnO_2 on its surface, providing easy access to the active sites for PET and EG.

In addition to mechanistic influence on reactants and the uniform dispersion of catalysts, supports can also play a role in altering the electronic structure of the catalysts. A density functional theory (DFT) study of IL adsorption onto GO concluded that the stronger IL-GO interactions led to increased reactivity of the ILs [61]. This was evidenced by a reduction in the energy gap between the highest occupied molecular orbital (HOMO) and lowest unoccupied molecular orbital (LUMO), suggesting a potential facilitation of charge transfer between ILs and the reactants. This finding is supported by similar work adsorbing ILs onto coronene fluorographene [62]. Notable for many of the aforementioned glycolysis catalysts, is their reusability. Due to their heterogeneous nature, separation processes are much simpler than with more commonly studied homogeneous ILs This recyclability improves the cost-effectiveness of the process and its potential scalability. Despite this, the supported

catalysts all contain transition-state metals, which may suffer from the leaching and toxicity issues described in **Section 2.1.1**.

Overall, it is clear from the results that the use of high surface area catalyst supports is a distinctively promising technology for the catalysis of PET glycolysis. The synergistic effects of both the catalyst and the support it is dispersed across, allow for extremely effective degradation of PET, and produce very high BHET yields. At the same time, the heterogeneous nature of these catalysts allows for their easy separation and reuse. By combining porous, high surface area catalyst supports with green catalysts dispersed across the surface, there is the potential for highly efficient and environmentally friendly catalysed PET glycolysis reactions.

2.2 PET glycolysis reaction mechanisms

A thorough comprehension of the reaction mechanism is essential for designing an efficient PET degradation process. It provides clarity for understanding the conditions and involved chemicals, resulting in more informed decision making. The general reaction mechanism of PET glycolysis is well-established. The nucleophilic hydroxyl group of EG attacks the carbonyl ester of PET *via* its lone electrons, resulting in chain cleavage and modification of the ester group. This sequence recurs until the polymer chain is completely fragmented, producing the final monomer products [63].

2.2.1 Lewis acid reaction mechanism

Although the intrinsic reaction mechanism remains the same, the use of a transesterification catalyst can significantly improve the efficiency of the process. This includes traditional catalysts such as zinc acetate [64], more novel technologies like metal oxide spinels [65] and easily recoverable superparamagnetic γ-Fe_2O_3

nanoparticles [58]. Once introduced into the system, interaction between the catalyst's Lewis acid site and the PET carbonyl oxygen act to create a highly positive charge on the ester carbon of the polymer, thus facilitating the subsequent nucleophilic attack. This general mechanism of PET glycolysis catalysed by a Lewis acid is shown in **Figure 2.1**.

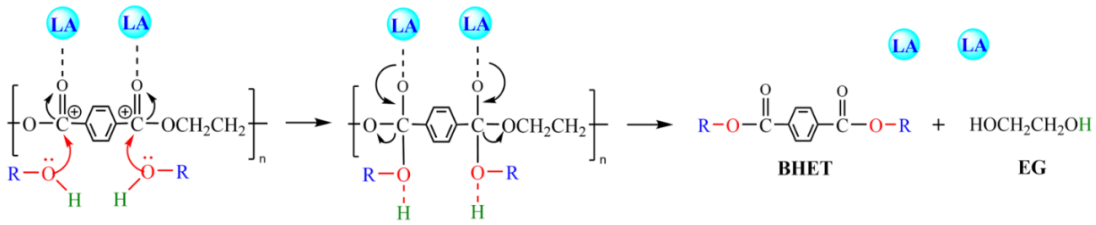

Figure 2.1. *Lewis acid reaction mechanism of catalysed PET glycolysis [63].*

The catalysts most commonly associated with the Lewis acid reaction mechanism are metal-based ones. The introduction of metal-centred catalysts can significantly enhance the degradation process due to their ability to coordinate with the ester functionalities of PET, reducing the electron density of the carbon atom to a greater degree than intermolecular interactions could alone [66].

The ligands corresponding to the metal centres can also play an important role. Their presence can impact reaction selectivity, catalyst solubility and longevity by mitigating deactivation pathways [67,68]. For instance, hard metals like magnesium tend to bind strongly with oxygen-based anions like acetate, which may suppress catalytic activity. In contrast, soft metals such as zinc demonstrate enhanced activity when coordinated with oxygen-based anions when compared with halide ligands [69].

2.2.2 Synergistic mechanism

As catalytic technologies have evolved, significant efforts have been directed toward enhancing the efficiency of PET degradation. One such advancement involves the design of catalysts that exhibit a synergistic catalytic effect. These include, but are

not limited to, deep eutectic solvents (DESs), polyoxometallates (POMs) and organometallic complexes [70–72]. While this mechanism shares similarities with the Lewis acid pathway illustrated in **Figure 2.1**, it relies more prominently on additional hydrogen bonding interactions between a nucleophile and a separate catalytic moiety, in addition to the Lewis acid interactions [73–75]. The term "synergistic" refers to the cooperative interaction between two distinct moieties, typically the cation and anion, functioning as a Lewis acid and base, respectively, to facilitate PET depolymerisation.

In the typical reaction mechanism, H-bonding between the anion of the catalyst and the reacting hydroxyl group of EG occurs. These interactions act to increase the polarity of the OH group, thus enhancing the nucleophilic attack ability. Simultaneously, the positively charged cation will engage with the PET carbonyl oxygen either covalently or non-covalently, protonating the ester carbon of PET. As a result, the nucleophilic hydroxyl group attacks the activated carbonyl carbon, leading to the cleavage of both the hydroxyl and ester bonds. A new C-O bond is then established between the hydroxyl oxygen and the PET carbonyl carbon, while the displaced hydrogen binds to another oxygen atom within the PET chain. This catalytic cycle continues iteratively, promoting the progressive breakdown of PET into oligomers, and ultimately yielding the desired monomeric products [63]. The overall synergistic Lewis acid-base mechanism is illustrated in **Figure 2.2**.

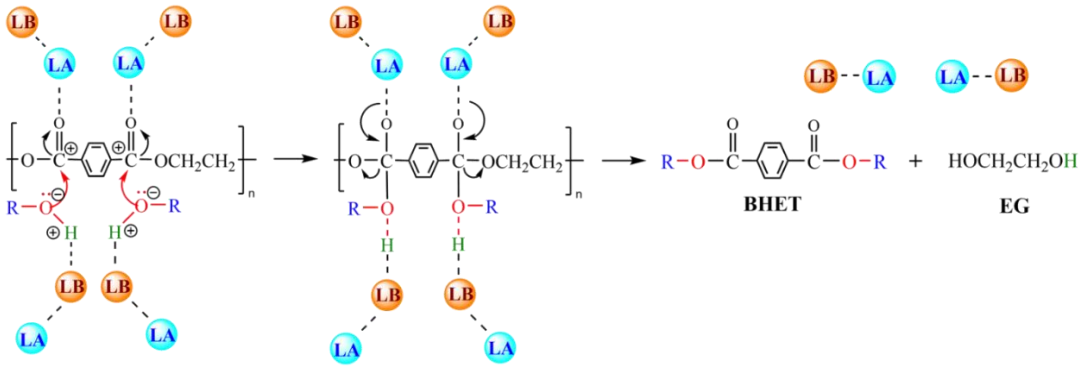

Figure 2.2. *Synergistic reaction mechanism of catalysed PET glycolysis [63].*

Catalysts that facilitate the synergistic catalytic effect are highly encouraged for PET glycolysis. The synergistic effect has been reported in PET glycolysis processes catalysed by various types of ILs, including metal acetate ILs [73,74], halometallate ILs [75–77] and non-metal ILs [78]. The observation arises through the co-catalysis caused by both cations and anions within ILs interacting with EG and PET, respectively. The presence of metal atom centres is an important factor in catalytic effectiveness, due to their coordination ability. Through this aspect, the catalysts can significantly facilitate PET degradation *via* bonds formed with the PET carbonyl oxygen. Conversely, organic ILs are limited to the formation of non-bonding complexes with PET. A critical consideration in the design of Lewis acid-base catalysts is achieving an optimal interaction strength between the two moieties. Excessively strong interactions can limit the availability of free acid or base sites needed to drive PET degradation, whereas overly weak interactions may compromise the catalyst's stability, increasing the risk of decomposition under reaction conditions [69,79]. It is well noted in existing literature reviews that many studies attribute their high performance to the synergistic effect created by the catalysts [80]. The near-ubiquitous IL-catalysed PET glycolysis reaction mechanism is shown in **Figure 2.3**.

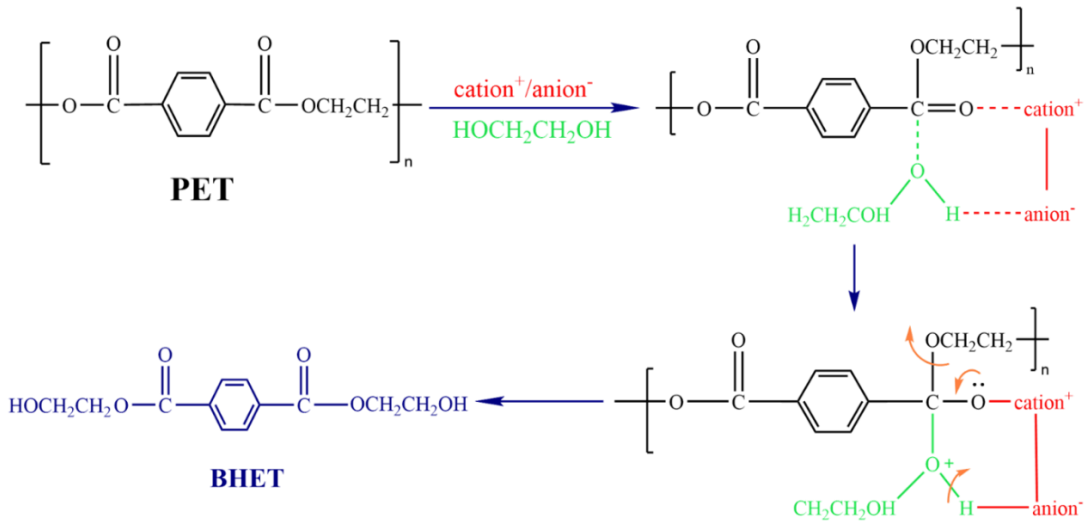

Figure 2.3. *General IL-catalysed PET glycolysis reaction mechanism [63].*

The combination of metal anion with organic cation is interesting from a mechanistic perspective. Wang et al. studied the use of [TMG]Cl/$ZnCl_2$ IL as a catalyst, applying DFT methods to explore the catalytic degradation process [23]. Their findings showed a reverse of the traditionally-established mechanism. In this case, the Zn metal centre of the anion acted "cationically", protonating the PET ester carbon *via* coordination with the carbonyl oxygen, while the organic guanidine-based cation interacted with the EG molecule *via* H-bonding. It should be noted that instead of testing full reaction complexes, their study focused only on isolated ion-reactant interactions. Therefore, the influence of steric hindrance may be limited, and thus influences how results should be interpreted.

Most DFT studies of IL catalysis for PET glycolysis relate to the intermolecular interactions on isolated systems, which are not necessarily reflective of the real reaction. To date, few papers have conducted deeper studies of the full system, including transition state theory to determine how these intermolecular interactions actually influence the energy barrier [81–83].

While the majority of DFT studies have described the conventional synergistic mechanism, some have introduced interesting variations. In a theoretical and experimental study of [bmim]OAc for PET glycolysis, Zhang et al. found that lone pair (LP) – π* (pi- anti-bonding) interactions between the carbonyl group of the acetate anion and the PET carbonyl were present, in addition to the more commonly described anion-EG H-bonding [84]. Work by Bura et al., [34] explored the use of biocompatible cholinic ILs through DFT, found that the mechanistic role of the choline cation was limited. Instead, they found that stabilisation of the PET carbonyl group could be conducted by EG molecules within the system, meaning that the replacement of the amino cation with a phosphonium-based one may be more effective. A similar lack of catalytic contribution by a choline cation was observed by Nosir et al. [85] through the use of molecular dynamics (MD) modelling. This contradicts the DFT results using the same choline-based ILs, found by Liu et al., which follows the more general catalytic mechanism [32]. These results serve as evidence that the IL-catalysed PET glycolysis reaction mechanisms are case-specific and cannot be easily described by an off-the-shelf catalytic mechanism, and that DFT modelling has been proven to be a valuable tool to elucidate these specific interactions.

2.3 Microwave heating

MW heating is rapidly emerging as an efficient tool in scientific processes, offering rapid and specific non-contact heating of materials. Through the dielectric and magnetic heating mechanisms, it offers reduced reaction times and lower energy consumption when compared with conventional heating methods. To date, MWs have been utilised in various processes including organic synthesis [86], pyrolysis [87],

polymerisation [88], among others. By utilising MW heating as the primary energy source, energy and cost efficiency of PET glycolysis can be improved.

2.3.1 Application of microwave heating in chemical engineering

MW-assisted heating, also known as dielectric heating, operates through two main mechanisms shown in **Figure 2.4**: 1) dipolar polarisation, where a dipole is subjected to an electric field and will attempt to align itself *via* repeated rotations, and 2) ionic conduction, where mobile charge carriers (such as free electrons and ions) will move back and forth within the material being subjected to the electric field. Initially, oppositely charged particles will move against each other to align with or against the electric field. However, at the high frequencies of MW irradiation, dipoles and charge carriers cannot fully follow the rapidly reversing field, resulting in a phase lag between field and molecular response. The repeated oscillations and subsequent collisions between molecules produce thermal energy resulting in the rapid volumetric heating associated with the technology [89]. Non-magnetic materials are only affected by these electric field-induced mechanisms, however, there is also a magnetic material-specific mechanism, where the magnetic field affects the spin of magnetic materials [90]. Unlike the electric field mechanisms, the motion of free electrons in this magnetic process is unaffected. Instead, heat energy is generated by the influence of the magnetic field on the electron spin, domain wall and orientation of domains within the material. As well as conduction losses, magnetic elements such as iron, nickel and cobalt will exhibit additional magnetic losses through hysteresis, eddy current, domain wall resonance and electron spin resonance [91]. Therefore, the combination of magnetic heating elements with permanent dipolar compounds is an attractive prospect for catalyst design to support efficient MW heating.

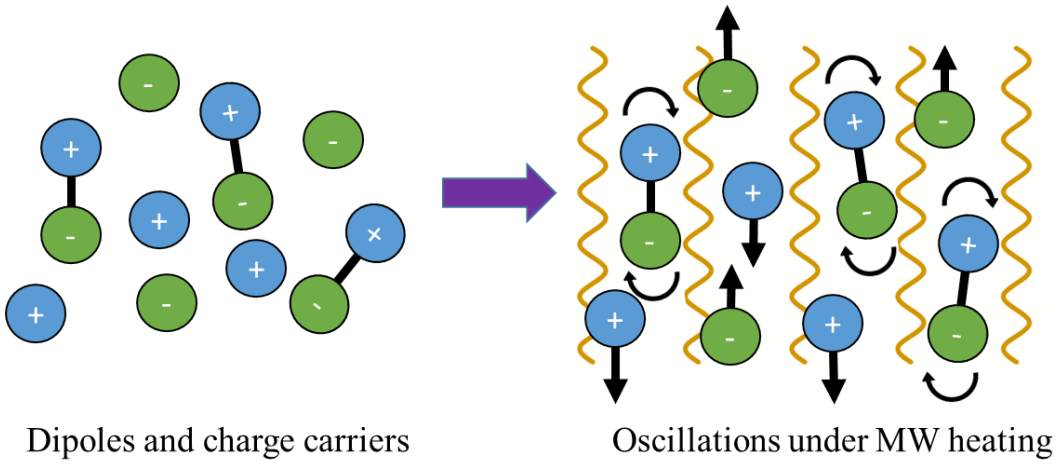

Figure 2.4. *Dielectric heating of molecules during microwave heating.*

The ability of a substance to convert the electromagnetic energy provided by the microwaves into heat is determined by the loss factor tanδ, which quantifies energy dissipation resulting from the lag between the applied field and the molecule's realignment. A substance with a high loss factor can absorb MWs extremely effectively to result in rapid heating. Using this information, catalysts and reagents can be selected specifically for their ability to absorb microwaves and improve the kinetics of the reaction.

2.3.2 Microwave-assisted PET glycolysis

MW-assisted glycolysis of PET has been explored as a more energy-efficient method compared to the conventionally-heated process. Conveniently for the glycolysis process, EG has an extremely high loss factor, owing to its polarity, compared to other solvents, meaning its use as a reagent in the microwave-assisted process is very effective. **Table 2.2** shows the loss factors of various commonly used chemical recycling solvents (EG, methanol and water).

Table 2.2. *Loss factors of common solvents used for PET chemical recycling [92].*

Solvent	tanδ
Ethylene glycol	1.350
Methanol	0.659
Water	0.123

MW heating has been employed successfully for PET glycolysis, using a number of varying organic and inorganic catalysts. Most commonly, zinc-based catalysts have been utilised, invariably concluding that MW heating reduced the reaction time significantly, with full conversion often being completed within 30 minutes [93–95]. Contrastingly, the conventionally-heated process often lasts up to 4 hours. Through the use of economic and environmental modelling, Luo et al. [96] evaluated the performance of an easily-separated heterogeneous ZnO catalyst for MW-assisted PET glycolysis. Following a life cycle assessment (LCA), it was found that BHET production through this approach significantly outperformed the traditional DMT-based process by a number of green metrics. The global warming potential (kg CO_2 eq/kg BHET) was reduced by a factor of ~7 due to the more energy-efficient heating associated with MW irradiation, as well as potential decarbonisation of the electricity grid. The chemical recycling process also qualitatively outperformed the petroleum-based one in a number of other categories including fossil fuel depletion, ecotoxicity and respiratory effects. Overall, the findings indicate that the energy-efficiency of MW heating, combined with the inherent carbon savings of using PET waste as a feedstock, offer a markedly lower environmental and economic footprint.

Whilst a number of catalysts have been tested, ILs, in particular, show great promise for use in microwave-assisted PET glycolysis due to their ability to heat at rates easily exceeding 10 °C s^{-1} without any significant pressure build-up. Such an

efficient interaction with microwave heating reduces the safety issues arising from over-pressurisation of heated closed-vessel reactions [97]. Indeed, ILs have commonly been used as "doping agents" for many microwave-assisted reactions. It has been found that the addition of just 0.1 mmol L^{-1} solvent is sufficient to obtain significant changes in the heating profile of a reaction medium [98]. As expected, ILs interact with microwaves predominantly *via* the ionic conduction mechanism, however if polar cations and/or magnetic moieties are introduced, they can also interact *via* the dipolar polarisation or magnetic heating mechanisms. Thus, the tuneability of ILs is a great advantage for microwave-assisted reactions.

Due to their exemplary MW-heating performance, IL-catalysed, MW-assisted PET glycolysis is a well-researched technology. A study by Scé et al. [99] found that the use of halometallate-based ILs under microwave heating not only significantly reduced the reaction time, but also increased the BHET yield from 74% to 77%, when compared with conventional heating. However, given the small magnitude of this difference, it is unlikely to represent a genuine enhancement attributable solely to microwave heating, and may instead fall within the experimental uncertainty of the process. They concluded that the reason for this was that the polar anion within the IL induced a faster heating rate due to its ability to heat through both dielectric heating mechanisms, whilst the traditional catalyst was a non-polar material. The improvement of not only reaction time but also product yield is a feature that has been noted before in other microwave-assisted chemical reactions. Shah et al. [100] found that, while synthesising benzotriazole derivatives under microwave irradiation, the product yield in every case was higher when microwave heating was chosen over conventional heating, with the maximal increase being as high as 23%.

It is notable that the majority of catalysts successfully used for MW-assisted PET glycolysis contain metal elements such as Zn, Fe and Co; understandably so, considering their enhanced MW absorbance. In addition to their suitability to MW heating, the reduced reaction times provide a method of offsetting the high cost of synthesis by reducing the process costs. However, these catalysts, although effective, will also suffer from the same shortcomings described in **Section 2.1** related to metal leaching and toxicity. As such, cheaper and more environmentally friendly alternatives, which are still capable of efficient MW-heating, are an exciting prospect. Choline-based materials have been utilised effectively for other MW-assisted chemical processes such as 5-hydroxymethylfurfural production and biomass pre-treatment [101,102]. Additionally, Casey et al. [103] conducted MW-assisted PET glycolysis using a metal-free SiO_2-supported guanidine-based heterogeneous catalyst, achieving a high BHET yield of ~80% after 30 minutes. Interestingly, the study found that the process was significantly more efficient when a carbon-based support was utilised instead of SiO_2, due to the enhanced MW absorbance. These publications open the door for the future use of organic, choline-based ILs in MW-assisted PET glycolysis, as a method of enhancing both the energy efficiency and effectiveness of the process at an industrial scale.

2.4 Biochar as catalyst support

BC is a carbonaceous material which is formed from the thermochemical degradation of cellulosic biomass. It is notably inexpensive, environmentally friendly and easily-produced compared to other carbon allotropes [104]. Owing to its high surface area, high porosity, functional groups and stability, BC is seen as a useful material for a number of catalytic processes. Consequently, it stands out for its

potential for use as an alternative to highly expensive catalyst supports for PET glycolysis, summarised in **Section 2.1.5.**

2.4.1 Application of biochar in catalysis

In preparation for catalysis, BC usually undergoes activation, which significantly increases its surface area, porosity and alters surface functional groups [105]. Physical activation typically involves thermal treatment with activating agents like CO_2, steam, air, or CO_2/N_2 mixtures [105]. In contrast, chemical activation uses agents such as acids (e.g., H_3PO_4), alkalis (e.g., KOH), and metal salts (e.g., $ZnCl_2$) under an inert atmosphere. It is generally more cost-effective, offering shorter reaction times, lower temperatures, higher yields, and greater surface area and porosity [106]. Notably, KOH enhances both porosity and the abundance of oxygen-containing functional groups, which are beneficial for adsorption applications [107].

Due to its excellent adsorptive properties, activated BC has been identified as a promising catalyst and/or catalyst support in various chemical processes. It has been used in a wide range of processes such as biodiesel production, microbial catalysis and NO_x reduction [108]. Waste-derived BC has several advantages over other porous carbon allotropes used for catalysis including its low cost, abundance, and contribution towards a circular economy [109]. Activated BC has also been utilised as a catalyst support for the methanation of syngas [110], in which rice husk-based BC was activated by KOH before having a ruthenium (Ru) catalyst grafted onto its surface. The results showed that the Ru catalyst adsorbed onto activated BC produced 10% higher CH_4 selectivity, at 95% confidence, than the case using the more expensively produced activated carbon support. This was attributed to the mixture of meso- and micropores on the surface of activated BC, due to its larger surface area and pore

volume. This allows for larger Ru particles to be dispersed across the surface and within the pores, subsequently leading to more catalyst-reactant interactions. Similarly, using a Ni-based catalyst and KOH-activated BC as a support, Villardon et al. [111] successfully hydrogenated CO_2 into methane, achieving a CO_2 conversion of 72.5% and a CH_4 selectivity of 95.4%. The enhanced results were once again explained by uniform dispersion of Ni allowing for improved accessibility to reactants. However, they also found that the abundant basic sites on the BC surface could also behave catalytically, thus creating a synergistic contribution to the catalytic mechanism.

In a similar study of CO_2 methanation, Renda et al. [112] did not observe evidence of this bi-functional role being played by BC, with its only mechanistic contribution appearing in the form of catalyst adsorption and dispersion. While the BC samples were derived from different feedstocks, the key difference in its properties lies in the activation method. In the former case, chemical activation was carried out using KOH, while the latter support was only physically activated using CO_2. This difference affects the presence of basic functional groups on the BC surface, capable themselves of activating reactants. The results show the importance of the BC support preparation process, which should be designed with specific processes in mind.

In addition to metal-based catalysts, greener alternatives have also been grafted onto activated BC catalyst supports. Sulfonated BC, produced when the BC surface is treated with sulfuric acid or other sulfonating agents, can be used as an organic and highly acidic catalyst for processes such as cellulose hydrolysis and biodiesel synthesis [113,114]. Following sulfonation, the BC is capable of further adsorbing catalytic species, including ILs. Work by Zhang et al. [115] used chlorozincate IL-functionalised sulfonated BC as a catalyst/support for cellulose hydrolysis under MW

irradiation, finding that the BC support played a synergistic mechanistic role. These results emphasise the potential for BC to be used as a support for immobilised IL catalysts. Despite this, the catalyst still suffered from a familiar problem of metal element leaching with repeated runs, indicating a familiar issue with metal-based catalysts.

2.4.2 Potential for use of biochar in PET glycolysis

The use of BC-based catalysts for plastic waste conversion has been reviewed by Li et al. [116], however the majority of studies focused on pyrolysis and photocatalytic processes. To date, and to the best of the author's knowledge, there have been few studies of PET glycolysis using BC-based catalysts/catalyst supports. Calcined ostrich egg samples were used as direct sources of CaO for the catalysis of PET glycolysis by Yunita et al., achieving a BHET yield of 76% [117]. A study by Laldinpuii et al. used bamboo leaf ash, a form of BC, as a direct catalyst for PET glycolysis [118]. Observing a BHET yield of 83%, they proposed that due to the lack of any other catalyst, the BC surface must be playing some catalytic role, namely through EG activation by the anionic active sites on its surface, occurring through oxidation of residual Ca, K, Mg, Mn and Fe elements. Similarly, BC derived from orange peels has been used as a heterogeneous catalyst for PET glycolysis [119]. As with, the previous example, a BHET yield of 79% was attributed to the presence of basic groups derived from potassium and calcium oxides on the BC surface. These studies, using BC as an isolated glycolysis catalyst, highlight the potential for a synergistic catalytic effect if functionalised by effective catalysts, such as ILs. A similar effect was observed with the use of other carbon allotropes, as outlined in **Section 2.1.5**.

2.5 Research gap and novelty

In summary of **Section 2.1**, ILs represent a promising catalyst for PET glycolysis due to their thermal stability and tuneable properties. Metal-based ILs, particularly those containing cobalt or zinc, have shown strong catalytic performance, but they suffer from toxicity and high costs, relative to other ILs, as well as the potential for leaching of active metals. In contrast, organic ILs, especially those based on choline, are non-toxic, biodegradable and inexpensive, yet they tend to be less catalytically active and are rarely reported as reusable. The following gaps in the research have been identified as areas for study in this endeavour:

1) **Systematic comparison on the performance of different ILs is lacking.**

The majority of studies are limited to a family of ILs, such as imidazolium-based, choline-based and metal-based. While valuable insights have been gathered, the lack of direct comparison between these groups can somewhat narrow the outlook of the work. By combining theoretical and experimental methods, the three groups can be systematically compared to evaluate their differences in performance.

2) **Traditional "off-the-shelf" mechanism is not universally applicable to IL-catalysed PET glycolysis systems.**

Mechanistic studies of IL-catalysed PET glycolysis usually describe the general, standardised reaction mechanism. However, some deeper DFT-based approaches have uncovered discrepancies in the established mechanism, suggesting the "off-the-shelf" approach may not be valid for all systems. Despite this, the general description still dominates the literature, suggesting more work must be done to critically challenge the established assumptions. Deep theoretical investigation is therefore required to elucidate the reaction mechanism further, in order to provide

bespoke catalytic mechanisms which can help inform future catalyst and process design.

3) An efficient, low-cost and sustainable approach to PET glycolysis is lacking

The potential for the industrialisation of successful PET glycolysis processes can be broadly judged on three categories: efficiency, cost and sustainability. While several IL-catalysed methods have displayed effectiveness in one or two of those groups, rarely are all three conditions satisfied. Therefore, future processes should be designed with these factors in mind.

Moisture is known to hinder the IL-catalysed PET glycolysis process, however systematic evaluation of the effects is lacking, despite its relevance in the context of real-world plastic waste. MW heating has been identified as an effective strategy to enable rapid, energy-efficient PET depolymerisation, and has the potential to enhance BHET yields. Most studies to date have utilised the excellent MW absorbance of metal-based ILs, while cheaper, more sustainable ILs such as those based on choline are yet to be investigated. Additionally, a common disadvantage shared by both metal and non-metal ILs is the unclear reusability, due to their homogeneous nature. Immobilisation atop carbon-based materials such as MWCNT and graphene have been shown to significantly improve BHET yields and ease of separation. This creates an opportunity to explore waste-derived BC as a novel alternative. BC is low-cost, renewable and rich in surface functional groups, offering high surface area and tuneable porosity that could enhance IL dispersion and reactivity. In combination with sustainable ILs, BC could enhance the effectiveness and reusability, while retaining the green credentials of the immobilised IL. Despite its promise, BC-based catalytic systems remain relatively unexplored, particularly with regards to PET glycolysis.

This work addresses these research gaps by systematically comparing two non-metal choline-based ILs, [Ch][For] and [Ch][OAc], and two imidazolium-based ILs, [bmim]Cl and $[bmim]_2[CoCl_4]$. The catalytic mechanisms of these ILs will be investigated to provide bespoke descriptions of the degradation process, providing insights for future process design. In an effort to enhance the efficiency, economics and sustainability of the IL-catalysed process, the effects of moisture will be explored systematically through experimental and theoretical methods. Additionally, the introduction of MW heating and, for the first time in PET glycolysis, a novel BC-based catalyst support will be evaluated with respect to the three aforementioned factors. Importantly, a focus will be made on bridging the gap in performance between the cheaper choline-based catalyst and its metal-based counterparts, without compromising its sustainable character. Progress in this respect would signal an important step in enhancing the suitability of these green chemicals for use on an industrial scale.

References

[1] Y. Chujo, H. Kobayashi, Y. Yamashita, Synthesis of aromatic dicarboxyl-terminated poly(methyl methacrylate) macromonomers, J Polym Sci A Polym Chem 27 (1989) 2007–2014. https://doi.org/10.1002/pola.1989.080270621.

[2] A. Aguado, L. Martinez, L. Becerra, M. Arieta-araunabena, S. Arnaiz, A. Asueta, I. Robertson, Chemical depolymerisation of PET complex waste : hydrolysis vs . glycolysis, J Mater Cycles Waste Manag 16 (2014) 201–210. https://doi.org/10.1007/s10163-013-0177-y.

[3] S.R. Shukla, V. Palekar, N. Pingale, Zeolite Catalyzed glycolysis of poly(ethylene terephthalate) bottle waste, J Appl Polym Sci 110 (2008) 501–506. https://doi.org/10.1002/app.28656.

[4] S.R. Shukla, K.S. Kulkarni, Depolymerization of poly(ethylene terephthalate) waste, J Appl Polym Sci 85 (2002) 1765–1770. https://doi.org/10.1002/app.10714.

[5] N.D. Pingale, S.R. Shukla, Microwave assisted ecofriendly recycling of poly (ethylene terephthalate) bottle waste, Eur Polym J 44 (2008) 4151–4156. https://doi.org/10.1016/j.eurpolymj.2008.09.019.

[6] J.R. Campanelli, M.R. Kamal, D.G. Cooper, Kinetics of glycolysis of poly(ethy1ene terephthalate) melts, J Appl Polym Sci 54 (1994) 1731–1740. https://doi.org/10.1002/app.1994.070541115.

[7] M. Imran, D.H. Kim, W.A. Al-Masry, A. Mahmood, A. Hassan, S. Haider, S.M. Ramay, Manganese-, cobalt-, and zinc-based mixed-oxide spinels as novel catalysts for the chemical recycling of poly(ethylene terephthalate) via glycolysis, Polym Degrad Stab 98 (2013) 904–915. https://doi.org/10.1016/j.polymdegradstab.2013.01.007.

[8] Y. Zhao, M. Liu, R. Zhao, F. Liu, X. Ge, S. Yu, Heterogeneous CaO(SrO, BaO)/MCF as highly active and recyclable catalysts for the glycolysis of poly(ethylene terephthalate), Res. Chem. Intermed. 44 (2018) 7711-7729. https://doi.org/10.1007/s11164-018-3582-y(0123456789().,-volV)(0123456789().,-volV).

[9] L.X. Yun, Y. Wei, Q. Sun, Y.T. Li, B. Zhang, H.T. Zhang, Z.G. Shen, J.X. Wang, Magnetic hollow micro-sized nanoaggregates for synergistically accelerating

PET glycolysis, Green Chem. 25 (2023) 6901–6913. https://doi.org/10.1039/d3gc01762a.

[10] Z. Fehér, J. Kiss, P. Kisszékelyi, J. Molnár, P. Huszthy, L. Kárpáti, J. Kupai, Optimisation of PET glycolysis by applying recyclable heterogeneous organocatalysts, Green Chem. 24 (2022) 8447–8459. https://doi.org/10.1039/d2gc02860c.

[11] C. Jehanno, I. Flores, A.P. Dove, A.J. Müller, F. Ruipérez, H. Sardon, Organocatalysed depolymerisation of PET in a fully sustainable cycle using thermally stable protic ionic salt, Green Chem. 20 (2018) 1205–1212. https://doi.org/10.1039/c7gc03396f.

[12] I. Olazabal, E.J. Luna Barrios, S. De Meester, C. Jehanno, H. Sardon, Overcoming the limitations of organocatalyzed glycolysis of poly(ethylene terephthalate) to facilitate the recycling of complex waste under mild conditions, ACS Appl Polym Mater (2024). https://doi.org/10.1021/acsapm.4c00326.

[13] C. Jehanno, J. Demarteau, D. Mantione, M.C. Arno, F. Ruipérez, J.L. Hedrick, A.P. Dove, H. Sardon, Selective chemical upcycling of mixed plastics guided by a thermally stable organocatalyst, Angew. Chem. Int. Ed. 60 (2021) 6710–6717. https://doi.org/10.1002/anie.202014860.

[14] J. Sutton, G. Grause, A. Al Rida Hmayed, S.T.G. Street, A.P. Dove, J. Wood, Organocatalytic glycolysis of polyethylene terephthalate and product separation by membrane filtration, Chem. Eng. J. 512 (2025). https://doi.org/10.1016/j.cej.2025.162400.

[15] A.P. Abbott, Deep eutectic solvents and their application in electrochemistry, Curr Opin Green Sustain Chem 36 (2022) 100649. https://doi.org/10.1016/j.cogsc.2022.100649.

[16] B. Liu, W. Fu, X. Lu, Q. Zhou, S. Zhang, Lewis acid-base synergistic catalysis for polyethylene terephthalate degradation by 1,3-dimethylurea/Zn(OAc)2 deep eutectic solvent, ACS Sustain Chem Eng 7 (2019) 3292–3300. https://doi.org/10.1021/acssuschemeng.8b05324.

[17] X. Wei, J. Qiu, H. Wang, W. Zheng, W. Sun, L. Zhao, Efficient glycolysis of Poly(ethylene terephthalate) to bis(hydroxyethyl) terephthalate catalyzed by non-metallic deep eutectic solvent, Chem. Eng. J. 508 (2025). https://doi.org/10.1016/j.cej.2025.161115.

[18] H. Wang, Y. Liu, Z. Li, X. Zhang, S. Zhang, Y. Zhang, Glycolysis of poly (ethylene terephthalate) catalyzed by ionic liquids, Eur Polym J 45 (2009) 1535–1544. https://doi.org/10.1016/j.eurpolymj.2009.01.025.

[19] P. Wasserscheid, W. Keim, Ionic liquidsÐnew [a]solutions[o] for transition metal catalysis, Angew. Chem. Int. Ed 39 (2000) 3772–3789.

[20] R.L. Vekariya, A review of ionic liquids: Applications towards catalytic organic transformations, J Mol Liq 227 (2017) 44. https://doi.org/10.1016/j.molliq.2016.11.123.

[21] Q. Wang, Y. Geng, X. Lu, S. Zhang, First-row transition metal-containing ionic liquids as highly active catalysts for the glycolysis of poly(ethylene terephthalate) (PET), ACS Sustain Chem Eng 3 (2015) 340–348. https://doi.org/10.1021/sc5007522.

[22] Y. Wang, T. Wang, L. Zhou, P. Zhang, Z. Wang, X. Chen, Synergistic catalysis of ionic liquids and metal salts for facile PET glycolysis, Eur Polym J 201 (2023). https://doi.org/10.1016/j.eurpolymj.2023.112578.

[23] T. Wang, X. Gong, C. Shen, G. Yu, X. Chen, Formation of Bis(hydroxyethyl) terephthalate from waste plastic using ionic liquid as catalyst, Polym Degrad Stab 190 (2021) 109601. https://doi.org/10.1016/j.polymdegradstab.2021.109601.

[24] K. Shi, L. Guo, R. Zheng, H. Wang, Y. Chen, Preparation of diacid comprising ionic liquid catalyst and its application in catalytic degradation of PET, Catal Letters 152 (2022) 1182–1193. https://doi.org/10.1007/s10562-021-03716-3.

[25] V.D. Lechuga-Islas, D.M. Sánchez-Cerrillo, S. Stumpf, R. Guerrero-Santos, U.S. Schubert, C. Guerrero-Sánchez, Thermo-responsive polymer catalysts for polyester recycling processes: switching from homogeneous catalysis to heterogeneous separations, Polym Chem 14 (2023) 1893–1904. https://doi.org/10.1039/d2py01520j.

[26] G. Kumar, K. Kumar, A. Bharti, Energy and environmental metrics-based comparison of ionic liquids/deep eutectic solvents-assisted chemical recycling of waste poly(ethylene terephthalate), Ind Eng Chem Res 63 (2024) 6024–6046. https://doi.org/10.1021/acs.iecr.3c04481.

[27] H. Srichandan, R.K. Mohapatra, P.K. Parhi, S. Mishra, Bioleaching approach for extraction of metal values from secondary solid wastes: A critical review, Hydrometallurgy 189 (2019). https://doi.org/10.1016/j.hydromet.2019.105122.

[28] M. Petkovic, K.R. Seddon, L.P.N. Rebelo, C.S. Pereira, Ionic liquids: A pathway to environmental acceptability, Chem Soc Rev 40 (2011) 1383–1403. https://doi.org/10.1039/c004968a.

[29] C.W. Cho, T.P.T. Pham, Y. Zhao, S. Stolte, Y.S. Yun, Review of the toxic effects of ionic liquids, Sci. Total Environ. 786 (2021). https://doi.org/10.1016/j.scitotenv.2021.147309.

[30] S. Stolte, M. Matzke, J. Arning, A. Böschen, W.R. Pitner, U. Welz-Biermann, B. Jastorff, J. Ranke, Effects of different head groups and functionalised side chains on the aquatic toxicity of ionic liquids, Green Chem. 9 (2007) 1170–1179. https://doi.org/10.1039/b711119c.

[31] W. Gouveia, T.F. Jorge, S. Martins, M. Meireles, M. Carolino, C. Cruz, T. V. Almeida, M.E.M. Araújo, Toxicity of ionic liquids prepared from biomaterials, Chemosphere 104 (2014) 51–56. https://doi.org/10.1016/j.chemosphere.2013.10.055.

[32] Y. Liu, X. Yao, H. Yao, Q. Zhou, J. Xin, X. Lu, S. Zhang, Degradation of poly(ethylene terephthalate) catalyzed by metal-free choline-based ionic liquids, Green Chem. 22 (2020) 3122–3131. https://doi.org/10.1039/d0gc00327a.

[33] W. Zheng, C. Liu, X. Wei, W. Sun, L. Zhao, Molecular-level swelling behaviors of poly (ethylene terephthalate) glycolysis using ionic liquids as catalyst, Chem Eng Sci 267 (2023). https://doi.org/10.1016/j.ces.2022.118329.

[34] D. Bura, L. Pedrini, C. Trujillo, S.J. Connon, Cholinium-based ionic liquid catalysts for polyethylene terephthalate glycolysis: understanding the role of solvent and a reappraisal of the cation contribution, RSC Sustain. 1 (2023) 2197–2201. https://doi.org/10.1039/d3su00336a.

[35] Fisher Scientific, Https://Www.Fishersci.Co.Uk/Gb/En/Home.Html (2025).

[36] J. Zhou, H. Sui, Z. Jia, Z. Yang, L. He, X. Li, Recovery and purification of ionic liquids from solutions: A review, RSC Adv 8 (2018) 32832–32864. https://doi.org/10.1039/c8ra06384b.

[37] M.H. Valkenberg, C. DeCastro, W.F. Hölderich, Immobilisation of chloroaluminate ionic liquids on silica materials, Top Catal 14 (2000) 139–144.

[38] M.P. Mudoi, P. Sharma, A.S. Khichi, A review of gas adsorption on shale and the influencing factors of CH4 and CO2 adsorption, J Pet Sci Eng 217 (2022). https://doi.org/10.1016/j.petrol.2022.110897.

[39] A. Thakur, H. Assad, S. Kaya, A. Kumar, Plant extracts as environmentally sustainable corrosion inhibitors II, in: Eco-Friendly Corrosion Inhibitors: Principles, Designing and Applications, Elsevier, 2022: pp. 283–310. https://doi.org/10.1016/B978-0-323-91176-4.00017-9.

[40] A. Wolny, A. Chrobok, Silica-based supported ionic liquid-like phases as heterogeneous catalysts, Molecules 27 (2022). https://doi.org/10.3390/molecules27185900.

[41] K. Donato, L. Matějka, R. Mauler, R. Donato, Recent applications of ionic liquids in the sol-gel process for polymer–silica nanocomposites with ionic interfaces, Colloids Interfaces 1 (2017) 5. https://doi.org/10.3390/colloids1010005.

[42] A. Maiti, A. Kumar, R.D. Rogers, Water-clustering in hygroscopic ionic liquids - An implicit solvent analysis, Phys. Chem. Chem. Phys. 14 (2012) 5139–5146. https://doi.org/10.1039/c2cp00010e.

[43] H. Wang, Y. Liu, Z. Li, X. Zhang, S. Zhang, Y. Zhang, Glycolysis of poly (ethylene terephthalate) catalyzed by ionic liquids, Eur Polym J 45 (2009) 1535–1544. https://doi.org/10.1016/j.eurpolymj.2009.01.025.

[44] Z. Ao, J. Deng, W. He, T. Liu, J. Wang, H. Yang, Z. Shen, J. Chen, Low-temperature one-step synthesis of surfactant-free ZnO nanoparticles for efficient glycolysis of PET, Chem. Eng. J. 494 (2024). https://doi.org/10.1016/j.cej.2024.153037.

[45] M. Chanda, Chemical aspects of polymer recycling, Adv. Ind. Eng. Polym. Res. 4 (2021) 133–150. https://doi.org/10.1016/j.aiepr.2021.06.002.

[46] S.A. Jabarin, E.A. Lofgren, Effects of water absorption on physical properties and degree of molecular orientation of poly (ethylene terephthalate), Polym Eng Sci 26 (1986) 620–625. https://doi.org/10.1002/pen.760260907.

[47] L. Wang, G.A. Nelson, J. Toland, J.D. Holbrey, Glycolysis of PET using 1,3-dimethylimidazolium-2-carboxylate as an organocatalyst, ACS Sustain Chem Eng 8 (2020) 13362–13368. https://doi.org/10.1021/acssuschemeng.0c04108.

[48] S. Marullo, C. Rizzo, N.T. Dintcheva, F. D'Anna, Amino acid-based cholinium ionic liquids as sustainable catalysts for PET depolymerization, ACS Sustain Chem Eng 9 (2021) 15157–15165. https://doi.org/10.1021/acssuschemeng.1c04060.

[49] B. Yilmaz, U. Müller, Catalytic applications of zeolites in chemical industry, Top Catal 52 (2009) 888–895. https://doi.org/10.1007/s11244-009-9226-0.

[50] H. Jüntgen, Activated carbon as catalyst support. A review of new research results, Fuel 65 (1986) 1436–1446. https://doi.org/10.1016/0016-2361(86)90120-1.

[51] Y.F. Li, M.Q. Guo, S.F. Yin, L. Chen, Y.B. Zhou, R.H. Qiu, C.T. Au, Graphite as a highly efficient and stable catalyst for the production of lactones, Carbon N Y 55 (2013) 269–275. https://doi.org/10.1016/j.carbon.2012.12.036.

[52] B. Majumdar, D. Sarma, T. Bhattacharya, T.K. Sarma, Graphene oxide as metal-free catalyst in oxidative dehydrogenative C-N coupling leading to α-ketoamides: importance of dual catalytic activity, ACS Sustain Chem Eng 5 (2017) 9286–9294. https://doi.org/10.1021/acssuschemeng.7b02267.

[53] M. Imran, K.G. Lee, Q. Imtiaz, B.K. Kim, M. Han, B.G. Cho, D.H. Kim, Metal-oxide-doped silica nanoparticles for the catalytic glycolysis of polyethylene

terephthalate, J Nanosci Nanotechnol 11 (2011) 824–828. https://doi.org/10.1166/jnn.2011.3201.

[54] A.M. Al-Sabagh, F.Z. Yehia, D.R.K. Harding, G. Eshaq, A.E. ElMetwally, Fe3O4-boosted MWCNT as an efficient sustainable catalyst for PET glycolysis, Green Chem. 18 (2016) 3997–4003. https://doi.org/10.1039/c6gc00534a.

[55] S. Bin Jin, J.M. Jeong, S.G. Son, S.H. Park, K.G. Lee, B.G. Choi, Synthesis of two-dimensional holey MnO2/graphene oxide nanosheets with high catalytic performance for the glycolysis of poly(ethylene terephthalate), Mater Today Commun 26 (2021) 101857. https://doi.org/10.1016/j.mtcomm.2020.101857.

[56] S. Najafi-Shoa, M. Barikani, M. Ehsani, M. Ghaffari, Cobalt-based ionic liquid grafted on graphene as a heterogeneous catalyst for poly (ethylene terephthalate) glycolysis, Polym Degrad Stab 192 (2021) 109691. https://doi.org/10.1016/j.polymdegradstab.2021.109691.

[57] H. Yao, L. Liu, D. Yan, Q. Zhou, J. Xin, X. Lu, S. Zhang, Colorless BHET obtained from PET by modified mesoporous catalyst ZnO/SBA-15, Chem Eng Sci 248 (2022) 117109. https://doi.org/10.1016/j.ces.2021.117109.

[58] L. Bartolome, M. Imran, K.G. Lee, A. Sangalang, J.K. Ahn, D.H. Kim, Superparamagnetic γ-Fe2O3 nanoparticles as an easily recoverable catalyst for the chemical recycling of PET, Green Chem. 16 (2014) 279–286. https://doi.org/10.1039/c3gc41834k.

[59] S. Najafi-Shoa, M. Barikani, M. Ehsani, M. Ghaffari, Cobalt-based ionic liquid grafted on graphene as a heterogeneous catalyst for poly (ethylene terephthalate) glycolysis, Polym Degrad Stab 192 (2021) 109691. https://doi.org/10.1016/j.polymdegradstab.2021.109691.

[60] S. Bin Jin, J.M. Jeong, S.G. Son, S.H. Park, K.G. Lee, B.G. Choi, Synthesis of two-dimensional holey MnO2/graphene oxide nanosheets with high catalytic performance for the glycolysis of poly(ethylene terephthalate), Mater Today Commun 26 (2021) 101857. https://doi.org/10.1016/j.mtcomm.2020.101857.

[61] Y. He, Y. Guo, F. Yan, T. Yu, L. Liu, X. Zhang, T. Zheng, Density functional theory study of adsorption of ionic liquids on graphene oxide surface, Chem Eng Sci 245 (2021). https://doi.org/10.1016/j.ces.2021.116946.

[62] D. Wagle, G. Kamath, G.A. Baker, Elucidating interactions between ionic liquids and polycyclic aromatic hydrocarbons by quantum chemical calculations, J. Phys. Chem. C 117 (2013) 4521–4532. https://doi.org/10.1021/jp310787t.

[63] S. Conroy, X. Zhang, Theoretical insights into chemical recycling of polyethylene terephthalate (PET), Polym Degrad Stab 223 (2024) 110729. https://doi.org/10.1016/j.polymdegradstab.2024.110729.

[64] Y. Hu, Y. Wang, X. Zhang, J. Qian, X. Xing, X. Wang, Synthesis of poly(ethylene terephthalate) based on glycolysis of waste PET fiber, J. Macromol. Sci., Part A 57 (2020) 430–438. https://doi.org/10.1080/10601325.2019.1709498.

[65] M. Imran, D.H. Kim, W.A. Al-Masry, A. Mahmood, A. Hassan, S. Haider, S.M. Ramay, Manganese-, cobalt-, and zinc-based mixed-oxide spinels as novel catalysts for the chemical recycling of poly(ethylene terephthalate) via glycolysis, Polym Degrad Stab 98 (2013) 904–915. https://doi.org/10.1016/j.polymdegradstab.2013.01.007.

[66] P. Fang, B. Liu, J. Xu, Q. Zhou, S. Zhang, J. Ma, X. lu, High-efficiency glycolysis of poly(ethylene terephthalate) by sandwich-structure polyoxometalate

catalyst with two active sites, Polym Degrad Stab 156 (2018) 22–31. https://doi.org/10.1016/j.polymdegradstab.2018.07.004.

[67] K.M. Engle, J.-Q. Yu, Developing ligands for palladium(II)-catalyzed C–H functionalization: intimate dialogue between ligand and substrate, J. Org. Chem. 78 (2013) 8927–8955. https://doi.org/doi:10.1021/jo400159y.

[68] E. Fazekas, P.A. Lowy, M. Abdul Rahman, A. Lykkeberg, Y. Zhou, R. Chambenahalli, J.A. Garden, Main group metal polymerisation catalysts, Chem Soc Rev 51 (2022) 8793–8814. https://doi.org/10.1039/d2cs00048b.

[69] K.R. Delle Chiaie, F.R. McMahon, E.J. Williams, M.J. Price, A.P. Dove, Dual-catalytic depolymerization of polyethylene terephthalate (PET), Polym Chem 11 (2020) 1450–1453. https://doi.org/10.1039/c9py01920k.

[70] E. Sert, E. Yılmaz, F.S. Atalay, Chemical recycling of polyethlylene terephthalate by glycolysis using deep eutectic solvents, J Polym Environ 27 (2019) 2956–2962. https://doi.org/10.1007/s10924-019-01578-w.

[71] P. Fang, B. Liu, J. Xu, Q. Zhou, S. Zhang, J. Ma, X. lu, High-efficiency glycolysis of poly(ethylene terephthalate) by sandwich-structure polyoxometalate catalyst with two active sites, Polym Degrad Stab 156 (2018) 22–31. https://doi.org/10.1016/j.polymdegradstab.2018.07.004.

[72] C. Qu, X. Han, H. Wang, R. Wang, Y. Zhang, W. Sun, Z. Shi, Y. Wang, P. Yin, Synergistic catalysis driven by solvent effect: efficient glycolysis of polyethylene terephthalate (PET) by the Zn(OAc)2/DBU-DMSO system, ACS Sustain Chem Eng 13 (2025) 12496–12508. https://doi.org/10.1021/acssuschemeng.5c03502.

[73] X. Zhou, X. Lu, Q. Wang, M. Zhu, Z. Li, Effective catalysis of poly(ethylene terephthalate) (PET) degradation by metallic acetate ionic liquids, Pure Appl. Chem. 84 (2012) 789–801. https://doi.org/10.1351/PAC-CON-11-06-10.

[74] A.M. Al-Sabagh, F.Z. Yehia, A.M.F. Eissa, M.E. Moustafa, G. Eshaq, A.M. Rabie, A.E. Elmetwally, Cu- and Zn-acetate-containing ionic liquids as catalysts for the glycolysis of poly(ethylene terephthalate), Polym Degrad Stab 110 (2014) 364–377. https://doi.org/10.1016/j.polymdegradstab.2014.10.005.

[75] Q. Wang, Y. Geng, X. Lu, S. Zhang, First-row transition metal-containing ionic liquids as highly active catalysts for the glycolysis of poly(ethylene terephthalate) (PET), ACS Sustain Chem Eng 3 (2015) 340–348. https://doi.org/10.1021/sc5007522.

[76] C. Shuangjun, S. Weihe, C. Haidong, Z. Hao, Z. Zhenwei, F. Chaonan, Glycolysis of poly(ethylene terephthalate) waste catalyzed by mixed Lewis acidic ionic liquids, J Therm Anal Calorim 143 (2020) 3489–3497. https://doi.org/10.1007/s10973-020-10331-8.

[77] H. Wang, R. Yan, Z. Li, X. Zhang, S. Zhang, Fe-containing magnetic ionic liquid as an effective catalyst for the glycolysis of poly(ethylene terephthalate), Catal Commun 11 (2010) 763–767. https://doi.org/10.1016/j.catcom.2010.02.011.

[78] Y. Liu, X. Yao, H. Yao, Q. Zhou, J. Xin, X. Lu, S. Zhang, Degradation of poly(ethylene terephthalate) catalyzed by metal-free choline-based ionic liquids, Green Chem. 22 (2020) 3122–3131. https://doi.org/10.1039/d0gc00327a.

[79] S. Naumann, P.B.V. Scholten, J.A. Wilson, A.P. Dove, Dual catalysis for selective ring-opening polymerization of lactones: evolution toward simplicity, J Am Chem Soc 137 (2015) 14439–14445. https://doi.org/10.1021/jacs.5b09502.

[80] Y. Feng, S.W. Lv, R. Zhang, X. Ren, J. Shen, Y. Cong, From waste to wealth: Glycolysis of PET for high-value resource utilization, Waste Manag. 200 (2025). https://doi.org/10.1016/j.wasman.2025.114768.

[81] A. Arunphacharawit, T. Poonsawat, T. Meechai, L. Chaicharoenwimolkul Chuaitammakit, E. Somsook, DFT study on the depolymerization of PET by Ca-catalyzed glycolysis reaction model, Heliyon 10 (2024). https://doi.org/10.1016/j.heliyon.2024.e34666.

[82] Z. Ju, L. Zhou, X. Lu, Y. Li, X. Yao, S. Cheng, G. Chen, C. Ge, Mechanistic insight into the roles of anions and cations in the degradation of poly(ethylene terephthalate) catalyzed by ionic liquids, Phys. Chem. Chem. Phys. 23 (2021) 18659–18668. https://doi.org/10.1039/d1cp02038b.

[83] É. Casey, R. Breen, J.S. Gómez, A.P.M. Kentgens, G. Pareras, A. Rimola, J.D. Holmes, G. Collins, Ligand-aided glycolysis of PET using functionalized silica-supported Fe2O3 nanoparticles, ACS Sustain Chem Eng 11 (2023) 15544–15555. https://doi.org/10.1021/acssuschemeng.3c03585.

[84] R. Zhang, P. Hao, X. Cheng, R.R. Neiber, L. Wang, Y. Li, J. Xu, D. Yan, Q. Zhou, J. Xin, X. Lu, A novel assessment method for the catalytic activity of ionic liquid degradation of PET, J Mol Liq 411 (2024). https://doi.org/10.1016/j.molliq.2024.125751.

[85] M.A. Nosir, M.A. Ortuño, Catalytic function of ionic liquids in polyethylene terephthalate glycolysis by molecular dynamics simulations, RSC Sustain. 2 (2024) 2677–2683. https://doi.org/10.1039/d4su00251b.

[86] C.O. Kappe, Controlled microwave heating in modern organic synthesis, Angewandte Chemie - International Edition 43 (2004) 6250–6284. https://doi.org/10.1002/anie.200400655.

[87] X. Zhao, J. Zhang, Z. Song, H. Liu, L. Li, C. Ma, Microwave pyrolysis of straw bale and energy balance analysis, J Anal Appl Pyrolysis 92 (2011) 43–49. https://doi.org/10.1016/j.jaap.2011.04.004.

[88] C. Guerrero-Sanchez, R. Hoogenboom, U.S. Schubert, Fast and "green" living cationic ring opening polymerization of 2-ethyl-2-oxazoline in ionic liquids under microwave irradiation, Chem. Commun. (2006) 3797–3799. https://doi.org/10.1039/b608364a.

[89] S. Mallakpour, Z. Rafiee, New developments in polymer science and technology using combination of ionic liquids and microwave irradiation, Prog. Polym. Sci. (Oxford) 36 (2011) 1754–1765. https://doi.org/10.1016/j.progpolymsci.2011.03.001.

[90] C. Bao, A. Serrano-Lotina, M. Niu, R. Portela, Y. Li, K.H. Lim, P. Liu, W. jun Wang, M.A. Bañares, Q. Wang, Microwave-associated chemistry in environmental catalysis for air pollution remediation: A review, Chem. Eng. J. 466 (2023). https://doi.org/10.1016/j.cej.2023.142902.

[91] R.R. Mishra, A.K. Sharma, Microwave-material interaction phenomena: Heating mechanisms, challenges and opportunities in material processing, Compos Part A Appl Sci Manuf 81 (2016) 78–97. https://doi.org/10.1016/j.compositesa.2015.10.035.

[92] K.K. Rana, S. Rana, Microwave reactors: A brief review on its fundamental aspects and applications, OAlib 01 (2014) 1–20. https://doi.org/10.4236/oalib.1100686.

[93] F. Chen, G. Wang, C. Shi, Y. Zhang, L. Zhang, W. Li, F. Yang, Kinetics of glycolysis of poly(ethylene terephthalate) under microwave irradiation, J Appl Polym Sci 127 (2013) 2809–2815. https://doi.org/10.1002/app.37608.

[94] S. Chaudhary, P. Surekha, D. Kumar, C. Rajagopal, P.K. Roy, Microwave assisted glycolysis of poly(ethylene terepthalate) for preparation of polyester polyols, J Appl Polym Sci 129 (2013) 2779–2788. https://doi.org/10.1002/app.38970.

[95] D. Ravikumar, P. Mani, N. Bernaurdshaw, S. Vajiravelu, Microwave-induced chemical recycling of colored polyester textile wastes promoted by Zn[(L)Proline]2, as a recyclable homogeneous catalyst, Waste Biomass Valorization 15 (2024) 4585–4598. https://doi.org/10.1007/s12649-024-02522-3.

[96] Y. Luo, E. Selvam, D.G. Vlachos, M. Ierapetritou, Economic and environmental benefits of modular microwave-assisted polyethylene terephthalate depolymerization, ACS Sustain Chem Eng 11 (2023) 4209–4218. https://doi.org/10.1021/acssuschemeng.2c07203.

[97] M. Deetlefs, K.R. Seddon, Improved preparations of ionic liquids using microwave irradiation, Green Chem. 5 (2003) 181–186. https://doi.org/10.1039/b300071k.

[98] N.E. Leadbeater, H.M. Torenius, A study of the ionic liquid mediated microwave heating of organic solvents, J. Org. Chem. 67 (2002) 3145–3148. https://doi.org/10.1021/jo016297g.

[99] F. Scé, I. Cano, C. Martin, G. Beobide, O. Castillo, I. De Pedro, Comparing conventional and microwave-assisted heating in PET degradation mediated by imidazolium-based halometallate complexes, New J. Chem. 43 (2019) 3476–3485. https://doi.org/10.1039/c8nj06090h.

[100] J. Shah, K. Mohanraj, Comparison of conventional and microwave-assisted synthesis of benzotriazole derivatives, Indian J Pharm Sci 76 (2014) 46–53.

[101] S. Phromphithak, T. Katongtung, P. Pholchan, N. Tippayawong, Microwave-heated pretreatment of corncob, giant juncao grass, and hemp using choline derivatives with glycerol, Bioenergy Res 18 (2025). https://doi.org/10.1007/s12155-024-10810-y.

[102] A.R. Mankar, A. Pandey, A. Modak, K.K. Pant, Microwave mediated enhanced production of 5-hydroxymethylfurfural using choline chloride-based eutectic mixture as sustainable catalyst, Renew Energy 177 (2021) 643–651. https://doi.org/10.1016/j.renene.2021.05.157.

[103] É. Casey, R. Breen, G. Pareras, A. Rimola, J.D. Holmes, G. Collins, Guanidine functionalized porous SiO2 as heterogeneous catalysts for microwave depolymerization of PET and PLA, RSC Sustain. 2 (2024) 1040–1051. https://doi.org/10.1039/d3su00425b.

[104] J.S. Cha, S.H. Park, S.C. Jung, C. Ryu, J.K. Jeon, M.C. Shin, Y.K. Park, Production and utilization of biochar: A review, J. Ind. Eng. Chem. 40 (2016) 1–15. https://doi.org/10.1016/j.jiec.2016.06.002.

[105] B.R. Patra, A. Mukherjee, S. Nanda, A.K. Dalai, Biochar production, activation and adsorptive applications: a review, Environ Chem Lett 19 (2021) 2237–2259. https://doi.org/10.1007/s10311-020-01165-9.

[106] D. Bergna, T. Varila, H. Romar, U. Lassi, Comparison of the properties of activated carbons produced in one-stage and two-stage processes, C (Basel) 4 (2018) 41. https://doi.org/10.3390/c4030041.

[107] C. Liu, W. Wang, R. Wu, Y. Liu, X. Lin, H. Kan, Y. Zheng, Preparation of acid- and alkali-modified biochar for removal of methylene blue pigment, ACS Omega 5 (2020) 30906–30922. https://doi.org/10.1021/acsomega.0c03688.

[108] P.R. Yaashikaa, P.S. Kumar, S. Varjani, A. Saravanan, A critical review on the biochar production techniques, characterization, stability and applications for circular bioeconomy, Biotechnol. Rep. 28 (2020) e00570. https://doi.org/10.1016/j.btre.2020.e00570.

[109] J. Lee, K.H. Kim, E.E. Kwon, Biochar as a catalyst, Renew. Sustain. Energy Rev. 77 (2017) 70–79. https://doi.org/10.1016/j.rser.2017.04.002.

[110] L. Zhu, S. Yin, Q. Yin, H. Wang, S. Wang, Biochar: A new promising catalyst support using methanation as a probe reaction, Energy Sci Eng 3 (2015) 126–134. https://doi.org/10.1002/ese3.58.

[111] A. Villardon, A. Alcazar-Ruiz, J. Cencerrero, A. Romero, L. Sanchez- Silva, F. Dorado, Olive stone-derived biochar as a sustainable catalyst support for CO2 methanation, J. CO2 Util. 96 (2025) 103102. https://doi.org/10.1016/j.jcou.2025.103102.

[112] S. Renda, C. Di Stasi, J.J. Manyà, V. Palma, Biochar as support in catalytic CO2 methanation: Enhancing effect of CeO2 addition, J. CO2 Util. 53 (2021). https://doi.org/10.1016/j.jcou.2021.101740.

[113] S. Dora, T. Bhaskar, R. Singh, D.V. Naik, D.K. Adhikari, Effective catalytic conversion of cellulose into high yields of methyl glucosides over sulfonated carbon

based catalyst, Bioresour Technol 120 (2012) 318–321. https://doi.org/10.1016/j.biortech.2012.06.036.

[114] K. Bouafina, F. Belferdi, F. Bouremmad, Sulfonated biochar derived from eucalyptus bark as natural catalyst in the Biginelli reaction, Russ J Gen Chem 95 (2025) 663–670. https://doi.org/10.1134/S1070363224613048.

[115] C. Zhang, Z. Fu, B. Dai, S. Zen, Y. Liu, Q. Xu, S.R. Kirk, D. Yin, Biochar sulfonic acid immobilized chlorozincate ionic liquid: An efficiently biomimetic and reusable catalyst for hydrolysis of cellulose and bamboo under microwave irradiation, Cellulose 21 (2014) 1227–1237. https://doi.org/10.1007/s10570-014-0167-9.

[116] F. Li, N. Wang, X. He, M. Deng, X. Yuan, H. Zhang, A. Nzihou, D.C.W. Tsang, C.H. Wang, Y.S. Ok, Biochar-based catalytic upgrading of plastic waste into liquid fuels towards sustainability, Commun Earth Environ 6 (2025). https://doi.org/10.1038/s43247-025-02286-1.

[117] I. Yunita, S. Putisompon, P. Chumkaeo, T. Poonsawat, E. Somsook, Effective catalysts derived from waste ostrich eggshells for glycolysis of post-consumer PET bottles, Chem. Pap. 73 (2019) 1547–1560. https://doi.org/10.1007/s11696-019-00710-3.

[118] Z. Laldinpuii, S. Lalhmangaihzuala, Z. Pachuau, K. Vanlaldinpuia, Depolymerization of poly(ethylene terephthalate) waste with biomass-waste derived recyclable heterogeneous catalyst, Waste Manag. 126 (2021) 1–10. https://doi.org/10.1016/j.wasman.2021.02.056.

[119] S. Lalhmangaihzuala, Z. Laldinpuii, C. Lalmuanpuia, K. Vanlaldinpuia, Glycolysis of poly(Ethylene terephthalate) using biomass-waste derived recyclable

heterogeneous catalyst, Polymers 13 (2021) 1–13. https://doi.org/10.3390/polym13010037.

Chapter 3
Methodology and Theory

Understanding catalytic processes at the molecular level benefits greatly from combining experimental studies with theoretical investigations. Experiments provide essential evidence of reaction outcomes and catalyst performance but often offer limited insight into underlying mechanisms. Quantum chemical calculations, particularly Density Functional Theory (DFT), complement experiments by revealing reaction pathways, energy profiles and electronic structures that are difficult to access otherwise. This combined approach is especially valuable in the study of this thesis. Experimental results highlight trends in catalyst efficiency and selectivity, while DFT modelling clarifies how catalyst structure, charge distribution and steric effects influence the depolymerisation process. Integrating experimental and theoretical methods thus enables a deeper mechanistic understanding and a more predictive framework for optimising ionic liquid (IL)-catalysed polyethylene terephthalate (PET) glycolysis. This chapter provides a full overview of the experimental and computational methodology, detailing any essential decision-making within the procedure. Then, the theory behind the modelling techniques and experimental characterisation is described in detail.

3.1 Methodology

3.1.1 Overview of computational methods

An overview of the computational methods used in this work is shown in a process diagram in **Figure 3.1**, grouped into four parts: DFT calculations of reaction pathways, intermolecular interactions analysis, modelling of moisture effects and IL adsorption on a biochar (BC) surface.

DFT calculations were employed to first screen IL catalysts through energy barrier calculations. Energy barriers were calculated based off of global minima determined for each IL using an iterative process combining geometric optimisation and transition state (TS) searching. Once global minima for each catalyst were confirmed *via* intrinsic reaction coordinate (IRC) analysis, intermolecular interactions were analysed using multiple techniques including natural bond orbital (NBO), quantum theory of atoms in molecules (QTAIM) and reduced density gradient (RDG) analyses. Additional charge transfer assessment methods such as bond order analysis, atomic dipole moment corrected Hirshfeld (ADCH) analysis and the highest occupied molecular orbital and lowest unoccupied molecular orbital (HOMO-LUMO) energy gap were employed. These tools were combined to elucidate the bespoke reaction mechanisms for each of the modelled ILs. Finally, a simplified BC model was used to evaluate the adsorption strength of one metal-based and one organic IL, based on their interaction with BC surface functional groups. More detailed theory behind the computational parameters considered for this study are included in **Sections 3.2.2** and **3.2.3**.

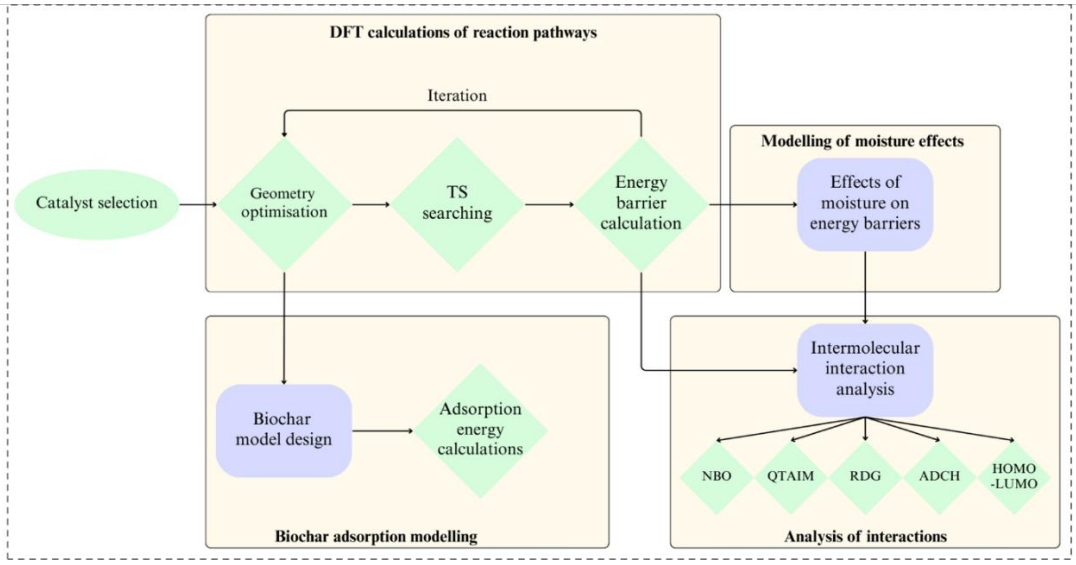

Figure 3.1. *Process flow diagram of computational method overview.*

3.1.1.1 Catalyst selection

In order to compare the effectiveness of cheap, environmentally-friendly choline-based ILs with the more commonly used metal, imidazolium-based counterparts, four ILs were selected for DFT screening. Two organic, choline-based ILs, [Ch][OAc] and [Ch][For] were chosen based on their performance in the study by Liu et al. [1]. Their inclusion represents a non-metal, inherently green IL which is cheap to produce. To represent the imidazolium family of ILs, as well as providing a comparison of metal and non-metal ILs, $[bmim]_2[CoCl_4]$ was selected for its high activity which is countered by higher toxicity and synthesis costs relative to other ILs. This metal-based IL is used as a highly effective reference for the cheaper, greener ILs to be compared to. As outlined in **Chapter 2**, previous studies of Co-based ILs has found them to produce yields ranging from 70% to 95% [2,3]. To isolate the mechanistic role of the metal-centred anion, [bmim]Cl was also selected for study.

3.1.1.2 DFT modelling of the reaction pathways of IL-catalysed PET glycolysis

Firstly, all reactants, catalysts and products were geometrically optimised, with frequency analysis confirming the existence of no imaginary frequencies. Electrostatic potential (ESP) mapping was conducted to identify nucleophilic and electrophilic regions of reactants and catalysts. This, alongside chemical intuition, allowed for initial guesses of geometries to be made, from which global minima could then be determined.

The calculation of activation barriers was carried out through an iterative process involving the identification of plausible TSs and their associated reactant geometries. Local minima were generated based on the known mechanism of IL-catalysed PET glycolysis (as well as any mechanistic discrepancies in the literature), with each minimum representing distinct relative orientations or interactions between the IL and PET. For each minimum, TS guesses were constructed and optimised, followed by IRC calculations to confirm connectivity to reactants and products. This process was repeated across all defined groups of minima until the TS associated with the lowest overall activation barrier was identified. The corresponding connected local minimum was considered the kinetically relevant reactant for that pathway. More details of this process are provided in **Chapter 4**.

While the global minimum on the potential energy surface may not always be directly involved in the reaction step, the focus was placed on the lowest-barrier path. Given the complexity of the system, as many iterations as were practically feasible were performed to explore the mechanistically relevant conformational space. Future work could benefit from machine learning or automated TS search algorithms to more

comprehensively sample the reaction landscape, but this was beyond the scope of the present study.

3.1.1.3 Analysis of intermolecular interactions

For a more detailed description of the intermolecular interactions taking place during the reaction, a number of additional methods were employed including NBO, QTAIM and population analysis. To date, a few studies of IL-catalysed PET glycolysis have shone light on the synergistic catalytic mechanism, using a number of supplementary tools such as NBO analysis, QTAIM and population analysis among others [4,5]. These methods were carried out using the Multiwfn package [6].

The optimised reactants from IRC analysis were used to explore the interactions which initiate the reaction. NBO and QTAIM represent the strength of interactions between certain moieties, while population analysis details the atomic charge transfer. For charge transfer analysis, ADCH was chosen due to its improved accuracy for highly polar systems, which is essential for IL-containing systems. Single-point energy calculations were carried out on the optimal IL configurations to determine the HOMO-LUMO gap, in order to determine the reactivity and stability of each catalyst, as well as the location of the occupied and unoccupied orbitals within the molecules. To provide qualitative analysis of the changing coordination chemistry of the cobalt-based anion within the metallic IL, fuzzy bond order analysis was employed at various stages along the reaction profile. Many of these methods have been used previously to quantify the interactions in IL-containing molecular systems [4,7,8].

3.1.1.4 Modelling of moisture effects

To explore the effects of moisture within the system, explicit water molecules were strategically added to the system, based on chemical intuition. Once added, energy barrier calculation was carried out to evaluate the suspected hindering of water, on metal- and organic-based IL-catalysed PET glycolysis. The optimised systems were then analysed using QTAIM, to investigate the interactions between catalysts, reactants and water molecules. The interaction strength was compared to the water-free system to quantify the influence of water on the reaction.

3.1.1.5 DFT modelling of IL adsorption on biochar

A catalyst surface was designed and optimised to represent the KOH-activated BC surface. Next, the charged adsorbates, bmim, choline, OAc and $CoCl_4$ were optimised individually and confirmed to be minimums. The optimised adsorbates were then placed strategically on top of the BC surface within the complex system. Various adsorption configurations were tested through geometric optimisation, with the lowest energy configuration being used as the optimal adsorption site.

It should be noted that this modelling work is significantly simplified as detailed modelling work of BC is still in its infancy. This work focuses on estimating the behaviours of ILs in contact with functional groups assumed to be on the BC surface, based on the activation by KOH, however it was not possible to model other properties such as porosity, amorphous regions and surface area. While there is ongoing research into developing complex models to accurately represent these structural characteristics, such approaches remain insufficiently defined and validated at this stage to be reliably applied within the scope of this study [9–12].

3.1.2 Experimental setup

The general experimental procedure begins with the synthesis of the IL catalysts, selected from DFT screening, which are characterised using Fourier transform infrared spectroscopy (FT-IR) and Raman spectroscopy. The ILs, with or without the addition of activated BC, are then added to the glycolysis reactor alongside select amounts of PET and ethylene glycol (EG), under argon. Upon completion of the reaction, the desired monomer, bis(2-hydroxyethyl) terephthalate (BHET), is removed *via* filtration. The production of BHET is then confirmed using FT-IR and nuclear magnetic resonance (NMR) characterisation. The process flow diagram is shown in **Figure 3.2**.

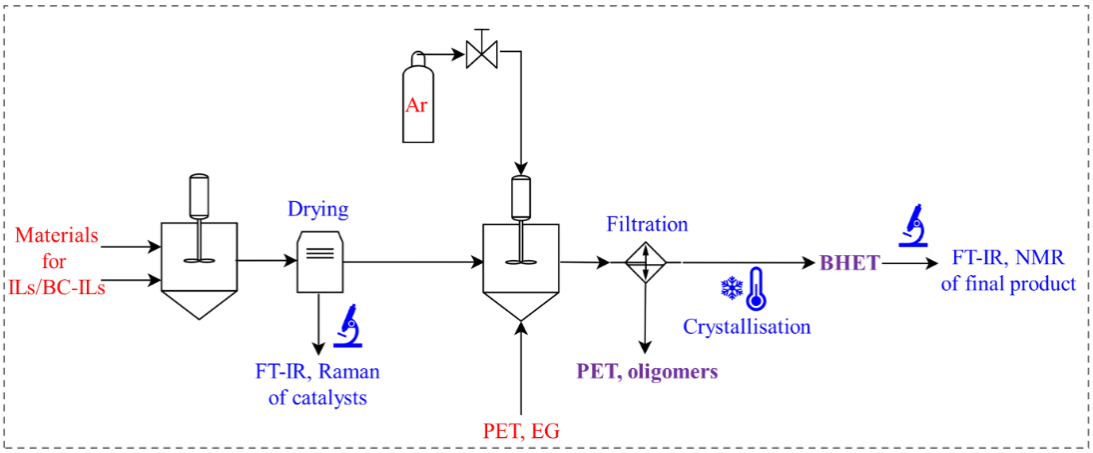

Figure 3.2. *Process flow diagram of the general experimental procedure.*

3.1.2.1 Materials

PET (30% glass fibre) was purchased from Sigma Aldrich. Although the average molecular weight of the polymer was unavailable from the supplier, it is estimated to be between 30000-40000 g/mol, based on the literature [13]. All remaining chemicals required for IL synthesis and glycolysis, including choline hydroxide (Alfa Aesar, 46% w/w aq. Soln.), acetic acid (Thermo Scientific, 99.7+%, ACS Reagent), formic acid (Thermo Scientific, 98+%), cobalt (II) chloride (Alfa

Aesar, anhydrous, 97%), 1-butyl-3-methylimidazolium chloride (Thermo Scientific, 98+%), dichloromethane (Alfa Aesar, 99+%, stabilised with *ca.* 50 ppm amylene), diethyl ether (Fisher Chemical, Stabilised with BHT), and EG (Alfa Aesar, 99%) were bought from Fisher Scientific. Spent coffee grounds (SCGs) of the Strath blend were collected from a café outlet at the University of Strathclyde.

3.1.2.2 Synthesis of organic ILs

Organic ILs [Ch][OAc] and [Ch][For] were synthesised using established literature methods [1,2,14]. As shown in **Figure 3.3**, the organic ILs are formed *via* a neutralisation reaction combining a cholinic base and a selected acid. The synthesis of [Ch][OAc] required a 0.1 mol aqueous solution of [Ch][OH], of which 12.12 g were loaded into a 250 mL round-bottom flask over an ice bath. A slight excess of 6.61 g acetic acid (0.11 mol) was gradually added dropwise and the reaction proceeded for 7 hours. Water was removed by rotary evaporation at 60 °C for 7 hours, followed by the elimination of unreacted acid using ~20 mL of diethyl ether. The final mixture, the IL, was then dried in a vacuum oven at 70 °C for 7 hours prior to use. It should be noted that laboratory safety restrictions prevented overnight running of the vacuum oven.

The synthesis of [Ch][For] followed the exact same procedure, with the exception of using formic acid instead of acetic acid.

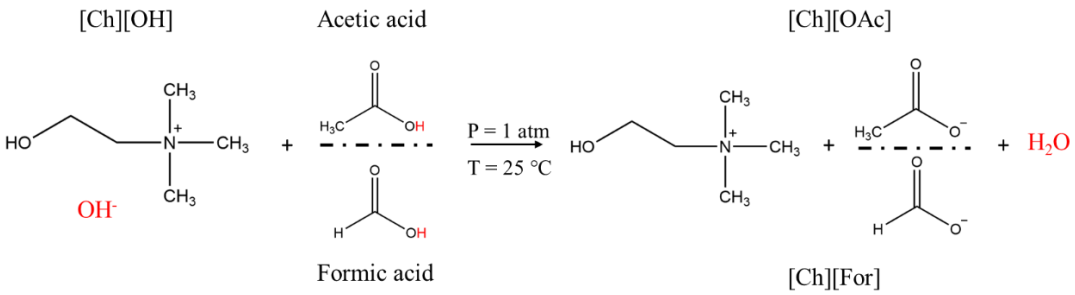

Figure 3.3. *Synthesis of organic ILs [Ch][OAc] and [Ch][For].*

3.1.2.3 Synthesis of metal-based IL

The metal IL $[bmim]_2[CoCl_4]$ was synthesised using the reaction shown in **Figure 3.4**. The crystal powder of [bmim]Cl (10 g) was first mixed in ~20 mL of dichloromethane with 3.72 g anhydrous $CoCl_2$ at a molar ratio of 2:1 ([bmim]Cl to metal chloride) and heated at 80 °C for 5 hours until a clear, transparent and homogeneous liquid formed. The obtained IL was then extracted with the addition of 10 mL of water at least three times. Water and dichloromethane remaining in the mixture were evaporated by a vacuum rotary evaporator at 50 °C for 7 hours. The resulting ILs were dried in a vacuum oven at 60 °C for 7 hours prior to use.

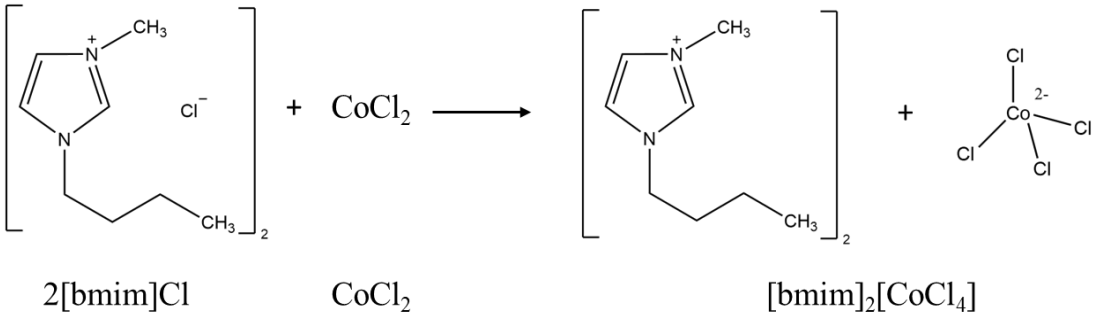

Figure 3.4. *Synthesis of metal-containing IL, $[bmim]_2[CoCl_4]$.*

3.1.2.4 Synthesis of BC-IL

The biomass pyrolysis and subsequent BC activation procedure was carried out by another PhD student within the Department of Chemical and Process Engineering, University of Strathclyde. The BC was prepared by first drying SCGs at 100 °C in a Memmert 298 oven before undergoing pyrolysis in a Carbolite Eurotherm 3508 horizontal tubular furnace and heated at a ramp rate of 20 °C/min to 600 °C, where they were held for one hour under a continuous flow of high-purity nitrogen (BOC, a Linde company; Oxygen-free nitrogen, 99.998% purity, 230 bar) at a flow rate of 100 mL/min.

The resulting BC was ground and mixed with potassium hydroxide (KOH) at a char:KOH mass ratio of 1:1. The mixture was transferred into an alumina boat crucible and placed inside the furnace and then heated at a ramp rate of 20 °C/min to a final temperature of 700 °C, where it was held for two hours in a nitrogen atmosphere. Following activation, the BC was thoroughly washed with deionised water to remove residual KOH and ash. The washed BC was then dried in an oven at 100 °C for 12 hours.

After obtaining the activated BC sample, all remaining experimental work was carried out by the author. ILs [Ch][OAc] and $[bmim]_2[CoCl_4]$ were grafted to the KOH-BC surface by mixing at a 1:1 (w/w) ratio in selected solvents (0.1 g/100 mL) at room temperature for 4 hours. Dichloromethane was used for [Ch][OAc]-BC and diethyl ether was used for $[bmim]_2[CoCl_4]$-BC. Once mixed, the samples were then filtered and washed with the corresponding solvents three times before being dried in an oven to a constant weight, at 100 °C.

Due to their hygroscopic nature, all synthesised catalysts were stored in a glovebox to mitigate moisture absorption from the air.

3.1.2.5 PET glycolysis experiments

The experimental setup featured a three-necked, 250 mL volumetric flask fitted with a thermocouple and a magnetic stirrer. The thermocouple was connected to a digital multimeter to monitor the reaction temperature. The flask was connected to a Schlenk line under argon to mitigate moisture effects. Following safety considerations, an aluminium heat-on block was chosen in place of an oil bath, unlike in literature. Using the metal block prevents the possibility of hot oil spillages and provides a more consistent heating at higher temperatures. The heat-on block was fitted with a

temperature probe connected to a magnetic hot-plate stirrer and temperature control. The reaction vessel was wrapped in aluminium foil to limit heat loss. The setup is shown in **Figure 3.5**.

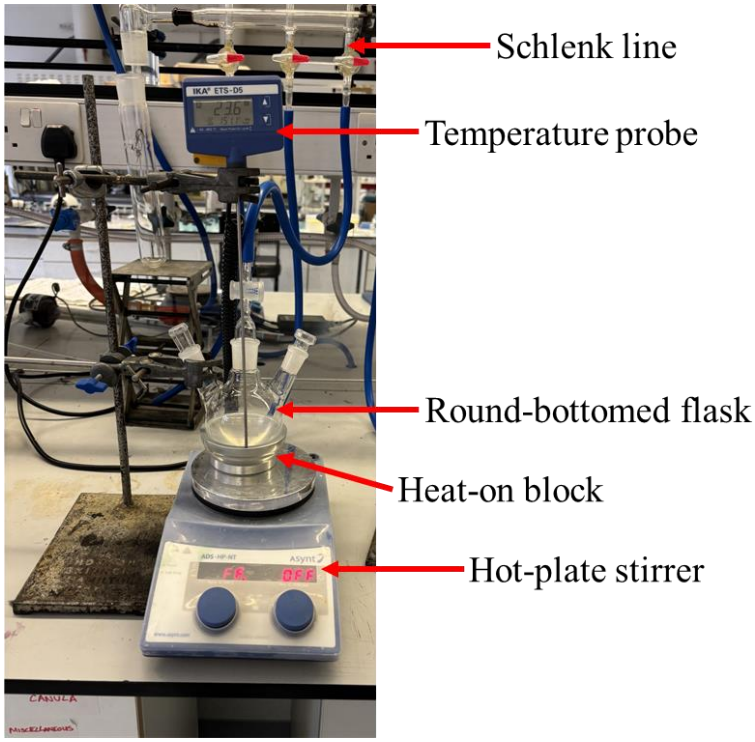

Figure 3.5. *Photograph of the experimental setup including Schlenk line-connected round-bottomed flask, heat-on block with temperature probe and hot-plate stirrer.*

The experimental procedure was designed based on numerous literature studies of catalysed PET glycolysis [1,2,15]. Selected weights of PET and catalyst were added to the flask and heated to the desired temperature, based on the heat-on block. EG was then injected into the flask and once the digital multimeter confirmed that the EG had reached the targeted temperature, the reaction was considered to have begun. During the time taken for EG to reach the equilibrium temperature of the reaction, PET degradation is minimal. The reaction was run for the desired length of time and once complete, filtered through a sieve. The remaining residue was washed with deionised water and dried in an oven at 70 °C until constant weight. Once dried, the residue was

weighed and determined to be unreacted PET. Using this, the PET conversion could be calculated as **Equation 3.1**:

$$PET\ Conversion = \frac{W_i - W_f}{W_i} \times 100 \quad (3.1)$$

Where W_i represents the initial weight of PET, W_f represents the final weight of PET.

Around 900 mL of deionised water was then added to the remaining filtrate and agitated vigorously at 70 °C using a large magnetic stirrer before being filtered again to remove any insoluble PET oligomers. The collected filtrate was then concentrated to approximately 100 mL by boiling, with heat supplied by a magnetic hot-plate stirrer. The concentrate was then stored at 5 °C in a refrigerator for 48 hours until white crystalline flakes formed. The flakes were separated through filtration and dried in an oven at 70 °C until a constant weight was achieved. The molar yield of BHET could be calculated using the weight of the crystals in **Equation 3.2**:

$$BHET\ Yield = \frac{{}^{W_{BHET}}/_{M_{BHET}}}{{}^{W_{PET}}/_{M_{PET}}} \times 100 \quad (3.2)$$

Where W_{BHET} and M_{BHET} represent the final weight and molecular weight of BHET, respectively, while W_{PET} and M_{PET} represent the initial weight and molecular weight of PET, respectively. The molecular weights of PET and BHET are 192 g/mol and 254 g/mol, respectively.

3.1.2.6 Material characterisation

FT-IR was selected to identify significant chemical functional groups on all catalysts, reactants and products. This approach was essential to confirming the production of the desired ILs, as well as their subsequent grafting to the BC surface. Additionally, it can be used to effectively mark the degradation journey of the PET, by tracing the evolution of the end-chain hydroxyl groups formed during glycolysis.

Specifically, ATR-FT-IR spectroscopy was performed using an ABB M83000 Spectrometer. A total of 32 scans were taken, with spectra recorded at 7 cm^{-1} intervals, covering a range of 4000-400 cm^{-1}. Catalyst, intermediate and final product samples were characterised three times and the mean spectroscopic value taken to account for variance within samples.

^{1}H NMR of the final degradation products was carried out to confirm the qualitative purity of BHET. This was selected over ^{13}C NMR as it is generally considered more sensitive and faster for the requirements of this work. NMR is a powerful complementary tool to FT-IR because while FT-IR identifies functional group effectively, oligomers of differing chain lengths will have overlapping spectra, therefore not providing a clear image of the purity of the product. Conversely, NMR provides detailed information of the hydrogen environments within the products, confirming the exact chemical structure and qualitative presence of impurities. The product was analysed by ^{1}H NMR (Bruker AVIII 400 MHz) in a deuterated dimethyl sulfoxide (DMSO-d_6) solvent (~5 mg/mL).

FT-IR spectra of pristine and IL-grafted BC samples were compared to determine the adsorption of ILs to the surface. Due to sloping baselines and reduced signal intensity of ATR-FT-IR-derived BC spectra, Raman spectroscopy was employed to characterise the pristine samples, as well as pure ILs, using a LabRAM HR system, with a Ventus 532 nm laser used to collect spectra over a wavenumber range of 100 cm^{-1} to 3500 cm^{-1}. As Raman spectra more effectively scan carbon frameworks, its use provides a much clearer image of BC interactions with ILs. Raman spectra of pure IL catalysts were compared with the BC-IL samples separated from the product mixture following glycolysis to evaluate how the ILs were grafted to the

surface, as well as the potential reusability of the BC-IL catalysts. Moisture content of EG samples was determined using Karl Fischer (KF) titration with a hybrid Karl Fischer Moisture Titrator, MKH700, Kyoto Electronics Manufacturing Co.

Further details of the chemical theory and physical relevance of the characterisation methods are included in **Section 3.2.4**.

3.2 Theory

3.2.1 Density Functional Theory (DFT)

DFT is a quantum chemistry approach to modelling molecular systems, making use of the observable electron density to determine the total energy of a system. The following section outlines the fundamental theory behind it.

3.2.1.1 DFT background

Understanding the structure and reactivity of molecules at the atomic level begins with quantum mechanics. The fundamental equation that governs all quantum systems is the Schrödinger Equation, as shown in **Equation 3.3**, which describes how the total energy of a system relates to its wavefunction, a mathematical object containing all the information about the system's electrons and nuclei [16]. In principle, Schrödinger Equation allows us to determine the energy and properties of any molecular system [17].

$$H\psi = E\psi \tag{3.3}$$

Where E is the total energy eigenvalue associated with the Hamiltonian operator (H) acting on the stationary eigenstate ψ (the wavefunction). H is a representation of the total energy, combining the kinetic and potential energy, assumed here to be independent of time.

In theory, solving Schrödinger Equation would provide all the observable properties of a molecular system, however, for systems with many atoms and electrons, the computational expense is too great. The intricacy of electron-electron interactions is extremely complex and grows rapidly with system size, known as the many-body problem [17].

There have been numerous mathematical approaches in the time since Schrodinger's breakthrough aimed at simplifying the problem. The Born-Oppenheimer approximation reduces the complexity by fixing the positions of the nuclei due to their relative size compared to the electrons [17,18]. Then, the Hartree theory was introduced which treats each electron as moving independently through a mean-field created by all other electrons in the system, creating a smooth approximation of their combined effect . This was then progressed using the Hartree-Fock method, which introduced the concept of exchange, where electrons of the same spin-state will avoid contact without directly repelling [17,19].

The above approximations go some way to simplifying the problem, however without the accurate description of electron-electron repulsion (correlation), energy predictions remained inaccurate. DFT shifts the complexity of the many-body wavefunction to another quantity, the electron density, which describes the spatial distribution of electrons in a system. It is proposed that the ground-state properties of a system, including the energy, can be determined from the electron density [20].

Fundamentally, DFT simulates a non-interacting system, the electron density of which matches that of the real system, thereby postulating that the ground state energy is also identical. The total energy of the system can then be broken down into several parts: kinetic energy, electron-nuclear attraction, electron-electron repulsion

and an additional term, the exchange-correlation energy, which accounts for the remaining quantum effects. **Equation 3.4** shows the total electron density of the system, using DFT:

$$E[\rho] = T_S[\rho] + V_{ext}[\rho] + V_H[\rho] + E_{xc}[\rho] \qquad (3.4)$$

Where T_S is the kinetic energy of non-interacting electrons, V_{ext} is the attraction between electrons and nuclei, V_H is the classical electron-electron repulsion calculated by the Hartree-Fock equation and E_{xc} is the exchange-correlation energy, which is an approximate error correction for the kinetic energy and electron-electron interaction.

The final term of the equation cannot be calculated exactly, however good approximations exist, such as the local (spin) density approximation (LDA) and the generalised gradient approximation (GGA).

3.2.1.2 Exchange-correlation functionals

The LDA is one of the earliest exchange-correlation functionals used in DFT. It assumes that the exchange-correlation energy at each point depends only on the local electron density, as in a uniform electron gas. While this provides a computationally efficient solution, it oversimplifies real systems by neglecting density gradients and long-range interactions. LDA tends to overestimate bond strengths and is best suited to systems with slowly varying densities.

GGA improves on LDA by considering the local electron density as well as its gradient. The density gradient is introduced into the calculations to account for the non-homogeneity of the real electron density. This reflects not only the electron density at a given point but also how the density varies from one point to another, allowing for more accurate calculations of complex systems [21].

3.2.1.3 Hybrid functionals

Hybrid functionals build upon GGA by incorporating a fraction of exact Hartree-Fock exchange, improving the description of electron correlation and charge transfer. This makes them especially useful in systems where long-range interactions or electronic excitation are important, such as in catalysis or organometallic chemistry. Popular examples include B3LYP and PBE0, which offer a good balance between accuracy and computational cost. Their semiempirical nature allows them to outperform pure GGA functionals in many practical applications [17].

3.2.1.4 Periodic and finite DFT

Two methods of DFT calculations are commonly used to gain insight into catalysed chemical reaction: periodic and finite. Periodic DFT is used generally for inorganic materials such as heterogeneous catalysts with systems composed of crystal structures, surfaces and extended materials. The technique employs periodic boundary conditions to account for the repetitive nature of the system. Conversely, organic molecular systems which operate in real space tend to use finite DFT. Finite DFT does not utilise periodic boundary conditions and is more suited to isolated molecules and solvated systems.

3.2.1.5 Basis sets

In DFT, basis sets are used to describe the electronic wavefunction. The choice of basis set significantly impacts computational accuracy and efficiency. The two main types are plane wave basis sets and localised basis sets. Plane wave basis sets employ delocalised functions that extend over the entire simulation cell, making them ideal for periodic systems such as crystals, surfaces and metals. Their size is controlled by an energy cutoff and they often require pseudopotentials to avoid explicit treatment of

core electrons. Plane waves systematically converge with increasing cutoff energy and do not suffer from basis set superposition error, but they are computationally expensive for non-periodic systems [22].

In contrast, localised basis sets, such as Gaussian-type orbitals, are centred around atoms and decay with distance, making them more efficient for isolated molecules and finite systems. They can introduce basis set error and do not naturally account for periodic boundary conditions. The larger and more accurate the basis set, the greater the computational expense, therefore, benchmarking must be conducted to identify the most balanced basis set to utilise in DFT calculations [22].

It is recommended that, for energy barrier calculation, at least triple-zeta quality (rather than double-zeta) basis sets are used [23]. “Zeta” refers to the number of basis functions used to represent each atomic orbital, with more functions correlating to better description of electron density details. Additional improvements can be made to any basis sets through the use of polarisation and/or diffuse functions. These additional functions are used to more accurately describe long-range electrostatic interactions. Without these terms, electron density is described as being concentrated around the atom nucleus, when in reality it is asymmetrically diffused a distance away from the nucleus. By introducing these terms, especially for heavier atoms, the electron density distribution becomes more flexible and long-range interactions become more accurate [24]. **Table 3.1** presents some of the most common functionals and basis sets, as well as their advantages and disadvantages [23,25,26]. Those included were selected based on their feasibility for use in this study as well as their frequent use in published work of similar systems [1,27,28].

Table 3.1. *Advantages and disadvantages of the common B3LYP and Minnesota functionals and their corresponding Pople and Ahlrich triple-zeta basis sets (F – Functional, BS – Basis set).*

F	Advantages	Disadvantages	BS	Advantages	Disadvantages
B3-LYP	Well-tested and widely used; Good for geometries and organics; Fast.	Poor for dispersion; Not ideal for transition metals; Inaccurate reaction energies.	**6-311G (d,p)**	Widely used; Built-in polarisation; Fast; Good for organics; Reasonable for energy barriers.	Poor for transition metals
M06	Accurate for transition metals; Includes some dispersion.	Slower convergence.	**Def2-TZVP**	Good for transition metals; Efficient.	Lacking in polarisation;
M06-2X	Very good for energy barriers; Accurate for non-covalent interactions.	Sensitive to basis set choice; Less suited to transition metals.	**Def2-TZVPP**	Better polarisation; Good for weak interactions; Good for transition metals.	Computationally expensive.

3.2.1.6 Solvation models

DFT calculations are carried out in the gas phase by default and so, in order to account for solvent effects within a molecular system, solvation models are required. Explicit solvent models, like those used in molecular dynamics (MD), are generally too computationally expensive to use in DFT calculations due to the large number of molecules which have to be modelled to simulate the solvated environment. DFT differs from MD in that it attempts to solve Schrodinger's equation for every atom within the system, whereas MD empirically determines interatomic interactions through predefined potential energy functions. To account for this, implicit solvation

models such as the polarisable continuum (PCM) and SMD have been designed. These models represent the solvent as a dielectric continuum surrounding the solute, rather than explicit molecules creating significant reductions in computational expense. Unlike PCM, where cavities are assumed to be rigid spheres, SMD cavities adjust dynamically based on the electron density of the solute, which is unevenly distributed around the nucleus. This allows for improved description of non-electrostatic effects [29].

3.2.1.7 Dispersion correction

Standard exchange-correlation functionals such as B3LYP and PBE rely on the effects of local electron density of atoms, meaning that weaker, long-range interactions such as van der Waals (vdW), π-π stacking and hydrogen bonding can be inaccurately described. To improve this, dispersion correction methods are commonly included. Empirical methods, such as Grimme's, which add a pairwise dispersion energy term to the DFT energy, are usually selected for molecular systems [30].

3.2.2 Application of DFT

Correctly parameterised DFT simulations are a powerful computational tool capable of providing valuable insights into the behaviour of molecules in a chemical system. In this work, four main forms of simulation are used: geometry optimisation, TS searching, frequency analysis and IRC.

3.2.2.1 Geometry optimisation

In order to calculate accurate ground-state energies for the system being investigated, it is important to ensure that the geometries are at their relative stationary points. A stationary point represents an energy minima along the potential energy

surface (PES), corresponding to an atom or molecule's most energetically stable configuration. To enable this, geometric optimisation is carried out.

During the optimisation process, self-consistent field (SCF) calculations are carried out on an initial guessed geometry to calculate the initial energy of the system. Next, the iterative optimisation process begins. The forces acting on each atom are computed and defined as the negative gradient of the total energy with respect to atomic positions, angles and dihedrals. These forces can be used as an indication of what geometric variations need to be made to reduce the total energy. The geometry is then update using the suggested variations from the force calculations and the total energy and forces are calculated once more. This process is repeated until the convergence criteria is met and the final geometry has been achieved. Convergence criteria is usually defined as a small maximum force or maximum energy change value [31].

3.2.2.2 Transition state searching

Unlike geometric optimisation, where global energy minima are sought, TS searching is the process of finding global energy maxima. Along the PES, TS's are critical points which represent the highest energy along the surface, known as saddle points. A saddle point is a point on the surface which is a minimum in one direction and a maximum in another. The down-sloped pathway connects the reactants and products, while all other pathways will increase the energy further.

There are a number of methods used for TS searching including the Structure Synchronous Transit-Guided Quasi-Newton Methods (QST2/QST3) and the Berny optimisation method. The key difference between them lies in the requirement of an additional guess TS structure in QST3 which helps constrain the interpolation process.

Following interpolation of the reactants and products, eigenvector following is carried out to refine the TS structure. These methods are useful when the reaction step is known but the TS structure is complex.

Conversely, the Berny method requires only a guess geometry of the TS structure. This method uses a gradient-based saddle-point search approach to locate a first-order saddle point which is then refined using force constants and nuclear gradients. Due to the use of direct optimisation instead of interpolation, TS is considered the most reliable approach, when applicable and is particularly useful when the reaction is complex and the products are unknown [31].

While this approach to TS location is effective and well-documented, it requires precise chemical knowledge of the target reaction and relies on a repetitive iterative process of testing and re-testing TSs until the pre-determined constraints are satisfied. These constraints can be based on a number of factors including the relative geometries of reactants and experimentally-verified energy barrier range, among others. Future TS prediction studies may make use of machine learning techniques, capable of creating high-level scans of PESs involving inputted reactants and products. Such methods are predicted to be significantly reduce both the time and computational expense of future DFT work, while increasing the throughput [32].

3.2.2.3 Frequency analysis

Frequency analysis of a system calculates the vibrational modes of a molecule based on its geometry. While it can provide physical insights such as IR spectra and thermodynamic properties, this work predominantly used it to indicate true minima and TSs.

Real frequencies, represented as positive numbers, indicate stable motions like stretching and bending. Alternatively, imaginary frequencies, shown as negative numbers, indicate unstable motions. Stable minima are confirmed through the presence of only real frequencies, indicating that the geometry is located at a PES minimum as any change in the geometry along the mode will increase in the energy of the system. Contrastingly, TSs are confirmed by the presence of a single imaginary (negative) frequency, as there is exactly one pathway along which the energy of the system will decrease, leading to the reactants and products [31].

3.2.2.4 IRC

Once TSs are confirmed by frequency analysis, an IRC calculation is carried out to follow the minimum energy path that connects the TS to the corresponding reactants and products. Following the downhill path, small geometric displacements are made which adhere to a continually decreasing energy [31].

This tool is essential for energy barrier calculation as it allows visual insights into the reaction mechanism while eliminating false TSs. Reactants and products are confirmed visually to ensure that the TS is associated to the intended chemical reaction.

3.2.3 Computational analysis techniques

There are a number of computational chemistry analysis tools which can provide mechanistic insight into a reaction. Quantification of the magnitude, nature and direction of intermolecular interactions is possible through the likes of NBO, QTAIM and RDG analyses, while electron distribution of individual atoms can be evaluated through population analysis, HOMO-LUMO energy gaps and bond order analysis.

3.2.3.1 Electrostatic potential

ESP analysis is a valuable tool for understanding intermolecular interactions in catalysis, particularly those driven by electrostatics such as hydrogen bonding, dipole-dipole interactions and ion pairing. ESP is derived directly from the spatial distribution of electron density and nuclear charges. It reflects the potential energy experienced by a positive test charge at various points around the molecule, offering a three-dimensional map of electrostatic influence [33].

This method provides a quantitative picture of how positive and negative regions are distributed around a molecule, often visualised as a color-coded surface: red indicating electron-rich (negative potential) areas and blue indicating electron-poor (positive potential) regions. ESP complements other analyses by highlighting areas of electrophilic or nucleophilic reactivity, aiding in the prediction of molecular interaction sites.

3.2.3.2 NBO

NBO analysis is another useful tool in evaluating intermolecular interactions in catalysis. Unlike QTAIM, which utilises the electron density, NBO focuses on localised bonding orbitals such as σ- and π- bonding, producing a Lewis-like representation of molecules. This is a more simplified outlook, which does not consider electrons to be delocalised, with them instead being described as localised bonds, lone pairs and antibonding [34]. While more simplistic, NBO can be related more easily to classical chemistry theories such as donor-acceptor interactions. Classical donor-acceptor interactions can be described and quantified through lone-pair - anti-bonding σ/π orbital (LP – BD*) interactions. These interactions have great relevance to catalytic systems, as the donation of electrons into anti-bonding orbitals

causes a weakening of existing bonds [35]. The main output of NBO analysis is the second-order perturbation energy, E(2), which quantifies the stabilisation energy arising from orbital interactions. It measures how much electron density is transferred from a donor orbital (e.g., a lone pair) to an acceptor orbital (anti-bonding orbital). A basic description of the concept of LP, σ- and π- bonding, and anti-bonding, as considered in NBO analysis, is shown in **Figure 3.6**.

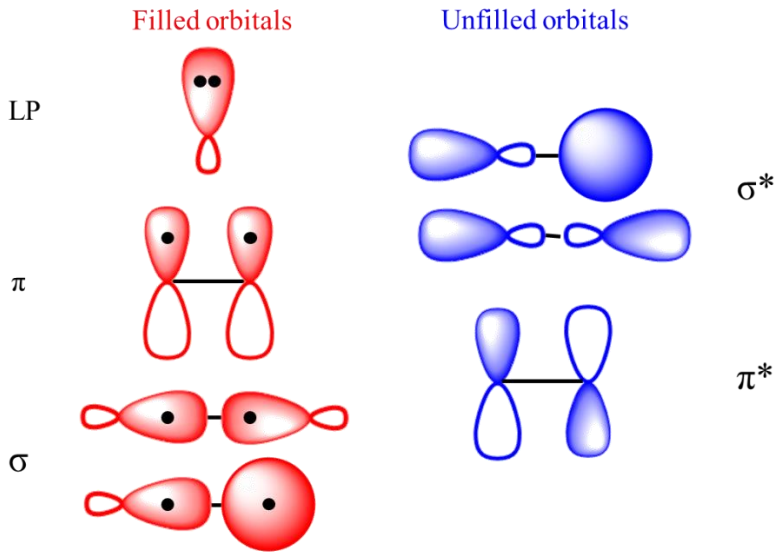

Figure 3.6. *Lewis-like description of molecular orbital overlap.*

3.2.3.3 QTAIM

QTAIM is a powerful topological analysis method used in DFT calculations to study electron density distributions in molecular systems. The technique identifies regions of significant electron density, known as critical points, which can be in the form of nuclear critical points at atomic centres, bond critical points (BCPs) between atoms, ring critical points in cyclic structures and cage critical points in three-dimensional frameworks. By analysing various parameters such as the electron density, Laplacian of electron density and the total energy density of BCPs,

interactions such as ionic, vdW and hydrogen bonding can be differentiated, allowing for a more specified analysis of intermolecular interactions.

While both QTAIM and NBO provide valuable insight into molecular interactions, QTAIM offers a more rigorous, model-independent analysis grounded in electron density. Unlike NBO, which simplifies bonding into localised orbitals, QTAIM can identify and quantify all types of interactions, including non-covalent and delocalised, through critical points in real space [36]. This makes QTAIM especially powerful for analysing weak interactions and complex bonding environments, such as those found in catalysis.

3.2.3.4 RDG analysis

RDG analysis is a computational method used to visualise and interpret non-covalent interactions in molecular systems. It is particularly useful for identifying weak interactions such as H-bonding, vdW and steric hindrance. By analysing the density distribution in molecular space, different types of non-covalent interactions can be distinguished from one another. It is typically presented as a scatter plot of RDG values against the electron density multiplied by the second eigenvalue of the Hessian matrix ($(\lambda_2)\rho$).

The eigenvalue of the Hessian matrix consists of second derivatives of electron density, with respect to spatial coordinates. It describes how the electron density changes in different directions, specifically whether they are attracted or repelled. Depending on a point's position on the plot, the nature of the interactions can be classified [37]. The relationships of position to interaction classification are shown in **Table 3.2**.

Table 3.2. *Relationship of RDG scatter plot to interaction type.*

$(\lambda_2)\rho$ value	Location on plot	Type of interaction
< 0	Left side	Hydrogen bonding, covalent
Near 0	Middle	Weak dispersion
> 0	Right side	Steric or Pauli repulsion

The scatter plot can then be compared with an isosurface, overlaid onto the molecular system, allowing for the most significant interactions to be classified.

3.2.3.5 Population analysis

Population analysis is a popular DFT approach used to estimate the distribution of electrons among atoms within a molecule. It is a valuable method as it provides atomic charges, bond orders and orbital populations which can help interpret reactivity, charge transfer and bonding interactions, helping to define reaction mechanisms and intermolecular interactions. There are a number of methods of population analysis including Mulliken and Hirshfeld however they are significantly basis set-dependent and in the case of Hirshfeld, tend to underestimate charge transfer. ADCH analysis improves on the Hirshfeld analysis by considering atomic dipole moments, making it more accurate for charged and highly polar systems [38]. This additional feature allows it to better represent polarisation effects and charge delocalisation, two attributes which are applicable to most catalytic systems.

3.2.3.6 HOMO-LUMO

The HOMO and LUMO are important concepts in molecular catalysis. The energy gap between the two orbitals can help determine a catalysts electronic properties, reactivity and stability. Generally, the smaller the energy gap, the more reactive a chemical species is, as electrons can transition between the two orbitals more

easily [39]. This reactivity is advantageous for catalysis as the molecule is more likely to partake in electron transfer. The LUMO energy is significantly reduced by properties such as delocalisation of electrons, π-systems and aromatic rings as the electrons are more spread out. However, the presence of a transition metal can further reduce this energy due to the partially-filled d-orbital electrons which can combine with the orbitals of a bonded ligand through ligand-field effects [40]. This reduction in LUMO energy creates a smaller energy gap, highlighting the importance of transition metals in chemical catalysis.

3.2.3.7 Bond order analysis

In classical chemistry, positive integers are commonly used to describe the strength and character of bonds (e.g. 1=single bond, 2=double bond). However, in DFT, these values present as continuous numbers, reflecting partial bonding and relative strength. Electron density data between two bonding, or non-bonding, atoms can be exported and used to estimate the bond strength. While the values will generally follow the same trend as the classical definitions, they are more useful for qualitative analysis of changing bond strengths which can help elucidate reaction mechanisms.

A common approach to bond order analysis is through the overlap population matrix, which describes the extent to which the orbitals of two atoms overlap. Fuzzy bond order however, a certain type of bond order analysis which uses real-space electron density rather than orbital overlap, can be particularly helpful in understanding catalyst coordination chemistry, without suffering from basis set error like the other methods [41]. That it is less sensitive to the choice of basis set is a major advantage when working with large molecular systems, where the use of large, highly-accurate basis sets is not feasible.

3.2.4 Characterisation techniques

A number of experimental characterisation techniques were utilised to validate the synthesis of the IL catalysts, as well as to confirm the attachment of ILs to the surface of the BC. The intermediate and final degradation products were also identified *via* various methods.

3.2.4.1 FT-IR

FT-IR is a non-destructive technique used to identify functional groups present in chemical compounds. When IR radiation is passed through a material, a portion of the radiation is absorbed by the sample, while some is allowed to pass through. Each peak in the IR spectrum is representative of a specific excitation of vibrational mode dependent on the molecules within the sample, allowing for the identification of functional groups [42].

Attenuated total reflectance (ATR) FT-IR is the most common technique, although there are others including transmission and diffuse reflectance. In ATR sampling, IR light passes through a high refractive index crystal, such as diamond, ZnSe or Ge, achieving full internal reflection upon impact with the end of the crystal. The sample is placed on the crystal at this internal reflection site and absorbs a proportion of the light, known as the evanescent wave, through molecular bonds at specific IR frequencies. The process is shown in **Figure 3.7**.

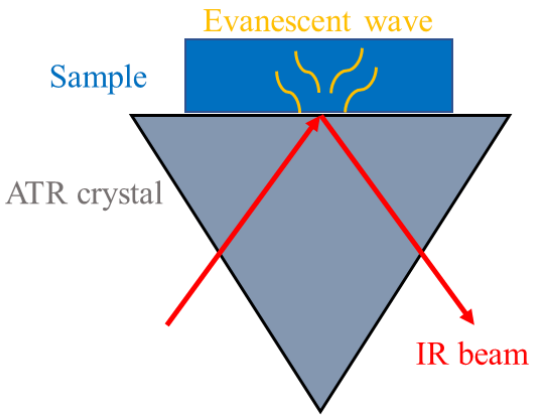

Figure 3.7. *Mechanism of ATR FT-IR.*

During the PET degradation process, the polymer backbone is cleaved, resulting in changes in the concentrations of certain functional groups and therefore, too, the FT-IR spectra. In the spectrum of the desired monomer, BHET, the hydroxyl and alkyl group peaks should be more prominent than in PET and any longer-chain oligomers. It is worth noting that, due to the similarities in functional groups, dimers will appear with only subtle differences to the peaks when compared with BHET. The key difference will be in the peak intensity of the hydroxyl group, as BHET has two free OH groups per unit, whereas longer chains have fewer free hydroxyls per mass. Therefore, BHET will have a much more intense peak at the corresponding wavenumbers.

In ATR FT-IR analysis of BC, sloping baselines are frequently observed due to the material's carbon black-like optical properties. BC, particularly when produced at high pyrolysis temperatures, contains extensive amorphous and aromatic carbon domains that exhibit strong, broad band IR absorption. This non-specific absorption leads to a gradual decrease in baseline intensity across the spectrum, especially in the fingerprint region (2000–500 cm^{-1}). Additionally, the internal reflection mechanism of ATR causes an evanescent IR wave to interact with the sample surface, and the high

refractive index and dispersive behaviour of carbon-rich BC can distort the effective penetration of the IR light. These effects contribute to baseline sloping and can complicate the interpretation of functional group signals [43,44]. Despite these drawbacks, subtle changes in spectra can still be used to indicate the presence of surface-bound molecules.

3.2.4.2 Raman spectroscopy

Similar to FT-IR, Raman spectroscopy is also a non-destructive technique used to study the vibrational, rotational and other low-frequency modes of molecules. When monochromatic light, typically from a laser source, is directed onto a material, most of the light is elastically scattered (Rayleigh scattering) without a change in wavelength. However, a small fraction of the light undergoes inelastic scattering, known as Raman scattering, where the scattered photons have either gained or lost energy corresponding to specific molecular vibrations [45]. The resulting Raman spectrum consists of peaks that represent these vibrational energy shifts, allowing detailed information about molecular bonds, functional groups and crystal structures to be obtained. The Raman scattering process is detailed in **Figure 3.8**.

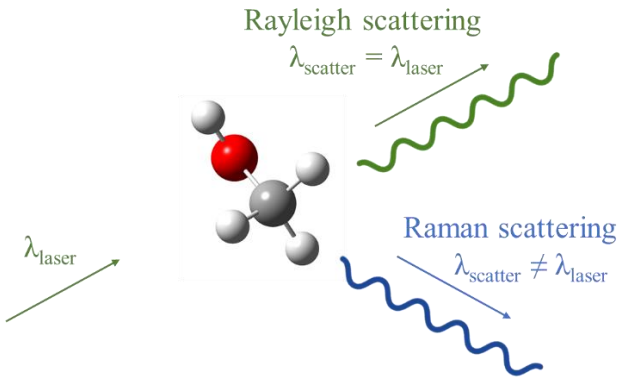

Figure 3.8. *Raman scattering and spectroscopy.*

Unlike FT-IR spectroscopy, which relies on changes in dipole moment, Raman scattering is sensitive to changes in the polarisability of molecular bonds. This difference makes Raman spectroscopy particularly complementary to FT-IR and especially useful for studying compounds with symmetric, non-polar bonds that may be weak or invisible in IR spectra [46]. Additionally, Raman is very well suited to the characterisation of carbon-based samples, showing sensitivity to the presence of both sp^2 and sp^3 hybridisation, while distinguishing between graphitic and amorphous carbon [47]. The sloping baseline effect, seen in ATR FT-IR spectra of black carbon samples, do not appear in Raman spectra of the same samples as the high refractive index does not have as significant a role.

3.2.4.3 Karl Fischer titration

KF titration is a method of titration used to quantify the presence of water in a sample, using two different approaches: volumetric and coulometric. The principle theory is based on the oxidation of sulphur dioxide by iodine in an alcohol-base solution (shown in **Equation 3.5**).

$$H_2O + I_2 + SO_2 + 2RN \rightarrow 2RNHI + RNSO_3 \qquad (3.5)$$

Where RN is an organic base.

The reaction only takes place when there is moisture present. In the volumetric method, the sample is mixed with the KF reagent (SO_2, iodine, a base and methanol) inside the vessel. An iodine-containing KF titrant is then added to the vessel, reacting with water in the sample. The process ends when all the water has reacted and free iodine accumulates, at which point the water content is calculated from the volume of titrant added and its water equivalence factor (mg/mL) [48]. This can be converted to a ppm value relative to the controlled amount of solvent inputted into the system. The

coulometric approach follows the same basic principle, differing only in respect to the addition of iodine to the vessel. Instead of being added manually through a titrant, iodine is electrochemically generated from iodide ions present in the original reagent. Volumetric KF titration is more often used for higher water content liquid samples, while the coulometric approach is advantageous for very dry samples such as powders.

3.2.4.4 NMR

NMR spectroscopy is an analytical technique used to determine the structure of organic molecules by probing the local magnetic environment of atomic nuclei. When a sample is placed in a strong magnetic field and exposed to radiofrequency radiation, certain nuclei absorb energy and shift between spin states. As they return to their original state, they release this energy which is detected by the NMR machine (**Figure 3.9**). The exact frequency at which this occurs is highly sensitive to the chemical surroundings of each nucleus, making NMR a highly informative tool for identifying molecular structure [49].

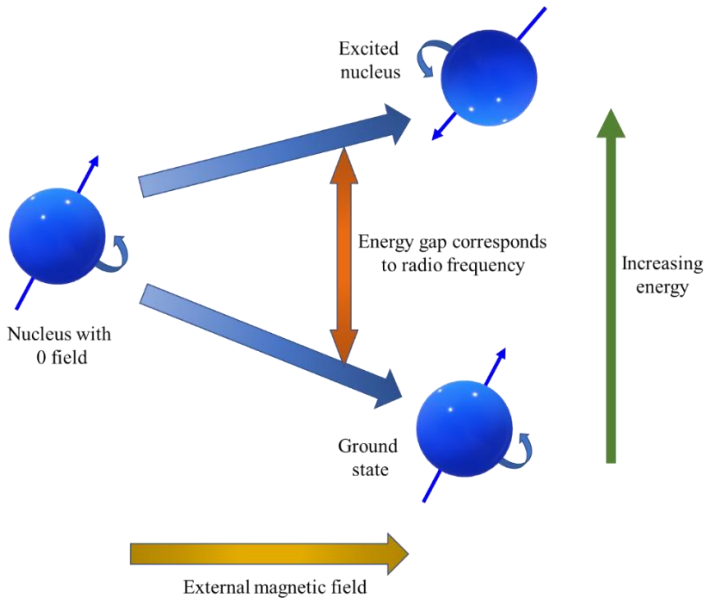

Figure 3.9. *Radiofrequency-induced excitement and precession of ground-state nuclei.*

In relation to PET glycolysis, NMR spectroscopy can be a powerful supplement to FT-IR analysis of BHET. While FT-IR can provide very valuable information regarding the presence of certain functional groups, complex product mixtures can create broad signal overlap of similarly structure molecules. Contrastingly, NMR confirms the full molecular structure by showing how atoms are bonded, while the relative intensities of certain can be utilised to distinguish between monomers, dimers and longer chain oligomers. Combining the two methods can provide a clear picture of both the molecular structure and purity of complex product mixtures.

References

[1] Y. Liu, X. Yao, H. Yao, Q. Zhou, J. Xin, X. Lu, S. Zhang, Degradation of poly(ethylene terephthalate) catalyzed by metal-free choline-based ionic liquids, Green Chem. 22 (2020) 3122–3131. https://doi.org/10.1039/d0gc00327a.

[2] Q. Wang, Y. Geng, X. Lu, S. Zhang, First-row transition metal-containing ionic liquids as highly active catalysts for the glycolysis of poly(ethylene terephthalate) (PET), ACS Sustain Chem Eng 3 (2015) 340–348. https://doi.org/10.1021/sc5007522.

[3] S. Najafi-Shoa, M. Barikani, M. Ehsani, M. Ghaffari, Cobalt-based ionic liquid grafted on graphene as a heterogeneous catalyst for poly (ethylene terephthalate) glycolysis, Polym Degrad Stab 192 (2021) 109691. https://doi.org/10.1016/j.polymdegradstab.2021.109691.

[4] Z. Ju, W. Xiao, X. Lu, X. Liu, X. Yao, X. Zhang, S. Zhang, Theoretical studies on glycolysis of poly(ethylene terephthalate) in ionic liquids, RSC Adv 8 (2018) 8209–8219. https://doi.org/10.1039/c7ra13173a.

[5] X. Wei, J. Qiu, H. Wang, W. Zheng, W. Sun, L. Zhao, Efficient glycolysis of Poly(ethylene terephthalate) to bis(hydroxyethyl) terephthalate catalyzed by non-metallic deep eutectic solvent, Chem. Eng. J. 508 (2025). https://doi.org/10.1016/j.cej.2025.161115.

[6] T. Lu, F. Chen, Multiwfn: A multifunctional wavefunction analyzer, J Comput Chem 33 (2012) 580–592. https://doi.org/10.1002/jcc.22885.

[7] J.A. Agwupuye, H. Louis, T.O. Unimuke, P. David, E.I. Ubana, Y.L. Moshood, Electronic structure investigation of the stability, reactivity, NBO analysis, thermodynamics, and the nature of the interactions in methyl-substituted imidazolium-based ionic liquids, J Mol Liq 337 (2021). https://doi.org/10.1016/j.molliq.2021.116458.

[8] P.A. Hunt, C.R. Ashworth, R.P. Matthews, Hydrogen bonding in ionic liquids, Chem Soc Rev 44 (2015) 1257–1288. https://doi.org/10.1039/c4cs00278d.

[9] A. Ngambia, O. Mašek, V. Erastova, Development of biochar molecular models with controlled porosity, Biomass Bioenergy 184 (2024). https://doi.org/10.1016/j.biombioe.2024.107199.

[10] H. Bamdad, S. Papari, S. MacQuarrie, K. Hawboldt, Study of surface heterogeneity and nitrogen functionalizing of biochars: Molecular modeling approach, Carbon 171 (2021) 161–170. https://doi.org/10.1016/j.carbon.2020.08.062.

[11] R. Wood, O. Mašek, V. Erastova, Developing a molecular-level understanding of biochar materials using public characterization data, Cell Rep Phys Sci 5 (2024). https://doi.org/10.1016/j.xcrp.2024.102036.

[12] D. López Barreiro, F.J. Martin-Martinez, C. Torri, W. Prins, M.J. Buehler, Molecular characterization and atomistic model of biocrude oils from hydrothermal

liquefaction of microalgae, Algal Res 35 (2018) 262–273. https://doi.org/10.1016/j.algal.2018.08.034.

[13] S. Farah, K.R. Kunduru, A. Basu, A.J. Domb, Molecular weight determination of polyethylene terephthalate, in: poly(ethylene terephthalate) based blends, Compos. Nanocompos., Elsevier Inc., 2015: pp. 143–165. https://doi.org/10.1016/B978-0-323-31306-3.00008-7.

[14] W. Zheng, C. Liu, X. Wei, W. Sun, L. Zhao, Molecular-level swelling behaviors of poly (ethylene terephthalate) glycolysis using ionic liquids as catalyst, Chem Eng Sci 267 (2023). https://doi.org/10.1016/j.ces.2022.118329.

[15] A.M. Al-Sabagh, F.Z. Yehia, A.M.M.F. Eissa, M.E. Moustafa, G. Eshaq, A.R.M. Rabie, A.E. Elmetwally, Glycolysis of poly(ethylene terephthalate) catalyzed by the Lewis base ionic liquid [Bmim][OAc], Ind Eng Chem Res 53 (2014) 18443–18451. https://doi.org/10.1021/ie503677w.

[16] E. Schrodinger, An Undulatory Theory of the Mechanics of Atoms and Molecules, Phys. Rev. 28 (1926). https://doi.org/10.1103/PhysRev.28.1049

[17] W. Koch, M.C. Holthausen, A chemist's guide to density functional theory, 2nd ed., Wiley, 2001. https://doi.org/10.1002/3527600043.

[18] M. Born, R. Oppenheimer, Zur Quantentheorie der Molekeln, Ann Phys 389 (1927) 457–484. https://doi.org/10.1002/andp.19273892002.

[19] J.C. Slater, A simplification of the Hartree-Fock method, Phys. Rev. 81 (1951) 385–390. https://doi.org/doi.org/10.1103/PhysRev.81.385.

[20] R.O. Jones, Density functional theory: Its origins, rise to prominence, and future, Rev Mod Phys 87 (2015). https://doi.org/10.1103/RevModPhys.87.897.

[21] A.D. Becke, Density-functional thermochemistry. III. The role of exact exchange, J Chem Phys 98 (1993) 5648–5652. https://doi.org/10.1063/1.464913.

[22] S. Tosoni, C. Tuma, J. Sauer, B. Civalleri, P. Ugliengo, A comparison between plane wave and Gaussian-type orbital basis sets for hydrogen bonded systems: Formic acid as a test case, J. Chem. Phys. 127 (2007). https://doi.org/10.1063/1.2790019.

[23] M. Bursch, J.-M. Mewes, A. Hansen, S. Grimme, Best-practice DFT protocols for basic molecular computational chemistry**, Angew. Chem. Int. Ed. (61) (2022). https://doi.org/10.26434/chemrxiv-2022-n304h.

[24] C.E. Check, T.O. Faust, J.M. Bailey, B.J. Wright, T.M. Gilbert, L.S. Sunderlin, Addition of polarization and diffuse functions to the LANL2DZ basis set for P-block elements, J. Phys. Chem. A 105 (2001) 8111–8116. https://doi.org/10.1021/jp011945l.

[25] L. Goerigk, S. Grimme, A thorough benchmark of density functional methods for general main group thermochemistry, kinetics, and noncovalent interactions, Phys. Chem. Chem. Phys. 13 (2011) 6670–6688. https://doi.org/10.1039/c0cp02984j.

[26] K.N. Kirschner, D. Reith, W. Heiden, The performance of Dunning, Jensen, and Karlsruhe basis sets on computing relative energies and geometries, Soft Mater 18 (2020) 200–214. https://doi.org/10.1080/1539445X.2020.1714656.

[27] Z. Ju, L. Zhou, X. Lu, Y. Li, X. Yao, S. Cheng, G. Chen, C. Ge, Mechanistic insight into the roles of anions and cations in the degradation of poly(ethylene terephthalate) catalyzed by ionic liquids, Phys. Chem. Chem. Phys. 23 (2021) 18659–18668. https://doi.org/10.1039/d1cp02038b.

[28] H. Yao, X. Lu, L. Ji, X. Tan, S. Zhang, Multiple hydrogen bonds promote the nonmetallic degradation process of polyethylene terephthalate with an amino acid

ionic liquid catalyst, Ind Eng Chem Res 60 (2021) 4180–4188. https://doi.org/10.1021/acs.iecr.0c06073.

[29] S.C. Liu, X.R. Zhu, D.Y. Liu, D.C. Fang, DFT calculations in solution systems: solvation energy, dispersion energy and entropy, Phys. Chem. Chem. Phys. 25 (2022) 913–931. https://doi.org/10.1039/d2cp04720a.

[30] S. Grimme, M. Steinmetz, Effects of London dispersion correction in density functional theory on the structures of organic molecules in the gas phase, Phys. Chem. Chem. Phys. 15 (2013) 16031–16042. https://doi.org/10.1039/c3cp52293h.

[31] J.B. Foresman, Æ. Frisch, Exploring chemistry with electronic structure methods, Gaussian, Inc., Wallingford, CT, 2015.

[32] S. Choi, Prediction of transition state structures of gas-phase chemical reactions via machine learning, Nat Commun 14 (2023). https://doi.org/10.1038/s41467-023-36823-3.

[33] M. Orozco, F.J. Luque, Generalization of the molecular electrostatic potential for the study of noncovalent interactions, in: 1996: pp. 181–218. https://doi.org/10.1016/S1380-7323(96)80044-6.

[34] F. Weinhold, Natural bond orbital analysis: A critical overview of relationships to alternative bonding perspectives, J Comput Chem 33 (2012) 2363–2379. https://doi.org/10.1002/jcc.23060.

[35] Y. Jean, F. Volatron, J. Burdett, An introduction to molecular orbitals, Oxford University Press, Inc., New York, 1993.

[36] F. Cortés-Guzmán, J.I. Rodríguez, J.S.M. Anderson, Introduction to QTAIM and beyond, in: Advances in Quantum Chemical Topology Beyond QTAIM, Elsevier, 2022: pp. 1–19. https://doi.org/10.1016/B978-0-323-90891-7.00021-9.

[37] G. Saleh, C. Gatti, L. Lo Presti, Non-covalent interaction via the reduced density gradient: Independent atom model vs experimental multipolar electron densities, Comput Theor Chem 998 (2012) 148–163. https://doi.org/10.1016/j.comptc.2012.07.014.

[38] Y. Zhao, M. Pan, X. Kang, W. Tu, H. Gao, X. Zhang, Gas separation by ionic liquids: A theoretical study, Chem Eng Sci 189 (2018) 43–55. https://doi.org/10.1016/j.ces.2018.05.044.

[39] R. Rijal, H.P. Lamichhane, K. Pudasainee, Molecular structure, homo-lumo analysis and vibrational spectroscopy of the cancer healing pro-drug temozolomide based on dft calculations, AIMS Biophys 9 (2022) 208–220. https://doi.org/10.3934/biophy.2022018.

[40] J.H. Cho, C. Lee, S.H. Hong, H.Y. Jang, S. Back, M. gi Seo, M. Lee, H.K. Min, Y. Choi, Y.J. Jang, S.H. Ahn, H.W. Jang, S.Y. Kim, Transition metal ion doping on ZIF-8 enhances the electrochemical CO2 reduction reaction, Adv. Mater. 35 (2023). https://doi.org/10.1002/adma.202208224.

[41] I. Mayer, P. Salvador, Overlap populations, bond orders and valences for “fuzzy” atoms, Chem Phys Lett 383 (2004) 368–375. https://doi.org/10.1016/j.cplett.2003.11.048.

[42] A.A. Ismail, F.R. van de Voort, J. Sedman, Chapter 4 Fourier transform infrared spectroscopy: Principles and applications, Tech. Instrum. Anal. Chem. 18 (1997) 93–139. https://doi.org/10.1016/S0167-9244(97)80013-3.

[43] Thermo Scientific, Carbon Black Analysis using FT-IR with Germanium and Diamond ATR, 2013. www.thermoscientific.com.

[44] Specac, ATR Crystal Choice and Quest Puck Guide, n.d. www.specac.com (accessed July 1, 2025).

[45] M.L. Zambrano-Zaragoza, D. Quintanar-Guerrero, R.M. González-Reza, Nanocontainers in food preservation: Techniques and uses, in: Smart Nanocontainers: Micro and Nano Technologies, Elsevier, 2019: pp. 137–155. https://doi.org/10.1016/B978-0-12-816770-0.00009-5.

[46] J. Thomas, P. Buzzini, G. Massonnet, B. Reedy, C. Roux, Raman spectroscopy and the forensic analysis of black/grey and blue cotton fibres: Part 1. Investigation of the effects of varying laser wavelength, Forensic Sci Int 152 (2005) 189–197. https://doi.org/10.1016/j.forsciint.2004.08.009.

[47] J. Xu, J. Liu, P. Ling, X. Zhang, K. Xu, L. He, Y. Wang, S. Su, S. Hu, J. Xiang, Raman spectroscopy of biochar from the pyrolysis of three typical Chinese biomasses: A novel method for rapidly evaluating the biochar property, Energy 202 (2020). https://doi.org/10.1016/j.energy.2020.117644.

[48] P. Rivera-Quintero, G.S. Patience, N.A. Patience, D.C. Boffito, X. Banquy, D. Schieppati, Experimental methods in chemical engineering: Karl Fischer titration, Can. J. Chem. Eng. 102 (2024) 2980–2997. https://doi.org/10.1002/cjce.25295.

[49] M. Kaliva, M. Vamvakaki, Nanomaterials characterization, in: Polymer Science and Nanotechnology: Fundamentals and Applications, Elsevier, 2020: pp. 401–433. https://doi.org/10.1016/B978-0-12-816806-6.00017-0.

Chapter 4
Computational and Experimental Evaluation of IL-catalysed PET Glycolysis

This chapter contains a comparison of various ionic liquids (ILs) as catalysts for PET glycolysis. The process involves the chemical depolymerisation of the PET chain to its monomer bis(2-hydroxyethyl) terephthalate (BHET), using ethylene glycol (EG) as a nucleophile. The reaction is outlined in **Figure 4.1**.

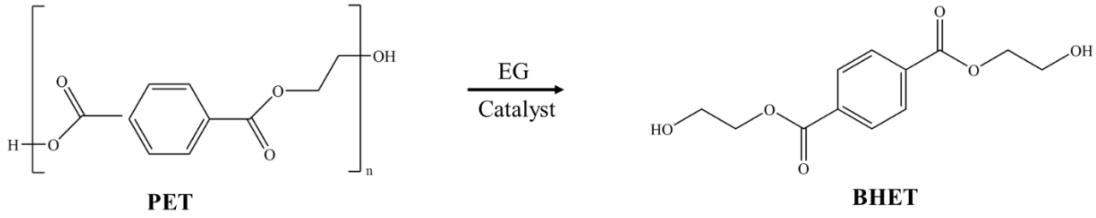

Figure 4.1. *General PET glycolysis reaction scheme.*

First, density functional theory (DFT) was used to screen potential ILs through energy barrier calculations. The best-performing catalysts were then selected for experimental investigation. The synthesis of IL catalysts and the results of the PET glycolysis (including PET conversion and BHET yield) are described. Experimental characterisation including Fourier-transform infrared (FT-IR), nuclear magnetic resonance (NMR) and Raman spectroscopy was performed to validate the catalysts

and the desired monomer, BHET. Finally, BHET yields were evaluated and compared with literature results.

4.1 Methodology

4.1.1 Selection of software package, functionals and basis sets

For its' reliability in modelling finite reactive systems, the Gaussian 16 package was selected to replicate the uncatalysed and IL-catalysed PET glycolysis systems [1]. Due to the liquid phase nature of the reaction and disorder of the catalysts, periodic simulations were not required. Selecting methods and basis sets for DFT modelling is a balance between computational expense and accuracy. There are several families of basis sets which were considered for use including Pople, Ahlrich and correlation-consistent (cc). The cc family is well-known to be extremely accurate for organic molecular systems, however it is highly expensive for medium- to large-sized systems. Only triple-zeta basis sets were considered as being sufficiently accurate for energy barrier calculation, in combination with two functionals: B3LYP and M06 . The former is very commonly used in literature and is geometrically accurate but is known to suffer from its inability to describe dispersion effects and transition metals. Conversely, the latter is much more electronically accurate but suffers from slow convergence.

Benchmarking was carried out to determine the most appropriate DFT method to use, based on the balance of electronic accuracy and computational expense. Reference energies were calculated using the coupled-cluster method, CCSD(T), widely regarded as the gold standard of DFT modelling due to its proven accuracy [2]. A number of combinations of M06 and B3LYP with different Pople and Ahlrich basis sets were tested, with the deviation of energies from the CCSD(T)-calculated values shown in **Figure 4.2**.

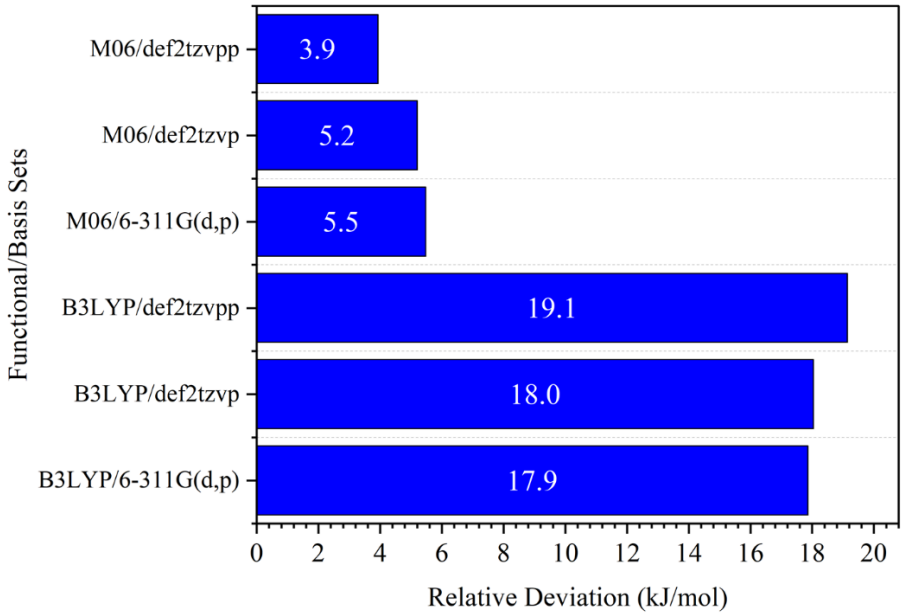

Figure 4.2. *Benchmarking of different functionals/basis sets, based on the deviation from the energy of an EG molecule calculated using CCSD(T).*

The results show an expected trend, that the M06 functional clearly outperforms B3LYP in terms of accuracy. Between basis sets (Def2TZVPP, Def2TZVP, 6-311G(d,p)) there is little difference and the energy differences may fall within error ranges. Although M06/Def2TZVPP shows the lowest deviation from CCSD(T), geometry optimizations at this level take a substantially longer time. Conversely, B3LYP/6-311G(d,p) provides a significantly more manageable computational cost, despite more significant deviation from the benchmark. While the deviation is larger, the error is assumed to be systematic, meaning that relative energy differences and overall trends remain reliable even if the absolute values are shifted. To compare the computational expense of triple-zeta Pople and Ahlrich basis sets, the simplest system modelled in this study (PET dimer and EG) was geometrically optimised to the same degree of convergence (**Table 4.1**). Both optimisations began from an identical geometry and run using the maximum number of compute processing

unit cores available, 40. To enhance the functionals' ability to model dispersion effects, a dispersion correction, D3, was applied.

Table 4.1. *Comparison of time taken for geometric optimisation of PET-EG system using B3LYP-D3/6-311G(d,p) and M06/Def2TZVPP.*

PET+EG Optimisation	
Method	Time to optimise (hrs)
B3LYP/6-311G(d,p)	12
M06/Def2TZVPP	144

From the results it can be seen that the B3LYP/6-311G(d,p) runs significantly faster than M06/Def2TZVPP for this calculation. The simple system contained just 11 atoms, while the largest IL-catalysed system used in this study contains 119 atoms, meaning large basis sets such as Def2tzvpp were considered to be not time-efficient. Therefore, due to the large through-put of DFT modelling required, B3LYP/6-311G(d,p), with an empirical dispersion term included, was selected for all remaining DFT calculations. Additionally, it has been used very recently to model similar systems [3–5]. A comprehensive review of a number of functionals and basis sets found that B3LYP performed generally well for energy barrier heights and other basic properties but poorly for reaction energies [6]. As the focus of the work is to compare energy barriers and explore reaction mechanisms, with less focus on the Gibb's free energy of reaction, this was considered a reasonable compromise. Therefore, while it is acknowledged that B3LYP/6-311G(d,p) has multiple shortcomings in its description of molecular systems, its use for examining qualitative trends in energy barriers and relative interaction strengths is justified. In order to more accurately describe the metal centre of the $CoCl_4$ anion, an effective core potential (ECP) basis set was used, in combination with 6-311G(d,p). ECPs are required for transition metal models, as they

model the inner core electrons as non-variable potentials, as opposed to explicitly calculating the energy of each one. This saves huge amounts of computational expense, while also improving accuracy, as "all-electron" basis sets tend to ill-describe relativistic effects, which occur due to the much larger size of metal atoms, compared with non-metal ones. The commonly used LANL2DZ, a double-zeta ECP basis set was selected to describe the energies of cobalt in all the calculations herein [7]. From herein, B3LYP-D3/6-311G(d,p) was used for all DFT modelling of non-metal atoms, while LANL2DZ was used for metals.

4.1.2 Computational details

Once the DFT method was finalised, all geometry optimisations, vibrational frequency calculations, transition state (TS) searching and intrinsic reaction coordinate (IRC) calculations were carried out at the same level: B3LYP/6-311G(d,p). To enhance the accuracy of non-covalent interaction description, a dispersion correction term, DFT-D3 by Grimme et al. [8], was included in all calculations. Solvation effects were considered by performing single-point energy calculations using the SMD model to replicate the EG solvent environment [9]. Reactants and products were optimised without constraints, and vibrational frequencies calculations were performed to ensure a true minimum had been achieved for these structures. TSs were identified using the same level of theory and vibrational frequencies were determined to ensure one imaginary frequency. IRC calculations were conducted to verify that the identified TS corresponded to the intended reactants and products. The activation energy (E_a) was then determined using **Equation 4.1**:

$$E_a = E_{TS} - E_R \tag{4.1}$$

Where E_R and E_{TS} represent the electronic energies of the reactants and transition state, respectively.

4.1.3 Experimental details

Based on DFT screening, the two best-performing ILs were selected for experimental study and synthesised using the methods outlined in **Chapter 3**. Active parameters were chosen by consulting the literature. Reaction time, temperature and catalyst weight were to be varied, while PET:EG ratio, rate of stirring and particle size were kept constant as far as reasonably practical. PET particle size was slightly variable, but always less than 10 mm, based on manufacturing values. **Table 4.2** displays the reaction scenarios tested for each IL catalyst. Ranges of parameter values for each catalyst were selected from literature.

Table 4.2. *Scenarios for experiments (* indicates where the calculated optimal parameter values were used).*

Run	Temperature (°C)	Catalyst:PET:EG ratio (w/w)	Reaction time (mins)
1	190	0.1:1:4	60
2	190	0.1:1:4	120
3	190	0.1:1:4	180
4	190	0.1:1:4	240
5	170	0.1:1:4	*
6	180	0.1:1:4	*
7	200	0.1:1:4	*
8	210	0.1:1:4	*
9	*	0.05:1:4	*
10	*	0.15:1:4	*

ATR-FT-IR spectroscopy was performed on synthesised catalysts, raw PET, intermediates, and main product using an ABB M83000 Spectrometer. A total of 32 scans were taken, with spectra recorded at 7 cm^{-1} intervals, covering a range of 4000-400 cm^{-1}. Synthesised ILs were also characterised using Raman spectroscopy performed using a LabRAM HR system, with a Ventus 532 nm laser used to collect

spectra over a wavenumber range of 100 cm^{-1} to 3500 cm^{-1}. The main degradation product was analysed by ^{1}H NMR (Bruker AVIII 400 MHz) in a deuterated dimethyl sulfoxide (DMSO-d_6) solvent.

4.2 Modelling of IL-catalysed PET glycolysis

4.2.1 Optimal conformations of catalysts and reactants

Potential configurations of the modelled catalysts and reactants are proposed through data from literature and chemical intuition. While this approach is not exhaustive, reasonable assumptions of initial configurations prior to optimisation do give a clear picture of the geometric positioning of atoms. To represent the PET polymer structure, with reasonable computational expense, a BHET dimer connected by C-O linkages was selected, as in the literature [10]. It is assumed that by isolating the C-O linkages, the general reaction mechanism is well represented by this structure. Several conformational isomers were tested by varying the cis/trans orientation of adjacent ester groups, either side of the benzene rings. The relative energies of each conformer, to that of the optimal one, are shown in **Figure 4.3**.

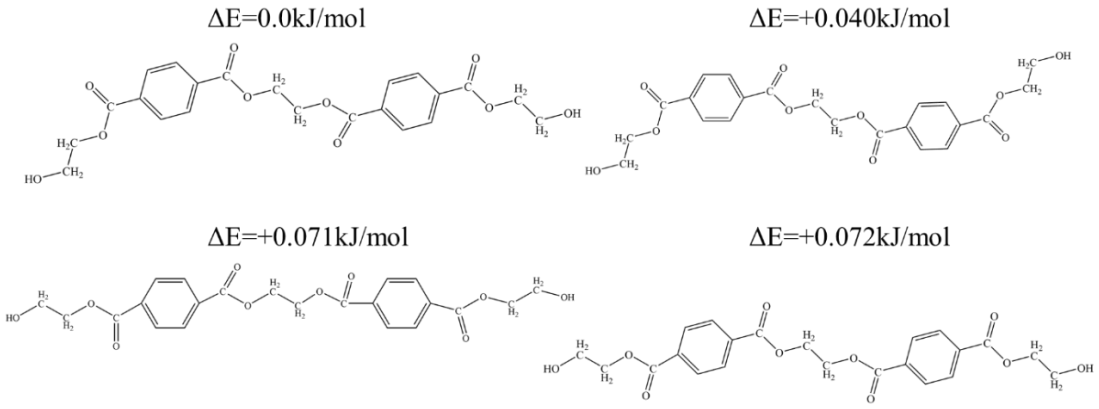

Figure 4.3. *Relative energies of PET dimer conformers.*

Following geometric optimisation of each conformational isomer, the free energies of the molecules were compared. Considering the dimer as two pairs of ester

groups, the DFT results demonstrate that the optimal configuration of the PET dimer features a cis then trans orientation of the paired groups. It should be noted that differences between the conformers are minimal. The electrostatic potential (ESP) of each reactant and catalyst was calculated using DFT and presented in **Figure 4.4**, allowing for the reactive site of each molecule to be predicted. The red and blue regions represent nucleophilic and electrophilic regions of the molecules, respectively, hence the distinct colourations of the anions and cations. In PET dimer and EG, the nucleophilic and electrophilic regions are mostly contained around the carbonyl and hydroxyl groups, the active sites for the reaction. For the bmim cation, the positive charge is centred around the aromatic ring, with the C-H bond located adjacent to the nitrogen atoms being the most electrophilic area of the molecule. In the case of the Ch ion, the positive charge is delocalised through the molecule, due to the polarity of the end chain hydroxyl group. The organic anions, For and OAc, show a highly polar ESP map, with the negative charge localised around the carboxylate group. Conversely, the symmetry of the tetrahedral $CoCl_4$ shows less polarity between the positive Co atom and chloride ions.

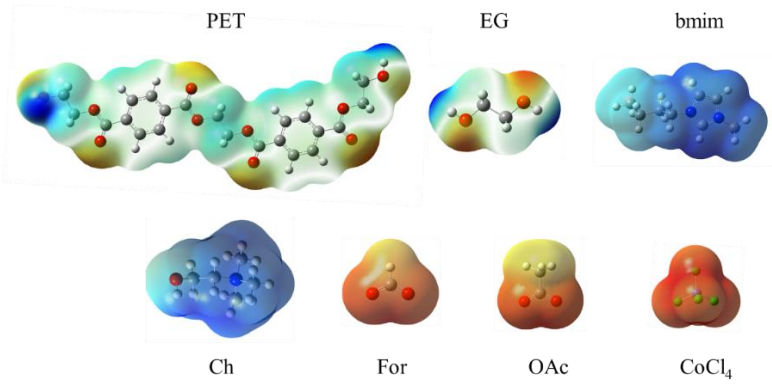

Figure 4.4. *ESP map of each modelled reactant and catalyst. Red represents the maximum ESP and blue the minimum. Atom colour code: Red – O, white – H, grey – C, dark blue – N, light blue – Co and green – Cl.*

Similar to the PET dimer, the IL catalysts had to be optimised prior to TS searching. For each IL, various conformers were tested based on estimated initial configurations taken from previous studies of ILs, as well as the ESP results [11–13]. For the imidazolium-based ILs, numerous conformers were tested (**Figure 4.5**). For the simplest IL, [bmim]Cl, the imidazolium cation forms an anti-anti butyl chain configuration [14]. When combined with the chloride ion, it was found that the optimal site for the anion was situated near to and in the same plane as the carbon located between nitrogen atoms within the imidazolium ring. As this is the most highly positive region of the molecule, due to the partially protonated nitrogen atoms, it is evident that electrostatic interactions are dominating.

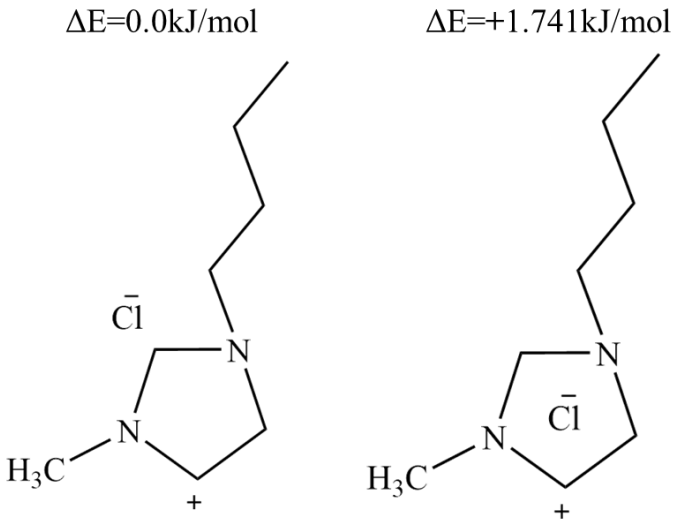

Figure 4.5. *Relative energies of [bmim]Cl conformers.*

Similarly, the primary ionic interactions within $[bmim]_2[CoCl_4]$ occur around the protonated imidazolium ring which also interacts through strong H-bonding with the chlorine atoms of the chlorometalate anion. Unlike [bmim]Cl, the butyl chains of $[bmim]_2[CoCl_4]$ were found to configure in an anti-gauche conformation, with each butyl chain pointing in opposite directions. The cations were also parallel to each other, either side of the chlorometalate anion. Due to the relatively large size of the chloride

ions, the tetrachlorocobaltate ion takes a distorted tetrahedral shape to avoid steric repulsion between the ligands [15,16]. The relative energies of the tested conformers are displayed in **Figure 4.6**.

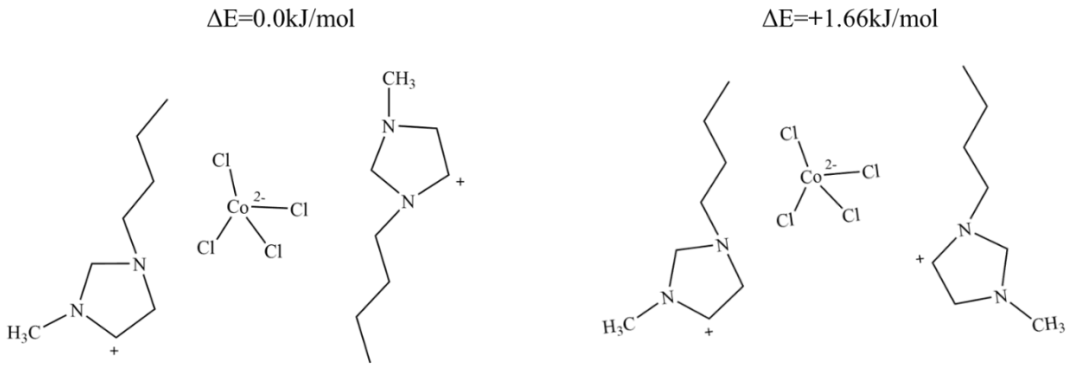

Figure 4.6. *Relative energies of [bmim]$_2$[CoCl$_4$] conformers.*

It was assumed that [Ch][OAc] and [Ch][For] share a similar configuration. DFT calculations by de Souza et al. have previously shown that the dominant conformation of the cation is *gauche*, which dominates over *anti* [17]. Both choline ILs feature strong ionic interactions between the single negative charge delocalised over the two anionic oxygen atoms and the cation. Therefore, configurations were tested based on cation interactions with the oxygen atoms specifically, with acetate interacting with the hydroxyl group of choline through H-bonding. This is likely due to the clouded nature of the positive choline nitrogen which is surrounded by methyl groups meaning access is more difficult for the acetate ion. The conformers, using [Ch][OAc] as an example, are shown in **Figure 4.7**.

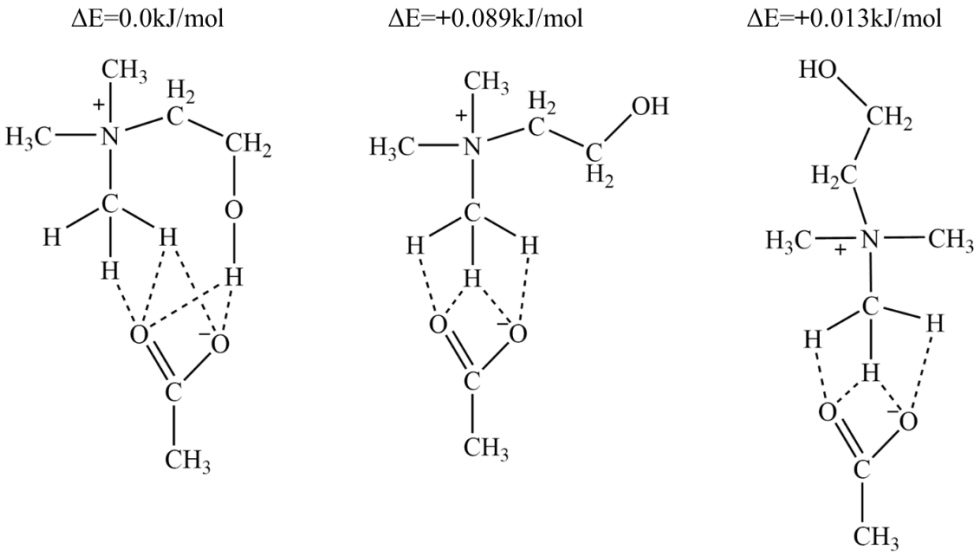

Figure 4.7. *Relative energies of [Ch][OAc] conformers.*

4.2.2 Vulnerable degradation site on the PET chain

Before introducing catalysts into the system, it was essential to determine the vulnerable degradation (bond cleavage) site on PET chain, as it significantly impacts the initial configurations of catalysed systems. It has previously been identified from electrostatic potential analysis that the ester linkage on the PET chain is the most vulnerable to nucleophilic attack due to its electronegativity, and due to the symmetry of the PET dimer, cleavage can occur at multiple points along the ester link [18]. **Figure 4.8** illustrates the PET dimer, highlighting the potential cleavage sites and their corresponding activation energies, together with the products from cleavage of that site.

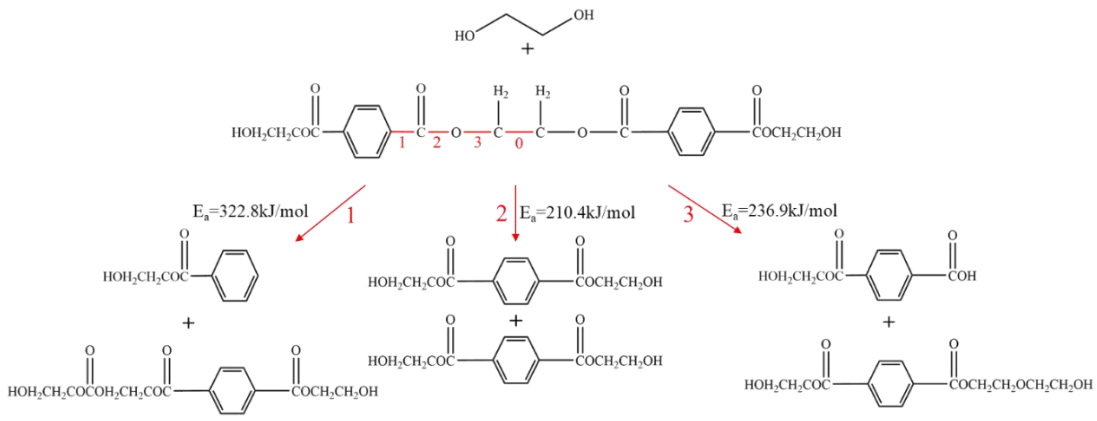

Figure 4.8. *Potential PET dimer degradation routes.*

Degradation *via* the site 0 cleavage proved challenging due to the perfect symmetry of the products. Due to the strength of this bond, it is unlikely that glycolysis would occur through this route. It was identified that the C-O bond of the ester link (site 2) is the weakest, with an energy barrier of 210.4 kJ/mol, facilitating the direct formation of BHET. This pathway involves the formation of a new C-O bond between the carbonyl carbon and the oxygen of EG, while simultaneously breaking the polyester's C-O bond, generating a cleaved chain fragment that subsequently combines with the dissociated EG H^+. To validate the three cleavage pathways, TS searching was carried out following by confirmation from IRC and frequency analysis. The activation energy for cleavage at site 2 was the lowest compared to site 1 and site 3, aligning with previously reported values in literature [18]. This work by Ju et al., using DFT calculations at the M06-2X-D3/6-311G(d,p) level, determined the energy barrier to be 209.2 kJ/mol. This confirms that cleavage at site 2 is the most favourable and that the model is valid.

4.2.3 Energy barriers derived from the use of different ILs

Based on the literature, several scenarios were tested through geometric optimisation. All scenarios contain the reactants, PET dimer and EG. Complex

catalysed systems include PET dimer, EG and one of the following ILs: [bmim]Cl, [Ch][For], [Ch][OAc] and $[bmim]_2[CoCl_4]$.

The uncatalysed system, containing just PET dimer and EG, showed that when interacting, the EG causes a folding of the usually linear polymer around the active site (**Figure 4.9**). This folding motion allows for easier access of the EG hydroxyl group to the C-O cleavage site.

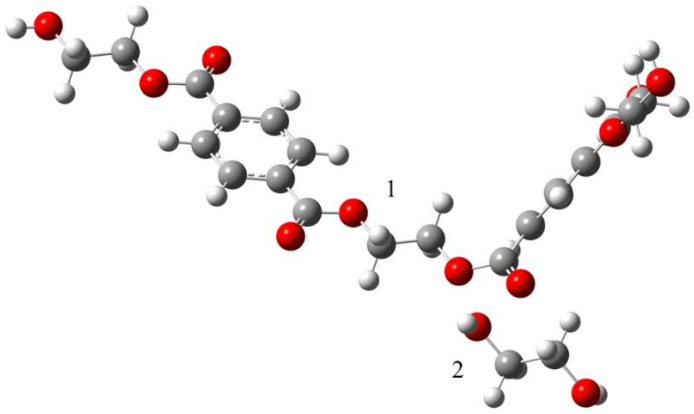

Figure 4.9. *PET dimer and EG reactant system.1) PET dimer and 2) EG.*

This finding was used as the basis for the construction of complex modelling systems containing ILs, PET dimer and EG. However, an interesting affect was noticed in these catalytic systems. When introducing the catalysts, many scenarios were tested. Two specific scenarios relative to PET and EG were those of the EG molecule being *inside* or *outside* the fold. It was assumed that the strong electrostatic forces between cations and anions would prevent ILs from separating and so, their spatial coordinates were kept close in all scenarios. Energy calculations of each scenario invariably showed the same interesting result, exemplified in **Figure 4.10** using the organic IL as an example. Hydrogen atoms have been omitted from the image for clarity. When the catalyst was introduced, it was found that the optimal configuration was for both cation and anion to be located on the same side of the PET dimer as the EG molecule.

However, due to the intermolecular interactions between the ILs and the PET dimer, the polymer is seen to fold towards the EG molecule. This has the effect of sterically preventing somewhat the access of EG to the active site. Once the spatial configuration of the ILs and EG was energetically confirmed to be *inside* the fold, the number of geometric variations were constrained as EG always had to be in close proximity to the PET ester.

Three constraints were used for all model building herein: 1) Location of ILs and EG *inside* the dimer fold, as per initial results 2) Close spatial proximity of cations and anion due to strong electrostatic interactions, and 3) Close spatial proximity of EG and dimer ester group, to facilitate the reaction.

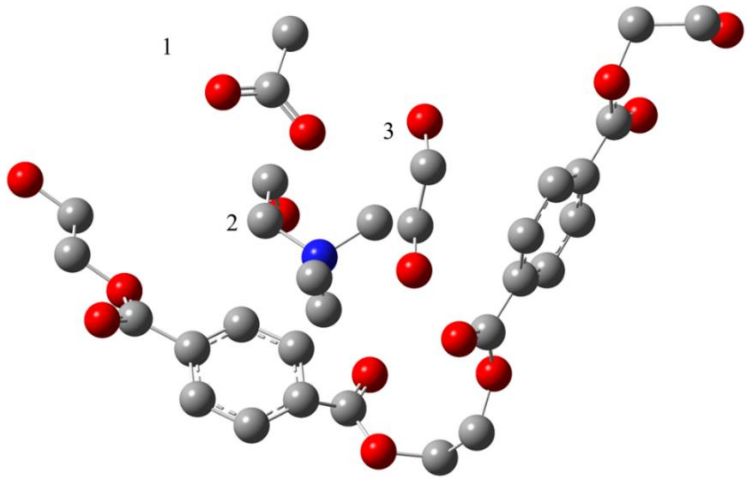

Figure 4.10. *Optimal configuration of [Ch][OAc]-catalysed system. 1) OAc, 2) Ch and 3) EG.*

In the case of the metal IL, the fold of the polymer is less pronounced, relative to the EG molecule (**Figure 4.11**). Instead, the active ester group is pulled towards the anion, thus exposing the site for nucleophilic attack by EG. It is proposed that this effect is due to the influence of the cobalt atom. In this case, although part of the anion, the Co(II) atom is capable of acting as a Lewis acid and interacting strongly with the

carbonyl O atoms of the dimer. In the organic IL systems, this is not the case, with the choline and imidazolium cations having less Lewis acidity.

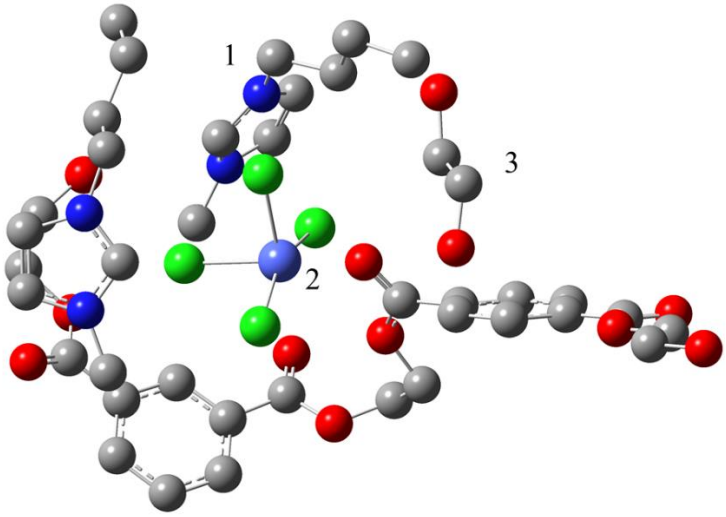

Figure 4.11. *Optimal configuration* of *$[bmim]_2[CoCl_4]$-catalysed system. 1) bmim, 2) $CoCl_4$ and 3) EG.*

Once the global minima were established, TS searching was carried out iteratively until the optimal reaction route was determined. The optimal route was based off of having the lowest energy barrier. **Table 4.3** contains both the gas and solvated phase energy values for each uncatalysed and catalysed system's reactant, TS and product. It can be seen that the introduction of the solvation model creates an increase in the energy barrier in all systems with the exception of the metal IL. Despite this, there is a clear trend in both the gas and solvated phase where the energy barriers are in the order: uncatalysed > [bmim]Cl > [Ch][For] > [Ch][OAc] > $[bmim]_2[CoCl_4]$.

Table 4.3. *System energies and activation energies, for gas phase and solvated systems, derived from DFT.*

System	Reactant (Gas) (a.u.)	TS (Gas) (a.u.))	Reactant (SMD) (a.u.))	TS (SMD) (a.u.))	Ea (Gas) (kJ/mol)	Ea (SMD) (kJ/mol)
Uncatalysed	-1834.862	-1834.783	-1834.708	-1834.628	202	210
[bmim]Cl	-2718.492	-2718.415	-2718.551	-2718.471	201	209
[Ch][For]	-2352.988	-2352.913	-2353.046	-2352.969	197	203
[Ch][OAc]	-2392.329	-2392.255	-2392.387	-2392.310	196	202
$[bmim]_2[CoCl_4]$	-4667.751	-4667.691	-4667.846	-4667.788	158	152

The computed energy barriers are displayed in **Figure 4.12**. The product energies are standardised for readability, as the activation energy is the main focus of the IL screening process. From herein, only SMD solvated energy barriers are reported.

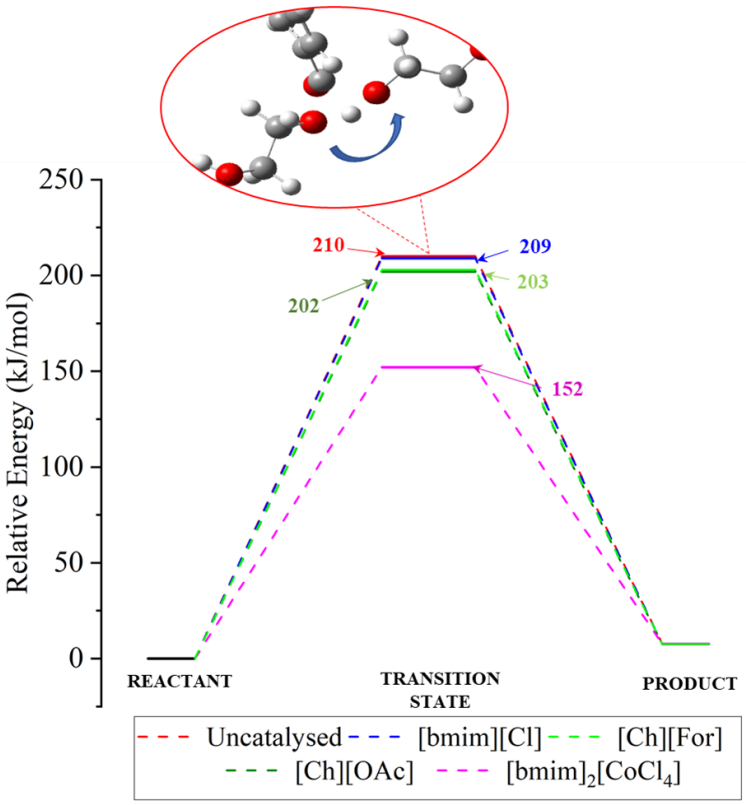

Figure 4.12. *Relative energy diagram with labelled energy barriers for each DFT system modelled. Insert shows TS snapshot and reaction mechanism for uncatalysed case.*

The reaction mechanism, shown in the insert, displays the hydrogen transfer between EG and the PET chain, which facilitates the degradation process. Each organic catalyst was found to catalyse the reaction intermolecularly, unlike $[bmim]_2[CoCl_4]$, which directly coordinated with the PET dimer. This mechanism will be explored in greater detail in **Chapter 5**. Generally, the energy barriers match well with DFT-calculated values from literature, albeit often with different catalysts. Using CaO, Arunphacharawit et al. [19] calculated an energy barrier of 207 kJ/mol, while Thomas et al. [20] determined activation energies of 166 kJ/mol and 204 kJ/mol for an IL-catalysed and uncatalysed reaction, respectively. Therefore, it is assumed that the results in **Figure 4.12** are within a reasonable range.

The decrease in energy barrier shows that each IL is somewhat effective in catalysing the reaction, to varying degrees. The simplest IL, [bmim]Cl, is the least effective, followed by [Ch][For] and [Ch][OAc], however, these values are likely to be within the estimated error of the calculations and therefore should not be used to definitively compare performance. As expected, the two choline ILs perform remarkably similar, due to their chemical similarity. The greatest reduction in energy barrier is shown by the metal IL, $[bmim]_2[CoCl_4]$, reducing it by more than 25%. By comparing the two halide-imidazolium ILs, [bmim]Cl and $[bmim]_2[CoCl_4]$, the influence of the metallic anion is made evident. The presence of the transition metal centre has a profound effect on the reaction, drastically reducing the energy barrier. This is to be expected, as transition metal catalysts are known to be extremely effective due to their incompletely filled d-orbitals, which facilitates the transfer of electrons to and from reactants, making them extremely active.

It is proposed that the reduction in energy barrier of the organic ILs is limited somewhat by the folding effect shown previously, as the EG molecule's access to the ester group is somewhat sterically restricted. That the EG molecule has much easier access to the vulnerable functional group explains the small difference in uncatalysed and organic IL-catalysed energy barriers. With this restriction, it is only the hydroxyl group activation of by the organic anion which facilitates the degradation, overcoming to an extent the steric hindrance. Based on these screening results, [Ch][OAc] and $[bmim]_2[CoCl_4]$ were selected for experimental investigation.

4.3 Experimental results of IL-catalysed PET Glycolysis

4.3.1 Catalyst synthesis and characterisation

The organic IL [Ch][OAc] was synthesised using the procedure described in **Chapter 3**. Acetic acid was added dropwise to the dissolved [Ch][OH], after which was formed a light- yellow clear liquid, containing a mixture of [Ch][OAc], water and solvent. Following the washing and drying process, the resultant IL was in the form of the extremely viscous brown liquid, which later crystallised at ambient temperature. The high viscosity of the IL is a result of both the high density and strong electrostatic interactions of the fluid [21]. The IL was then characterised using FT-IR spectroscopy to determine the functional groups. **Figure 4.13** displays the spectrum produced by FT-IR, which matches will with those of the literature.

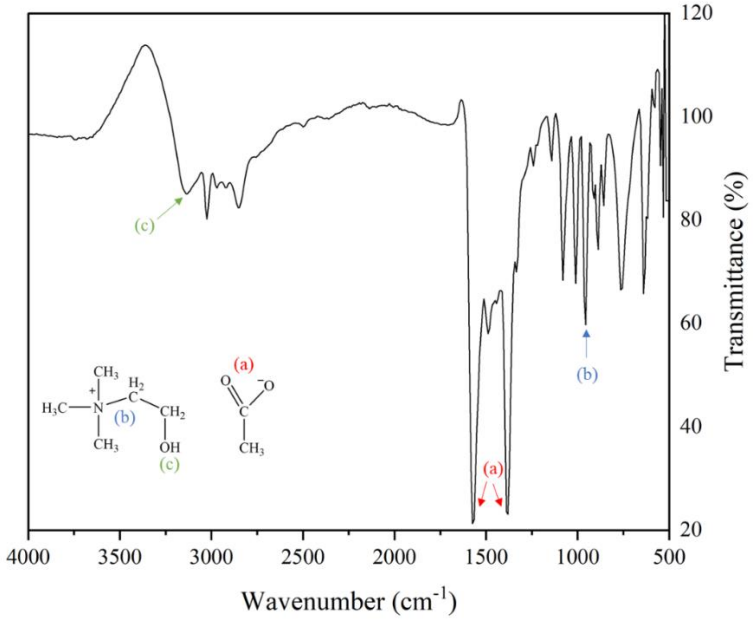

Figure 4.13. *FT-IR spectroscopy spectra of [Ch][OAc].*

The peak at ~1500 cm^{-1} (a) and the peak next to it, represent the symmetric stretching vibration of the C=O bond within the acetate anion. The peak (b) situated around 950 cm^{-1} is indicative of N-C stretching. The broader peak (c) represents the stretching vibration of an O-H bond in the choline cation. The peaks associated with the asymmetric stretching of the methyl groups at ~2900 cm^{-1} are reduced in their intensity due to the broad O-H peaks. The presence of these peaks confirms the production of [Ch][OAc] [11,22]. **Figure 4.14** displays the Raman spectrum of the organic IL. The peaks at ~716 and ~770 cm^{-1} represent different configurations of the N-CH_3 group within the choline cation, suggesting a dominant mix of *gauche* (red) rather than *anti* (green) conformations, matching well with the DFT calculations. This mixture of conformations is a result of the sample being a combination of crystalline and amorphous phases, as in the literature [17]. The peak at ~915 cm^{-1} (blue) is indicative of the C-C band of the acetate anion.

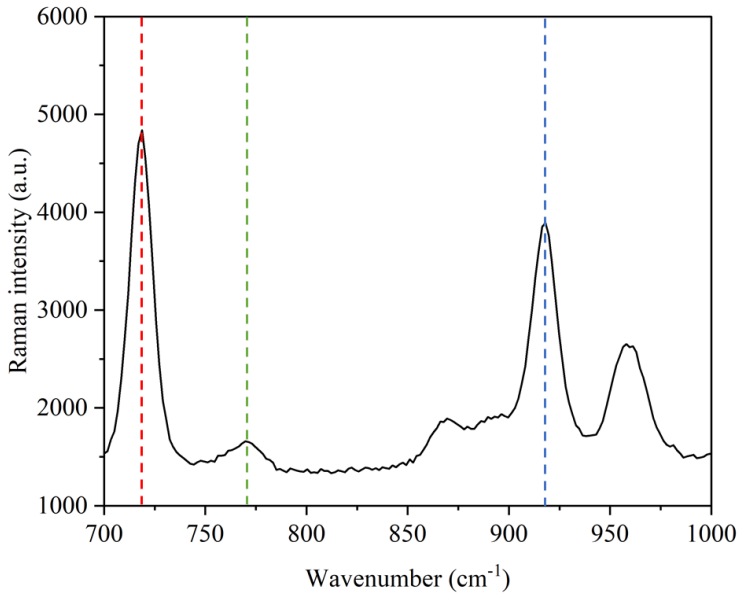

Figure 4.14. *Raman spectroscopy of [Ch][OAc].*

Once the composition of the catalyst was confirmed, it was stored in a glovebox to prevent exposure to atmospheric moisture. It should be noted that some atmospheric

moisture exposure is unavoidable during the synthesis process. The vacuum drying process should mitigate this, however during transfer to the glovebox, located in a separate lab, there will be some limited water uptake.

The metal IL, $[bmim]_2[CoCl_4]$, was synthesised using the procedure outlined in **Chapter 3**. The materials were mixed until the liquid formed a clear blue-green colour. Following extraction with dichloromethane and water, three times each, the liquid was placed in a rotary evaporator followed by a vacuum oven. Once excess solvent had been evaporated, the IL was in the form of an extremely viscous, dark blue liquid which crystallised when cooled. The FT-IR spectrum of the synthesised catalyst is shown in **Figure 4.15**. Spectra of the imidazolium-based cation were observed, including the peaks around 2950 cm^{-1} originating from C–H stretching vibration of the butyl chain. The peak at 1560 cm^{-1} represents the stretching vibration of C = N in the imidazole ring, while the one at 1170 cm^{-1} is indicative of the C-H within the aromatic ring. The 750 cm^{-1} peak can also be assigned to the imidazole ring. The spectra match well with other imidazolium-based ILs from literature, confirming the cationic structure [23].

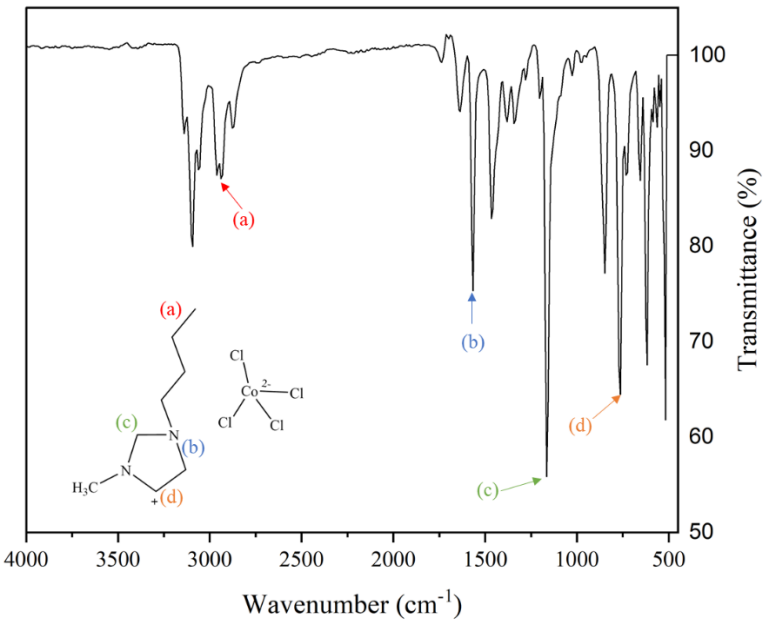

Figure 4.15. *FT-IR spectroscopy of [bmim]$_2$[CoCl$_4$]*.

In order to characterise the metallic anion, Raman spectroscopy was employed, as shown in **Figure 4.16**. The distinct peak at 265 cm^{-1} corresponds to the Co-Cl stretching vibration, confirming the synthesis of the desired IL [23].

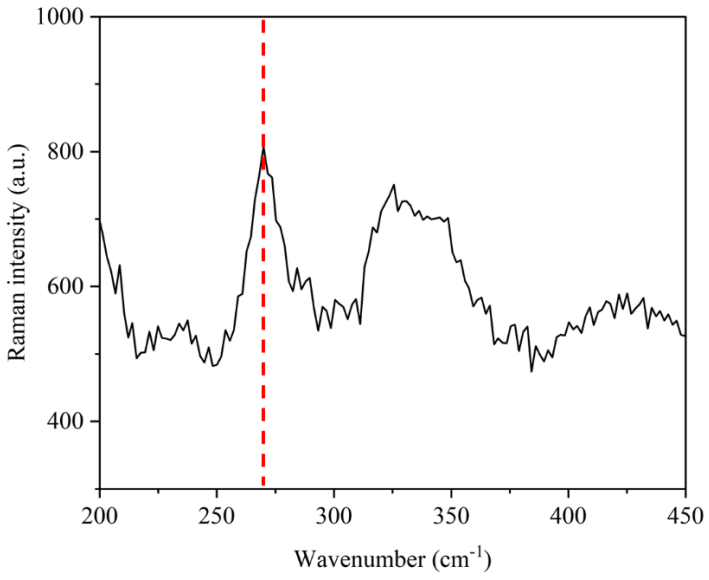

Figure 4.16. *Raman spectroscopy of [bmim]$_2$[CoCl$_4$]*.

4.3.2 Effect of catalyst weight

As the synthesis of ILs required expensive chemicals, the catalyst amount was considered the highest priority variable in order to prevent unnecessary use. A range of 0.25-0.75 g of catalyst was tested, using the reaction time of 120 mins and temperature of 190 °C, based on literature [11,24]. It can be seen that, generally, the PET conversions are very high, showing that it is not significantly affected by the catalyst amount (**Figure 4.17**). Generally, the more IL is in the system, the more cationic and anionic interactions take place, facilitating the degradation process. However, with an over-increase in catalyst amount, there is the potential for the promotion of the re-polymerisation reaction of BHET, due to the presence of unreacted EG [25,26]. At the reaction conditions, the temperature approaches the boiling point of EG (196 °C), meaning small amounts of EG will be lost. The effects of solvent loss are expected to be mitigated by loading an excess amount of EG, thereby supporting the suggestion that re-polymerisation is the limiting factor.

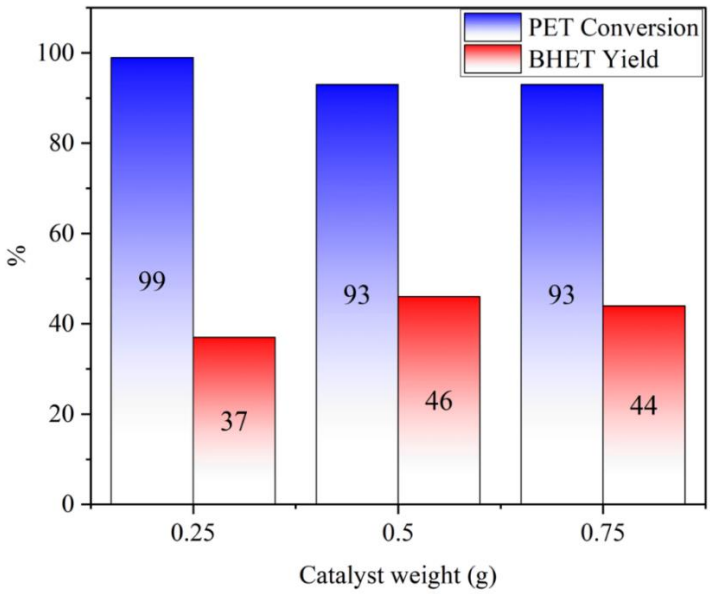

Figure 4.17. *Effect of catalyst weight on [Ch][OAc]-catalysed PET glycolysis (5 g PET, 20 g EG, 120 mins,* 190 °C).

Based on these results, it was decided that, in order to prevent catalyst wastage, the catalyst amount was not varied for the metal IL. It is assumed that, similar to the other varied parameters, the BHET yield in the metal IL cases would follow the same trend and 0.5 g of the catalyst would be the optimal amount.

4.3.3 Effect of reaction time

Initially, it is shown from **Figure 4.18** that the time-dependence of the reaction is significant, when 0.5 g [Ch][OAc] is used at 190 °C. The PET conversions remain high no matter the reaction time, however the BHET yield is minimal at times below two hours. There are a number of proposed reasons for this. Firstly, while the calculated PET conversion signifies the initial degradation of the polymer chain, it does not represent the extent to which this degradation occurs. For example, in the lower BHET yield cases, there is a substantial amount of intermediate removed from the product mixture. This is likely to consist of longer chain oligomers which are not fully soluble in water. Additionally, there is the potential for separation inefficiencies to be having an effect. The reduced BHET yields after 120 mins has been previously noted in literature, and is attributed to the reverse re-polymerisation previously discussed [25,26]. The BHET yield is at a maximum after 120 minutes of reaction, so it was decided that the reduced energy demands of the shorter reaction outweighed the increase in PET conversion, meaning 120 minutes was chosen henceforth as the optimal reaction time.

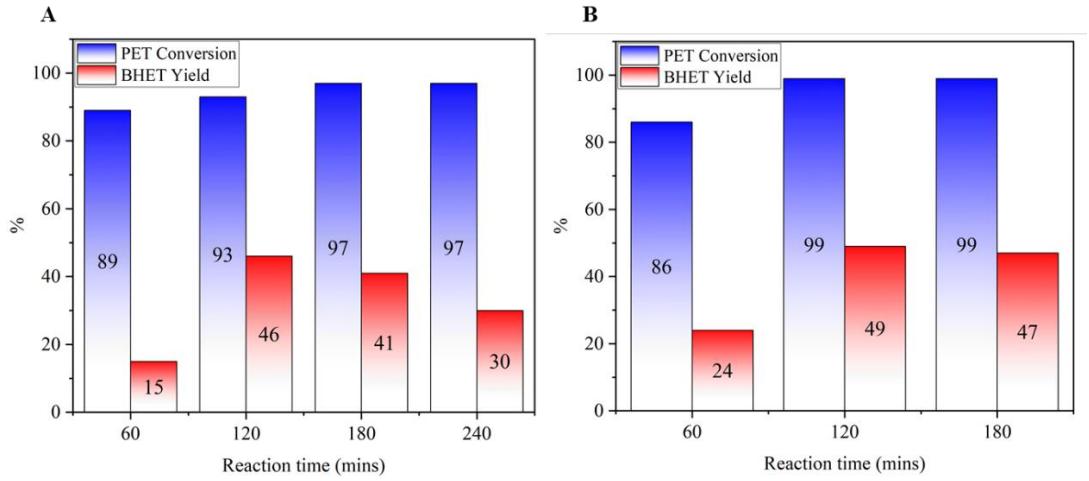

Figure 4.18. *Effect of reaction time on IL-catalysed PET glycolysis using A) [Ch][OAc] and B) $[bmim]_2[CoCl_4]$ (5 g PET, 20 g EG, 190 °C, 0.15 g cat.).*

For the metal IL case, the reaction was run until the decrease in BHET yield caused by re-polymerisation was observed. As before, this was seen at the 120-minute mark, which clearly represents an equilibrium point for the reaction, after which BHET yield begins to decrease. For each tested reaction time, the metal IL facilitates greater degradation of the PET chain, producing greater yields of BHET. Previous studies of similar PET glycolysis processes have estimated the BHET yield error to be between 1-7% [27–29]. Possible sources of errors include measurement uncertainty and losses during crystallisation and filtration of the product. Using this error estimation as a guide, the metal IL outperforms the organic one within the uncertainty range.

4.3.4 Effect of temperature

Initially, a temperature range of 170-210 °C was selected, based on literature ranges [11,24]. Both ILs were tested at this temperature range, for a reaction time of 120 mins and catalyst weight of 0.15 g, with the PET conversion and BHET yield presented in **Figure 4.19**.

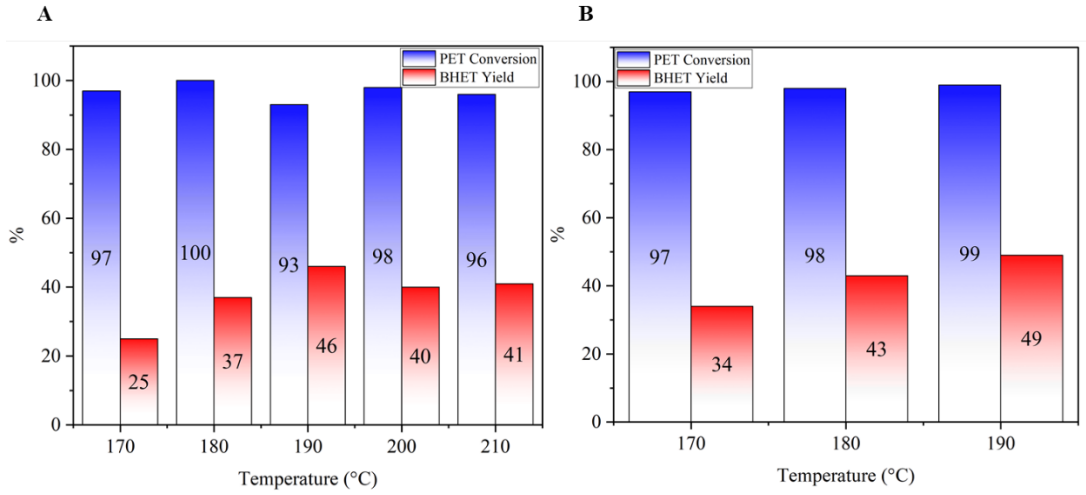

Figure 4.19. *Effect of reaction temperature on IL-catalysed PET glycolysis using A) [Ch][OAc] and B) $[bmim]_2[CoCl_4]$ (5 g PET, 20 g EG, 120 mins, 0.5 g cat.).*

As before, the PET conversion remains high at all of the tested temperatures. However, the BHET yield is low at temperatures below 180 °C, showing that the complete degradation of PET is sensitive to the reaction temperature. It was found that the optimal reaction temperature for BHET yield is 190 °C. At higher temperatures, the BHET yield begins to decrease. It is somewhat surprising that the BHET yield does not decrease more significantly at temperatures of 200 °C and above, due to the boiling point of EG being 196 °C, meaning that the reaction would be expected to be limited by the evaporation of the solvent. This suggests that a small reduction in EG weight does not have a significant impact on the reaction, due to the excess amount being used. For subsequent experiments using the metal IL, the temperature range was capped at 190 °C, with the assumption that the BHET yield would not increase further. Additionally, from a safety perspective, operating above a solvent's boiling point can lead to excessive evaporation, pressure build-up and potential safety hazards, increasing operational costs and requiring specialised high-pressure equipment, which complicates scalability and commercial viability.

A similar trend can be seen in the case of $[bmim]_2[CoCl_4]$ to the organic IL, in that the BHET yield generally increases with the temperature, reaching a peak at 190 °C. Additionally, the PET conversion is very high in each case, even when BHET yields are low. This effect has been noted in a previous study using choline-based ILs for PET glycolysis [30]. For each temperature tested, the BHET yield is greater in the case of the metal IL, matching well with the DFT-derived energy barriers.

That, in each studied scenario, the PET conversion is far greater than the BHET yield, provides some insight into the nature of the chain scission during the process. Previous kinetic studies have observed that the degradation process initiates through the random chain scission of PET amorphous tie-chain regions, while highly-ordered crystalline regions remain inaccessible to EG molecules, resulting in increased relative crystallinity of the polymer [31,32]. This step can be promoted through catalytically-induced swelling of PET, allowing for easier access to amorphous regions [3,33]. Subsequently, once amorphous PET tie chains have been degraded, the smaller and untethered remaining crystalline regions may become more dispersed and partially dissolved [34,35]. If these regions become small or dispersed enough to no longer become visible, this will influence the PET conversion which is measured by the weighing of visible solids. Therefore, while PET conversion is technically high due to the lack of visible, insoluble PET granules, the discrepancy between BHET yield and PET conversion likely indicates the accumulation of soluble oligomeric intermediates.

In a kinetic study of PET glycolysis, using differential scanning calorimetry (DSC) to characterise the product mixture residues following extraction with hot water, Lopez-Fonseca et al. [36] proposed that their exists an equilibrium between the monomer and dimer and that this final depolymerisation step is rate-determining. The

results showed that with increasing reaction time, the concentration of dimers and other oligomers began to increase, limiting the yield of BHET. This reversible, rate-determining step likely provides explanation for the reduced BHET yields seen in this study.

4.3.5 Characterisation of main degradation products

Figure 4.20 presents the FT-IR spectra of the separated residues, as well as the final crystallised product. The increasing length of the O-H peaks at ~3400 cm^{-1} and the alkyl C-H bonds at ~2900 cm^{-1} signifies the polymer's degradation journey as the concentration of hydroxyl groups and CH content increases as more bonds are cleaved. These peaks align with previously reported data for BHET and PET [37]. The results of the FT-IR characterisation support the theory that BHET yield is lost through either the incomplete degradation of PET or the re-polymerisation of BHET. The separated intermediate, the FT-IR spectrum of which shows a hydroxyl peak intensity between that of PET and BHET, was found in greater quantities in low BHET yield runs.

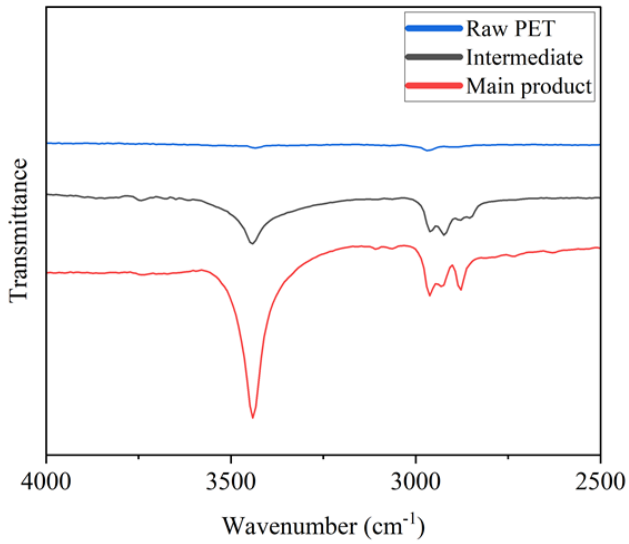

Figure 4.20. *FT-IR spectra of raw PET, intermediate and final degradation product.*

^{1}H NMR of the final glycolysis product dissolved in deuterated dimethyl sulfoxide provides further confirmation of the production of BHET, rather than longer-chain oligomers (**Figure 4.21**). The appearance of an intense singlet peak at 8.13 ppm indicates the aromatic ring protons, present on all degradation products of PET. The peak most characteristic of BHET is the triplet peak at 4.97 ppm, representing the terminal OH proton. That this peak is more intense than the adjacent methylene groups (4.32 and 3.72 ppm, respectively), confirms the preferential production of BHET over longer-chain oligomers [38–40]. The former methylene group is bonded to the -COO- group, while the latter is bonded to the -OH.

The sign around 2.5 ppm is attributed to the solvent, while the very intense signal at 3.3 ppm is caused by residual and contaminant water within the sample, a feature commonly noted in the literature [41,42]. It should be noted that NMR was carried out on samples long after gravimetric quantification, when they would have been driest. The lack of a notable peak at 4.7 ppm, characteristic of the inner methylene groups between two benzene rings, confirms the negligible concentration of dimers in the sample [39].

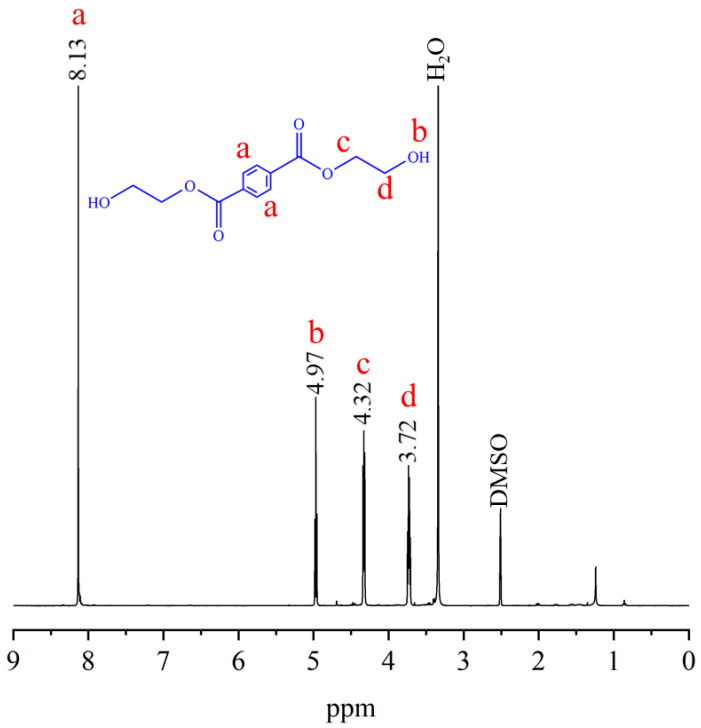

Figure 4.21. *[1]H NMR spectra of final degradation product (BHET).*

4.4 Comparison with literature

The results enclosed in this chapter evidenced the successful synthesis of IL catalysts, as well as the production of the desired monomer, BHET, with the results matching generally well with the theoretical DFT calculations in that the metal IL outperforms the organic one. Generally, as shown in **Figure 4.22**, the PET conversion is very high, while the BHET yield lags behind, as is often the case in the literature [43–45]. Indeed, the variance in PET conversion is limited run-to-run, likely within the measurement of the scales used for weighing the unconverted pellets, meaning that it is not appropriate to compare catalysts in this respect. It was proposed that the higher conversion relative to BHET yield is a result of the initial scission of amorphous tie-chains, allowing smaller crystalline regions to become more disperse and eventually dissolve at higher temperatures, despite not being fully converted to monomers. It is

acknowledged that this approach to quantifying PET conversion, although ubiquitous in the literature, likely results in the overestimation of the conversion. The BHET yields conversely, showed much greater variance due to the increased handling of the final product, creating more opportunity for losses during filtration or crystallisation.

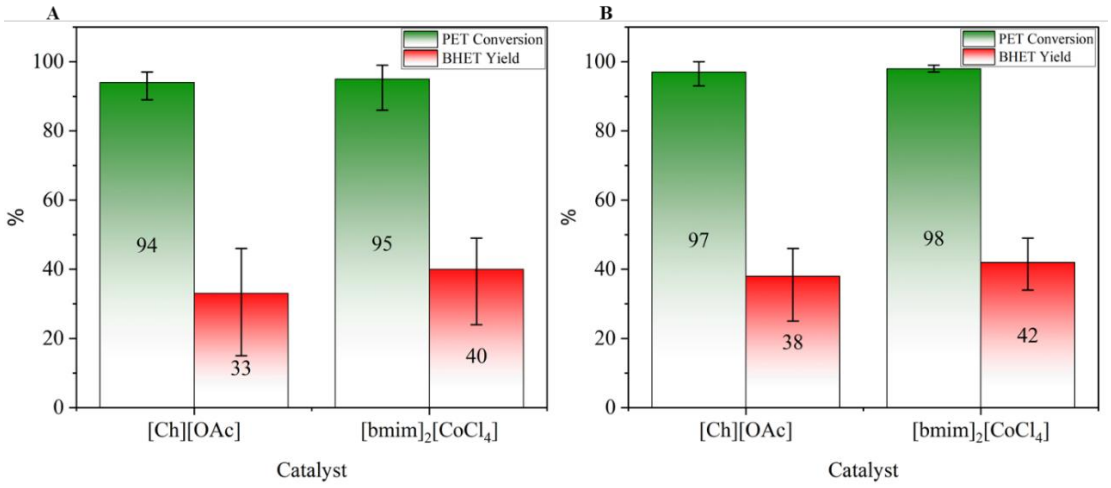

Figure 4.22. *Standard deviation of PET conversion and BHET yield using [Ch][OAc] and [bmim]$_2$[CoCl$_4$] with changing A) Temperature (5 g PET, 20 g EG, 120 mins, 0.5 g cat.) and B) Reaction time (5 g PET, 20 g EG, 190 °C, 0.5 g cat.).*

Notably, when compared with literature values, the BHET yields are low. In recent years, as outlined in **Chapter 2**, novel catalytic PET glycolysis processes have been shown to achieve upwards of 90% BHET yields. For the two ILs studied here, the BHET yield data is variable. The metal IL, [bmim]$_2$[CoCl$_4$] has only been studied once, where the BHET yield wasn't reported directly, however it was likely > 80% due to the excellent PET conversion and BHET selectivity that was reported [24]. The organic IL, [Ch][OAc], has been reported a number of times, with BHET yields ranging between 63-85% [11,33,46]. In any case, all BHET yields are significantly higher than those reported in this study, where the maximum BHET yield was found

to be 49%. An attempt to bridge this gap in performance using microwave heating and a biochar catalyst support will be evaluated in **Chapter 6**.

Regarding the low yields observed in this chapter, there are a number of proposed reasons:

1) **Moisture contamination:**
    - The use of hygroscopic reactants and ILs may introduce water into system, interfering with the degradation process.
    - Leads to more complex product mixtures, including oligomers formed from incomplete depolymerisation and potential hydrolysis of BHET, however the latter was not observed in the results.
    - Increase in solubility of BHET inhibits crystallisation and therefore reduces product yield.
2) **Handling and storage conditions**
    - Lack of pre-drying of PET and ILs due to laboratory restrictions.
    - Exposure to ambient humidity during the transferring of materials.
3) **Re-polymerisation of oligomers**
    - The rate-determining step of the process is the reversible conversion of dimers to BHET. As this reverse reaction occurs, the BHET yield is subsequently limited.

Moisture effects were mitigated as far as reasonably practical with the facilities available. Gloveboxes and Schlenk lines were utilised for storage and the carrying out of reactions, however water contamination was unavoidable. The influence of H_2O interference on the reaction will be explore more deeply in **Chapter 6**.

4.5 Conclusions

In this chapter, theoretical screening of ILs for PET glycolysis was carried out through DFT calculations. The results showed that while all tested ILs reduced the energy barrier to some degree, the metal IL, $[bmim]_2[CoCl_4]$, outperformed the organic ILs by a significant margin, reducing the energy barrier of PET glycolysis from 210 kJ/mol to 152 kJ/mol. This was initially attributed to coordination between the PET carbonyl O atom and Co. The intrinsic reaction catalytic mechanism of the ILs will be further elucidated in **Chapter 5**. Consequently, the two best-performing ILs, metal-based $[bmim]_2[CoCl_4]$ and organic [Ch][OAc], were selected for experimental investigation.

Organic and metal-containing ILs, [Ch][OAc] and $[bmim]_2[CoCl_4]$ were synthesised based on literature procedures, before FT-IR and Raman spectroscopy were used to validate their chemical structure. FT-IR and NMR characterisation showed that both ILs successfully degraded PET to its monomer BHET. The effects of various reaction parameters, including temperature, time and catalyst amount were tested. Overall, PET conversion is facile, with > 90% conversion seen in almost every tested case. However, BHET yield is considerably lower, suggesting that the short-chain scission of dimers into monomer is the rate-determining step. The significant lag between conversion and yield provides insight into the progression of chain scission during the reaction. It was proposed that, initially, the depolymerisation proceeds through random chain scission of amorphous regions, before the rate is slowed due to the more difficult end-chain scission of crystalline regions required to form BHET. Despite this, at all reaction conditions tested, the metal IL outperformed the organic one, matching well with the DFT results. In comparison to the literature, the BHET

yields are low, the maximum values for $[bmim]_2[CoCl_4]$ and [Ch][OAc] were 49% and 46%, respectively. This is likely due to moisture contamination caused by the hygroscopicity of the reactants and ILs, as well as storage and handling issues. The role of moisture, as well as the mechanism of its effect, will be explored further in **Chapter 6**. In addition, the re-polymerisation of BHET monomer is proposed as a limiting factor. To mitigate this, it is proposed that the reaction times are minimised.

References

[1] M.J. Frisch, G.W. Trucks, H.B. Schlegel, G.E. Scuseria, M.A. Robb, J.R. Cheeseman, G. Scalmani, V. Barone, G.A. Petersson, H. Nakatsuji, X. Li, M. Caricato, A. V. Marenich, J. Bloino, B.G. Janesko, R. Gomperts, B. Mennucci, H.P. Hratchian, J. V. Ortiz, A.F. Izmaylov, J.L. Sonnenberg, D. Williams-Young, F. Ding, F. Lipparini, F. Egidi, J. Goings, B. Peng, A. Petrone, T. Henderson, D. Ranasinghe, V.G. Zakrzewski, J. Gao, N. Rega, G. Zheng, W. Liang, M. Hada, M. Ehara, K. Toyota, R. Fukuda, J. Hasegawa, M. Ishida, T. Nakajima, Y. Honda, O. Kitao, H. Nakai, T. Vreven, K. Throssell, J.A. Montgomery, Jr, J.E. Peralta, F. Ogliaro, M.J. Bearpark, J.J. Heyd, E.N. Brothers, K.N. Kudin, V.N. Staroverov, T.A. Keith, R. Kobayashi, J. Normand, K. Raghavachari, A.P. Rendell, J.C. Burant, S.S. Iyengar, J. Tomasi, M. Cossi, J.M. Millam, M. Klene, C. Adamo, R. Cammi, J.W. Ochterski, R.L. Martin, K. Morokuma, O. Farkas, J.B. Foresman, D.J. Fox, Gaussian 16, (2016).

[2] J. Řezáč, L. Šimová, P. Hobza, CCSD[T] describes noncovalent interactions better than the CCSD(T), CCSD(TQ), and CCSDT methods, J Chem Theory Comput 9 (2013) 364–369. https://doi.org/10.1021/ct3008777.

[3] E. Luna, I. Olazabal, M. Roosen, A. Müller, C. Jehanno, M. Ximenis, S. de Meester, H. Sardon, Towards a better understanding of the cosolvent effect on the low-

temperature glycolysis of Polyethylene Terephthalate (PET), Chem. Eng. J. 482 (2024). https://doi.org/10.1016/j.cej.2024.148861.

[4] F. Li, X. Yao, R. Ding, Y. Bao, Q. Zhou, D. Yan, Y. Li, J. Xu, J. Xin, X. Lu, Directional glycolysis of waste PET using deep eutectic solvents for preparation of aromatic-based polyurethane elastomers, Green Chem. (2024). https://doi.org/10.1039/d4gc00292j.

[5] X. Wei, J. Qiu, H. Wang, W. Zheng, W. Sun, L. Zhao, Efficient glycolysis of Poly(ethylene terephthalate) to bis(hydroxyethyl) terephthalate catalyzed by non-metallic deep eutectic solvent, Chem. Eng. J. 508 (2025). https://doi.org/10.1016/j.cej.2025.161115.

[6] L. Goerigk, S. Grimme, A thorough benchmark of density functional methods for general main group thermochemistry, kinetics, and noncovalent interactions, Phys. Chem. Chem. Phys. 13 (2011) 6670–6688. https://doi.org/10.1039/c0cp02984j.

[7] C.E. Check, T.O. Faust, J.M. Bailey, B.J. Wright, T.M. Gilbert, L.S. Sunderlin, Addition of polarization and diffuse functions to the LANL2DZ basis set for P-block elements, J. Phys. Chem. A 105 (2001) 8111–8116. https://doi.org/10.1021/jp011945l.

[8] S. Grimme, J. Antony, S. Ehrlich, H. Krieg, A consistent and accurate ab initio parametrization of density functional dispersion correction (DFT-D) for the 94 elements H-Pu, J. Chem. Phys. 132 (2010). https://doi.org/10.1063/1.3382344.

[9] A. V. Marenich, C.J. Cramer, D.G. Truhlar, Universal solvation model based on solute electron density and on a continuum model of the solvent defined by the bulk dielectric constant and atomic surface tensions, J. Phys. Chem. B 113 (2009) 6378–6396. https://doi.org/10.1021/jp810292n.

[10] Z. Ju, W. Xiao, X. Lu, X. Liu, X. Yao, X. Zhang, S. Zhang, Theoretical studies on glycolysis of poly(ethylene terephthalate) in ionic liquids, RSC Adv 8 (2018) 8209–8219. https://doi.org/10.1039/c7ra13173a.

[11] Y. Liu, X. Yao, H. Yao, Q. Zhou, J. Xin, X. Lu, S. Zhang, Degradation of poly(ethylene terephthalate) catalyzed by metal-free choline-based ionic liquids, Green Chem. 22 (2020) 3122–3131. https://doi.org/10.1039/d0gc00327a.

[12] C. Zhong, T. Sasaki, A. Jimbo-Kobayeshi, E. Fujiwara, A. Kobayashi, M. Tada, Y. Iwasawa, Syntheses, structures, and properties of a series of metal ion-containing dialkylimidazolium ionic liquids, Bull Chem Soc Jpn 80 (2007) 2365–2374. https://doi.org/10.1246/bcsj.80.2365.

[13] L. Del Olmo, C. Morera-Boado, R. López, J.M. García De La Vega, Electron density analysis of 1-butyl-3-methylimidazolium chloride ionic liquid, J Mol Model 20 (2014). https://doi.org/10.1007/s00894-014-2175-y.

[14] N. Kotov, A. Šturcová, A. Zhigunov, V. Raus, J. Dybal, Structural transitions of 1-butyl-3-methylimidazolium chloride/water mixtures studied by Raman and FTIR spectroscopy and WAXS, Cryst Growth Des 16 (2016) 1958–1967. https://doi.org/10.1021/acs.cgd.5b01551.

[15] J.J. Criado, A. Jime Â Nez-Sa, F.H. Cano, R. Sa Â Ez-Puche, E. Rodrõ Âguez-Ferna Â Ndez, Preparation and characterization of tetrachlorocobaltates(II) of a,x-alkylenediammonium. Magnetic and thermal properties. Crystal structure of [NH3(CH2)5NH 3]CoCl4, Acta Cryst. 55 (1999) 947-952. https://doi.org/10.1107/S0108768199005698

[16] H.Q. Ye, D.D. Zhou, X.Q. Cai, J.J. Yang, Y.L. Qian, L.J. Su, X.P. Liu, L.M. Yang, J.R. Zhou, C.L. Ni, Syntheses, characterization, and crystal structures of two

tetrachlorocobaltate(II) salts with 4-substituted benzyl triphenylphosphonium, Synth. React. Inorg. Met.-Org. Nano-Met. Chem. 44 (2014) 672–677. https://doi.org/10.1080/15533174.2013.783866.

[17] Í.F.T. de Souza, M.C.C. Ribeiro, A Raman spectroscopy and rheology study of the phase transitions of the ionic liquid choline acetate, J Mol Liq 322 (2021). https://doi.org/10.1016/j.molliq.2020.114530.

[18] Z. Ju, L. Zhou, X. Lu, Y. Li, X. Yao, S. Cheng, G. Chen, C. Ge, Mechanistic insight into the roles of anions and cations in the degradation of poly(ethylene terephthalate) catalyzed by ionic liquids, Phys. Chem. Chem. Phys. 23 (2021) 18659–18668. https://doi.org/10.1039/d1cp02038b.

[19] A. Arunphacharawit, T. Poonsawat, T. Meechai, L. Chaicharoenwimolkul Chuaitammakit, E. Somsook, DFT study on the depolymerization of PET by Ca-catalyzed glycolysis reaction model, Heliyon 10 (2024). https://doi.org/10.1016/j.heliyon.2024.e34666.

[20] D. Thomas, K.P. Vijayalakshmi, C.H. Suresh, B.K. George, Insights into 1-ethyl 3-methyl imidazolium dicyanamide-catalysed glycolysis of polyethylene terephthalate, New J. Chem. (2025). https://doi.org/10.1039/D5NJ02489G.

[21] F. Philippi, D. Rauber, K.L. Eliasen, N. Bouscharain, K. Niss, C.W.M. Kay, T. Welton, Pressing matter: why are ionic liquids so viscous?, Chem Sci 13 (2022) 2735–2743. https://doi.org/10.1039/d1sc06857a.

[22] K. Mulia, E. Krisanti, F. Terahadi, S. Putri, Selected natural deep eutectic solvents for the extraction of α-Mangostin from mangosteen (Garcinia mangostana L.) pericarp, Int. J. Technol. 6 (2015) 1211–1220. https://doi.org/10.14716/ijtech.v6i7.1984.

[23] R. Xie, W. He, G. Qu, H.H. Wu, Z. Li, J. Li, W. Li, Low-temperature catalytic pyrolysis of cellulose to directional products 5-methylfurfural by magnetic ionic liquid, Bioenergy Res 16 (2023) 1108–1120. https://doi.org/10.1007/s12155-022-10494-2.

[24] Q. Wang, Y. Geng, X. Lu, S. Zhang, First-row transition metal-containing ionic liquids as highly active catalysts for the glycolysis of poly(ethylene terephthalate) (PET), ACS Sustain Chem Eng 3 (2015) 340–348. https://doi.org/10.1021/sc5007522.

[25] A.M. Al-Sabagh, F.Z. Yehia, A.M.F. Eissa, M.E. Moustafa, G. Eshaq, A.M. Rabie, A.E. Elmetwally, Cu- and Zn-acetate-containing ionic liquids as catalysts for the glycolysis of poly(ethylene terephthalate), Polym Degrad Stab 110 (2014) 364–377. https://doi.org/10.1016/j.polymdegradstab.2014.10.005.

[26] R. López-Fonseca, I. Duque-Ingunza, B. de Rivas, S. Arnaiz, J.I. Gutiérrez-Ortiz, Chemical recycling of post-consumer PET wastes by glycolysis in the presence of metal salts, Polym Degrad Stab 95 (2010) 1022–1028. https://doi.org/10.1016/j.polymdegradstab.2010.03.007.

[27] M. Schlüter, J. Zimmer, C. Held, K. Wohlgemuth, Enhancing sustainability in PET glycolysis by closed-loop recycling, Chem Eng Sci 307 (2025). https://doi.org/10.1016/j.ces.2025.121337.

[28] L. Zhou, E. Qin, H. Huang, Y. Wang, M. Li, PET Glycolysis to BHET efficiently catalyzed by stable and recyclable Pd-Cu/γ-Al2O3, Molecules 29 (2024). https://doi.org/10.3390/molecules29184305.

[29] D.T. Van-Pham, Q.H. Le, T.N. Lam, C.N. Nguyen, W. Sakai, Four-factor optimization for PET glycolysis with consideration of the effect of sodium bicarbonate

catalyst using response surface methodology, Polym Degrad Stab 179 (2020). https://doi.org/10.1016/j.polymdegradstab.2020.109257.

[30] S. Marullo, C. Rizzo, N.T. Dintcheva, F. D'Anna, Amino acid-based cholinium ionic liquids as sustainable catalysts for PET depolymerization, ACS Sustain Chem Eng 9 (2021) 15157–15165. https://doi.org/10.1021/acssuschemeng.1c04060.

[31] A. Sangalang, L. Bartolome, D.H. Kim, Generalized kinetic analysis of heterogeneous PET glycolysis: Nucleation-controlled depolymerization, Polym Degrad Stab 115 (2015) 45–53. https://doi.org/10.1016/j.polymdegradstab.2015.02.012.

[32] J. Cao, H. Liang, J. Yang, Z. Zhu, J. Deng, X. Li, M. Elimelech, X. Lu, Depolymerization mechanisms and closed-loop assessment in polyester waste recycling, Nat Commun 15 (2024). https://doi.org/10.1038/s41467-024-50702-5.

[33] W. Zheng, C. Liu, X. Wei, W. Sun, L. Zhao, Molecular-level swelling behaviors of poly (ethylene terephthalate) glycolysis using ionic liquids as catalyst, Chem Eng Sci 267 (2023). https://doi.org/10.1016/j.ces.2022.118329.

[34] S. Watson-Sanders, M. Dadmun, More efficient chemical recycling of poly(ethylene terephthalate) by intercepting intermediates, ChemSusChem 17 (2024). https://doi.org/10.1002/cssc.202301698.

[35] S.F. Llopis, E. Verdejo, O. Gil-Castell, A. Ribes-Greus, Partial glycolytic depolymerisation of poly(ethylene terephthalate) (PET) in the solid state: Modelling the contribution of time and temperature, Polym Degrad Stab 221 (2024). https://doi.org/10.1016/j.polymdegradstab.2024.110695.

[36] R. López-Fonseca, I. Duque-Ingunza, B. de Rivas, L. Flores-Giraldo, J.I. Gutiérrez-Ortiz, Kinetics of catalytic glycolysis of PET wastes with sodium carbonate, Chem. Eng. J. 168 (2011) 312–320. https://doi.org/10.1016/j.cej.2011.01.031.

[37] M.J. Chinchillas-Chinchillas, V.M. Orozco-Carmona, C.G. Alvarado-Beltrán, J.L. Almaral-Sánchez, S. Sepulveda-Guzman, L.E. Jasso-Ramos, A. Castro-Beltrán, Synthesis of recycled poly(ethylene terephthalate)/polyacrylonitrile/styrene composite nanofibers by electrospinning and their mechanical properties evaluation, J Polym Environ 27 (2019) 659–669. https://doi.org/10.1007/s10924-019-01379-1.

[38] J. Sutton, G. Grause, A. Al Rida Hmayed, S.T.G. Street, A.P. Dove, J. Wood, Organocatalytic glycolysis of polyethylene terephthalate and product separation by membrane filtration, Chem. Eng. J. 512 (2025). https://doi.org/10.1016/j.cej.2025.162400.

[39] M. Imran, D.H. Kim, W.A. Al-Masry, A. Mahmood, A. Hassan, S. Haider, S.M. Ramay, Manganese-, cobalt-, and zinc-based mixed-oxide spinels as novel catalysts for the chemical recycling of poly(ethylene terephthalate) via glycolysis, Polym Degrad Stab 98 (2013) 904–915. https://doi.org/10.1016/j.polymdegradstab.2013.01.007.

[40] Y. Cha, Y.J. Park, D.H. Kim, Hydrodynamic synthesis of Fe2O3@MoS20D/2D-nanocomposite material and its application as a catalyst in the glycolysis of polyethylene terephthalate, RSC Adv 11 (2021) 16841–16848. https://doi.org/10.1039/d1ra02335g.

[41] V. Gayathri, R.T.B. Sheyara, N. Devassy, D. Samanta, Investigating the degradation of PET utilizing NHC-based catalysts and effective reuse of the

degradation product as an additive with polyurethane adhesive material, J Appl Polym Sci 139 (2022). https://doi.org/10.1002/app.52474.

[42] G.R. Lima, W.F. Monteiro, R. Ligabue, R.M.C. Santana, Titanate nanotubes as new nanostrutured catalyst for depolymerization of PET by glycolysis reaction, in: Materials Research, Universidade Federal de Sao Carlos, 2017: pp. 596–602. https://doi.org/10.1590/1980-5373-mr-2017-0645.

[43] B. Shojaei, M. Abtahi, M. Najafi, Chemical recycling of PET: A stepping-stone toward sustainability, Polym Adv Technol 31 (2020) 2912–2938. https://doi.org/10.1002/pat.5023.

[44] A.M. Al-Sabagh, F.Z. Yehia, G. Eshaq, A.M. Rabie, A.E. ElMetwally, Greener routes for recycling of polyethylene terephthalate, Egypt. J. Pet. 25 (2016) 53–64. https://doi.org/10.1016/j.ejpe.2015.03.001.

[45] J. Xin, Q. Zhang, J. Huang, R. Huang, Q.Z. Jaffery, D. Yan, Q. Zhou, J. Xu, X. Lu, Progress in the catalytic glycolysis of polyethylene terephthalate, J Environ Manage 296 (2021) 113267. https://doi.org/10.1016/j.jenvman.2021.113267.

[46] D. Bura, L. Pedrini, C. Trujillo, S.J. Connon, Cholinium-based ionic liquid catalysts for polyethylene terephthalate glycolysis: understanding the role of solvent and a reappraisal of the cation contribution, RSC Sustain. 1 (2023) 2197–2201. https://doi.org/10.1039/d3su00336a.

Chapter 5
Mechanistic Insights into PET Glycolysis

Generally, the ionic liquid (IL)-catalysed polyethylene terephthalate (PET) glycolysis mechanism is investigated widely in the literature, with many studies conducting experimental and theoretical methods to validate it. However, as outlined in **Chapter 2**, some deeper theoretical studies have uncovered discrepancies specific to each system, suggesting that overarching "off-the-shelf" mechanisms cannot be applied to all systems and that in order to understand individual cases fully, further analysis must be carried out. Traditionally, it was thought that ILs catalyse the reaction through a synergistic mechanism whereby the cation protonates the ester carbon via interactions with the PET carbonyl and the anion interacts with reactive hydroxyl group of ethylene glycol (EG) (**Figure 5.1A**). However, recent studies have disputed this, suggesting that the role of the cation is mechanistically limited, with the EG molecule capable of protonating the ester in its stead (**Figure 5.1B**). Additionally, in the case of metallic anions, the roles of the ions can swap as the metal centre coordinates with the PET carbonyl group (**Figure 5.1C**). These reappraisals serve as evidence of the case-specific nature of the reaction mechanisms, which need to be reviewed systematically for the corresponding catalysts, rather than assumed to be applicable to one general mechanism.

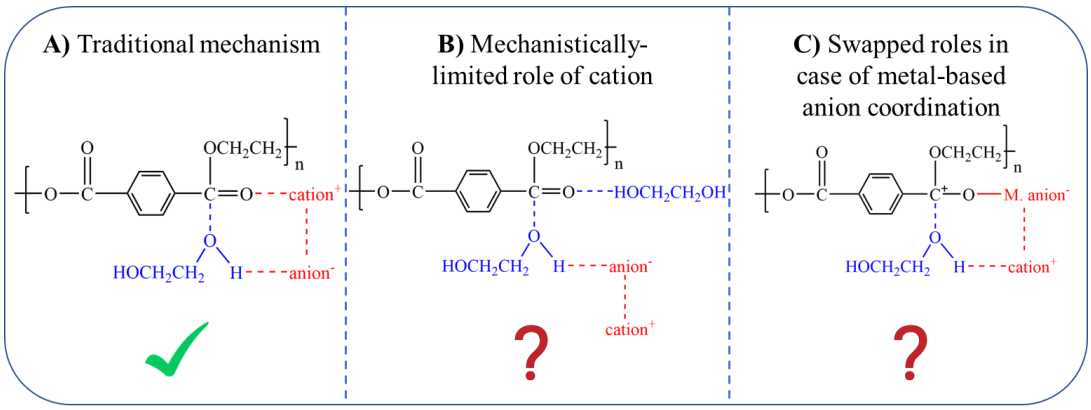

Figure 5.1. *Traditional IL-catalysed PET glycolysis mechanism compared to new, case-specific proposed mechanisms.*

This chapter provides specific mechanistic insights into the organic and metal-based IL-catalysed PET glycolysis process, focusing on the individual roles played by each ion. The intermolecular interactions for each system are quantified and compared using various density functional theory (DFT)-based methods, including highest occupied molecular orbital and lowest unoccupied molecular orbital (HOMO-LUMO) energy gaps, natural bond orbital (NBO), bond order theory, quantum theory of atoms in molecules (QTAIM) analysis, population analysis and reduced density gradient (RDG). These analyses, combined with the energy barriers calculated in **Chapter 4**, will elucidate the effectiveness of each catalyst, with a focus on the differences between metal and non-metal ILs. By developing a better understanding of the intermolecular interactions which drive the PET glycolysis reaction, recommendations can be made which will inform future catalyst and process design.

5.1 Methodology

All DFT calculations described in this chapter were carried out using Gaussian 16 package [1] and external Multiwfn software [2]. Multiwfn is a powerful electronic wavefunction analyser tool, allowing users to conduct numerous analysis techniques from Gaussian output files. The same DFT functional and basis set were used as in **Chapter 4**: B3LYP-D3/6-311G(d,p) for non-transition metal atoms, while the LANL2DZ basis set was used for transition metal atoms [3–5]. The SMD model was used to replicate the EG solvent environment [6]. Single-point energy calculations of the optimised reactant and transition state (TS) systems were carried out at the same level, with the output files being inputted into Multiwfn for further analysis.

QTAIM charges of reactant systems were computed through Multiwfn. Critical points including nuclear critical points at atomic centres, bond critical points (BCPs) between atoms, ring critical points in cyclic structures, and cage critical points were searched. As this chapter investigates intermolecular interactions between atoms, only BCPs were analysed. Key topology parameters, including electron density ($e\rho$), Laplacian of electron density, and energy density, were calculated for the IL-catalysed systems.

The electron density at a BCP reflects the extent of electron accumulation and stabilisation between two atoms. A study by Emamiam et al. [7] fitted a linear model of electron densities against high-accuracy CCSD(T)-derived binding energies between charged moieties, proving that they serve as reliable descriptors of interaction energies arising predominantly from electrostatic forces. **Equation 5.1** enables the direct use of BCP electron densities as a proportional indicator of the interaction energy within IL-containing systems.

$$Interaction\ energy\ \left(\frac{kcal}{mol}\right) = -332.34 \times \rho BCP\ (a.u.) - 1.0661 \qquad (5.1)$$

Only BCPs with an electron density ranging from 0 to 0.15 (a.u.) were considered, as values above 0.15 are indicative of covalent bonding [8].

NBO analysis within Gaussian 16 was employed to further explore the intermolecular non-bonding interactions. While the NBO output provides a variety of data, only the second order perturbative estimates of donor-acceptor interaction (E(2)) are included. In this context, the unperturbed operator represents an idealised Lewis-like system, where all bonding and lone-pair orbitals are perfectly localised and no delocalisation occurs. The perturbation, on the other hand, accounts for the mixing between these donor (filled) and acceptor (empty or partially filled) orbitals, reflecting how electrons can be partially transferred or shared between them. The interaction strength threshold used for producing data was 0.50 kcal/mol. The second-order perturbation stabilisation energy (E(2)), as presented in the results, was calculated using **Equation 5.2:**

$$E(2) = q_i \frac{F(i,j)^2}{\varepsilon_i - \varepsilon_j} \qquad (5.2)$$

Where i and j represent donor and acceptor atoms, respectively, ε represents the orbital energy, F represents the Hamiltonian operator and qi represents the occupancy of the orbital. The E(2) value is assumed to be proportional to the interaction energy between intermolecular atoms within the system and can therefore be used for comparative purposes.

RDG calculations were carried out using the Multiwfn software package. The RDG and the product of the electron density (ρ) with the sign of the second Hessian eigenvalue (sign(λ_2)ρ) were computed throughout the molecular space. These two scalar quantities are plotted against each other to distinguish different types of

interactions. To facilitate the visualisation of non-covalent interaction regions, isosurfaces of the RDG function were generated at an isovalue of 0.5 a.u. and overlaid onto the corresponding molecular systems they represent.

Population analysis was conducted through Multiwfn, using the Atomic Dipole Moment Corrected Hirshfeld (ADCH) method. The energy gap between the HOMO and LUMO were calculated by subtracting the last occupied eigenvalue (HOMO) from the first virtual eigenvalue (LUMO), both located in the Gaussian single-point energy output file. This was conducted for each ion pair.

5.2 Results

5.2.1 HOMO-LUMO energy gap

To evaluate the catalytic reactivity of the selected ILs, their frontier molecular orbitals, HOMO and LUMO, as well as the associated energy gaps and charge distributions, were analysed using DFT calculations. These parameters provide insight into the electron-donating and accepting abilities of the ILs, which are crucial for understanding their activity in PET glycolysis. The HOMO-LUMO gap, in particular, serves as a useful indicator of chemical reactivity: a smaller energy gap generally corresponds to a more chemically active system . **Figure 5.2** displays the HOMO-LUMO energy gap of each catalyst.

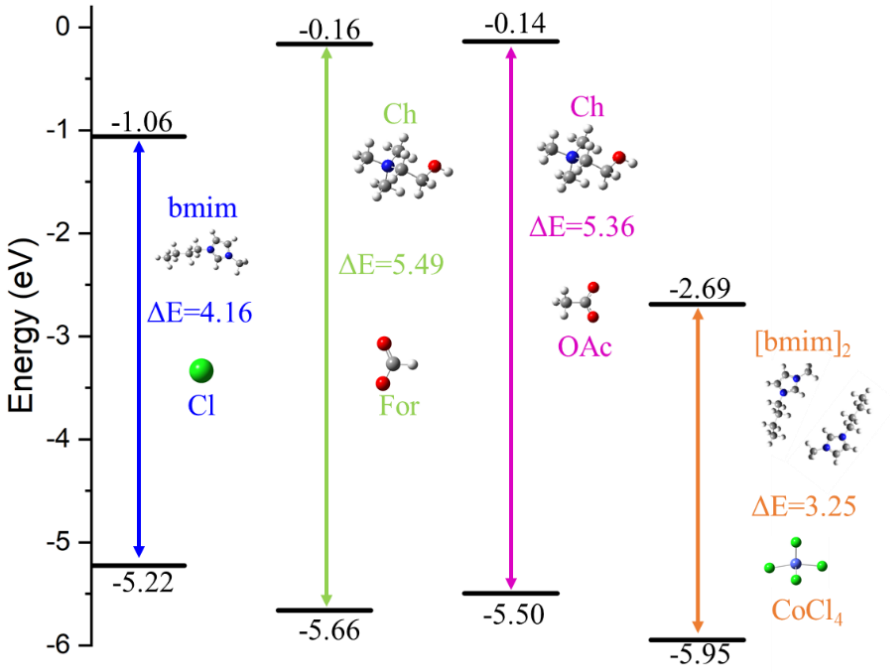

Figure 5.2. *HOMO-LUMO energy gaps (eV) for each ion pair.*

Generally, the energy gap values are within a reasonable range. In a study of imidazolium-based ILs, Agwupuye et al. [9] determined the HOMO-LUMO gaps to be within a range of 3.85 – 6.05 eV, depending on the choice of anion. Among the ILs studied, [Ch][For] exhibited the largest energy gap, indicating relatively lower reactivity, followed by [Ch][OAc] and [bmim]Cl, with $[bmim]_2[CoCl_4]$ showing the smallest gap. This decreasing trend in energy gap correlates well with the observed catalytic activity from **Chapter 4**, **Figure 4.11**, highlighting the enhanced reactivity of metal-based ILs like $[bmim]_2[CoCl_4]$, which can more readily participate in electron transfer processes during the PET depolymerisation reaction. The correlation between HOMO-LUMO energy gap and activation energy has been noted in literature [10]. However, the low energy gap of [bmim]Cl is somewhat surprising, as it produces the highest energy barrier of the catalysts chosen for study. In all cases, the LUMO orbitals tend to localise around electronegative atoms, suggesting their role in accepting

electron density during the reaction. Meanwhile, HOMO orbitals are often centred on the anionic moieties [11]. **Figure 5.3** identifies specifically which component of the ion pairs represents the HOMO and LUMO.

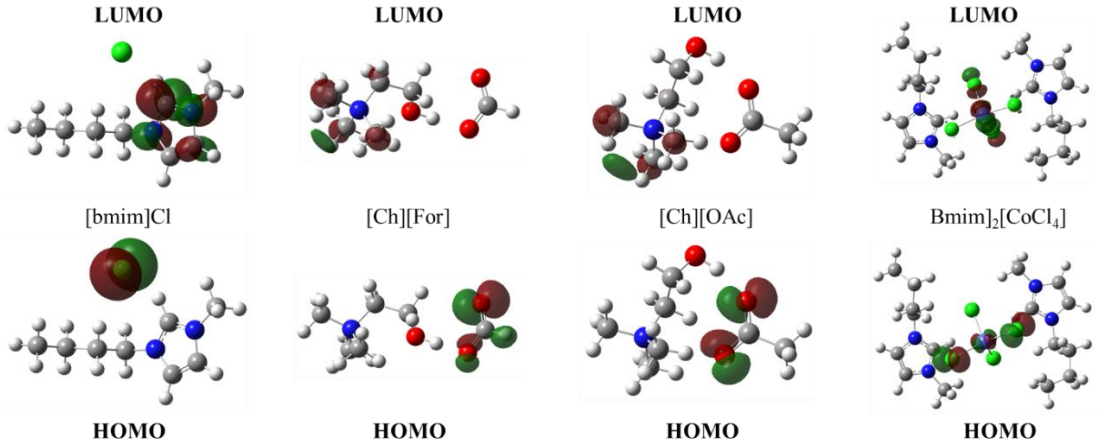

Figure 5.3. *HOMO and LUMO energies of each ion pair.*

In most cases, the HOMO and LUMO energies are located across the anion and cation, respectively. However, it is notable that in the case of the metal IL, the $CoCl_4$ anion contains both the HOMO and LUMO, indicating its importance in the catalytic activity of the IL, as well providing an explanation for its significantly different energy gap, when compared to the relatively chemically similar [bmim]Cl. These results demonstrate the interesting dual-functioning role played by the transition-metal centre. While the energy gap does provide insight into the reactivity of the ILs, it was modelled on a closed system with no external reactants. Therefore, further analysis of the direction and magnitude of electron transfer has to be carried out in order to elucidate its influence on the reaction.

5.2.2 NBO Analysis

Second-order perturbation theory was carried out to explore the intermolecular interactions in a quantifiable manner. Interactions within each system were categorised based on the moieties involved: cation-anion, cation-PET, cation-EG, anion-EG,

anion-PET and PET-EG interactions are included. The omission of any of these combinations is resultant of negligible interactions. Only prominent interactions are considered herein. For the [bmim]Cl system, a more comprehensive list of interactions is included in **Table 5.1** as an example, with **Figure 5.4** showing the corresponding atom numbers. Accompanying numbered atomic schemes are merely for visualisation purposes and are not indicative of true reaction mechanism.

Table 5.1. *NBO analysis for [bmim]Cl system.*

Structures	**Donor (i)**	**Acceptor (j)**	**E(2) (kJ/mol)**	**ε(i) – ε(j)**	**F (i,j)**
Anion - Cation	LP1 Cl86	σ* C66-H80	6.61	1.01	0.036
	LP2 Cl86	σ* C66-H80	0.46	0.66	0.008
	LP3 Cl86	σ* C66-H80	5.52	0.66	0.027
	LP4 Cl86	σ* C66-H80	84.77	0.66	0.103
PET - Cation	LP1 O24	σ* C63-H75	0.63	1.15	0.012
	LP1 O24	σ* C63-H75	1.63	0.73	0.015
Anion - EG	LP1 Cl86	σ* O88-H90	2.427	1.08	0.022

	LP2 Cl86	σ* O88- H90	0.837	0.73	0.011
	LP3 Cl86	σ* O88- H90	42.342	0.73	0.077
	LP4 Cl86	σ* O88- H90	0.962	0.73	0.012
	LP4 Cl86	σ* C57- H58	2.092	0.7	0.017
EG - PET	LP1 O60	σ* C23- O24	1.172	0.6	0.012
	LP2 O60	σ* C23- O24	0.962	0.3	0.008
EG - Cation	LP1 O88	σ* C64- H78	42.049	1.1	0.094

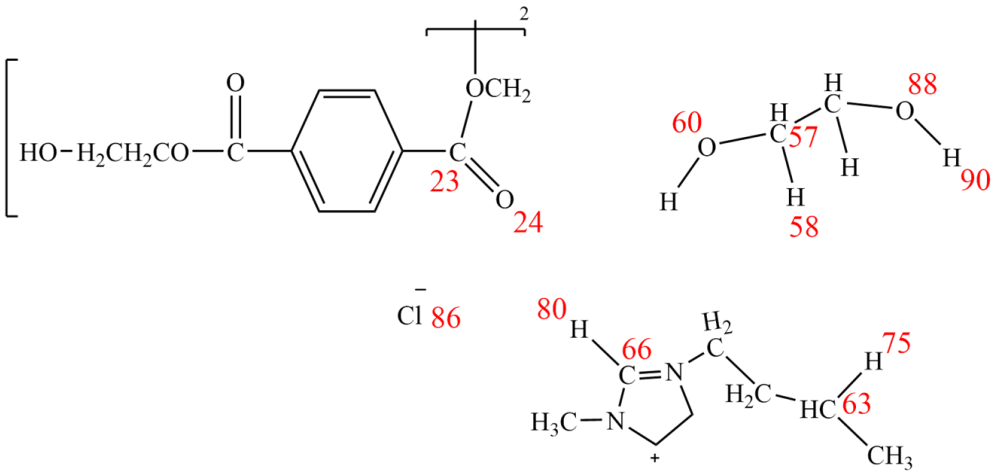

Figure 5.4. *[bmim]Cl with red-numbered atoms of importance. EG hydroxyl group closest to PET is considered the "reacting" group.*

Before analysing the data, there is a clear discrepancy between the NBO results and the classical understanding of a chloride ion: the NBO analysis describes four distinct LPs of electrons, when there is known to be only three. **Table 5.2** supplements the analysis to provide an explanation for this discrepancy, showing the hybridisation and occupancy of the LPs.

Table 5.2. *Hybridisation and occupancy details for Cl LPs.*

LP	s character	p character	Occupancy
LP1 Cl86	s (74.51%)	0.71p (25.49%)	-1.99
LP2 Cl86	s (5.97%)	0.71p (94.02%)	-1.99
LP3 Cl86	s (8.96%)	0.71p (91.02%)	-1.95
LP4 Cl86	s (10.59%)	0.71p (89.39%)	-1.92

It should be noted that there is a small amount of d-character for each LP which rounds up to 100% but is not considered chemically important. By observing the hybridisation, it can be seen that LP1 displays unusual character, in that it is mainly s-characterised, when it would be predicted to be strongly p-characterised, like the other three LPs, which all have roughly ≥ 90% p-characteristics [12]. This suggests that it most likely represents a core-like electron, rather than valence. This effect can be seen when very strong intermolecular interactions distort the molecular orbital, resulting in the NBO model splitting it into two separate localised LPs. In this case, the very strong interactions between Cl LP4 and the C-H bond of the cation result in this discrepancy.

The E(2) values for the chloride ion in **Table 5.1** represent the relative interactions with different moieties. It is clear from their magnitudes that the most prominent anionic interactions are with the C-H anti-bonding orbital, as in the literature [12]. This represents the -CH group located between the nitrogen atoms of

bmim, across which the positive charge is localised. This interaction is stronger than the anion – EG interactions, which activate the reaction, resulting in the limited catalytic effect of this IL. Indeed, the E(2) value for anion-EG interaction is still high, 42 kJ/mol, however, it is with the hydroxyl group at the opposite end to the active site on EG (O88-H90). It is unsurprising that the anionic contribution is greater than that of the cation, as the literature commonly states that this is the most significant, mechanistically [13,14].

The third greatest interaction is between the non-reacting O atom of EG and a C-H bond located on the bmim butyl side-chain. This charge transfer will act to make the O atom less negative, potentially increasing nucleophilicity of the opposite end of the EG molecule. Additionally, there is a small amount of interaction with the adjacent methylene group of EG, C57-H58. The results also show weak H-bonding between the cation and PET carbonyl oxygen, as in the theoretical study of IL-catalysed PET glycolysis by Ju et al. [15], which will somewhat protonate the reacting carbon atom within the polymer chain. However, their work found that this interaction was the most prominent cationic contribution, contrasting with the weaker contribution observed in this study. The weak H-bonding between EG-PET, around the reaction site, suggests that the glycolysis reaction is a result of the initial activation via the catalytic interactions.

As these interactions are for comparison purposes between ILs, the results herein will provide additive E(2) values, combining the values for each LP belonging to the same atom. The $\varepsilon(i) - \varepsilon(j)$ and F (i,j) values will be omitted.

Table 5.3. *NBO Analysis for [Ch][For] system.*

Structures	Donor (i)	Acceptor (j)	E(2) (kJ/mol)
Anion - Cation	LP O84	σ* O62-H69	149.704
	LP O84	σ* C68-H82	3.515
Anion - EG	LP O84	σ* O87-H88	48.745
	LP O84	σ* C55-H56	1.674
	LP O84	σ* C57-H59	0.920
PET - EG	LP O24	σ* O60-H61	12.510

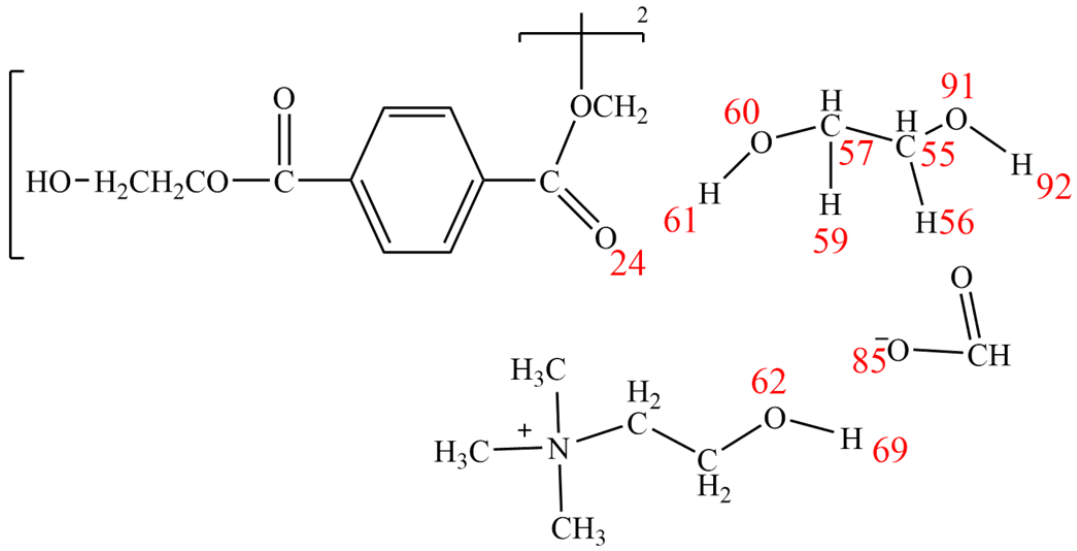

Figure 5.5. *[Ch][For] system with red-numbered atoms of mechanistic importance.*

Table 5.3 and **Figure 5.5** show the most significant donor - acceptor stabilisation energies for the [Ch][For] system. The strongest interactions are between the anion and cation, however there are no significant interactions between the cation and PET, meaning only the anion is influencing the reaction directly. The most prominent anionic interactions, other than with the cation, are between the LPs of the

formate's oxygen and the non-reacting hydroxyl group of EG, while there is an E(2) value of 1.674 kJ/mol with the adjacent C-H bond. Additionally, there is a 0.920 kJ/mol strength anionic interaction with the methylene group (C57-H59) next to the reacting OH group. Compared to the [bmim]Cl NBO analysis, the [Ch][For] system has more interactions between EG and the anion, which likely creates the reduction in energy barrier. Additionally, there is H-bonding between the carbonyl oxygen of PET (O24) and the hydroxyl group of EG [13,14]. Through this interaction, the EG molecule is acting similar to the cation in the traditionally published reaction mechanism. Contrasting with the accepted mechanism reported in the literature [16,17], the findings indicate no evidence of cationic interactions with the PET dimer. Such an observation has been noted in a few very recent theoretical studies of IL-catalysed PET glycolysis [13,14]. The other choline-based IL, [Ch][OAc], shows similar results following NBO analysis (**Table 5.4** and **Figure 5.6**).

Table 5.4. *NBO analysis for [Ch][OAc] system.*

Structures	Donor (i)	Acceptor (j)	E(2) (kJ/mol)
Anion - Cation	O85	σ* O62-H69	160.080
Anion - EG	O85	σ* O91-H92	56.484
	O85	σ* C55-H56	1.632
	O85	σ* C57-H59	0.753
PET - EG	O24	σ* O60-H61	13.431

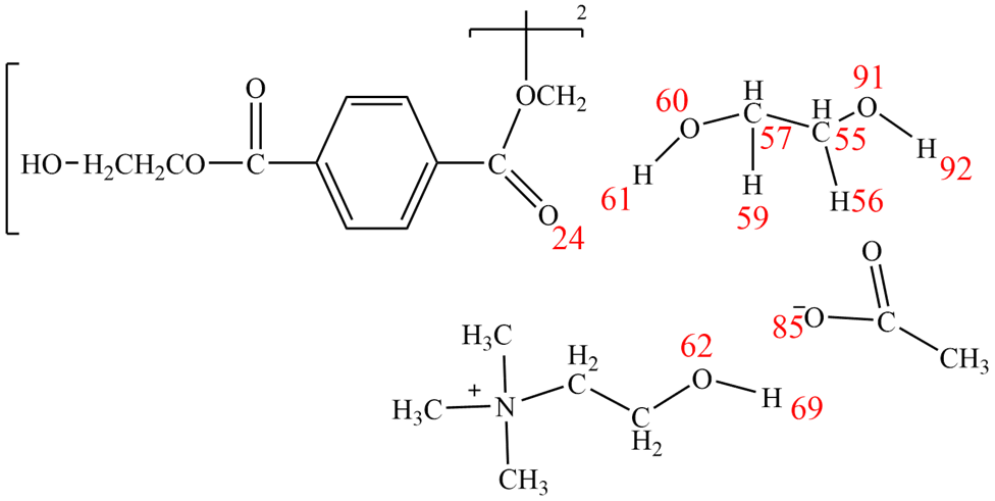

Figure 5.6. *[Ch][OAc] system with red-numbered atoms of mechanistic importance.*

As with the formic-based IL, the strongest interactions are between anion and cation. However, in this case, the anion – EG interactions are stronger, likely resulting in the reduced energy barrier. As with [Ch][For], the anion interacts predominantly with the hydroxyl group opposite to the reaction site, as well the adjacent -CH_2 group. Despite being extremely molecularly similar, the acetate ion is more basic than the formate one, resulting in increased polarity and charge transfer [18]. The catalytic effect of the EG molecule is seen once more, with a 13.431 kJ/mol stabilisation energy between the carbonyl oxygen LPs and the EG hydroxyl group. Accordingly, there are no cation - PET interactions, limiting the choline's role within the reaction. The metal IL case was also studied, with the results shown in **Table 5.5** and **Figure 5.7**.

Table 5.5. *NBO analysis for $[bmim]_2[CoCl_4]$ system.*

Structures	Donor (i)	Acceptor (j)	E(2) (kJ/mol)
Anion – Cation 1	Cl	σ* C66-H77	4.728
	Cl	σ* N69-C70	8.242
	Cl	σ* C70-H84	4.392
Anion – Cation 2	Cl	σ* N94-C95	8.780
	Cl	σ* C95-H109	10.878
	Cl	σ* C99-H114	3.556
Anion - EG	Cl	σ* O4-H5	32.552
	Cl	σ* C6-H7	1.046
PET - Anion	O28	σ* Co115-Cl117	61.212
PET - EG	O28	σ* O4-H5	4.853

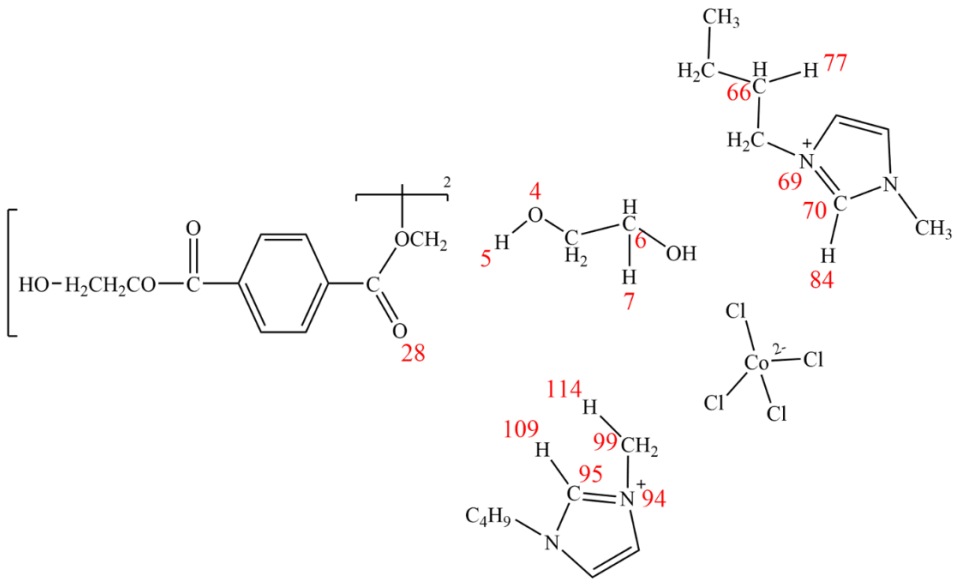

Figure 5.7. *$[bmim]_2[CoCl_4]$ system with red-numbered atoms of mechanistic importance.*

In the metal IL case, there are more potential sites for intermolecular interactions, due to the d-orbitals of Co and the multiple LPs located on each chloride ion, as well as the presence of two cationic molecules. The LPs of each chloride ion have combined for presentation in **Table 5.5**.

It was confirmed that the BD* orbital between Co and Cl, seen to interact strongly with the carbonyl group, is characterised as being 53.21% d-orbital contributed, confirming that it is the presence of d-orbital electrons which allow for such strong additional interactions with PET. Coordination between metal-based moieties and PET dimer has commonly been reported in the literature and are highly effective in promoting the reaction [19,20]. In comparison with the other ILs, the anion - EG interactions of the metal IL system are generally weaker, however, they are directed almost entirely towards the reacting OH group of EG, suggesting that the position of the anion relative to EG is of importance in addition to the strength of the interaction. As before, there is some activation of the PET carbonyl via the EG molecule, however this is less pronounced in the metal case. Instead, the PET carbon is heavily protonated through interactions between the carbonyl LP and the anti-bonding orbital of Co-Cl, with an E(2) value of 61.212 kJ/mol, almost 6 times the strength of the carbonyl interactions in the cases of the choline-based ILs.

5.2.3 QTAIM analysis

There are some limitations in the way that NBO analysis represents H-bonding via the second-order perturbation energy E(2). While this energy is useful for comparisons of systems, it more accurately corresponds to a charge transfer energy from LP to empty or anti-bonding orbitals, thus somewhat negating the important electrostatic and polarisation effects which do not always involve orbital overlap [21].

Additionally, it can be corrupted by errors associated with the chosen basis set. In contrast, QTAIM displays the topological electron density between atoms and is commonly viewed as the most representative description of intermolecular interactions. Additionally, it does not suffer from any errors derived from choice of basis set.

With the NBO results as a basis, the most important interactions of each system could be explored through QTAIM. BCPs of interest for the [bmim]Cl, as well as their topological parameters, are displayed in **Table 5.6** in decreasing order of electron density.

Table 5.6. *Topological parameters of electron density (ρ), Laplacian of electron density ($\nabla^2 e\rho$) and energy density (H) for [bmim]Cl system. All units are in a.u.*

Molecules	Atoms	Electron density (ρ)	Laplacian ($\nabla^2 e\rho$)	Energy density (H)
Cation - anion	H80-Cl86	3.26E-02	7.73E-02	-1.47E-03
Anion - EG	Cl86-H90	2.29E-02	6.28E-02	7.53E-04
Cation - EG	H79-O88	9.80E-03	3.02E-02	8.37E-04
Cation - PET	O24-H75	8.64E-03	2.65E-02	7.21E-04
Cation - EG	H74-088	8.14E-03	2.46E-02	6.50E-04
Anion - EG	Cl86-H58	7.64E-03	2.29E-02	1.02E-03
EG – PET	O60-O22	7.20E-03	2.63E-02	7.23E-04
EG - PET	H55-O24	7.07E-03	2.13E-02	6.08E-04

There are general rules of thumb for the results of QTAIM, by which intermolecular interactions can be broadly categorised. Focusing on the interactions most applicable to the IL systems, H-bonding, the electron density of a strong H-bond is > 0.05 a.u., while weak is < 0.02 a.u. The Laplacian and energy density are both negative for strong bonding and positive for weak bonding. Cases where energy density is negative and Laplacian is positive represent medium strength H-bonding [22].

The results match the NBO analysis well, with the strongest interactions forming between the anion and the C-H bond located between the nitrogen atoms of bmim, followed by the anionic interactions with the non-reacting hydroxyl group of EG. The range of these values suggest medium H-bonding between the moieties. The additional anion – EG interactions between Cl86-H58 are also confirmed.

For the [Ch][For] and [Ch][OAc] systems, the electron density topologies are displayed in **Table 5.7** and **Table 5.8**. Only chemically important interactions of electron densities of > 0.01 a.u. are discussed herein, to prevent repetition.

Table 5.7. *Topological parameters of electron density (ρ), Laplacian of electron density (∇2eρ) and energy density (H) for [Ch][For] system.*

Molecules	Atoms	Electron density (ρ)	Laplacian ($\nabla^2 e\rho$)	Energy density (H)
Anion - Cation	O84-H69	5.70E-02	1.23E-01	-1.05E-02
Anion - EG	O84-H88	3.35E-02	1.05E-01	-3.98E-04
EG - PET	H61-O24	2.57E-02	9.13E-02	1.39E-03

As before, the result match well with the previous NBO analysis. There appears strong, electrostatically-supported H-bonding between the anion and cation, while

there is medium-strength H-bonding between the formate anion and the non-reacting hydroxyl group of EG. To a lesser degree, there are some stabilising interactions between the reacting hydroxyl group of EG and the carbonyl oxygen of PET.

Table 5.8. *Topological parameters of electron density (ρ), Laplacian of electron density (∇2eρ) and energy density (H) for [Ch][OAc] system.*

Molecules	Atoms	Electron density (ρ)	Laplacian ($\nabla^2 e\rho$)	Energy density (H)
Anion - Cation	O84-H69	6.00E-02	1.47E-01	-1.18E-02
Anion - EG	O84-H88	3.74E-02	1.22E-01	-1.09E-03
EG - PET	H61-O24	2.57E-02	1.02E-01	2.75E-03

The QTAIM result of the [Ch][OAc] system is remarkably similar to the [Ch][For] case, with only the magnitude of the strongest interactions varying. In each case of anionic interactions, the interactions are stronger in the acetate example, due to its increased basicity over the formate ion, while the EG stabilisation of the carbonyl is ~0.008 a.u. stronger in the acetate case. This could be due to increased polarity brought on by the stronger anionic interaction with EG.

Table 5.9. *Topological parameters of electron density (ρ), Laplacian of electron density (∇2eρ) and energy density (H) for [bmim]$_2$[CoCl$_4$] system.*

Molecules	Atoms	Electron density (ρ)	Laplacian ($\nabla^2 e\rho$)	Energy density (H)
Anion - PET	Co-O28	7.69E-02	4.82E-01	-5.05E-03
Anion - Anion	Co-Cl1	7.35E-02	2.25E-01	-9.68E-03
Anion - EG	Cl1-H5	2.26E-02	6.55E-02	9.80E-04

Table 5.9 features the QTAIM analysis for the $[bmim]_2[CoCl_4]$ system. The results displayed emphasise the uniqueness of the metal-based IL, compared to the other ILs studied. As with the NBO results, the metal centre of the anion is seen to interact very strongly with the carbonyl oxygen of atom, while the chloride ions engage the reacting hydroxyl group of EG.

Generally, the QTAIM results overall match well with the NBO analysis, thus validating its use as a method of quantifying the intermolecular interactions within each IL-catalysed system. A summary of the interactions derived from NBO and QTAIM are displayed in **Figure 5.8A** and **B**, respectively.

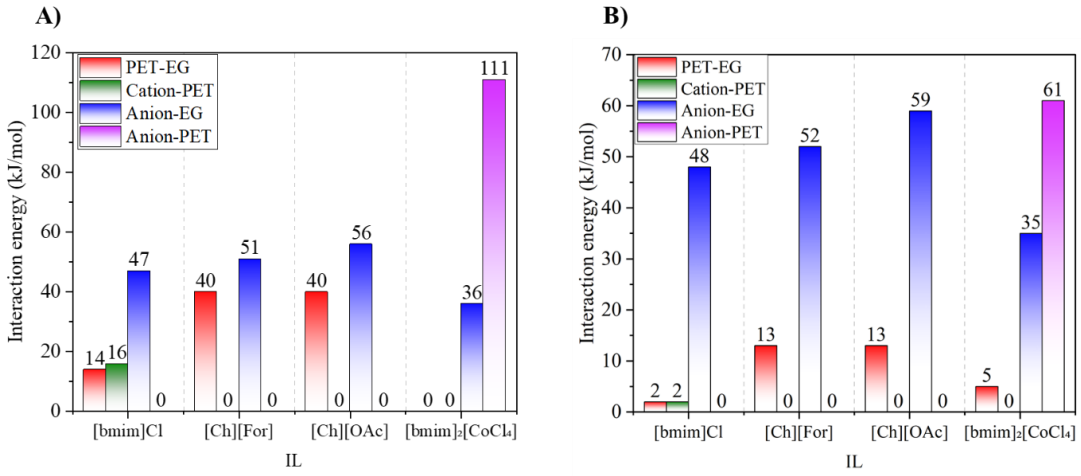

Figure 5.8. *Intermolecular interactions derived from A) NBO and B) QTAIM analyses.*

5.2.4 RDG analysis

RDG scatter plots of the reactant systems were developed to supplement the NBO and QTAIM analyses, as in the theoretical study of IL-catalysed PET glycolysis by Ju et al. [15]. Each point within the scatterplot represents a cartesian coordinate onto which the isosurface value is projected. By combining both visual methods, scatter plot and isosurface, weak intermolecular interactions can be identified, located

and defined. For the simplest system, the uncatalysed one, the RDG scatter plot and projected isosurface are shown in **Figure 5.9**.

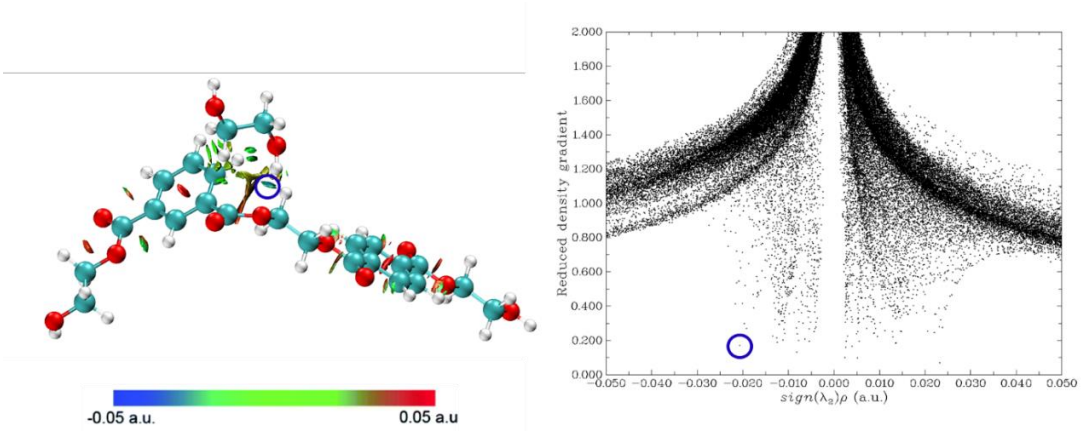

Figure 5.9. *RDG scatter plot and corresponding isosurface for uncatalysed system. Blue ring indicates region of strongest attractive interaction. Atomic colour code: Cyan – carbon, red – oxygen and white – hydrogen. Isosurface colour bar: Blue represents strong attraction, green represents weak attraction and red represents repulsion.*

The x-axis, the sign of the second Hessian eigenvalue, signifies whether the interactions are attractive or repulsive, with the near-zero region representing weak interactions such as vdW, while the y-axis indicates the localisation of the electron density [23]. Only y-axis values close to zero are considered important, as too high an RDG suggests that interactions are highly delocalised and diffuse.

In the example above, the strongest intermolecular interactions are indicated by the blue ring. On the scatter plot, this is presented as the most negative x-axis value close to zero on the y-axis. By plotting the coordinates of the corresponding isosurface, this interaction can be identified as H-bonding between the hydroxyl group of EG and the single-bonded O atom in the ester bond of PET, i.e. the active reaction site. This process was then repeated for three catalysed systems: [bmim]Cl, [Ch][OAc] and

[bmim]$_2$[CoCl$_4$] ([Ch][For] was not analysed as it is assumed to be the same as [Ch][OAc]). The RDG scatter plots and isosurfaces are displayed in **Figure 5.10A-C**.

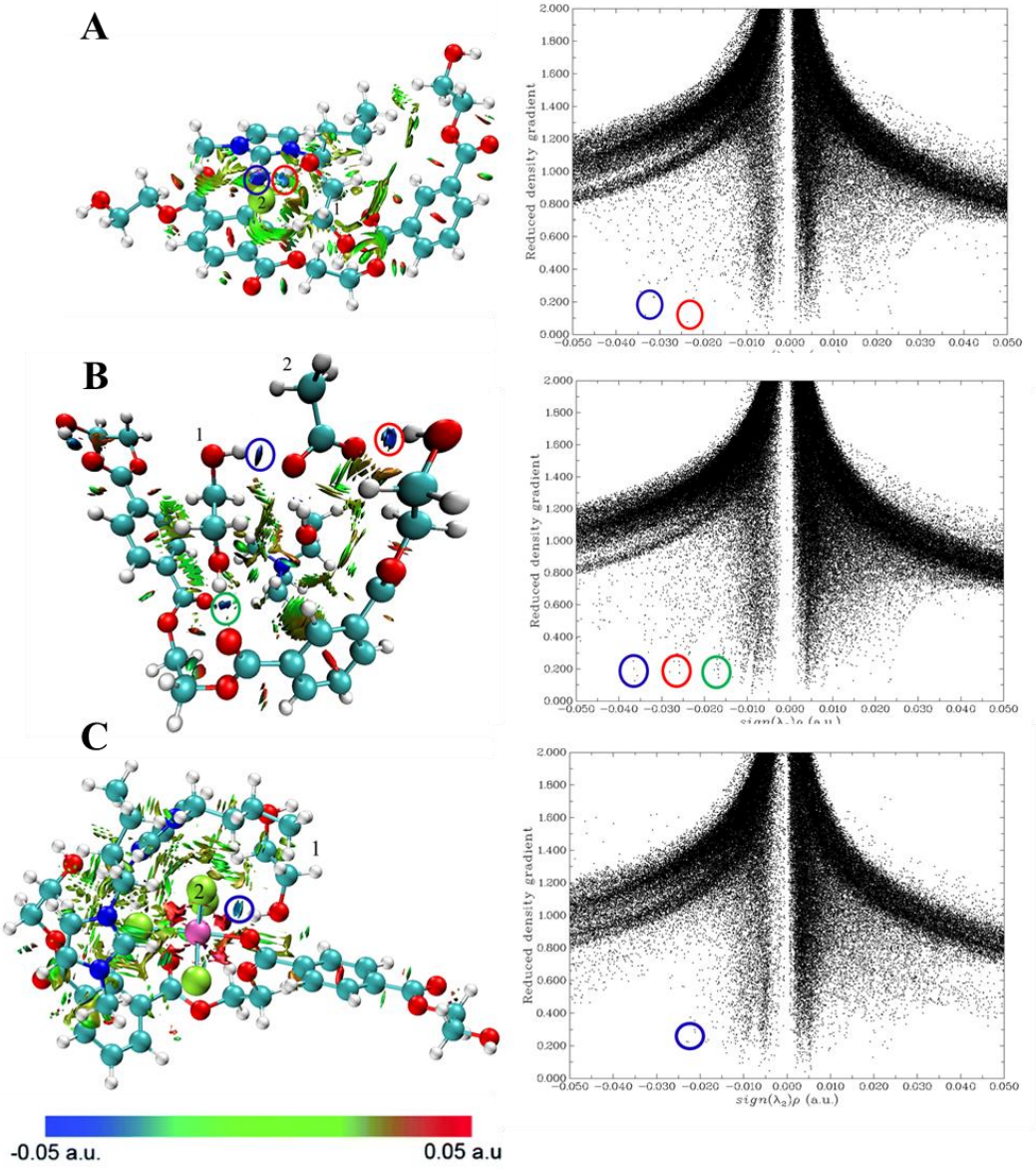

Figure 5.10. *RDG scatter plots and corresponding isosurfaces for A) [bmim]Cl, B) [Ch][OAc] and C) [bmim]$_2$[CoCl$_4$]. Atomic colour code: Blue – nitrogen, green – chlorine, pink – Co. Numbers 1 and 2 on the isosurfaces represent anion and EG, respectively.*

For the simplest catalyst, [bmim]Cl, there are two main regions of strong attractive interactions, shown as a blue isosurface. The strongest is located between the anion and cation, suggesting strong electrostatic forces, and is signified by the blue ring. The red ring, the second strongest area of attraction, displays the H-bonding between the chloride anion and the non-reacting EG hydroxyl group. This indicates that the chloride ion's influence is somewhat hindered by its location adjacent to its cation. The close proximity of the anion to the C2 hydrogen atom adjacent to the positively charged nitrogen of bmim, and thus the electron density it donates, makes it less available to interact with the active end of EG to facilitate the degradation. This relates to previous studies which emphasise the importance of balancing the strength of interactions between ion pairs. If interactions are too strong, there is a resultant insufficiency of "free" acidity or basicity to significantly influence the reaction [24,25].

In the case of [Ch][OAc], according to the peaks of the RDG plot, there are similarly strong interactions compared to the [bmim]Cl system. The blue, red and green rings represent interactions between OAc and EG, OAc and PET, and EG and PET, respectively. Although the strength of interaction is similar to the [bmim]Cl system, around -0.035 a.u., the moieties involved are more varied. Indeed, the strongest H-bonding occurs between OAc and the non-reacting hydroxyl group of EG, while there is weaker interaction between the anion and cation. This is resultant of the optimal configuration of the ion pair, shown in **Chapter 4**, which aligns the anionic oxygens proximal to the cationic hydroxyl group, rather than the localised positive charge surrounding the nitrogen of choline. Too strong interactions between cation and anion may result in hindering the catalytic effect, as shown by the calculated energy

barriers. Additionally, the green ring on **Figure 5.10B** represents the stabilising EG-PET interaction, discussed previously.

The metal IL results showcase the difference in importance between intermolecular non-bonding interactions and covalent bonding. By scanning the RDG plot, the intermolecular interactions are clearly weaker in the case of $[bmim]_2[CoCl_4]$, with a sign of the second Hessian eigenvalue value of ~-0.023 a.u., which is more positive than the organic IL cases. This emphasises the importance of the cobalt centre in activating the carbonyl oxygen of PET, which is shown to be more influential than any anion – EG interactions, as seen by the vastly reduced energy barrier produced by $[bmim]_2[CoCl_4]$. This activation of the carbonyl group is not represented by the RDG scatter plot, as it is not within the selected isovalue range. Additionally, the results highlight the influence of selective anionic interactions with EG, which in the metal IL case are weaker but targeted closer to the active site.

5.2.5 Charge analysis

As explored above, anionic interactions can heavily influence the reaction by inducing a partial negative charge on the reacting hydroxyl group oxygen of EG, thus affecting the O-H bond length [26,27]. Through ADCH analysis, this partial charge can be quantified and is shown, for each catalytic system, in **Figure 5.11**. Also included is the partial positive charge of the dimer's reacting C atom, which reflects the protonation caused by interaction with the carbonyl group from an external molecule [27].

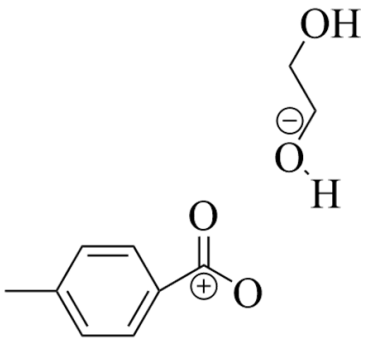

System	Charge on O	Charge on C	O-H bond length (Å)
[bmim]Cl	-0.443	0.799	0.961
[Ch][For]	-0.373	0.331	0.966
[Ch][OAc]	-0.369	0.334	0.966
$[bmim]_2[CoCl_4]$	-0.473	0.354	0.971

Figure 5.11. *Charge analysis and EG hydroxyl O-H bond lengths for each catalytic system.*

The charges of the oxygen atoms are in the order of system: $[bmim]_2[CoCl_4]$ < [bmim]Cl < [Ch][For] < [Ch][OAc]. The two choline-based ILs inducing a similar charge is unsurprising, while the close proximity of the metallic anion to the reacting hydroxyl group clearly influences the negativity of the oxygen atom, as expected. However, the charge value produced by [bmim]Cl, the worst-performing IL, is significantly more negative than both choline ILs. Additionally, the carbonyl C^+ is extremely more partially positive than any other system.

In theory, the more partially negative the O atom, the longer the O-H bond, due to repulsive forces between the LPs of oxygen and the bonding electrons. Subsequently, the longer O-H bond should be easier to break and activate the glycolysis reaction. However, the bond lengths were measured following geometric optimisation with DFT and the results follow the same trend as the energy barriers for each catalyst, with a longer O-H bond inducing a lower energy barrier, contrasting with the trend in partially negative charges. These results are surprising and suggest that the catalytic mechanism is not restricted to just electrostatic effects.

It is proposed that in addition to the electronic redistribution caused by intermolecular interactions, there are stabilising effects which holds the EG molecule

in a more favourable geometric position for the reaction to take place [13,14,28]. Therefore, the interaction between the PET carbonyl and EG hydroxyl group, which is very prominent in the choline IL cases, should be considered as a key interaction. While there is interaction between the PET and EG in the [bmim]Cl case, it is very weak. This causes the EG molecule to align out of plane with the PET dimer, requiring it to re-orient during the reaction process, thus increasing the energy barrier. For the new C-O bond to form upon the scission of the PET chain, the C_{BZ}-C-O_{EG} bond angle, where C_{BZ} is the benzene ring carbon, C is the PET ester carbon and O_{EG} is the reacting oxygen of EG, has to re-orient somewhat to form the appropriate bonds for the production of the monomer, according to the reaction models in this study. The re-orientation of the angle for each system is shown in **Table 5.10**.

Table 5.10. *Re-orientation of C_{BZ}-C-O_{EG} angle during PET glycolysis.*

System	Reactant C_{BZ}-C-O_{EG} angle (°)	TS C_{BZ}-C-O_{EG} angle (°)	Re-orientation required (°)
[bmim]Cl	83	105	22
[Ch][For]	107	113	6
[Ch][OAc]	107	112	5
$[bmim]_2[CoCl_4]$	96	109	13

The required re-orientation values match the exact trend of EG – PET carbonyl O interactions shown by the NBO and QTAIM analyses, confirming the geometric stabilisation these interactions create. The significant re-orientation required in the case of [bmim]Cl reiterates that the lack of stabilising interaction with PET is the most likely cause of the high energy barrier. While the re-orientation of EG in the metal IL

case is greater than the choline-based ILs, the polymer chain scission is much easier due to the role played by the cobalt centre.

5.3 Discussion

Based on the above, the reaction mechanisms for [Ch][OAc] and $[bmim]_2[CoCl_4]$, in comparison with the traditional mechanism described in the literature, are displayed in **Figure 5.12**. In contrast with the traditional mechanism, where the anion and cation work synergistically by interacting with EG and the PET carbonyl, respectively, both mechanisms observed here showed no significant cationic interactions. Instead, EG was seen to itself play a partially-catalytic role, or that of a geometric stabiliser, by interacting with the dimer, while the anion often facilitates the reaction through an inductive effect, rather than engaging with the reacting hydroxyl group directly. In the case of the metal IL, the Co-based anion was seen to be bifunctional, acting as both Lewis acid and base, explaining its excellent performance. Further details of the role played by both anion and cation are discussed below.

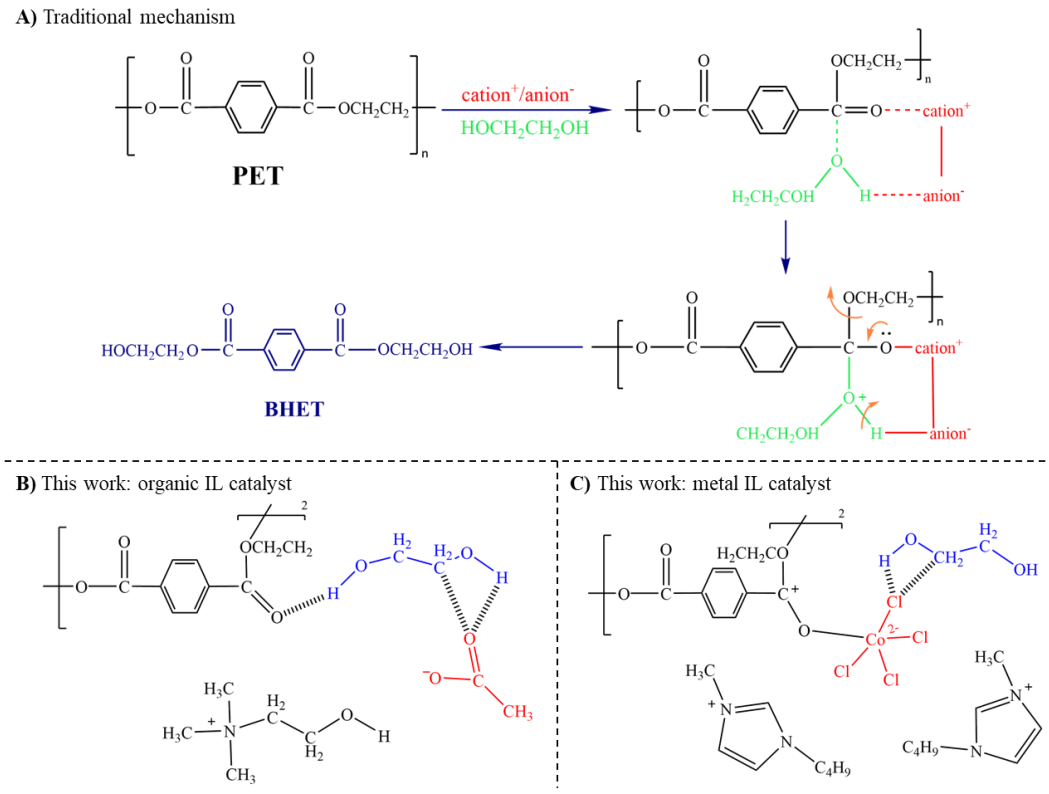

Figure 5.12. *Comparison of the conventional reaction mechanism to the [Ch][OAc] and [bmim]$_2$[CoCl$_4$] catalyst mechanisms derived in this work.*

5.3.1 Role of the anion

The previous analysis of the intermolecular interactions, charge transfer and energy barrier calculation, creates a clearer picture of the difference in roles played by metal-containing and non-metal anions. In each case, there exists anionic interactions with EG, as described by the traditionally-used reaction mechanism. However, due to the multitudes of varying sizes and compositions of anions, the current description of H-bonding between anions and the reactive hydroxyl group is an oversimplification.

Anions are usually accompanied by a bulkier cation, which, following the folding of the PET chain seen in **Chapter 4**, often prevents the anion from being located close to the active site and therefore, the reacting hydroxyl group. While the majority of mechanistic studies describe anionic interactions with the reacting

hydroxyl group of EG [18], the results here show that the most likely interactions are between the anion LPs and either the opposite EG hydroxyl group, or the methylene groups. What occurs after is an inductive-like effect, where the electron density is redistributed through the molecule [29]. To assess the difference in charge distribution, based on the position of the anion, relative to the EG molecule, single-point energy calculations were carried out and are displayed in **Figure 5.13**. An isolated EG molecule was included as the control example. Distances between the negatively charged conjugate oxygen and the selected hydrogen of EG were kept constant at 1.50 Å.

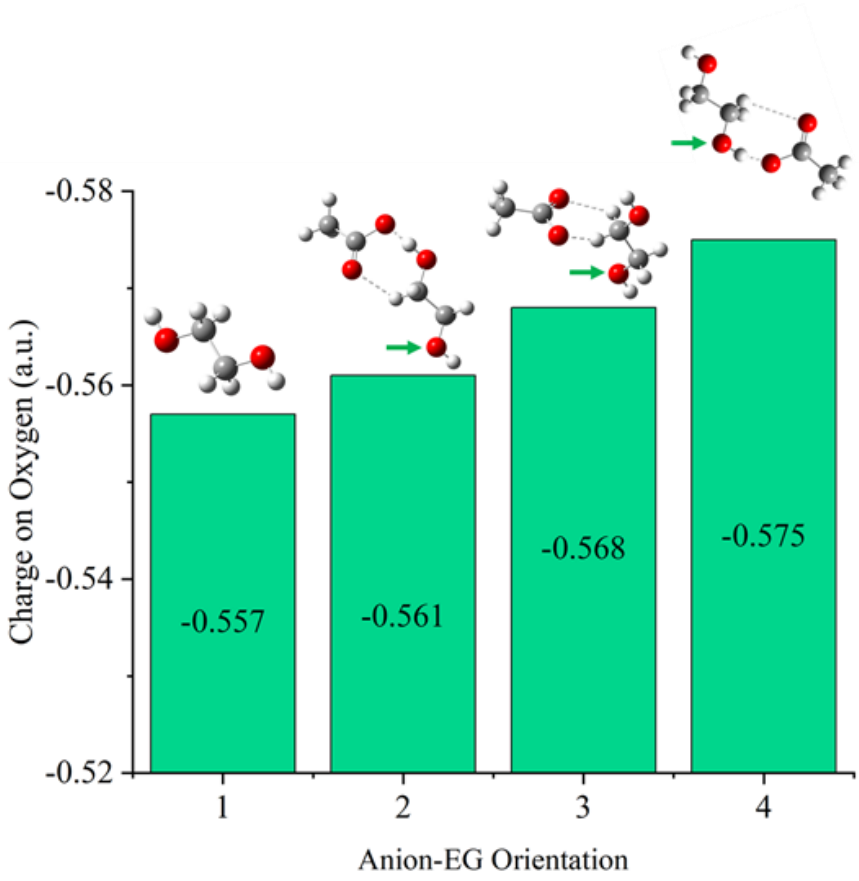

Figure 5.13. *Electronic charge of reacting EG hydroxyl oxygen atom, varying with relative position of anion (using OAc as an example). Green arrows point to the reacting O atom.*

The charge analysis of the EG molecule shows that, as expected, the reacting hydroxyl oxygen has the most negative charge in the idealistic case, where the acetate anion is located directly adjacent to it (orientation 4). In the cases of orientations 2 and 3, located along the EG molecule, the induced polarity is increasingly reduced as the acetate moves away from the active site. However, compared to the isolated system with no anion (orientation 1), each positional configuration does cause a redistribution of charge, enhancing the nucleophilic nature of EG. This serves as evidence of the inductive-like effect described above, meaning that despite steric hindrance preventing the anion from accessing the active site, it is still having an electronic effect on the nucleophile. However, reducing steric hindrance and prevention of access to the active site for anions should be considered for future catalyst design.

The metal IL, $[bmim]_2[CoCl_4]$, demonstrates an interestingly dynamic coordination capability. The cobalt centre is initially coordinated with chloride ions, forming a stable anionic complex. During the reaction, these cobalt-chloride bonds can temporarily weaken, creating open coordination sites on the cobalt. This allows cobalt to interact directly with the PET molecule, facilitating the scission of its polymeric structure, while the temporarily released chloride ion's increased negative charge interacts more strongly with the H atoms of EG.

The ability of cobalt to dynamically coordinate with PET enables a more efficient catalytic process. Organic catalysts, in contrast, lack this capability of providing a metal centre that can flexibly alter its coordination environment to stabilise transition states and lower activation energies. Instead, they are limited to the formation of non-covalent bonding complexes with EG. Consequently, the unique coordination chemistry of $[bmim]_2[CoCl_4]$ and its ability to engage in dynamic ligand

exchange make it a more effective compound for the catalytic degradation of PET [30]. A similar effect, where partial ligand dissociation facilitates the coordination between substrate and metal centre, has previously been reported in catalysed water oxidation systems [31].

Indeed, by conducting analysis of the bond orders in both the reactant and TS systems, the strength of covalent bonds could be monitored. **Figure 5.14** highlights the selected bond orders of atoms surrounding the active site in the metal IL-catalysed system. It should be noted that covalent bond types are generally in the bond order range shown in **Table 5.11**.

Reactant

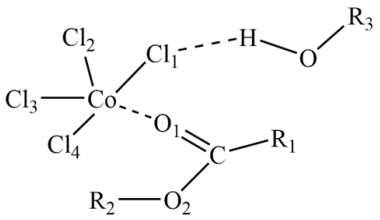

Bond	Bond order
Co – O1	0.82
Co – O2	0.07
C – O1	1.68
Co – Cl1	0.99

TS

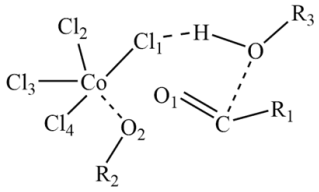

Bond	Bond order
Co – O1	0.41
Co – O2	0.99
C – O1	1.92
Co – Cl1	0.92

Figure 5.14. *Bond order analysis of selected atoms surrounding the active site during $[bmim]_2[CoCl_4]$-catalysed PET glycolysis. R1 and R2 represent separate ends of the dimer chain, while R3 represents the remainder of the EG molecule.*

Table 5.11. *Corresponding bond order ranges for covalent bond types.*

Bond order range	Bond type
1.8 – 2.1	Double
0.9 – 1.1	Single
0.6 – 0.9	Weak single
0.3 – 0.6	Partial
< 0.2	Nonbonded

From the representation of the reactant system, it can be seen that as the $CoCl_4$ anion approaches the PET/EG interface, it reorients itself to expose the metal centre to the dimer. Initially, it forms a bond with the double-bonded oxygen of the PET ester group, similar to what is described as the role of the cation in the literature reaction mechanisms. This bond results in protonation of the PET carbon and subsequent weakening of the C-O2 bond. At this point, interaction between Co and O2 is minimal. During the TS, the C-O1 bond has returned to its state of a double bond, with a bond order of 1.92, meanwhile Co has formed a clear single bond with O2, thus facilitating the scission of the dimer. Between the reactant and TS stage, there is a redistribution of electrons within the anion, highlighted by the weakening Co-Cl1 bond, freeing the electrons of the chloride ion to be donated to EG, aiding the nucleophilic attack.

The bond order analysis helps to conclude that the presence of the metal centre within the anion, allows it to perform both roles of the IL, within the synergic mechanism. The positive metal centre acts as a Lewis acid, while the dynamically attached chlorides act as Lewis bases. The full role of $[bmim]_2[CoCl_4]$ in the PET glycolysis process is outlined in **Figure 5.15**.

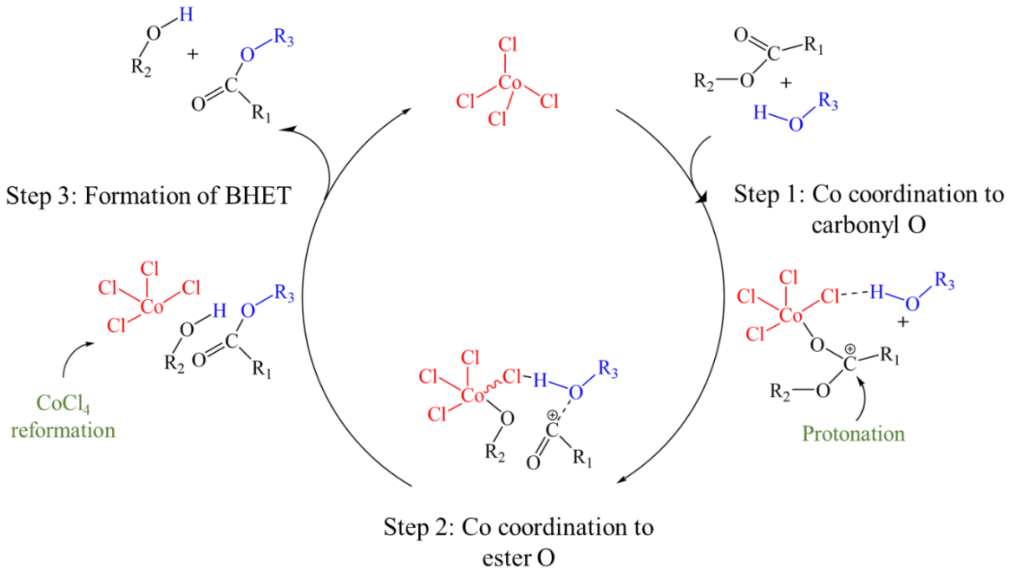

Figure 5.15. *Catalytic cycle of $CoCl_4^{2-}$ anion during glycolysis reaction. R1 and R2 represent separate ends of the dimer chain, while R3 represents the remainder of the EG molecule.*

In comparison to the organic systems, the anionic interaction with EG, previously noted to be the dominating catalytic influencing factor, is shown to be of less importance than the coordination ability of the anion's metallic centre as the electron density of the anion-EG BCP is considerably greater in the organic IL cases. However, it should be noted that, as mentioned before, the chloride ions of $CoCl_4$ interact directly with the reacting hydroxyl group of EG. Clearly, the strongest interactions within the metal IL system are between the cobalt atom and the carbonyl oxygen of PET, which results in protonation of the ester carbon atom, thus facilitating the degradation of the polymer chain. This effect, supplemented by very specific H-bonding with the reacting hydroxyl group of EG, are what make the metal IL a more effective catalyst, as shown by the energy barriers and experimental results in **Chapter 4**.

5.3.2 Role of the cation

Unlike the anions tested, the roles of the cations studied rarely resemble those described generally in the literature, where cationic interactions with the PET carbonyl oxygen act to protonate the ester carbon. In the cases of the choline-based ILs, [Ch][For] and [Ch][OAc], there are no significant interactions between the cation and PET. Instead, the carbonyl is stabilised via interactions from the reacting hydroxyl group. These results serve as further validation of the work carried out by Bura et al., as discussed in **Chapter 2** [14]. Their study also used DFT calculations to determine energy barriers of several scenarios. One traditional configuration, where the anion interacts with EG and the choline interacts with the carbonyl PET, and another scenario where there is the same anionic interaction, but the choline's role is simply to stabilise the anion, while another EG molecule interacts with the PET carbonyl. The results found that the lowest energy barrier was produced from the second scenario. The DFT results from this study agree well with their theory that, while the cation's "green" credentials are undeniable, its' mechanistic contribution is limited.

The imidazolium-based cation of [bmim]Cl is also seen to not behave as described in literature, instead interacting via H-bonding with the EG molecule. The long butyl chain of the cation comes into contact with the EG molecule and may contribute mechanistically towards its increasing polarity. However, it is potentially this larger size which causes steric hindrance and reduces the effectiveness of the catalyst [32,33]. Additionally, the results show that the only significant catalytic interactions are between anion-EG and cation-EG, suggesting that while anionic interactions are vital to the mechanism, there must still be some interaction with the PET carbonyl group to facilitate the reaction.

In the case of $[bmim]_2[CoCl_4]$, there is a similar lack of mechanistic contribution from the cation. Once more, the two cation molecules seem to only stabilise the charge of the anion. However, in this case, the Co atom acts as a Lewis acid while the chloride ions act as bases. Therefore, in the absence of mechanistic contribution from the bmim molecules, there is "cationic" contribution from the metal centre of the anion. This differs from previous studies of metal-based anions, which postulate that the roles of the ions swap when metal-based anions are used [34]. Instead, the bi-functionality of the anion negates the need for the cation, other than for charge stabilisation. While these results show that previous descriptions of IL-catalysed glycolysis mechanism are likely oversimplified, they do validate the general conclusion in the literature that a synergic mechanism promotes greater degradation [24]. Whether this is in the form of a more acidic organic cation or the central atom of a metal-based anion, Lewis acid protonation of the ester carbon via interactions with the carbonyl group are important for more effective degradation. While the choline cation's mechanistic ineffectiveness is notable, its biodegradability and cheap synthesis provide some positive contribution to the system. However, as outlined in **Chapter 2**, imidazolium-based ILs are relatively expensive and toxic. These results provide a justification to explore the replacement of bmim cations for PET glycolysis, if their contribution is indeed further confirmed to be limited, with greener and cheaper alternative cations.

5.3.3 Summary of reaction mechanism

From the DFT analysis discussed, there are various mechanisms through which the ILs can catalyse the PET glycolysis reaction:

- Organic anions interact non-covalently with EG through H-bonding, acting to enhance the polarity of the reacting hydroxyl group. An inductive-like effect can occur depending on the relative location of the molecules. Interactions with hydrogens closest to the reacting hydroxyl group will create more polarity than those further away.
- In each studied case, the mechanistic role of the cation is limited. In the choline- and metal-based ILs, there are no significant cation-PET interactions, meaning the role of the cation is merely a charge-stabilising one. In the case of [bmim]Cl, H-bonding between the butyl chain of the cation and EG may help polarise the hydroxyl group, however this is likely offset by the steric hindrance which brings them together in the first place.
- Metal-based anions are capable of performing bi-functionally, to effectively enhance the degradation process. The metal centre first protonates the PET carbon by coordinating with the carbonyl oxygen, before dynamically re-coordinating with the ester oxygen, meanwhile weakening its bonding to the chloride ions, allowing them to interact with the EG hydroxyl group. In this way, the $CoCl_4$ anion acts both as a Lewis acid and Lewis base. This dynamic coordination is not seen in the cases of the organic ILs and is therefore concluded to contribute significantly towards its enhanced catalytic effectiveness.
- In the absence of cation-PET interactions, H-bonding between the EG hydroxyl group and the carbonyl oxygen of PET, which seems to stabilise the geometry, facilitates the convenient nucleophilic attack of the polymer chain. These interactions not only have an electronic effect but a geometric one too. By

strongly interacting with the polymer chain, the EG molecule remains in plane with PET, preventing the need for significant re-orientation during the reaction.

5.4 Conclusions

This chapter presents a detailed mechanistic study of PET glycolysis catalysed by both metal- and organic-based ILs, supported by DFT-based analyses including NBO, QTAIM, RDG and population studies. The conventional mechanism focused on hydrogen bonding between anion and the reacting hydroxyl group of EG, and protonation of the PET carbonyl by the cation. This was re-evaluated in light of steric and electronic factors.

The results revealed that the position of the anion relative to the EG active site does indeed influence its effect on the extent of nucleophilicity of the hydroxyl group, although the inductive-like polarising effect was witnessed in all the organic IL cases. While anion-EG and interactions were found to be important, as in the literature, additional H-bonding between EG and the PET carbonyl group is proposed to provide geometric stability to the EG molecule, preparing it for convenient nucleophilic attack of the polymer chain. In all cases, the results showed that the mechanistic impact of the cation was limited. Instead of interacting strongly with the PET carbonyl, as proposed by literature, its primary role was in stabilising the charge distribution of the anion. This raises the notion that these catalysts could be redesigned with a more influential cation in mind.

In contrast to the organic ILs, $[bmim]_2[CoCl_4]$ exhibits a versatile coordination behaviour, wherein the cobalt centre temporarily weakens its ligand bonds, allowing direct coordination with the PET ester group: first with the carbonyl oxygen, then the ester oxygen. Bond order analysis reinforces this mechanism, showing that cobalt

plays a dual role: acting “cationically” as a Lewis acidic centre, while its associated chlorides function as reactive anions. The bmim cations primarily serve to stabilise the anionic framework, once again opening the door to redesign of ILs, as imidazolium-based cations could be replaced by greener and cheaper alternatives. Thus, $CoCl_4$ functions as a self-sufficient catalytic entity, capable of flexibly modulating its electronic and structural configuration to promote PET depolymerisation. This bifunctional behaviour, absent in organic ILs, underpins the superior catalytic efficiency of metal-based ILs in this system.

Overall, the DFT calculations and additional analyses emphasise the need for a deep mechanistic understanding of IL-catalysed systems, with “off-the-shelf” degradation mechanisms often misrepresenting the true interactions. By gaining more insight into the roles played by each ion pair, future catalyst and process design can be more effectively informed.

References

[1] M.J. Frisch, G.W. Trucks, H.B. Schlegel, G.E. Scuseria, M.A. Robb, J.R. Cheeseman, G. Scalmani, V. Barone, G.A. Petersson, H. Nakatsuji, X. Li, M. Caricato, A. V. Marenich, J. Bloino, B.G. Janesko, R. Gomperts, B. Mennucci, H.P. Hratchian, J. V. Ortiz, A.F. Izmaylov, J.L. Sonnenberg, D. Williams-Young, F. Ding, F. Lipparini, F. Egidi, J. Goings, B. Peng, A. Petrone, T. Henderson, D. Ranasinghe, V.G. Zakrzewski, J. Gao, N. Rega, G. Zheng, W. Liang, M. Hada, M. Ehara, K. Toyota, R. Fukuda, J. Hasegawa, M. Ishida, T. Nakajima, Y. Honda, O. Kitao, H. Nakai, T. Vreven, K. Throssell, J.A. Montgomery, Jr, J.E. Peralta, F. Ogliaro, M.J. Bearpark, J.J. Heyd, E.N. Brothers, K.N. Kudin, V.N. Staroverov, T.A. Keith, R. Kobayashi, J. Normand, K. Raghavachari, A.P. Rendell, J.C. Burant, S.S. Iyengar, J. Tomasi, M.

Cossi, J.M. Millam, M. Klene, C. Adamo, R. Cammi, J.W. Ochterski, R.L. Martin, K. Morokuma, O. Farkas, J.B. Foresman, D.J. Fox, Gaussian 16, (2016).

[2] T. Lu, F. Chen, Multiwfn: A multifunctional wavefunction analyzer, J Comput Chem 33 (2012) 580–592. https://doi.org/10.1002/jcc.22885.

[3] J.P. Perdew, K. Burke, Generalized gradient approximation for the exchange-correlation hole of a many-electron system, Phys Rev B Condens Matter Mater Phys 54 (1996) 16533–16539. https://doi.org/10.1103/PhysRevB.54.16533.

[4] Axel D. Becke, Density-functional thermochemistry. III. The role of exact exchange, J Chem Phys 98 (1993) 5648.

[5] C. Lee, W. Yang, R.G. Parr, Development of the Colle-Salvetti correlation-energy formula into a functional of the electron density, Phys Rev B Condens Matter Mater Phys 37 (1988) 785–789. https://doi.org/10.1103/PhysRevB.37.785.

[6] A. V. Marenich, C.J. Cramer, D.G. Truhlar, Universal solvation model based on solute electron density and on a continuum model of the solvent defined by the bulk dielectric constant and atomic surface tensions, J. Phys. Chem. B 113 (2009) 6378–6396. https://doi.org/10.1021/jp810292n.

[7] S. Emamian, T. Lu, H. Kruse, H. Emamian, Exploring nature and predicting strength of hydrogen bonds: A correlation analysis between atoms-in-molecules descriptors, binding energies, and energy components of symmetry-adapted perturbation theory, J Comput Chem 40 (2019) 2868–2881. https://doi.org/10.1002/jcc.26068.

[8] P.A. Hunt, C.R. Ashworth, R.P. Matthews, Hydrogen bonding in ionic liquids, Chem Soc Rev 44 (2015) 1257–1288. https://doi.org/10.1039/c4cs00278d.

[9] J.A. Agwupuye, H. Louis, T.O. Unimuke, P. David, E.I. Ubana, Y.L. Moshood, Electronic structure investigation of the stability, reactivity, NBO analysis, thermodynamics, and the nature of the interactions in methyl-substituted imidazolium-based ionic liquids, J Mol Liq 337 (2021). https://doi.org/10.1016/j.molliq.2021.116458.

[10] J.A. Murillo-Hernández, S. López-Ramírez, J.M. Domínguez, C. Duran-Valencia, I. García-Cruz, J.A. González-Guevara, Survey on ionic liquids effect based on metal anions over the thermal stability of heavy oil, J Therm Anal Calorim 95 (2009) 173-179. https://doi.org/10.1007/s10973-007-8919-5.

[11] M.I. Ofem, C.A. Ayi, H. Louis, T.E. Gber, A.A. Ayi, Influence of anionic species on the molecular structure, nature of bonding, reactivity, and stability of ionic liquids-based on 1-butyl-3-methylimidazolium, J Mol Liq 387 (2023). https://doi.org/10.1016/j.molliq.2023.122657.

[12] L. Del Olmo, C. Morera-Boado, R. López, J.M. García De La Vega, Electron density analysis of 1-butyl-3-methylimidazolium chloride ionic liquid, J Mol Model 20 (2014). https://doi.org/10.1007/s00894-014-2175-y.

[13] M.A. Nosir, M.A. Ortuño, Catalytic function of ionic liquids in polyethylene terephthalate glycolysis by molecular dynamics simulations, RSC Sustain. 2 (2024) 2677–2683. https://doi.org/10.1039/d4su00251b.

[14] D. Bura, L. Pedrini, C. Trujillo, S.J. Connon, Cholinium-based ionic liquid catalysts for polyethylene terephthalate glycolysis: understanding the role of solvent and a reappraisal of the cation contribution, RSC Sustain. 1 (2023) 2197–2201. https://doi.org/10.1039/d3su00336a.

[15] Z. Ju, W. Xiao, X. Lu, X. Liu, X. Yao, X. Zhang, S. Zhang, Theoretical studies on glycolysis of poly(ethylene terephthalate) in ionic liquids, RSC Adv 8 (2018) 8209–8219. https://doi.org/10.1039/c7ra13173a.

[16] S. Conroy, X. Zhang, Theoretical insights into chemical recycling of polyethylene terephthalate (PET), Polym Degrad Stab 223 (2024) 110729. https://doi.org/10.1016/j.polymdegradstab.2024.110729.

[17] Q. Wang, Y. Geng, X. Lu, S. Zhang, First-row transition metal-containing ionic liquids as highly active catalysts for the glycolysis of poly(ethylene terephthalate) (PET), ACS Sustain Chem Eng 3 (2015) 340–348. https://doi.org/10.1021/sc5007522.

[18] Y. Liu, X. Yao, H. Yao, Q. Zhou, J. Xin, X. Lu, S. Zhang, Degradation of poly(ethylene terephthalate) catalyzed by metal-free choline-based ionic liquids, Green Chem. 22 (2020) 3122–3131. https://doi.org/10.1039/d0gc00327a.

[19] P. Anggo Krisbiantoro, Y.W. Chiao, W. Liao, J.P. Sun, D. Tsutsumi, H. Yamamoto, Y. Kamiya, K. C.-W. Wu, Catalytic glycolysis of polyethylene terephthalate (PET) by solvent-free mechanochemically synthesized MFe2O4 (M = Co, Ni, Cu and Zn) spinel, Chem. Eng. J. 450 (2022). https://doi.org/10.1016/j.cej.2022.137926.

[20] M. Schlüter, R. Enomoto, S. Makino, L. Weihs, C.L. Stamm, K. Wohlgemuth, C. Held, Boosting the kinetics of PET glycolysis, React Chem Eng 9 (2024) 3038–3046. https://doi.org/10.1039/d4re00235k.

[21] A.J. Stone, Natural bond orbitals and the nature of the hydrogen bond, J. Phys. Chem. A 121 (2017) 1531–1534. https://doi.org/10.1021/acs.jpca.6b12930.

[22] P.A. Hunt, C.R. Ashworth, R.P. Matthews, Hydrogen bonding in ionic liquids, Chem Soc Rev 44 (2015) 1257–1288. https://doi.org/10.1039/c4cs00278d.

[23] C. Guerra, J. Burgos, L. Ayarde-Henríquez, E. Chamorro, Formulating reduced density gradient approaches for noncovalent interactions, J. Phys. Chem. A 128 (2024) 6158–6166. https://doi.org/10.1021/acs.jpca.4c01667.

[24] K.R. Delle Chiaie, F.R. McMahon, E.J. Williams, M.J. Price, A.P. Dove, Dual-catalytic depolymerization of polyethylene terephthalate (PET), Polym Chem 11 (2020) 1450–1453. https://doi.org/10.1039/c9py01920k.

[25] S. Naumann, P.B.V. Scholten, J.A. Wilson, A.P. Dove, Dual catalysis for selective ring-opening polymerization of lactones: Evolution toward simplicity, J Am Chem Soc 137 (2015) 14439–14445. https://doi.org/10.1021/jacs.5b09502.

[26] Z. Bai, Z. Bao, H. Hu, Chemical recycling of catalytic glycolysis of polyethylene terephthalate with potassium-rich biomass, Recycling 10 (2025). https://doi.org/10.3390/recycling10030085.

[27] H. Yao, X. Lu, L. Ji, X. Tan, S. Zhang, Multiple hydrogen bonds promote the nonmetallic degradation process of polyethylene terephthalate with an amino acid ionic liquid catalyst, Ind Eng Chem Res 60 (2021) 4180–4188. https://doi.org/10.1021/acs.iecr.0c06073.

[28] I. Olazabal, E.J. Luna Barrios, S. De Meester, C. Jehanno, H. Sardon, Overcoming the limitations of organocatalyzed glycolysis of poly(ethylene terephthalate) to facilitate the recycling of complex waste under mild conditions, ACS Appl Polym Mater (2024). https://doi.org/10.1021/acsapm.4c00326.

[29] Y. Kong, Z. Song, S. Wang, Z. Xia, Q. Liu, Charge transfer, local structure, and the inductive effect in rare-earth-doped inorganic solids, Inorg Chem 57 (2018) 12376–12383. https://doi.org/10.1021/acs.inorgchem.8b02141.

[30] P. Fang, B. Liu, J. Xu, Q. Zhou, S. Zhang, J. Ma, X. lu, High-efficiency glycolysis of poly(ethylene terephthalate) by sandwich-structure polyoxometalate catalyst with two active sites, Polym Degrad Stab 156 (2018) 22–31. https://doi.org/10.1016/j.polymdegradstab.2018.07.004.

[31] B. Das, A. Orthaber, S. Ott, A. Thapper, Water oxidation catalysed by a mononuclear CoII polypyridine complex; Possible reaction intermediates and the role of the chloride ligand, Chem. Commun. 51 (2015) 13074–13077. https://doi.org/10.1039/c5cc04148a.

[32] Z. Guo, J. Wu, J. Wang, Chemical degradation and recycling of polyethylene terephthalate (PET): a review, RSC Sustain. 3 (2025) 2111–2133. https://doi.org/10.1039/d4su00658e.

[33] L. Nguyet Thi Ho, D. Minh Ngo, J. Cho, H.M. Jung, Enhanced catalytic glycolysis conditions for chemical recycling of glycol-modified poly(ethylene terephthalate), Polym Degrad Stab 155 (2018) 15–21. https://doi.org/10.1016/j.polymdegradstab.2018.07.003.

[34] T. Wang, X. Gong, C. Shen, G. Yu, X. Chen, Formation of Bis(hydroxyethyl) terephthalate from waste plastic using ionic liquid as catalyst, Polym Degrad Stab 190 (2021) 109601. https://doi.org/10.1016/j.polymdegradstab.2021.109601.

Chapter 6
Enhancements in PET glycolysis processes

Chapter 4 of this thesis showed the capability of two ionic liquids (ILs), [Ch][OAc] and $[bmim]_2[CoCl_4]$, to catalyse the glycolysis of polyethylene terephthalate (PET) to its monomer bis(2-hydroxyethyl) terephthalate (BHET), however BHET yields are still low. Theoretical studies in **Chapter 5** further revealed that the enhanced performance of the metal-based IL arises from its unique ability to coordinate with PET. However, the use of heavy metal-containing catalysts like Co-based ones is being phased out due to the toxicity of the metal and high cost. Contrastingly, choline-based ILs are considered to be environmentally friendly and cheap, but less effective than metal-based ones. While these IL catalysts do not achieve the three pillars of sustainability, low-cost and effectiveness, their use in industry will always be limited. Therefore, the focus of this chapter is to design a process which satisfies these requirements by exploring three strategies:

1) Microwave (MW) heating - to reduce reaction time and energy consumption, while enhancing catalytic performance;
2) Exploration of moisture effects - to relate the process to real-world plastic waste conditions;
3) Biochar-supported IL catalysts - using waste biomass-derived biochar (BC) as a catalyst support to enhance catalyst recovery and performance.

6.1 Methodology

6.1.1 MW heating

MW heating experiments were carried out by mixing ILs, PET and EG at a w/w ratio of 0.1:1:4 in a glass flask and loading into a CEM microwave reactor. Due to equipment specifications, reaction mixtures had to be reduced in weight by a factor of 10. The heating responses of [Ch][OAc] and $[bmim]_2[CoCl_4]$ were compared by running the scenarios shown in **Table 6.1**, three times. Once the target temperature was achieved, the reaction was continued for five minutes to monitor the temperature fluctuation.

Table 6.1. *Reaction parameters for MW heating response of each IL.*

Catalyst	Temperature (°C)	Catalyst:PET:EG ratio (w/w)	Reaction time (mins)
[Ch][OAc]	190	0.1:1:4	5
$[bmim]_2[CoCl_4]$	190	0.1:1:4	5

The best-performing IL was then selected for further study. PET glycolysis experiments were carried out using the same procedure in **Chapter 3**, **Section 3.1.2.5**, testing the three scenarios outlined in **Table 6.2**.

Table 6.2. *Experimental runs of MW-heated PET glycolysis.*

Catalyst	Temperature (°C)	Catalyst:PET:EG ratio (w/w)	Reaction time (mins)
$[bmim]_2[CoCl_4]$	190	0.1:1:4	15
$[bmim]_2[CoCl_4]$	190	0.1:1:4	30
$[bmim]_2[CoCl_4]$	190	0.1:1:4	45

6.1.2 Moisture content testing

To evaluate the effects of moisture, both ordinary ethylene glycol (EG) and an anhydrous EG sample were purchased from Sigma Aldrich. The moisture content of

the original and anhydrous solvent was then measured using Karl Fischer (KF) titration. Each sample was characterised three times for reliability. Two scenarios, one "wet" and one "dry", were tested using [Ch][OAc] and $[bmim]_2[CoCl_4]$ as IL catalysts under the same reaction conditions, stated in **Table 6.3**.

Table 6.3. *Scenarios tested to compare "wet" and "dry" EG for two IL catalysts.*

Run	Catalyst	Solvent	Temperature (°C)	Catalyst:PET:EG ratio (w/w)	Reaction time (mins)
1	[Ch][OAc]	Wet EG	190	0.1:1:4	120
2	[Ch][OAc]	Dry EG	190	0.1:1:4	120
3	$[bmim]_2[CoCl_4]$	Wet EG	190	0.1:1:4	120
4	$[bmim]_2[CoCl_4]$	Dry EG	190	0.1:1:4	120

The PET glycolysis process was carried out as above, with PET conversion and BHET yield calculated for each scenario. In order to validate the quality of the in-house synthesised organic IL, a pure [Ch][OAc] was purchased from Sigma Aldrich and used.

6.1.3 BC-supported IL-catalysed glycolysis

BC-supported IL catalysts were prepared using the procedure outlined in **Chapter 3, Section 3.1.2.4**. Only the purchased, pure [Ch][OAc], instead of the in-house synthesised sample, was used for the BC study. The in-house synthesised $[bmim]_2[CoCl_4]$ was used for the BC support investigation.

To validate the presence of the ILs on the BC surface, Fourier transform infrared (FT-IR) and Raman spectroscopy of the pristine and IL-grafted BC samples was performed. Both spectra were determined as in **Chapter 4**.

Once the catalysts were prepared, the glycolysis process was carried out as before, using the anhydrous EG as solvent. Due to the limited amounts of BC available for use, only one experimental run was carried out for each supported IL (**Table 6.4**).

The optimal scenario, determined in **Chapter 4**, was used for both catalysts. FT-IR and nuclear magnetic resonance (NMR) spectra of degradation products were recorded as before.

Table 6.4. *Experimental scenarios for BC-supported IL-catalysed PET glycolysis.*

Run	Catalyst	Solvent	Temperature (°C)	Catalyst:PET:EG ratio (w/w)	Reaction time (mins)
1	BC-[Ch][OAc]	Wet EG	190	0.1:1:4	120
2	BC-$[bmim]_2[CoCl_4]$	Wet EG	190	0.1:1:4	120

In addition to the PET conversion and BHET yield, the greenness of the BC-supported process was analysed using the atom economy, E-factor and energy efficiency coefficient (ε) as green metrics, determined using **Equations 6.1**, **6.2** and **6.3**, respectively.

$$Atom\ economy = \frac{M_{BHET}}{M_{PET}+M_{EG}} \times 100 \quad (6.1)$$

$$E - factor = \frac{W_{PET}+W_{EG}-W_{BHET}}{W_{BHET}} \quad (6.2)$$

$$\varepsilon = \frac{W_{BHET}}{T\tau} \quad (6.3)$$

Where M_{BHET}, M_{PET} and M_{EG} are the molecular weights of BHET, PET and EG, respectively. W_{PET} and W_{EG} are the initial weights of PET and EG loaded into the system, respectively, while W_{BHET} is the final mass of BHET produced. T and τ represent the reaction temperature (°C) and time (minutes), respectively.

6.1.4 Computational details

All density functional theory (DFT) modelling of the effects of moisture were carried out using Gaussian 16 package [1], with the same methods previously used in **Chapters 4** and **5**: B3LYP-D3/6-311G(d,p) for non-transition metal atoms, while the

LANL2DZ basis set was used for transition metal atoms [2–4]. The solvation model using density (SMD) model was used to replicate the EG solvent environment [5] and dispersion correction was carried out using Grimme's D3 method [6]. Energy barrier calculations were carried out using the same procedure as in **Chapter 4**, using **Equation 4.1** to calculate the activation energy. Intrinsic reaction coordinate (IRC) and frequency analysis were carried out as before to confirm the desired reactants and products. Quantum theory of atoms in molecules (QTAIM) analysis of the intermolecular interactions within the water-doped systems were conducted as described in **Chapter 5**.

To validate the role played by the BC catalyst support, adsorption calculations were carried out. Due to the partially crystalline nature of the BC, periodic DFT was employed through the CASTEP code in the BIOVIA Materials Studio software package. DFT modelling of a KOH-activated BC surface was carried out using the CASTEP code as part of the BIOVIA Materials Studio package [7,8]. For adsorption calculations, the generalized gradient approximation (GGA) and Perdew-Burke-Ernzerhof functional were employed to account for exchange-correlation energy [9]. Although hybrid functionals such as HSE06 are known to be more accurate, they are extremely computationally expensive and so, were ruled out for use here [10]. The projector augmented wave pseudopotentials and van der Waals (vdW) interactions were described using the Grimme DFT-D3 method [11]. The Kohn-Sham equations were solved with a convergence criterion of 2.0×10^{-5} eV/atom for energy and 0.05 eV $Å^{-1}$ for force. Additionally, k-point sampling was carried out using the Monkhorst–Pack scheme with a (1 ×1 × 1) grid, and a cut-off energy of 400 eV was applied. Adsorption energies were calculated using **Equation 6.4.**

$$E_{Ads} = E_{AB} - E_A - E_B \quad (6.4)$$

Where E_{AB} is the energy of the complex system, E_A is the energy of the adsorbent and E_B is the energy of the adsorbate.

6.2 MW-heated PET glycolysis

6.2.1 MW heating performance of ILs

First, the thermal response of the ILs to the dielectric heating mechanism was investigated. By comparing the heating properties of mixtures of identical catalyst:PET:EG ratios, the influence of the specific catalyst being used can be compared. **Figure 6.1** represents the time taken for each catalytic system, containing PET, EG and IL, to reach the desired reaction temperature of 190 °C. As each system contains the same amounts of PET, EG and IL, the time taken to reach the target temperature is assumed to be a direct indication of the IL's ability, or inability, to efficiently absorb MW irradiation.

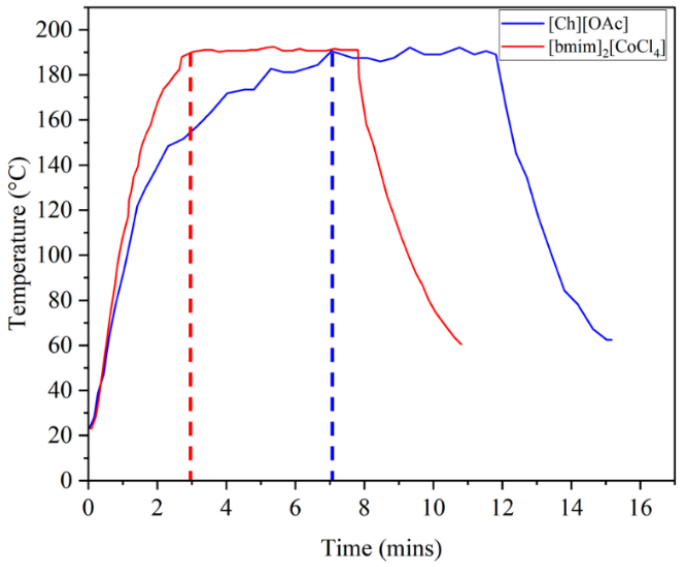

Figure 6.1. *Heating profile of PET, EG, IL systems using MW heating. Red and blue dotted lines indicate the time at which the target temperature is reached, using [bmim]$_2$[CoCl$_4$] and [Ch][OAc], respectively.*

The results show the time taken to reach the target temperature, followed by 5 minutes during which this temperature is sustained, and finally a cool-down period. It should be noted that the reaction was stopped once the system reached a temperature of 60 °C during cool-down. Evidently, the system containing the metal IL is more effectively heated by the MWs, reaching the target temperature after just 3 minutes, around 4 minutes faster than the organic IL. Additionally, there is less temperature fluctuation associated the metal IL, providing a much more steady and reliable system heating. Another indicator of the ILs response to MW heating, is the power output required to achieve and then maintain the target temperature. The power output of the reactor is what supplies heat to the system, *via* the MW irradiation. **Figure 6.2** shows the power gradient with time for both catalytic systems at 190 °C.

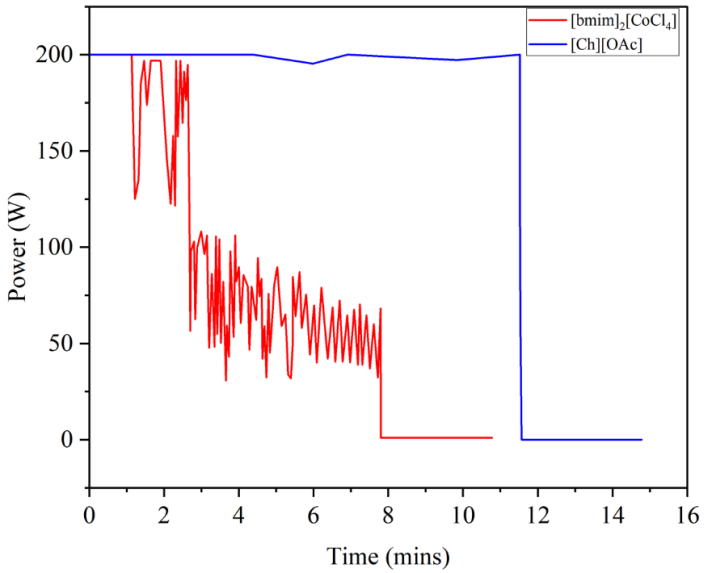

Figure 6.2. *Power output profile of PET, EG, IL systems, heated to a target temperature of 190 °C and sustained for 5 minutes.*

The reactor operates by ramping the heat in the system as quickly as possible, initially maximising its power output (200 W) until the target temperature is reached. Then, assuming there is enough heat present in the closed system, the output reduces,

only increasing to apply small amounts of heat when required. This effect is seen in the metal IL system, where other than a few fluctuations, the power operates comfortably at over half the maximum output value. Contrastingly, the organic IL system requires maximum power for the duration of the reaction, just to maintain the temperature. From a safety perspective, this creates the potential for thermal overshoots and overpressure of the reaction vessel [12]. The results indicate that the organic IL, [Ch][OAc], is unsuitable for consideration for a MW-assisted PET glycolysis process, due to the its relative MW transparency compared to alternative ILs. Therefore, it was not considered for further investigation. Previous studies have successfully combined choline-based deep eutectic solvents (DESs) with MW heating, however DES:solvent ratios were as high as 1:4, as opposed to the 1:40 IL:EG ratio used in this study, making the catalyst lifecycle costs unviable for PET glycolysis [13]. Future work could potentially combine choline-based ILs with MW doping agents to enhance their response. “Cladding” materials for MW-transparent materials in the form of carbonaceous supports, such as graphite, carbon nanotubes (CNT) and BC can generate microplasma due to their excellent response to MWs [14–16].

In conventionally heated systems, usually controlled by thermally regulated hot plates, there exists a conservative heating ramp to prevent these thermal overshoots which causes the slow heating rate. Indeed, the conventional heating time for the same reaction mixture is 20 minutes. Therefore, the extremely fast and non-fluctuating heating seen in the metal IL system, as well as the reduced energy demands of the power ramping, is an attractive prospect. In the event that a higher power MW reactor was available, it is likely that the target temperature could be reached in an even shorter

time. Although MW-induced intensification of the process will reduce operating costs, the issues of high synthesis costs and toxicity of the metal IL remain.

It should be noted that, while MW heating can theoretically enhance the energy efficiency of the process, there remain numerous challenges for scalable MW technology. From an economic perspective, a major drawback is the incompatibility of MW systems with conventional ones, meaning that the currently-used systems would have to be fully replaced, at significant capital investment [17]. On a technical level, concerns have been raised regarding the actual energy efficiency of MW heating, due to the necessity for the use of electrical energy for operation, as opposed to lower grade recycled heat energy used in conventional processes [18]. However, this can be balanced by the considerably shortened reaction times, as well as the reduced power input required once the reaction has been initiated. Beyond energy efficiency, another scale-up issue is the penetration depth of the materials being heated, meaning the distance into the material over which the MW power decreases significantly compared to its surface value [19]. Upon scale-up, the inability of PET to absorb MW heating could significantly promote this issue without efficient mixing, even in the presence of the highly polar medium, EG.

While the industrialisation of MW-heated PET glycolysis is still in its infancy, there exists some evidence of viable processes. DEMETO, a project funded by the EU's Horizon programme, utilises a MW-assisted, catalysed chemical recycling system, which has been validated at full pilot plant scale, while a partnership between gr3n and Schneider Electric is planning on building a 40000 ton/year production plant as of March, 2024 [20,21]. While both plants operate a PET hydrolysis process, they serve as a proof of concept of the scalability of MW-assisted chemical recycling of

PET. Indeed, their continuous reactor approach, in contrast to the industry standard batch reactor, effectively solves many of the challenges of MW chemistry at scale, including penetration depth and temperature control, while intensifying the process. However, it should be noted that, while several lab- and pilot-scale studies show evidence of reduced energy consumption, public data at an industrial scale is lacking and so, it is difficult to conclusively ascertain that total energy consumption is reduced inherently, when using MW heating.

As introduced in **Chapter 2**, MW heating generally relies on the dipolar polarisation and/or ionic conduction mechanisms to heat a sample. Many ILs are notable for their polarity, while clearly the presence of ions will support of the latter mechanism, in any case. Examination of the DFT-calculated permanent dipole moment of each ion was carried out. **Figure 6.3** shows that, unlike the other ions, the $CoCl_4$ anion does not contain a permanent dipole moment due to its tetrahedral geometry. Also shown is the dipole moment of EG, meaning that in all systems, the solvent is also contributing towards the dipolar polarisation mechanism.

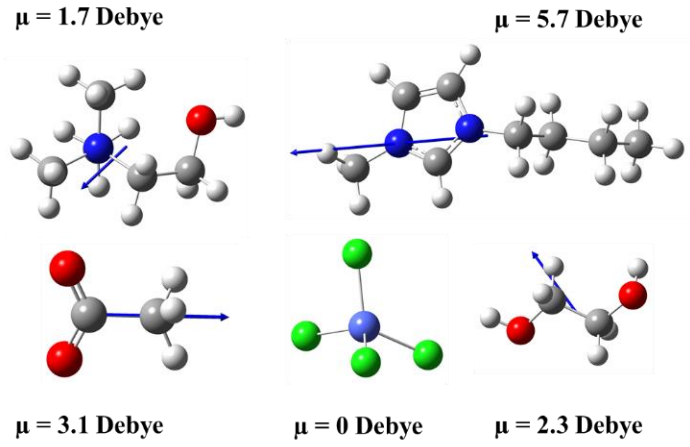

Figure 6.3. *DFT-derived dipole moment for each ion, as well as EG, showing the magnitude and direction of the dipole moment vector. (L-R) Ch, bmim, OAc, $CoCl_4$ and EG.*

Unlike other metal ions, Co^{2+} does not have any 4s electrons which are free to conduct, instead containing more localised d-orbital electrons. However, in addition to the two main dielectric heating mechanisms, there is also a magnetic material-specific mechanism, where the magnetic field affects the spin of magnetic materials [22]. The cobalt(II) ion can exist in one of two spin states: high (S=3/2) or low (S=1/2), depending on the nature of the ligand. In the tetrahedral tetrachlorocobaltate ion, the chloride ions form a weak-field ligand, resulting in a high state spin for cobalt. It is this high spin state and unpaired d electrons which give the anion its paramagnetism, meaning the metal IL is capable of being heated through both dielectric and magnetic MW heating mechanism, thus explaining its enhanced response in this study. There are many studies using cobalt-based complexes for their MW absorption capacities which serve to validate the results, especially in combination with a compound which utilises the dielectric heating mechanism more strongly – bmim and EG in this case [23,24]. In addition to other ions, the dielectric component can be contributed towards by porous carbon materials such as BC-derived activated carbon (AC), meaning their combination with cobalt complexes could enhance the rapid heating effect even further [25]. It should be noted that other transition metals such as Fe, likely have even greater effectiveness for heating under MW due to their increased magnetism [26].

6.2.2 MW heated glycolysis experiments

Having shown the efficient MW heating of the $[bmim]_2[CoCl_4]$-catalysed reaction sample, the reaction time was extended to 15, 30 and 45 minutes, respectively, to investigate the PET conversion and BHET yield at 190 °C and a 0.1:1:4 (IL:PET:EG w/w) ratio. The results, displayed in **Figure 6.4**, show that a reasonable PET conversion of 59% was achieved after just 15 minutes. At the same point in the

conventionally-heated reaction, using the same catalyst and reaction conditions, the PET conversion was negligible. As discussed in **Chapter 4**, the glycolysis reaction is known to proceed initially through random chain scission of amorphous tie-chain regions, producing soluble oligomers and short-chain fragments. This effect causes PET to appear highly "converted" in gravimetric terms while BHET yield lags behind due to lack of complete depolymerisation. **Figure 6.4** serves as further evidence of this effect, as the PET conversion increases rapidly under MW heating (random scission of amorphous tie-chains) while the BHET lags behind due to the difficulty in breaking down the more inaccessible end-chain crystalline regions. Essentially, under MW irradiation, PET can be converted very easily and rapidly into oligomers, but BHET yield will remain low as the depolymerisation is incomplete.

The rapidly enhanced PET conversion can be caused by a number of factors. In MW heating, the general heat transfer rate is significantly improved, as outlined in the catalyst heating tests. However, in addition to this, it is likely that the $[bmim]_2[CoCl_4]$ present in the sample provides localised "hot spots" of extremely fast reaction kinetics, even if the bulk temperature remains moderate [27]. From previous studies of IL and MW heating relationships, it is possible that the catalyst reaches the reaction temperature and higher in under 20 seconds, without increasing the pressure of the vessel [28]. Despite the rapid PET conversion, BHET yields are considerably low even at 45 minutes, suggesting other factors may be limiting the reaction such as diffusion rates or the presence of contaminants. For this reason, while the enhanced thermal and kinetic effects of MW-heated $[bmim]_2[CoCl_4]$ shows promise for drastically reducing reaction times and energy demand, more work must be completed to investigate the potential for increased yields, as well as PET conversion. Novel work

by Li et al. [29] show the potential for DFT modelling of a MW-heated, Co-catalysed system which could help elucidate the effects.

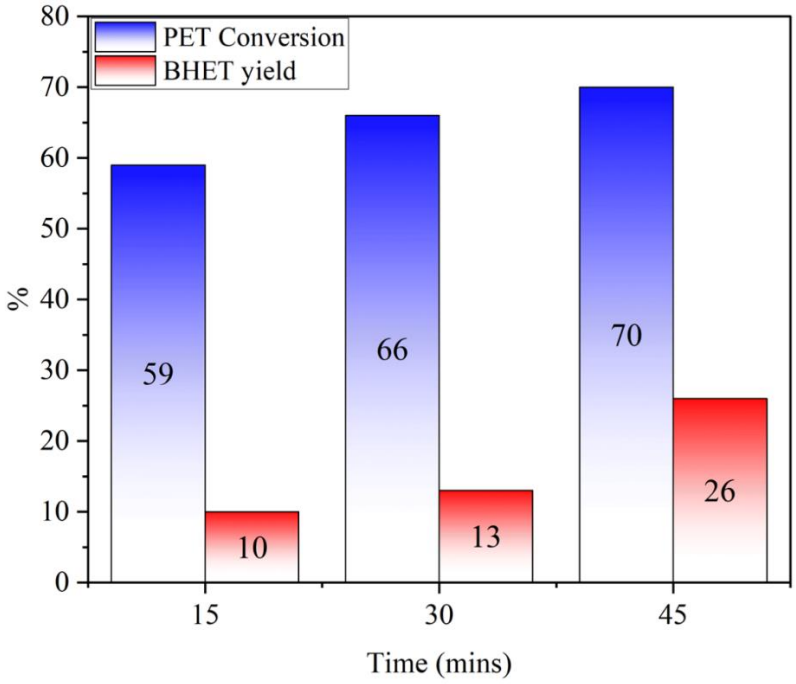

Figure 6.4. *PET conversion and BHET yield of [bmim]$_2$[CoCl$_4$]-catalysed PET glycolysis under MW heating (1 g PET, 4 g EG, 0.1 g cat., 190 °C).*

6.3 Effects of moisture

As outlined in **Chapter 4**, the effects of moisture are potentially hindering to the PET glycolysis process, and, as the likelihood of water presence is very high within real-world plastic waste, moisture mitigation is a very important topic. By understanding the effects of water on the reaction, researchers can more specifically improve the scalability of these novel processes.

6.3.1 Experimental comparison of moisture content

As the studied ILs are known to be very hygroscopic, great care was taken in avoiding exposure to the atmosphere. By drying in a vacuum oven and storing in a glovebox, moisture exposure was mitigated as far as reasonably practical. However,

as described in **Chapter 4**, avoidance of all moisture was impossible due to the synthesis methods. This is expected to hinder the glycolysis process, reducing the BHET yields compared to the literature. However, while this may influence the effectiveness of the catalysts, a far greater issue is the hygroscopicity of the solvent. Due to the w/w ratio of solvent to catalyst (40:1), the moisture content of EG negates any moisture present within the catalyst. Therefore, the amount of water present in the EG samples was chosen to be varied.

Two EG samples, referred to herein as "wet" and "dry", were prepared. The dry sample was purchased as anhydrous EG, while the wet sample was not. Volumetric KF titration was carried out to determine the water content of the two EG samples. The averaged results and the standard deviation of the titration are shown in **Table 6.5**.

Table 6.5. *Moisture content of wet and dry EG samples, derived from KF titration.*

Sample	Moisture content (ppm)
Wet EG	320 ± 15
Dry EG	205 ± 15

The calculated moisture contents show a significant decrease when the anhydrous EG is used. However, despite being labelled as anhydrous, the water content of the dry sample is still considerable. Abbasi et al. [30] found that a moisture content above 0.005% (w/w) was potentially capable of hydrolysing the PET, creating unwanted competitive degradation. The (w/w) % of water and PET in this case is ~0.08%. The difficulty in removing water from EG stems from its affinity for water molecules. While EG and water do not have an azeotrope, the strong H-bonding occurring due to the diols can form very strong interaction networks which require energy intensive heating to break. On an industrial scale, recent research has gone into

improving the water/EG separation process, which is made difficult due to the production method, which involves the hydrolysis of ethylene oxide [31]. It is considered out-with the scope of the project to attempt to improve upon the moisture content standards of the manufacturer, and so, due to safety restrictions and practical limitations, further distillation of the sample was not undertaken.

Figure 6.5 shows the difference in PET conversions and BHET yields when using wet and dry EG with the IL catalysts (5 g PET, 20 g EG, 0.5 g cat., 190 °C, 120 mins).

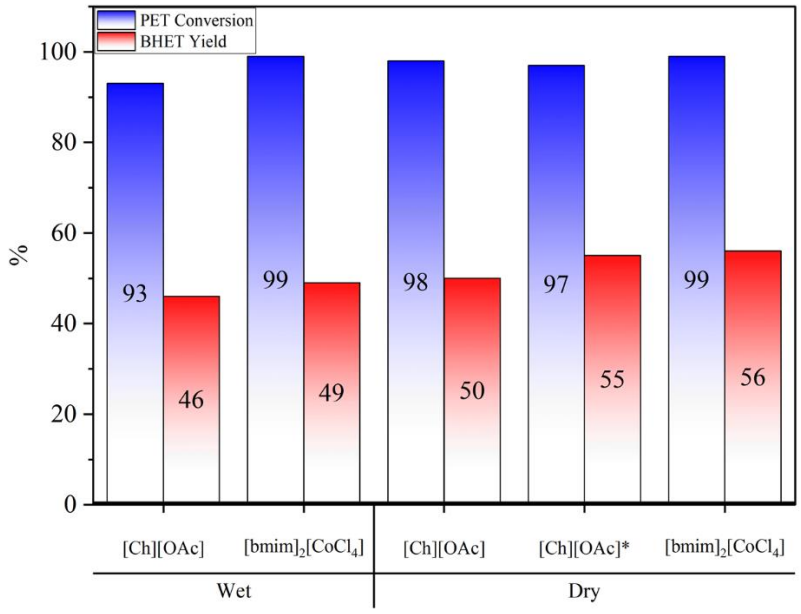

Figure 6.5. *PET conversion and BHET yield for in-house [Ch][OAc], purchased [Ch][OAc]* and $[bmim]_2[CoCl_4]$ using EG with varying moisture content (5 g PET, 20 g EG, 0.5 g cat., 190 °C, 120 mins).*

With the removal of water from the solvent, there is seen to be a clear but small increase in PET conversion and BHET yield, showing that the moisture content is a hindering factor to the process. In the reduced moisture environment, both catalysts induce almost complete conversion of the plastic, while the yields increase by 4% and

7%, respectively, for the organic and metal IL. These results suggest that compared with [Ch][OAc], the metal IL suffers from greater interference by water molecules within the system, potentially due to its capacity for stronger H-bonding. While the BHET yields are improved in the dry case, compared to literature values they are still low. It is unknown what the moisture content is of the EG used in literature and so it cannot be validated that this is the main factor in the reduced yields.

To investigate this further, a pre-synthesised pure [Ch][OAc] catalyst was purchased for comparison for the in-house synthesised version. With the use of the purer catalyst, the PET conversion surprisingly decreases slightly, however this is likely down to variance as the PET conversion is still seen to be almost complete. The BHET yield is increased, as expected, when the pure catalyst is used, however this is still lower than the largest values seen in literature [32]. As every reasonable precaution had been taken to mitigate moisture, i.e. the use of gloveboxes and Schlenk lines, it is assumed that the significant moisture content within the solvent is still the limiting factor hindering the process. It should be noted that as the margins are fairly small in **Figure 6.5**, additional experimental runs are required to make more quantitative conclusions. However, due to limited time and resources, only repeated reactions at the optimal conditions, determined from **Chapter 4**, were ran.

6.3.2 DFT modelling of moisture effects

6.3.2.1 Moisture effects on energy barriers

The hindering effects of moisture was validated through DFT energy barrier calculation. Using the molecular systems optimised in **Chapter 4**, for [Ch][OAc] and $[bmim]_2[CoCl_4]$, explicit water molecules were strategically added to represent their presence within the solvent. It was deemed that the most likely site for moisture

interference is adjacent to the reacting hydroxyl group of EG, interacting with both the reactant and the anion. It should be noted that this is representative of a worst-case scenario as, in reality, there are other locations within the system that H_2O could be found which would not have such a significant effect on the reaction. Due to the limitations of computational expense with respect to system size, only one explicit water molecule was initially added for calculation. **Figure 6.6** displays the compared energy barriers for the [Ch][OAc] and $[bmim]_2[CoCl_4]$, with and without an additional H_2O molecule. As the energy barrier increase is less pronounced in the case of the organic IL, a further three water molecules were added.

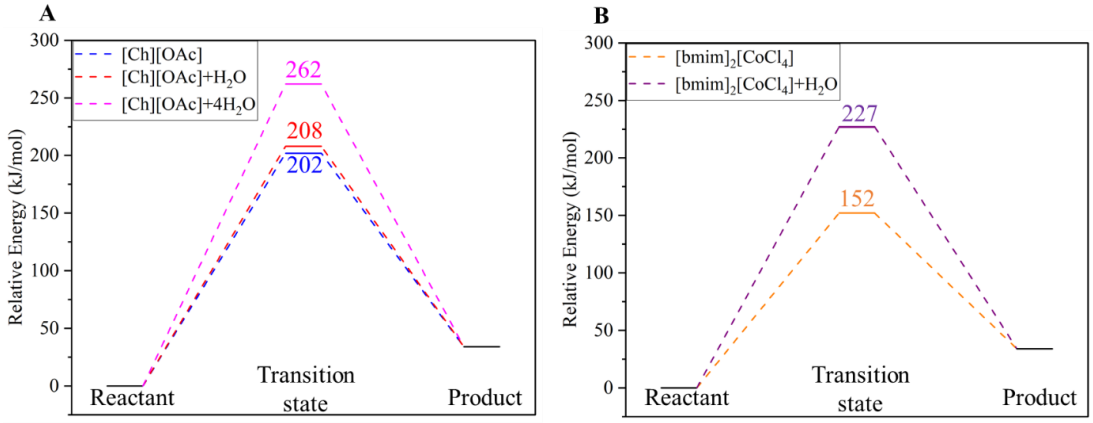

Figure 6.6. *Energy barriers with varying explicit water molecule presence using A) [Ch][OAc] and B) $[bmim]_2[CoCl_4]$ as catalysts.*

The results show that the presence of explicit water molecules increases the energy barrier, in every case. When one H_2O molecule is added, the increase in activation energy is 6 kJ/mol and 75 kJ/mol for the [Ch][OAc] and $[bmim]_2[CoCl_4]$ catalyst systems, respectively, showing a significantly higher moisture sensitivity in the metal IL system. Indeed, even with four strategically placed H_2O molecules, the increase in energy barrier for the organic IL system is still only 60 kJ/mol, which 15 kJ/mol less than the metal IL system with one additional water molecule. In the wider

context of sustainable engineering, it is a favourable result that the greener and cheaper choline-based IL seems to be less sensitive to the presence of moisture that is ubiquitously present in real-world plastic waste.

The results show that with increasing water concentration, there too is an increase in energy barrier to glycolysis. It is likely that this shift in activation energy is caused by the interfering H-bonding of the water molecules, preventing the catalyst from activating the reaction through intermolecular interactions, however further DFT analysis was required to validate this proposal. It should be noted that the model is idealised and assumes easy access of water molecules to the active site all along the polymer chain, meaning the energy barriers could be somewhat overestimated compared to the uncatalysed case in **Chapter 4**. The energy barriers are included here for qualitative purposes, to show the hindering effect of water.

6.3.2.2 Intermolecular interactions in water-doped system

QTAIM analysis of the catalytic systems in **Chapter 5** identified several intermolecular interactions which are essential for PET glycolysis catalysis. In the case of the organic IL, [Ch][OAc], H-bonding between the anion's carboxylate group and EG helps facilitate the reaction through an inductive-like polarisation effect. Additionally, while the choline cation's mechanistic role was seen to be minimal, strong interactions between EG and the PET carbonyl group act to stabilise the geometry, maintaining the reactants proximal location relative to each other. **Figure 6.7** shows selected key interactions, with the electron density for the original system, as well as with 1 and 4 explicit H_2O molecules added, respectively.

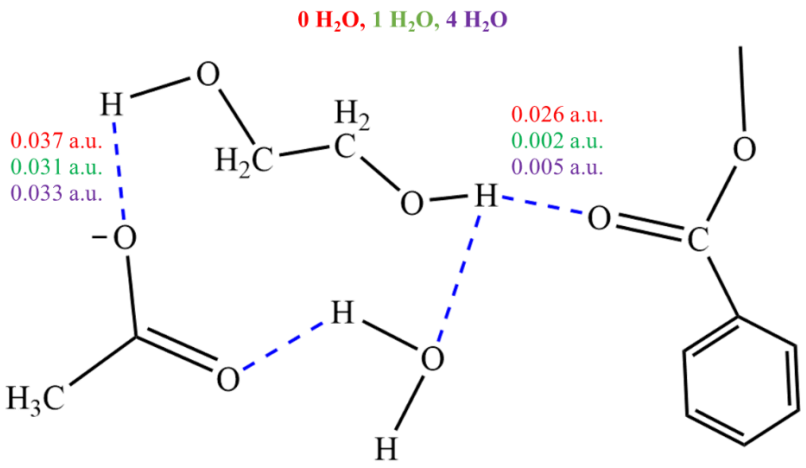

Figure 6.7. *Key interactions and electron densities between EG, OAc, H_2O and PET dimer.*

The blue dashed lines represent key H-bonding between the moieties within the system, showing the interaction complex formed by the four molecules. The QTAIM results are somewhat surprising in that there is little difference between the $1H_2O$ and $4H_2O$ systems in terms of electron density transfer, despite a significant increase in energy barrier. In both water systems, the anion – EG H-bonding is reduced slightly compared to the waterless case, likely due to charge delocalisation caused by anionic interaction with water. This redistributes a fraction of the electron density to the other oxygen atom of OAc.

The more significant change in electron density is between EG and the carbonyl oxygen of the PET dimer, with a decrease of around ~20 a.u. for each water-containing system. In **Chapter 5** this interaction was proposed to be important in stabilising the geometry of the EG molecule, preventing it from re-orienting to an angle relative to PET which is not conducive to the reaction. However, as shown in **Table 6.6**, the re-orientation of the molecules is not significantly higher in the $4H_2O$ molecules case. Therefore, it is unlikely that the orientation of EG with respect to the

dimer is the limiting factor. EG in both systems is pulled out of plane by the additional H-bonding of the water molecules.

Table 6.6. *Geometric re-orientation of EG molecule in water-free and water-doped [Ch][OAc]-catalysed systems.*

System	Reactant C_{BZ}-C-O_{EG} angle (°)	TS C_{BZ}-C-O_{EG} angle (°)	Re-orientation required (°)
[Ch][OAc]	107	112	5
[Ch][OAc]+1H_2O	75	113	38
[Ch][OAc]+4H_2O	71	111	40

However, another noticeable effect is the folding of the PET dimer, again initiated through increased H-bonding on account of the additional water molecules. Comparison of the PET dimer folding is shown in **Figure 6.8**, with all other molecules removed. To quantify the folding effect, the change in internal angle of the dimer is presented, with the greatest folding corresponding to the largest change in angle. This effect likely induces steric repulsion due to the narrowing of the path for EG to access the reaction site. Comparing the two water-containing samples, the folding of the dimer is clearly more evident in the 4H_2O system, which may be the cause of the significant increase in energy barrier.

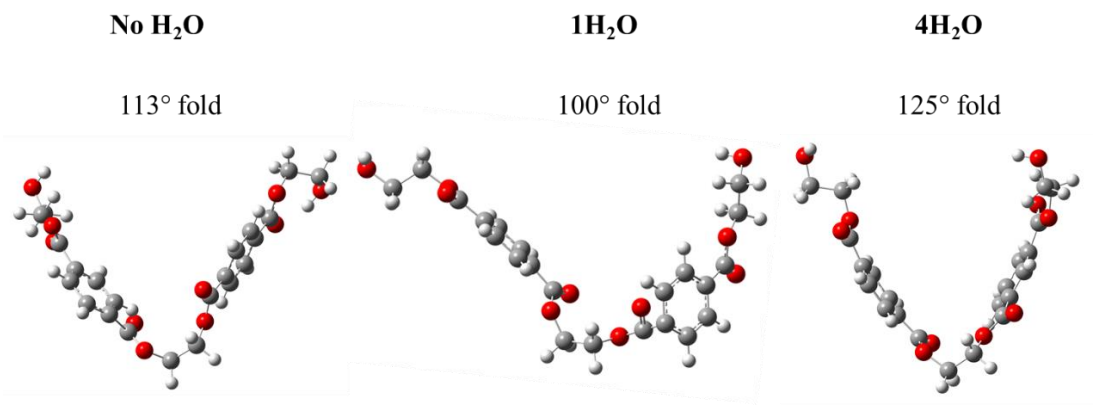

Figure 6.8. *Folding effect of PET dimer in no H_2O-, $1H_2O$- and $4H_2O$-doped [Ch][OAc]-catalysed systems.*

The results suggest that, in the [Ch][OAc] system, the mechanistic hindrance caused by the presence of moisture is in two parts: 1) with initial contact between EG and water, the redistribution of electron density between the EG hydroxyl group and PET carbonyl results in increasing the required re-orientation of the EG molecule prior to the reaction and 2) with increasing moisture content, there occurs a folding of the PET dimer, creating steric hindrance and preventing easy access to the active site for the EG molecule.

For the metal IL system with a single water molecule, there is a clearer picture of the hindering effects. By analysing the electron density, shown in **Figure 6.9**, with a focus on the anion, EG, dimer and H_2O, the role of the water is clear. In the absence of water, there is a strong Co – PET coordination which protonates the ester carbon and facilitates the reaction. Additionally, one of the chloride ions electrostatically interacts with the reacting hydroxyl group of EG, creating a largely negative partial charge on the EG oxygen. However, upon the introduction of a water molecule, the electron distribution significantly changes. The Co – PET O bond distance increases, reducing the electron density at the BCP, therefore reducing the protonation of the

ester carbon atom. Additionally, the Cl – EG interactions shifts away from the reacting to hydroxyl group to the adjacent CH_2 of EG, due to the pulling influence of the nearby H_2O. While there is still a polarising effect, the negative partial charge of the oxygen is reduced, explaining the large increase in energy barrier.

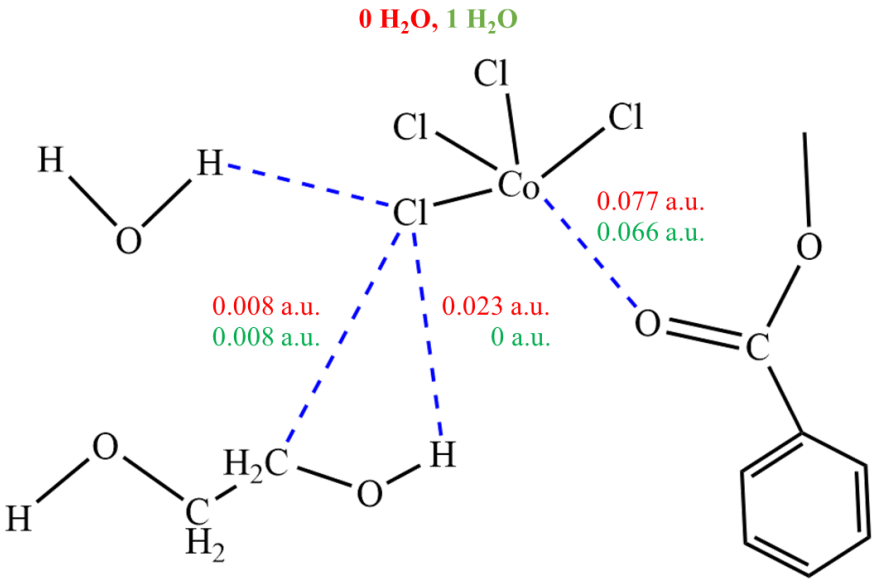

Figure 6.9. *Key interactions and electron densities between EG, $CoCl_4$, H_2O and PET dimer.*

These results show the heavily hindering effects of moisture within the PET glycolysis system. Due to the high expense of a large-scale solvolysis process, the presence of moisture has to be considered for mitigation, or else energy intensive industrial scale drying is required. Work by Stoski et al. [33] suggested that the presence of water at 1% and 2% v/v with respect to EG could result in the production of terephthalic acid, a competing side-product formed through the hydrolysis of PET. However, FT-IR and NMR analysis of the final degradation products shows no evidence of its formation, suggesting that the influence of moisture at the studied concentration is merely an interfering one, rather than being a competitive reactant with EG.

6.4 BC-supported IL-catalysed PET glycolysis

The use of waste-derived BC catalyst supports has the potential to enhance the catalytic efficiency, as outlined in **Chapter 2**, while also contributing to the circular economy through its synthesis from a waste valorisation process. These factors make it an attractive prospect for use in the PET glycolysis process, a method already contributing impactfully toward sustainable chemistry.

6.4.1 BC-IL characterisation

Grafting of the IL to the BC surface was confirmed using a number of characterisation techniques. **Figure 6.10** shows the FT-IR spectrum for the organic IL-grafted BC sample, compared with that of the pure BC sample. A notable feature of the spectra are the sloping baselines, as described in **Chapter 3**.

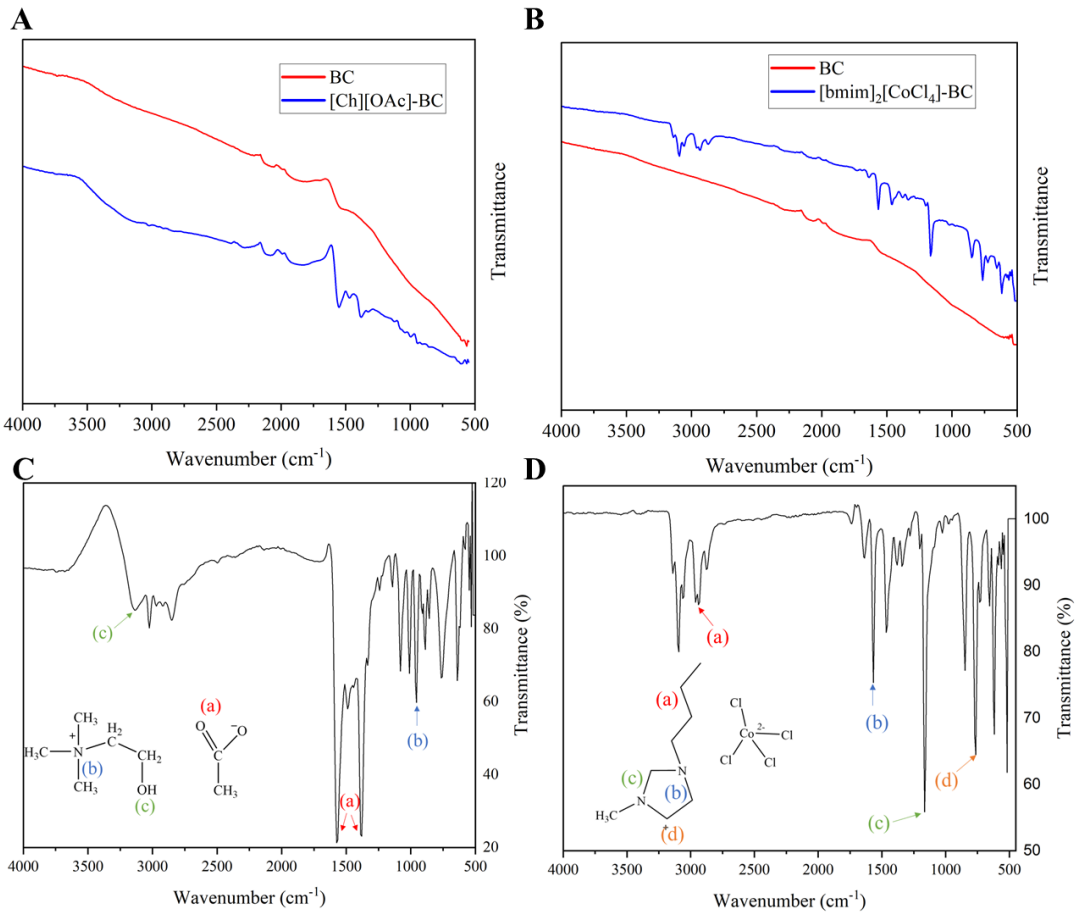

Figure 6.10. *FT-IR spectra of A) pristine BC and [Ch][OAc]-BC samples, B) pristine BC and $[bmim]_2[CoCl_4]$-BC samples, C) pure [Ch][OAc] sample and D) pure $[bmim]_2[CoCl_4]$ sample.*

The spectra present some evidence of the grafting of the ILs to the surface, however, the shortness of the peaks is surprising considering the 1:1 (w/w) ratio of IL:BC. It is expected that with such a high loading content, taken from literature [34], that much more distinct IL peaks would form, assuming their effective adsorption onto the BC. It is proposed that the high refractive index of the BC significantly distorts the spectra, including peak ratios, potentially making the results unreliable for estimating the relative adsorbed contents of the two ILs [35]. Instead, they are included here as qualitative evidence of IL adsorption, rather than to estimate relative surface

adsorption. Future work could include additional techniques such as thermogravimetric analysis (TGA) to verify relative IL dispersion but were not available for this work.

Despite the sloping baselines, there is a clear change in the distinct peaks when the IL is introduced. For the organic IL, new peaks in the fingerprint region including ~950 cm^{-1} likely show evidence of the C-N stretches of the choline cation. Additionally, there are very weak peaks indicative of the choline's alkyl group present at ~2850-3000 cm^{-1}. The COO- peaks at ~1550-1410 cm^{-1} are typical of the acetate anion. Generally, the fingerprint region peaks (1000-1500 cm^{-1}) show the IL functional groups are still present on the BC after washing and that the ILs have been somewhat adsorbed to the surface. The wide -OH peak at around 3400 cm^{-1} is indicative of water present in the synthesised sample, as described previously.

Similarly, the metal IL spectra present evidence of adsorption atop the BC surface after washing. The appearance of peaks at ~3000 cm^{-1} represent the presence of the butyl chain of the cation [34]. Also observed are the characteristic peaks of the C-H and C=N groups within the imidazolium ring (~1170 and ~1570 cm^{-1}), further indicating the presence of the cation on the surface. As outlined in **Chapter 3**, the presence of Co-Cl is difficult to determine from FT-IR, however it is assumed that the metal anions are electrostatically bound to the cations and therefore present in the new heterogeneous catalyst.

6.4.2 BC-IL-catalysed PET glycolysis

Experimental testing of BC-IL catalysts was carried out as described above, with the scenarios outlined in **Table 6.4**. **Figure 6.11** shows that the presence of BC increases the BHET yield for both ILs, with the performance of the organic IL

improving by a remarkable 24% (5 g PET, 20 g EG, 0.5 g cat., 190 °C, 120 mins). The metal IL sees a less marked improvement; however, the yield does rise by 3%.

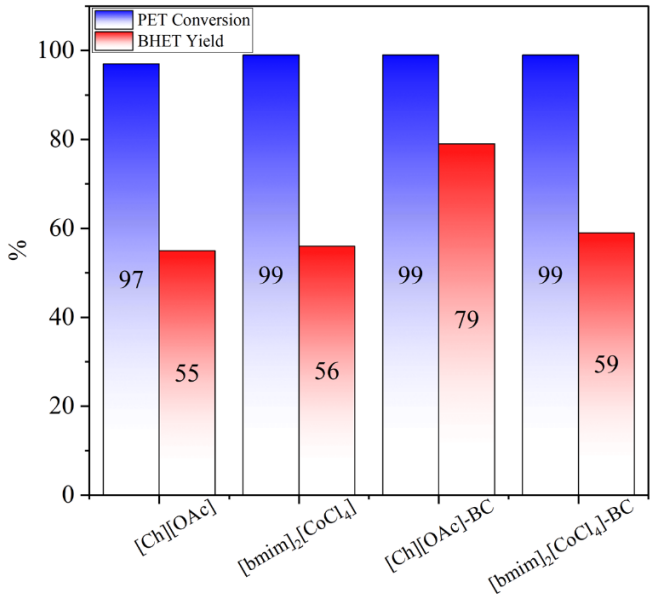

Figure 6.11. *PET conversion and BHET yield when [Ch][OAc]-BC and $[bmim]_2[CoCl_4]$-BC are used as catalysts (5 g PET, 20 g EG, 0.5 g cat., 190 °C, 120 mins).*

The 79% yield of BHET when [Ch][OAc] is supported by KOH-activated BC brings the work much more in line with literature standards for PET glycolysis and valorises an abundant and cheap feedstock. Additionally, while the metal IL's cobalt centre provides mechanistic superiority, the toxicity of the element and potential for its leaching into the environment, mean that more environmentally friendly alternatives should be explored [36]. Therefore, the clear enhancement of catalytic performance of the organic IL, when combined with the waste-derived support, is an exciting initial result.

The theoretical atom economy of PET glycolysis is 100% when BHET is utilised as the desired product, as excess EG and the production of oligomers are not considered. Therefore, the E-factor and ε can provide additional insight as to the actual

greenness of the process, when catalysed by ILs and BC-supported ILs, with a high ε and low E-factor being desirable. **Figure 6.12** highlights the green metrics of the different systems, which align with the BHET yields. As expected, the [Ch][OAc]-BC system outperforms the others tested, due to the significantly higher yield producing an increase in the efficiency of the system, from both a waste reduction and energy consumption perspective. The use of green metrics for PET glycolysis is limited in the literature, however a previous study of a MW-assisted, CaO-catalysed process achieved values of ε = 0.00084 and E-factor = 1.44 [37]. The E-factor value accounts for the production of undesired oligomers, as well as the treatment of excess EG. In comparison to the literature value, there is actually fewer waste oligomers produced when [Ch][OAc], due to the higher yield of BHET, however, the lack of EG recycling creates a substantial amount of waste. The discrepancy in E-factor highlights the importance of EG recycling consideration for potential scale-up, from an economic perspective. Despite this, the value falls between the <1 – 5 range that is industry standard [38]. Following the methodology of Zangana et al. [37], ε is reported as a dimensionless penalised productivity index and is therefore presented without units. This metric is used solely for the relative comparison of reaction conditions and does not represent a thermodynamic energy efficiency. In their work, ε is clearly higher when MW heating is used, due to the reduced reaction times. However, while the value of 2.84E-4 in this work compares unfavourably, it is still a reasonable value and the "greenness" is enhanced due to the use of a waste-derived catalyst support and non-toxic IL, compared to the metal-based catalyst in the literature, representing an acceptable trade-off.

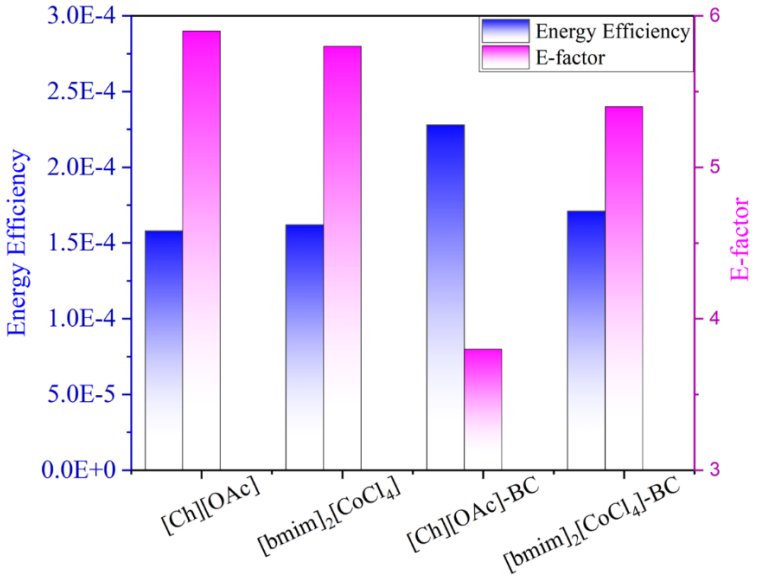

Figure 6.12. *Green metrics including energy efficiency coefficient and E-factor for PET glycolysis using ILs and BC-ILs (5 g PET, 20 g EG, 0.5 g cat., 190 °C, 120 mins).*

It is also plausible that the BC support contributes to moisture mitigation in the system. Given its porous structure and known hygroscopic properties, BC may act as a moisture absorber during the reaction, reducing the concentration of free water molecules in the vicinity of the catalytic sites [39,40]. This effect could partially explain the enhanced BHET yields observed, given that water interference was previously identified as a major limiting factor. Despite this, further testing must be carried out at varying reaction conditions, while also ideally reducing the water content of the solvent, to make more reliable conclusions and potentially enhance the performance even further. The production of BHET as the main degradation product was carried out by FT-IR, shown in **Figure 6.13**.

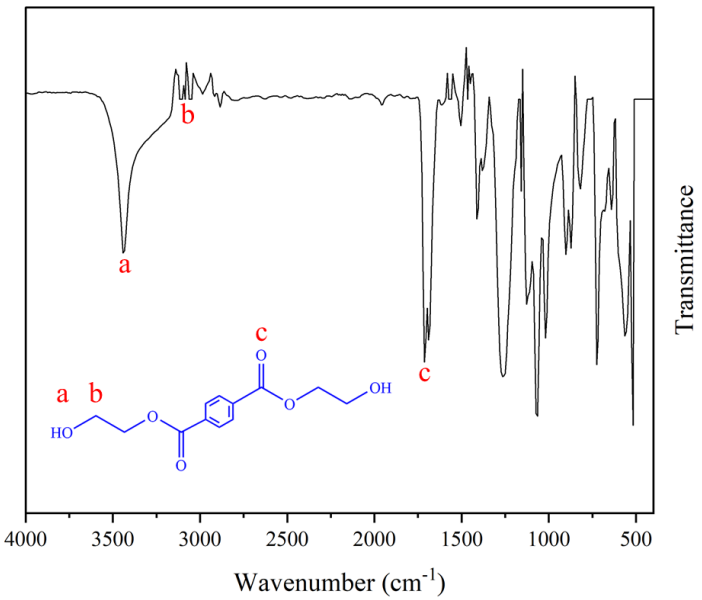

Figure 6.13. *FT-IR spectra of main degradation product from PET glycolysis catalysed by A) [Ch][OAc]-BC.*

In order to assess the purity of the final product, ^{1}H NMR was carried out. **Figure 6.14** displays the NMR spectrum for the main product of PET glycolysis catalysed by [Ch][OAc]-BC.

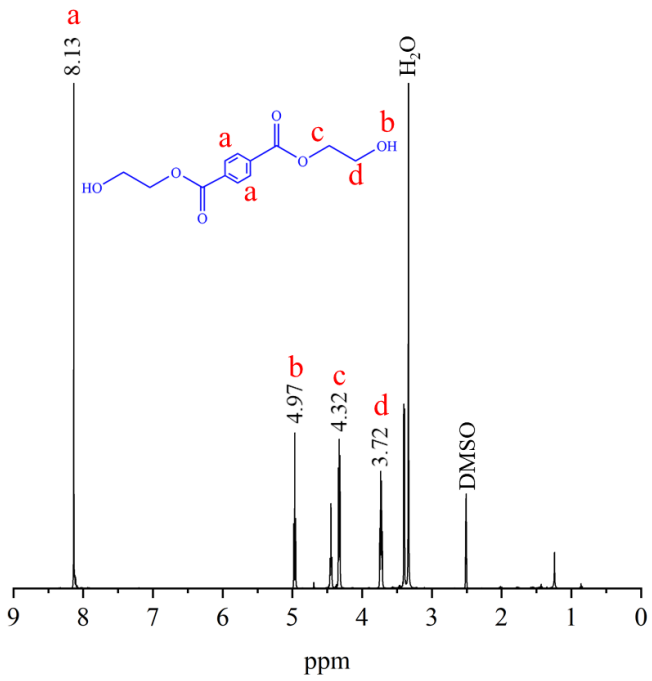

Figure 6.14. *^{1}H NMR of main degradation product using [Ch][OAc]-BC.*

As in **Chapter 4**, the NMR spectrum of the main degradation product reveals the characteristic peaks of BHET at 8.13 ppm (aromatic ring), 4.97 ppm (terminal OH groups), 4.32 ppm and 3.72 ppm (adjacent methylene groups). The intensity of the hydroxyl group peak is indicative of BHET production and in the absence of a significant dimer peak at 4.7 ppm, it is unlikely that there is a large amount of oligomer in the sample. However, compared with the NMR results from **Chapter 4**, there are a number of impurities present. That these only occurred in the NMR spectra of the BC-catalysed samples implies that they are resultant of contaminants within the BC, a common effect of biomass-based materials [41]. The results highlight that although BHET production is greatly increased, the purity may be compromised somewhat. Further work is required to first identify the impurities, then mitigate this issue and prepare the produced BHET for polymer production.

In order to evaluate the potential recyclability of the BC-IL catalyst, Raman spectroscopy of the pristine BC sample was carried out, followed by the post-reaction separated BC-IL sample. **Figure 6.15** shows a comparison of the three spectra. The pristine BC sample shows two distinct peaks representing carbon sp^3 and sp^2 hybridisation, which are indicative of amorphous and crystalline structure, respectively [42].

The two BC-IL spectra show a clear increase in the crystallinity of the sample upon mixing with the reactants and IL, as reported in the literature [43]. The key distinction between the two BC-IL spectra is the presence of distinct peaks between 700 and 1000 cm^{-1} in the [Ch][OAc]-BC sample, representing the continued attachment of the organic IL to the surface, even after separation from the product mixture. These peaks correspond to C-N stretches of the cation, previously mentioned

in **Chapter 4**, shifted left slightly due to intermolecular interactions with BC. This serves as evidence of the strong binding to the BC surface, as well as highlighting the potential reusability of the catalyst. Due to its homogeneous nature, easy catalyst separation was previously not possible in this study. Therefore, the addition of the heterogeneous BC catalyst support provides a promising result which could ease scalability of the process.

Contrastingly, the Raman spectrum for the BC sample removed from the metal IL-catalysed system shows an absence of any distinct IL peaks. It is likely that the IL is washed away with the solvent during the reaction or post-reaction processing. The experimental characterisation of the two IL-BC catalysts suggests that the organic IL is more strongly adsorbed onto the support surface. This adsorption is likely the key factor in enhancing the BHET yield.

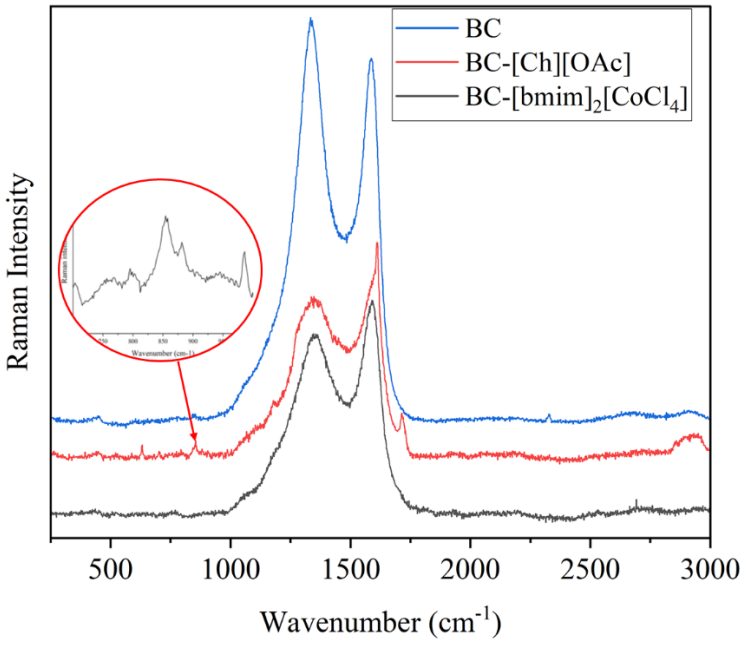

Figure 6.15. *Raman spectroscopy of pristine BC sample and both the organic and metal BC-IL samples.*

6.4.3 DFT modelling of BC-IL system

The adsorption capabilities of the ion pairs on top the BC surface were tested through DFT modelling to validate the experimental results. The BC model was constructed based on the work by Masrura et al. [44], who modelled KOH-activated BC for adsorption of tetracycline in water by BC. Their work defined the BC surface as a graphitic structure with abundant -OH groups. **Figure 6.16** represents the top layer of the BC, showing the aromatic structures with numerous hydroxyl groups and a furan group. This matches well with physical characterisation of KOH-activated BC in literature [45].

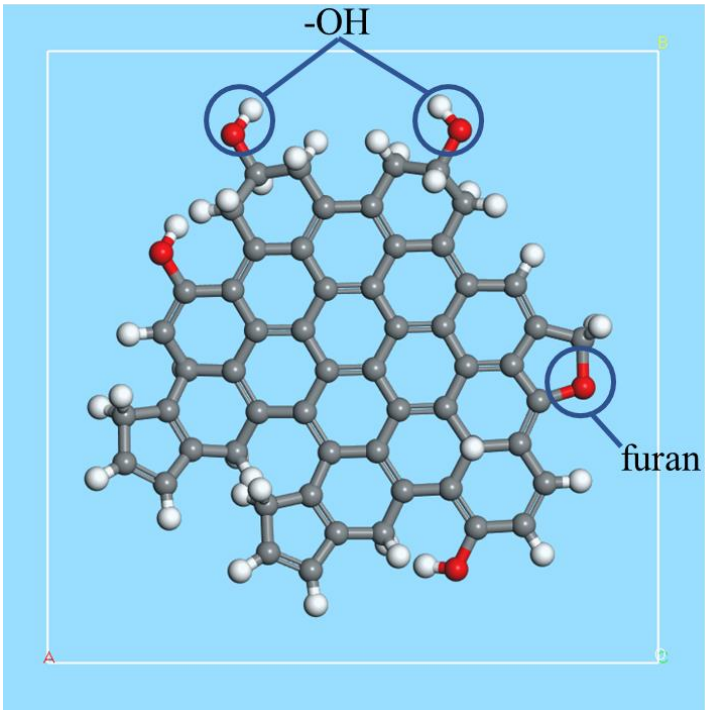

Figure 6.16. *Chemical structure of DFT-modelled BC with identified functional groups.*

Also shown in the figure are the periodic boundary conditions, indicated by the white box. These represent the boundaries after which the contents of the box are repeated, allowing for the crystal structure of the BC to be represented. Due to the

mixed crystalline/amorphous morphology of the BC, identification of specific facets through powder x-ray diffraction is made difficult, therefore the model does not follow an exact crystal facet structure [46]. Although there are precedents for the model in the literature, to guarantee correspondence to the BC used in this study, elemental analysis would have to be carried out. However, the targeted functional groups present in the model are widely known to exist on the surface of KOH-activated BC and therefore the model is assumed to give a qualitative analysis of the adsorption of ion pairs.

The dispersion of the catalyst across a support can provide a reactant with easy access to the active sites. The strength of the catalyst's adhesion to the surface, whether through chemical or physical adsorption, can be quantified through DFT adsorption investigation, while the abundance of viable adsorption sites can elucidate the degree of dispersion across the surface. The energy difference between the sites acts as a diffusion barrier, preventing the agglomeration of ions. For each ion (Ch, bmim, OAc, $CoCl_4$), three adsorption sites were tested based on the functional group: the hydroxyl groups, the furan group and the graphitic carbon-based aromatics.

Figure 6.17 displays for each ion, the adsorption energy at the corresponding adsorption site, based on the targeted BC functional group, as well as the mean adsorption energy for the ion. The three tested adsorption sites include the hydroxyl groups, furan group and directly over the aromatic carbons, labelled as "C" in the figure.

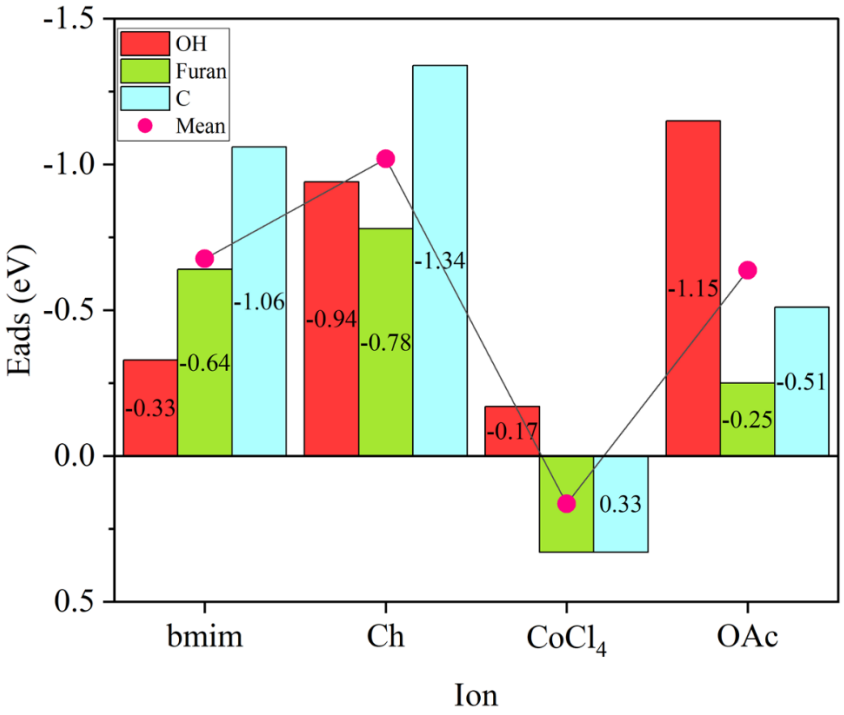

Figure 6.17. *Adsorption energies of each IL ion at various adsorption sites.*

The DFT calculations match well with the Raman spectroscopy shown previously, in that the organic IL adsorbs more strongly to the BC support than the metal IL. Treating each ion individually, the results show that generally the cations adsorb more easily than the anions, with the aromatic carbons being the most optimal cationic adsorption site. The adsorption energies for both cations fall within the range for chemisorption (0.8 to 2.5 eV) [47]. It was expected that the strongest cationic adsorption site would be located on the OH or furan group, due to the partial negative charge of the O atoms.

In the case of bmim, the key interactions are *via* π-stacking of the aromatic imidazolium group with the aromatic carbons atop the BC surface. The Ch cation, despite its lack of delocalised electrons, has been previously seen to adsorb through cation-π interactions with aromatics [48]. The overall improved adsorption of the cationic species is unsurprising, it is well known from the literature that KOH-

activated BC has a nucleophilic nature, attracting positively charged moieties such as Ch and bmim [49,50]. This explains also why generally the anions do not adsorb as strongly. While the overall surface is nucleophilic, there are still regions on the BC where strong H-bonding can take place with the negatively charged ions, especially near the edges. Therefore, it is unsurprising that both anions are adsorbed most easily on the hydroxyl groups, where the H atoms will have their most positive partial charge.

The OAc ion forms strong H-bonds with the hydroxyl group and is capable of physisorbing atop the other adsorption sites. The $CoCl_4$ anion, however, is only capable of adsorbing onto the hydroxyl groups, while its doubly negative charge is electrostatically repelled by the furan and aromatic sites. The reduced energy of adsorption compared to OAc is due to the oxygen atoms being more capable of strong H-bonding with the BC surface than the chloride ions are. **Figure 6.18** shows the optimal adsorption configurations for each ion, as well as the corresponding energies.

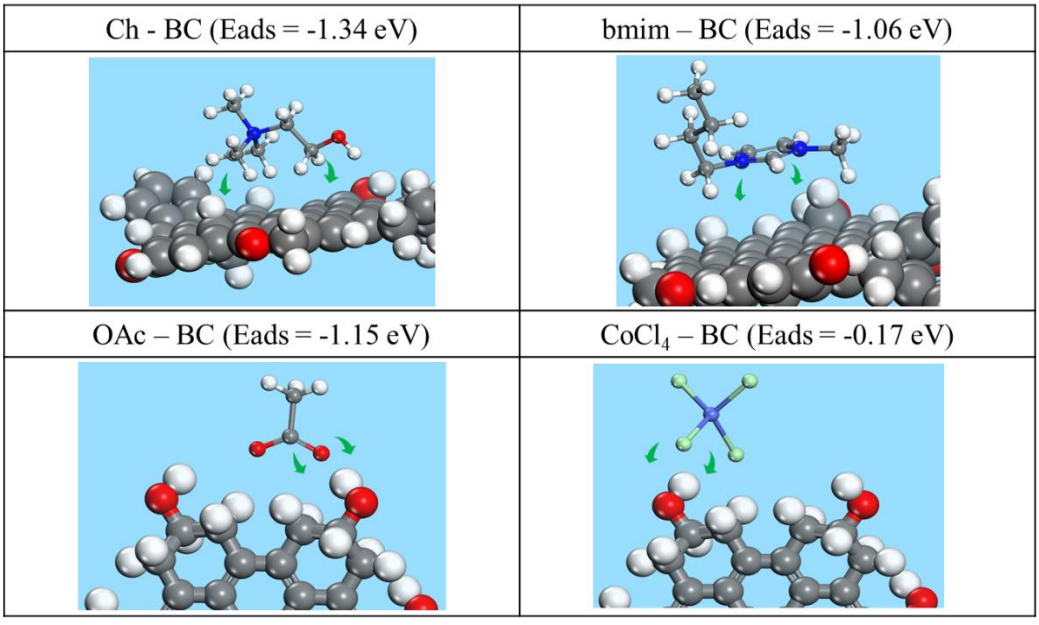

Figure 6.18. *Optimal adsorption configurations and energies for each ion atop BC.*

The adsorption results support the enhanced performance of the organic IL grafted on the BC surface and suggest that the organic IL's more facile adsorption onto the BC surface stabilises the ion pair, allowing its active sites to interact more freely with PET and EG. Additionally, that both choline and acetate, but choline in particular, can adsorb onto each site more easily than the corresponding ion of the metal IL, suggests that they are more widely dispersed atop the BC surface, a key feature in catalyst support chemistry. That the metal IL predominantly adsorbs through its cation, with the anion strongly attached to it through the electrostatic interactions discussed in **Chapter 5**, means that it may not be as efficiently dispersed across the surface. Despite this, the cation's adsorption is seemingly enough to cause a slight increase in catalytic effectiveness and BHET yield. The choline cation's strong adsorption enhances its role in the degradation mechanism, as the previous results showed its mechanistic contribution to the reaction to be negligible. While this is still the case when adsorbed atop the BC surface, its strong interactions with neighbouring OAc ions should anchor them similarly, allowing for increased anionic interactions with EG.

6.4.4 Proposed mechanism of BC-IL-catalysed PET glycolysis

The mechanistic contribution of the BC support is postulated to be through a number of possible mechanisms:

1. **Dispersion and enhancement of catalyst:**

   The primary role of the BC support is observed as uniform dispersion of well-adsorbed ILs across the catalyst surface, allowing for easy access to reactants. Additionally, it has been suggested in the literature that a catalyst support is capable of reducing the HOMO-LUMO gap of the adsorbed ILs, enhancing their catalytic activity [51,52].

2. **Synergistic role of BC:**

Besides supporting the ILs, the additional effect of the support is two-fold: first, through a π-π stacking adsorption mechanism, PET can be anchored to the BC surface, providing stability to the reactant. Secondly, favourable H-bonding between the graphitic structure and EG may enhance the reaction, similar to the mechanism discussed in **Chapter 5**. Previous studies have shown that through H-bonding, graphitic carbon is capable of strongly interacting with nucleophilic reactants [53]. The multi-functional role of the BC has been noted in several studies of carbon-based catalyst supports [34,54,55].

3. **Moisture content mitigation:**

The hygroscopic and porous nature of the BC surface may help to mitigate the hindering moisture effects. Rather than cause interfering interactions, water may be absorbed by the support

6.5 Proposed approach to sustainable, low-cost and effective PET glycolysis

This thesis set out to propose a novel approach to enhancing the sustainability, economics and effectiveness of IL-catalysed PET glycolysis. Choline-based ILs were identified as promising catalysts, due to their green credentials and low-cost. Despite this, their catalytic activity consistently underperforms compared to their metal counterparts. MW heating has previously been shown to significantly enhance performance and energy-efficiency of PET glycolysis reactions, however the lack of MW absorbance by [Ch][OAc] within the system meant that it was deemed an unsuitable strategy for future use. Contrastingly, a combined strategy of moisture

mitigation and a novel KOH-activated BC support saw a significant BHET yield increase from 46% to 79%. It is likely that with further water removal, this value could increase further. Additionally, experimental characterisation of the post-process mixture suggests the potential for catalyst recycling, an important consideration in designing cost-effective catalytic processes. In the context of sustainable IL-catalysed glycolysis of PET, the results represent an important development in the use of biodegradable choline-based ILs. While they have been shown previously to be less catalytically active than their metal-based counterparts, in addition to their unclear recyclability, the introduction of BC signifies a dramatic increase in performance which brings them closer in line to the state of the art. That the support is formed from the utilisation of a waste-stream helps promote the sustainability of the choline-catalysed process.

From a sustainability perspective, the use of BC derived from waste biomass in combination with the already environmentally friendly [Ch][OAc] is a clear improvement on ILs produced from metal-containing anions or imidazolium-based cations. Additionally, in comparison to alternative carbonaceous supports, which are commonly derived from petroleum resources and require energy-intensive and expensive synthesis, BC offers a promising alternative [56]. Activated BC is an extremely abundant and diverse material which offers practically limitless future options. As the high synthesis costs of ILs has been a major drawback to their acceptance in industry, combining this low-cost material with cheaply-synthesised choline-based ILs is an exciting prospect. In summary, the integration of BC support with [Ch][OAc] represents a promising approach for PET glycolysis, satisfying the

three conditions of sustainability, low-cost and effectiveness. Therefore, it is proposed from this work that it be considered for future process design for PET glycolysis.

6.6 Conclusions

This chapter has explored three yield- and sustainability-enhancing strategies for PET glycolysis catalysed by ILs: MW heating, moisture content control and the use of BC as a catalyst support. Each approach was assessed through a combination of experimental work and DFT modelling, providing a comprehensive understanding of how these variables influence reaction performance.

MW-assisted glycolysis demonstrated significantly improved heating efficiency with the metal-based IL $[bmim]_2[CoCl_4]$, achieving rapid, stable heating with reduced power demand compared to the organic IL [Ch][OAc]. This was attributed to a dual heating mechanism, involving both dielectric and magnetic interactions, facilitated by the high-spin Co^{2+} centre, whereas the choline-based IL has relatively high MW transparency compared to other ILs. PET glycolysis experiments under MW heating using the metal IL were found to enhance the PET conversion in short reaction times, achieving 59% in just 15 minutes. As before, BHET yield lagged behind PET conversion, further demonstrating the ease with which PET chains are randomly severed, in contrast to the difficulty in converting short-chain oligomers to monomer. Such performance highlights the potential for energy-efficient process intensification of the process using the more expensive metal IL, however, the issues of sustainability and synthesis costs still remain. While MW heating is a promising technology, its use has been largely limited to pilot and lab-scale processes, however recent developments do provide evidence of scalability.

The investigation of moisture effects revealed that water content in EG can hinder PET depolymerisation, primarily by disrupting key hydrogen bonding and charge-transfer interactions. DFT results confirmed that water raises the energy barrier for glycolysis, especially in the metal IL system, where protonation of the ester group and coordination interactions are more severely disrupted. Therefore, due to the high moisture content of municipal plastic waste, the prevention of moisture effects must be focused on as a key prerequisite for the scalability of IL-catalysed PET glycolysis. The reduced moisture sensitivity of [Ch][OAc] further strengthen its claim for future use in industrial PET glycolysis processes involving real-world plastic waste.

Finally, supporting ILs on waste-derived BC proved effective in enhancing BHET yield, particularly for [Ch][OAc], which showed a remarkable 24% increase. However, NMR spectroscopy revealed that the BHET purity may be compromised somewhat by impurities originating from the BC. Spectroscopic and DFT adsorption analyses indicated stronger and more uniform adsorption of organic ILs to the BC surface, suggesting improved catalyst dispersion and potentially a synergistic role of the BC in facilitating the reaction. While the metal IL also benefitted from BC support, the enhancement was modest, likely due to weaker IL-support interactions. As organic ILs are considerably cheaper to produce and more sustainable than metal ones, these results represent a promising method for bridging the gap in performance, while retaining the low-cost and green credentials of the individual BC-[Ch][OAc] moieties. However, it should be noted that further experimental analysis must be carried out to determine the potential for scalability.

References

[1] M.J. Frisch, G.W. Trucks, H.B. Schlegel, G.E. Scuseria, M.A. Robb, J.R. Cheeseman, G. Scalmani, V. Barone, G.A. Petersson, H. Nakatsuji, X. Li, M. Caricato, A. V. Marenich, J. Bloino, B.G. Janesko, R. Gomperts, B. Mennucci, H.P. Hratchian, J. V. Ortiz, A.F. Izmaylov, J.L. Sonnenberg, D. Williams-Young, F. Ding, F. Lipparini, F. Egidi, J. Goings, B. Peng, A. Petrone, T. Henderson, D. Ranasinghe, V.G. Zakrzewski, J. Gao, N. Rega, G. Zheng, W. Liang, M. Hada, M. Ehara, K. Toyota, R. Fukuda, J. Hasegawa, M. Ishida, T. Nakajima, Y. Honda, O. Kitao, H. Nakai, T. Vreven, K. Throssell, J.A. Montgomery, Jr, J.E. Peralta, F. Ogliaro, M.J. Bearpark, J.J. Heyd, E.N. Brothers, K.N. Kudin, V.N. Staroverov, T.A. Keith, R. Kobayashi, J. Normand, K. Raghavachari, A.P. Rendell, J.C. Burant, S.S. Iyengar, J. Tomasi, M. Cossi, J.M. Millam, M. Klene, C. Adamo, R. Cammi, J.W. Ochterski, R.L. Martin, K. Morokuma, O. Farkas, J.B. Foresman, D.J. Fox, Gaussian 16, (2016).

[2] J.P. Perdew, K. Burke, Generalized gradient approximation for the exchange-correlation hole of a many-electron system, Phys Rev B Condens Matter Mater Phys 54 (1996) 16533–16539. https://doi.org/10.1103/PhysRevB.54.16533.

[3] Axel D. Becke, Density-functional thermochemistry. III. The role of exact exchange, J Chem Phys 98 (1993) 5648.

[4] C. Lee, W. Yang, R.G. Parr, Development of the Colle-Salvetti correlation-energy formula into a functional of the electron density, Phys Rev B Condens Matter Mater Phys 37 (1988) 785–789. https://doi.org/10.1103/PhysRevB.37.785.

[5] A. V. Marenich, C.J. Cramer, D.G. Truhlar, Universal solvation model based on solute electron density and on a continuum model of the solvent defined by the bulk

dielectric constant and atomic surface tensions, J. Phys. Chem. B 113 (2009) 6378–6396. https://doi.org/10.1021/jp810292n.

[6] S. Grimme, J. Antony, S. Ehrlich, H. Krieg, A consistent and accurate ab initio parametrization of density functional dispersion correction (DFT-D) for the 94 elements H-Pu, J. Chem. Phys. 132 (2010). https://doi.org/10.1063/1.3382344.

[7] S.J. Clark, M.D. Segall, C.J. Pickard Ii, P.J. Hasnip, M.I.J. Probert, K. Refson, M.C. Payne, First principles methods using CASTEP, n.d. www.accelrys.com/references/castep/.

[8] BIOVIA, BIOVIA Materials Studio, (2020).

[9] J.P. Perdew, K. Burke, M. Ernzerhof, Generalized Gradient Approximation Made Simple, Phys Rev Lett 77 (1996) 3865–3868.

[10] H.D. Saï¿ nick, C. Cocchi, Electronic structure of cesium-based photocathode materials from density functional theory: Performance of PBE, SCAN, and HSE06 functionals, Electron. Struct. 3 (2021). https://doi.org/10.1088/2516-1075/abfb08.

[11] S. Grimme, J. Antony, S. Ehrlich, H. Krieg, A consistent and accurate ab initio parametrization of density functional dispersion correction (DFT-D) for the 94 elements H-Pu, J. Chem. Phys. 132 (2010). https://doi.org/10.1063/1.3382344.

[12] D. Obermayer, D. Znidar, G. Glotz, A. Stadler, D. Dallinger, C. Oliver Kappe, Design and Performance Validation of a Conductively Heated Sealed-Vessel Reactor for Organic Synthesis, J. Org. Chem. 81 (2016) 11788–11801. https://doi.org/10.1021/acs.joc.6b02242.

[13] J. González-Rivera, E. Husanu, A. Mero, C. Ferrari, C. Duce, M.R. Tinè, F. D'Andrea, C.S. Pomelli, L. Guazzelli, Insights into microwave heating response and

thermal decomposition behavior of deep eutectic solvents, J Mol Liq 300 (2020). https://doi.org/10.1016/j.molliq.2019.112357.

[14] S. Chandrasekaran, T. Basak, R. Srinivasan, Microwave heating characteristics of graphite based powder mixtures, Int. Commun. Heat Mass Transf. 48 (2013) 22–27. https://doi.org/10.1016/j.icheatmasstransfer.2013.09.008.

[15] R. Singh, C. Lindenberger, A. Chawade, V. Vivekanand, Unveiling the microwave heating performance of biochar as microwave absorber for microwave-assisted pyrolysis technology, Sci Rep 14 (2024). https://doi.org/10.1038/s41598-024-59738-5.

[16] E. Vázquez, M. Prato, Carbon nanotubes and microwaves: Interactions, responses, and applications, ACS Nano 3 (2009) 3819–3824. https://doi.org/10.1021/nn901604j.

[17] P. Priecel, J.A. Lopez-Sanchez, Advantages and limitations of microwave reactors: from chemical synthesis to the catalytic valorization of biobased chemicals, ACS Sustain Chem Eng 7 (2019) 3–21. https://doi.org/10.1021/acssuschemeng.8b03286.

[18] I.J. Siddique, A.A. Salema, E. Antunes, R. Vinu, Technical challenges in scaling up the microwave technology for biomass processing, Renew. Sustain. Energy Rev. 153 (2022). https://doi.org/10.1016/j.rser.2021.111767.

[19] Demeto, Demeto, (2021). https://www.demeto.eu/ (accessed October 28, 2025).

[20] R. Lingle, New (Micro) Wave of PET Recycling Technology Arrives, Plastics Today (2024). https://www.plasticstoday.com/advanced-recycling/new-micro-wave-of-pet-recycling-technology-arrives (accessed October 28, 2025).

[21] C. Bao, A. Serrano-Lotina, M. Niu, R. Portela, Y. Li, K.H. Lim, P. Liu, W. jun Wang, M.A. Bañares, Q. Wang, Microwave-associated chemistry in environmental catalysis for air pollution remediation: A review, Chem. Eng. J. 466 (2023). https://doi.org/10.1016/j.cej.2023.142902.

[22] C. Luo, S. Liu, G. Yang, P. Jiang, X. Luo, Y. Chen, M. Xu, E. Lester, T. Wu, Microwave-accelerated hydrolysis for hydrogen production over a cobalt-loaded multi-walled carbon nanotube-magnetite composite catalyst, Appl Energy 333 (2023). https://doi.org/10.1016/j.apenergy.2022.120538.

[23] J.Y. Yusuf, H. Soleimani, Noorhana yahya, Y.K. Sanusi, L.L. Adebayo, S. Sikiru, F.A. Wahaab, Recent advances and prospect of cobalt based microwave absorbing materials, Ceram Int 46 (2020) 26466–26485. https://doi.org/10.1016/j.ceramint.2020.07.244.

[24] G.J.H. Melvin, Z. Wang, Q.-Q. Ni, N.J. Siambun, Md.M. Rahman, Electromagnetic wave absorption properties of rice husks carbonized at 2500 °C, AIP Conf Proc (2017). https://doi.org/10.1063/1.5010439.

[25] S. Cot, M.K. Leu, A. Kalamiotis, G. Dimitrakis, V. Sans, I. de Pedro, I. Cano, An oxalate-bridged binuclear iron(III) ionic liquid for the highly efficient glycolysis of polyethylene terephthalate under microwave irradiation, Chempluschem 84 (2019). https://doi.org/10.1002/cplu.201900075.

[26] C.O. Kappe, Controlled microwave heating in modern organic synthesis, Angew. Chem. Int. Ed. 43 (2004) 6250–6284. https://doi.org/10.1002/anie.200400655.

[27] A.F. Visentin, T. Dong, J. Poli, M.J. Panzer, Rapid, microwave-assisted thermal polymerization of poly(ethylene glycol) diacrylate-supported ionogels, J Mater Chem A Mater 2 (2014) 7723–7726. https://doi.org/10.1039/c4ta00907j.

[28] W. Li, K. Qian, Z. Yang, X. Ding, W. Tian, D. Chen, Promotion effect of cobalt doping on microwave-initiated plastic deconstruction for hydrogen production over iron catalysts, Appl Catal B 327 (2023). https://doi.org/10.1016/j.apcatb.2023.122451.

[29] M. Abbasi, M.R.M. Mojtahedi, A. Khosroshahi, Effect of spinning speed on the structure and physical properties of filament yarns produced from used PET bottles, J Appl Polym Sci 103 (2007) 3972–3975. https://doi.org/10.1002/app.25369.

[30] L. Yan, P.M. Witt, T.F. Edgar, M. Baldea, Static and dynamic intensification of water-ethylene glycol separation using a dividing wall column, Ind Eng Chem Res 60 (2021) 3027–3037. https://doi.org/10.1021/acs.iecr.0c06139.

[31] Y. Liu, X. Yao, H. Yao, Q. Zhou, J. Xin, X. Lu, S. Zhang, Degradation of poly(ethylene terephthalate) catalyzed by metal-free choline-based ionic liquids, Green Chem. 22 (2020) 3122–3131. https://doi.org/10.1039/d0gc00327a.

[32] A. Stoski, M.F. Viante, C.S. Nunes, E.C. Muniz, M.L. Felsner, C.A.P. Almeida, Oligomer production through glycolysis of poly(ethylene terephthalate): effects of temperature and water content on reaction extent, Polym Int 65 (2016) 1024–1030. https://doi.org/10.1002/pi.5146.

[33] S. Najafi-Shoa, M. Barikani, M. Ehsani, M. Ghaffari, Cobalt-based ionic liquid grafted on graphene as a heterogeneous catalyst for poly (ethylene terephthalate) glycolysis, Polym Degrad Stab 192 (2021) 109691. https://doi.org/10.1016/j.polymdegradstab.2021.109691.

[34] Thermo Scientific, Carbon Black Analysis using FT-IR with Germanium and Diamond ATR, 2013. www.thermoscientific.com.

[35] S. Gupta, R. Fernandes, R. Patel, M. Spreitzer, N. Patel, A review of cobalt-based catalysts for sustainable energy and environmental applications, Appl Catal A Gen 661 (2023). https://doi.org/10.1016/j.apcata.2023.119254.

[36] K.H. Zangana, A. Fernandez, J.D. Holmes, Simplified, fast, and efficient microwave assisted chemical recycling of poly (ethylene terephthalate) waste, Mater Today Commun 33 (2022). https://doi.org/10.1016/j.mtcomm.2022.104588.

[37] R.A. Sheldon, Metrics of Green Chemistry and Sustainability: Past, Present, and Future, ACS Sustain Chem Eng 6 (2018) 32–48. https://doi.org/10.1021/acssuschemeng.7b03505.

[38] K. Tan, Y. Qin, T. Du, L. Li, L. Zhang, J. Wang, Biochar from waste biomass as hygroscopic filler for pervious concrete to improve evaporative cooling performance, Constr Build Mater 287 (2021). https://doi.org/10.1016/j.conbuildmat.2021.123078.

[39] X. Bao, M. Li, R. Niu, J. Lu, S. Panigrahi, A. Garg, C. Berretta, Hygroscopic water retention and physio-chemical properties of three in-house produced biochars from different feedstock types: Implications on substrate amendment in green infrastructure, Water 13 (2021). https://doi.org/10.3390/w13192613.

[40] H. Han, W. Buss, Y. Zheng, P. Song, M. Khalid Rafiq, P. Liu, O. Mašek, X. Li, Contaminants in biochar and suggested mitigation measures – a review, Chem. Eng. J. 429 (2022). https://doi.org/10.1016/j.cej.2021.132287.

[41] M. González-Hourcade, G. Simões dos Reis, A. Grimm, V.M. Dinh, E.C. Lima, S.H. Larsson, F.G. Gentili, Microalgae biomass as a sustainable precursor to

produce nitrogen-doped biochar for efficient removal of emerging pollutants from aqueous media, J Clean Prod 348 (2022). https://doi.org/10.1016/j.jclepro.2022.131280.

[42] Y. Yu, Z. Ren, L. Li, J. Han, Z. Tian, C. Liu, J. Chen, Ionic liquid-induced graphitization of biochar: N/P dual-doped carbon nanosheets for high-performance lithium/sodium storage, J Mater Sci 56 (2021) 8186–8201. https://doi.org/10.1007/s10853-021-05823-3.

[43] S.U. Masrura, T. Abbas, H. Heidari, S.R. Rothee, A. Javed, E. Khan, Density functional theory for selecting modifiers for enhanced adsorption of tetracycline in water by biochar, Waste Dispos Sustain Energy 5 (2023) 25–35. https://doi.org/10.1007/s42768-022-00125-z.

[44] W. Chen, M. Gong, K. Li, M. Xia, Z. Chen, H. Xiao, Y. Fang, Y. Chen, H. Yang, H. Chen, Insight into KOH activation mechanism during biomass pyrolysis: Chemical reactions between O-containing groups and KOH, Appl Energy 278 (2020). https://doi.org/10.1016/j.apenergy.2020.115730.

[45] Y. Trivedi, A. Sharma, M. Sharma, R.K. Mishra, J.B. Joshi, A.B. Gupta, B. Achintya, K. Shah, K.K. Pant, Mechanistic assessment of functionalised biochar derived from customised pyrolyzer for nitrate removal, Results Eng. 26 (2025). https://doi.org/10.1016/j.rineng.2025.104672.

[46] A. Thakur, H. Assad, S. Kaya, A. Kumar, Plant extracts as environmentally sustainable corrosion inhibitors II, in: Eco-Friendly Corrosion Inhibitors: Principles, Designing and Applications, Elsevier, 2022: pp. 283–310. https://doi.org/10.1016/B978-0-323-91176-4.00017-9.

[47] H.M. Khan, P.C.T. Souza, S. Thallmair, J. Barnoud, A.H. De Vries, S.J. Marrink, N. Reuter, Capturing Choline-Aromatics Cation-πInteractions in the MARTINI Force Field, J Chem Theory Comput 16 (2020) 2550–2560. https://doi.org/10.1021/acs.jctc.9b01194.

[48] M. Lawrinenko, D.A. Laird, Anion exchange capacity of biochar, Green Chem. 17 (2015) 4628–4636. https://doi.org/10.1039/c5gc00828j.

[49] N. Musa, K.S. Khan, J.C. Blankinship, S.S. Ijaz, Z. Akram, M.S. Alwahibi, M.A. Ali, M. Yousra, Sorption-desorption of phosphorus on manure- and plant-derived biochars at different pyrolysis temperatures, Sustainability 16 (2024). https://doi.org/10.3390/su16072755.

[50] J. Fang, Y. Zhang, Y. Wang, Y. Li, H. Li, C. Li, The molecular design and experimental study on the catalytic cleavage of linkages in lignin with binuclear ionic liquid, J Mol Liq 308 (2020). https://doi.org/10.1016/j.molliq.2020.113128.

[51] Y. He, Y. Guo, F. Yan, T. Yu, L. Liu, X. Zhang, T. Zheng, Density functional theory study of adsorption of ionic liquids on graphene oxide surface, Chem Eng Sci 245 (2021). https://doi.org/10.1016/j.ces.2021.116946.

[52] D. Cheshmedzhieva, S. Ilieva, B. Galabov, Hydrogen bonding to graphene surface: A comparative computational study, Inorganica Chim Acta 551 (2023). https://doi.org/10.1016/j.ica.2023.121454.

[53] M.R. Nabid, Y. Bide, N. Fereidouni, B. Etemadi, Maghemite/nitrogen-doped graphene hybrid material as a reusable bifunctional catalyst for glycolysis of polyethylene terephthalate, Polym Degrad Stab 144 (2017) 434–441. https://doi.org/10.1016/j.polymdegradstab.2017.08.033.

[54] A.M. Al-Sabagh, F.Z. Yehia, D.R.K. Harding, G. Eshaq, A.E. ElMetwally, Fe3O4-boosted MWCNT as an efficient sustainable catalyst for PET glycolysis, Green Chem. 18 (2016) 3997–4003. https://doi.org/10.1039/c6gc00534a.

[55] R. Cancelliere, M. Cianciaruso, K. Carbone, L. Micheli, Biochar: A sustainable alternative in the development of electrochemical printed platforms, Chemosensors 10 (2022). https://doi.org/10.3390/chemosensors10080344.

Chapter 7
Conclusions and future work

7.1 Conclusions

This study presents a comprehensive exploration of polyethylene terephthalate (PET) glycolysis catalysed by selected organic and metal-based ionic liquids (ILs), integrating theoretical modelling with experimental validation. The aim of the work was to bridge the gap in activity between highly active metal ILs and their greener, cheaper choline-based counterparts, while elucidating the reaction mechanism.

Density Functional Theory (DFT) calculations enabled the theoretical screening of a range of ILs, identifying $[bmim]_2[CoCl_4]$ as the most promising candidate due to its ability to significantly lower the reaction energy barrier. Coordination between the cobalt centre and PET's ester group was shown to facilitate chain scission more effectively than organic ILs, such as [Ch][OAc], which rely solely on non-covalent interactions. Experimental validation confirmed the superior catalytic performance of $[bmim]_2[CoCl_4]$, though monomer bis(2-hydroxyethyl) terephthalate (BHET) yields remained limited, highlighting challenges in short-chain scission and the potential of moisture effects.

Mechanistic insights from advanced DFT analyses revealed fundamental differences in the catalytic role of metal-based and organic ILs, both differing from the traditional mechanism described in **Chapter 2**, **Section 2.2**. Organic ILs exhibited a reliance on hydrogen bonding and charge redistribution to enhance EG nucleophilicity, but lacked the dynamic coordination behaviour observed in metal-based systems. The cobalt-based anion acted as a bifunctional catalytic moiety, offering both Lewis acidic and nucleophilic functionality *via* dynamic ligand exchange, resulting in its superior efficiency. In both cases, the mechanistic role of the cation was found to be limited to charge stabilisation, contrary to the established mechanism. The results emphasise the

need for bespoke mechanistic studies of catalyst-specific systems, in place of "off-the-shelf" general reaction mechanisms which incorrectly imply uniformity across all systems.

Overall, the DFT results in this thesis both rationalise the experimentally-observed catalyst performance and provide predictive mechanistic insights beyond qualitative chemical reasoning. By quantifying electronic interactions and energy barriers, the calculations identify design principles that can be applied to develop next-generation ionic liquid and metal-based catalysts for PET glycolysis, including desirable functional groups and the influence of steric bulk and charge localisation. In this way, DFT serves not only as a post-experiment rationalisation tool but also as a forward-looking guide for catalyst optimisation.

Although metal-based ILs are more catalytically active, the heavy metals they contain are being phased out of use due to their high cost and toxicity. Choline-based ILs, contrastingly, offer much cheaper synthesis and greener credentials, at the expense of reduced activity and unverified recyclability. Therefore, to enhance the sustainability and effectiveness of the ILs, microwave (MW) heating, moisture control and the introduction of a waste-derived biochar (BC) catalyst support were explored. Through a dual dielectric-magnetic heating mechanism, the rate of PET conversion under $[bmim]_2[CoCl_4]$ catalysis was significantly enhanced, while [Ch][OAc] did not respond efficiently, making its use for future MW-assisted PET glycolysis studies unsuitable unless combined with more absorbent materials. Further enhancement of the MW-assisted process could be achieved by the introduction of MW-absorbing cladding materials such as BC. Although the metal IL shows promise for MW heated glycolysis, BHET yields remained very low.

Moisture was identified as a critical inhibitor to the glycolysis process, disrupting hydrogen bonding and coordination pathways. This is an important finding in the context of real-world plastic waste, suggesting that rigorous pre-drying of plastic waste would be required for the technology to be feasible on an industrial scale, at great energetic expense. The organic IL was observed both experimentally and theoretically to be less sensitive to moisture, further cementing its position as the more promising catalyst for an industrial-scale process.

IL immobilisation on BC, demonstrated a promising strategy to enhance monomer yields and catalyst dispersibility, particularly for [Ch][OAc], which showed a remarkable 24% BHET yield increase, whilst showing potential for recyclability. DFT calculations, coupled with Raman spectroscopy, attribute the superior catalytic performance of the supported choline-based IL to stronger and more uniform adsorption of the ions, while an additional catalytic and moisture mitigating role of the BC is postulated. The results highlight the potential for BC-supported [Ch][OAc] as cheap, green and effective catalyst for PET glycolysis. However, nuclear magnetic resonance (NMR) spectroscopy revealed that while the main degradation product was BHET, its purity was somewhat compromised, most likely by impurities present within BC. It is advised that future work should investigate the further purification of the monomer during separation of the catalyst.

Overall, the work enclosed in this thesis underscore the potential for use of cheap, environmentally-friendly ILs for PET glycolysis catalysis. By implementing theoretical calculations for mechanistic understanding, processes can be selectively enhanced to bridge the activity gap between the greener choline-based ILs and their metallic counterparts. Of the strategies tested, the novel waste-derived BC catalyst

support represent an exciting technology, while moisture mitigation is identified as a key factor for future processes on a micro- and macroscopic scale.

7.2 Future work

The results from this thesis provide the opportunity for both experimental and theoretical future work to be conducted, particularly in regards to the BC support.

7.2.1 Systematic investigation of BC-supported [Ch][OAc]

Chapter 6 of the thesis highlighted potential of the BC-supported [Ch][OAc] catalyst, achieving a remarkable increase in BHET yield. While the BHET yield significantly increased, the purity was somewhat compromised. High-Performance Liquid Chromatography (HPLC) could assist in the identification, and subsequent mitigation, of the impurities. Regrettably, due to limited BC resources, the glycolysis experiments could not be further optimised, potentially preventing the BHET yield from reaching its maximum. Although clear conclusions can be made from the results, an obvious next step would be to test more experimental scenarios as well as alternative support materials. To provide a fuller picture of the effects, future work should incorporate a Design of Experiment (DoE) approach to optimising the process through multiple repeated experiments. The effectiveness of the BC as a support opens up possibilities for task-specific catalyst design due to the materials' diversity. The BC in this study was derived from spent coffee grounds and activated with KOH, however if extracted from another biomass source and activated through a different method, the surface properties could alter significantly. This represents an opportunity for a systematic approach to comparing different BC's for PET glycolysis, aided by experimental tools such as x-ray photoelectron spectroscopy (XPS) or energy dispersive x-ray spectroscopy (EDS), which were out-with the scope of this project.

Additionally, it was observed that the MW-assisted performance of [Ch][OAc] was limited due to its relative MW transparency compared with the cobalt-based IL. As a known MW cladding material, BC could significantly enhance the dielectric heating response of [Ch][OAc].

It should be noted that these findings could also be applied to alternative systems involving chemically-similar compounds, such as in the use of deep eutectic solvents (DESs) for plastic composite recycling. As ILs and DESs are so chemically similar, and are often choline-based, it is reasonable to suggest that they too could be combined with a BC support to form an effective, low-cost and sustainable heterogeneous catalyst.

7.2.2 Advanced modelling of biochar

While the DFT modelling in this work goes some way to predicting the behaviours of ILs adsorbed to certain functional groups believed to be on the BC surface, the model is highly simplified. As mentioned briefly in **Chapter 3**, molecular modelling of BC is extremely complex and, to date, there exists very few computational studies. Whilst the interactions between adsorbates and the functional groups of BC provide some valuable information, they do not account for many characteristics such as microporosity and surface area. Paired with the vast diversity of the materials, this signifies a large gap in the research. DFT modelling of inorganics, functional groups and heteroatoms could be paired with advanced molecular dynamics models capable of replicating macroscopic properties. This work, combined with experimental characterisation techniques, could create accurate, bespoke models of the BC actually being used rather than being restricted to predicted functional groups, opening the door for potential screening of BCs for PET glycolysis.

7.2.3 Mechanistic results informing future catalyst design

Mechanistic analysis undertaken in **Chapter 5** validate recent literature which highlight the limited catalytic role of choline cations. In the case of $[bmim]_2[CoCl_4]$ too, the cation molecules were seen to not contribute significantly. However, [bmim]Cl, the worst-performing IL, did show some cationic contribution, suggesting that in some cases the cation do play the role outlined in the traditionally-used mechanism. These results suggest that potentially, the acetate anion could be paired with an alternative cation which contributes to the catalytic degradation while retaining the cholinium's green credentials. Some very recently published work has found that a phosphonium cation exerts more catalytic effect compared to choline due to increased lipophilicity, however this was found to reduce the biodegradability of the IL. The work serves as evidence of the tuneability of ILs due to the near-unlimited number of potential pairs. Future work would be aimed at testing new combinations of ion pairs based on their functionalities, first through DFT modelling and validated by experiment.